Universidade de Aveiro Departamento de Ciências Médicas
2018

Mafalda Raquel da Conceição Santos

ELUCIDAR O PAPEL DOS PROTEOMAS ESTATÍSTICOS NO CANCRO EM HUMANOS

UNRAVELLING THE ROLES OF STATISTICAL PROTEOMES IN HUMAN CANCER

Universidade de Aveiro Departamento de Ciências Médicas
2018

Mafalda Raquel da Conceição Santos

Elucidar o papel dos proteomas estatísticos no cancro em humanos

Unravelling the roles of statistical Proteomes in human cancer

Tese apresentada à Universidade de Aveiro para cumprimento dos requisitos necessários à obtenção do grau de Doutor em Biomedicina, realizada sob a orientação científica do Doutor Manuel António da Silva Santos, Professor Associado do Departamento de Ciências Médicas da Universidade de Aveiro e co-orientação da Doutora Carla Isabel Gonçalves Oliveira, Professora Afiliada da Faculdade de Medicina da Universidade do Porto e Investigadora Principal no Ipatimup/i3S – Instituto de Patologia e Imunologia Molecular da Universidade do Porto/ Instituto de Investigação e Inovação em Saúde.

Apoio financeiro da FCT e do FSE no âmbito do III Quadro Comunitário de Apoio.

“The important thing is not to stop questioning. Curiosity has its own reason for existence. One cannot help but be in awe when he contemplates the mysteries of eternity, of life, of the marvelous structure of reality. It is enough if one tries merely to comprehend a little of this mystery each day.he art and science of asking questions is the source of all knowledge.” – Albert Einstein

Dedico este trabalho à minha família e amigos.

o júri

Presidente

Prof. Doutor Amadeu Mortágua Velho da Maia Soares
Professor Catedrático, Universidade de Aveiro

Prof. Doutor Manuel António da Silva Santos
Professor Associado, Universidade de Aveiro

Prof. Doutora Maria Alexandra Marques Moreira Mourão do Carmo
Investigadora Principal, Universidade do Porto

Doutor Peter Jordan
Investigador Coordenador, Instituto Nacional de Saúde Ricardo Jorge

Prof. Doutora Luísa Alejandra Helguero
Professora Auxiliar, Universidade de Aveiro

Agradecimentos

Em primeiro lugar quero agradecer ao meu Orientador, Professor Doutor Manuel Santos, pela orientação deste trabalho, por todos os conselhos e pela confiança que depositou em mim ao aceitar-me no seu laboratório para fazer este trabalho, sem me conhecer antecipadamente.

À minha co-Orientadora, Doutora Carla Oliveira, por tudo o que fez por mim durante estes anos; por me ter ajudado a desenvolver as competências necessárias para a realização do trabalho, por todas as ideias, entusiasmo e por me ter acolhido no seu laboratório sempre que tinha de desenvolver uma técnica nova.

À Fundação para a Ciência e Tecnologia o meu muito obrigado por ter financiado este trabalho através de uma bolsa de Doutoramento, SFRH/BD/91020/2012 e do projecto FCT-ANR/IMI-MIC/0041/2012. Ao CESAM, ao iBiMED (UID/BIM/04501/2013), ao IPATIMUP e ao I3S por terem proporcionado as condições necessárias à realização deste trabalho.

À Doutora Luisa Helguero e à Doutora Daniela Ribeiro por me terem disponibilizado as suas salas de cultura de células para poder realizar este trabalho.

À Mónica Almeida, por me ter ajudado a estabelecer as linhas estáveis por electroporação (num dia 23 de Dezembro), quando eu já estava a perder a esperança de que fosse conseguir.

À Patrícia Pereira que iniciou a colaboração entre estes dois grupos fantásticos (Biologia do RNA e ERiC) e que iniciou este trabalho.

Agradecimentos (Continuação)

A toda a gente do grupo da Biologia do RNA. Apesar de cada um trabalhar no seu tópico, todos nos apoiamos para progredir. Em especial, quero agradecer à Ana Soares e à Ana Rita Bezerra por todas as discussões científicas, por me ajudarem a organizar o tempo e a prioritizar tarefas, mas também por todas as gargalhadas no trabalho. À Rita Guimarães pela nossa jornada no meio de espectros, tempos de retenção, péptidos sintéticos, digestões e afins e por todos os momentos de convívio fora do lab. À Inês Santana, porque sem ela não tinha material para trabalhar, sobretudo os anticorpos. À Andreia Reis, por todos os scripts que desenvolveu para podermos analisar os dados de espectrometria de massa. Aos que já não estão presentes, Rita Araújo e Violeta Ferreira, pela amizade que permaneceu depois de terem saído do laboratório. À Ana Fidalgo, por tudo o que me fizeste crescer como pessoa e "cientista". Obrigado por todas as caminhadas que fizemos juntas até ao Departamento de Química, carregadas com o material às costas e por todos os ensaios que fizemos juntas. À Sofia Varanda, por tudo e por nada, porque é impossível colocar em palavras todo o trabalho e convívio nestes últimos anos.

Ao grupo ERIC. Sem vocês este trabalho tinha sido sem dúvida mais pobre. À Joana Carvalho, porque sem ti os tRNAs NUNCA teriam sido detectados. À Patrícia Oliveira, porque me incentivaste a ser melhor e a provar que o símbolo de Bioquímica de Coimbra afinal era mais interessante do que aquilo que parecia ao início e por teres escrito um projecto fantástico com os nossos resultados preliminares. À Gabriela Almeida, por todas as salas que marcaste por mim, por toda a burocracia de que trataste, por todo o planeamento do trabalho que fizemos sobretudo com os fármacos, por todo o apoio que deste nas experiências e por todas as discussões científicas que fomos tendo. À Diana Martins, por toda a ajuda que deste nas experiências de metastização e de resistência aos fármacos e por me teres arranjado aquele software fantástico de análise de imagem para quantificar as áreas de metastase. À Carla Pereira, por teres preparado sempre a cisplatina nos dias dos

Agradecimentos (Continuação)

tratamentos e pela disponibilidade que sempre demonstraste em ajudar. À Sara Rocha por me ter ajudado com as imunohistoquímicas. Ao Hugo Pinheiro, à Sofia Valente, à Anabela Ferro, à Sara Teles por todas as discussões nos lab meetings, por todo o companheirismo que sempre demontraram e por todo o carinho com que me receberam sempre que ia ao IPATIMUP e por me dizerem sempre onde estavam as coisas.

Ao Nuno Mendes, por tudo o que me ensinaste e pela confiança que sempre depositaste em mim quando eu dizia que não conseguia fazer alguma coisa com os bichinhos. Sem ti não teria conseguido fazer os ensaios todos que fiz.

Ao Rui Vitorino e ao Fábio Trindade, por toda a ajuda com a espectrometria de Massa. Obrigado por acreditarem que era possível detectarmos as "misincorporações".

À Carolina Silva, à Rita Faria e à Doutora Catarina Almeida, por me terem ajudado a estabelecer a técnica de medição da taxa de síntese proteica por citometria.

Ao Miguel Aroso, por me teres ajudado com a microscopia e com a análise de imagens.

À Fátima Camões, por todo o trabalho que fazes para manter as salas de cultura do iBiMED a funcionar, por todos os testes ao micoplasma que fizeste e pela disponibilidade para resolver todos os problemas e esclarecer dúvidas.

Ao Doutor Phillipe Pierre por nos ter gentilmente cedido o anticorpo anti-puromicina.

Às meninas da tuna, em especial à Gladys Caldeira, por todos as escapadelas musicais, amizade, "cumbíbio" e diversão.

Agradecimentos (Continuação)

Aos meus amigos de sempre, Ana Monteiro, Diogo Freitas, Joana Contramestre, Rui Albino, Joana Santos, Nuno Monteiro, Elsa Monteiro, por me apoiarem sempre e por me lembrarem que há mais vida para além da tese. Obrigado por tudo!

Ao meu noivo, Zé Sousa, por todo o apoio que me deste ao longo destes anos. É preciso ser alguém especial para aturar as longas horas que passava no laboratório, a falta de tempo para as coisas mais básicas e mesmo assim insistir para que eu tivesse sempre um bocadinho para mim. Por teres cuidado de mim, do cão e da casa praticamente sozinho durante estes últimos meses. Obrigado por tudo o que fizeste por mim, por me fazeres feliz e por nunca me deixares baixar os braços.

À minha família, sobretudo àqueles que são os meus quatro pilares fundamentais: Mãe Luce, Lena, Tia Lena e Avó Maria Helena. Sem vocês nunca teria conseguido chegar aqui, obrigado por tudo aquilo que sempre fizeram por mim e por me ajudarem a tornar na pessoa que sou hoje. Obrigado às outras grandes mulheres da minha família, Tia Raquel, Tia Catarina e Avó Joaquina, pelo exemplo de força e resiliência em todas as circunstâncias da vida. Obrigado por me incentivarem a ser sempre melhor.

palavras-chave

Erros na síntese proteica, *Unfolded Protein Response*, desregulação de tRNAs, *misreading* tRNAs, cancro, invasão local, resistência à cisplatina.

resumo

A desregulação dos componentes da maquinaria de síntese proteica, tais como tRNAs, aminoacil-tRNA sintetases, e enzimas modificadoras dos tRNAs, é comum em tumores, levantando a hipótese de que a fidelidade da síntese proteica pode estar comprometida em tumores.

Para clarificar esta hipótese, determinámos a taxa de erro da síntese proteica e observámos que os tumores produzem mais erros na síntese de proteínas que os tecidos normais. De modo a compreender o papel dos erros de tradução na biologia tumoral, expressámos tRNAs de Serina mutantes que incorporam Ser em locais de Ala (erro frequente) e Ser em locais de Leu (erro raro) na linha celular NIH3T3. O tRNA que incorpora Ser em locais de Ala, promoveu o crescimento tumoral com uma cinética semelhante à induzida pela mutação K-ras^{V12}. A activação da via AKT e a activação diferencial da UPR, dependendo do tRNA expresso, também foram observadas. No entanto, a expressão dos tRNAs mutantes nas linha celulares derivadas das NIH3T3 não permitiu clarificar o papel dos tRNAs recombinantes na iniciação ou na progressão tumoral. Para tal, expressámos um tRNA de Serina WT e o tRNA mutante insere Ser em locais de Ala em células derivadas de epitélio bronquial normal, BEAS-2B, e em células derivadas de Carcinoma de células grandes do pulmão, H460. A expressão destes tRNAs na linha celular normal, aumentou a proliferação celular, a taxa de síntese proteica e a activação de biomarcadores da via da UPR, a qual é dependente do tRNA expresso. Ambos os tRNAs favoreceram a formação de colónias *in vitro*. O aumento da expressão do tRNA de Serina WT foi suficiente para iniciar a formação de tumores de crescimento lento. Quando expressámos os mesmos tRNAs nas células tumorais H460, observámos um aumento na cinética de crescimento tumoral e no potencial de invasão local das células, embora os resultados obtidos não permitam tirar uma conclusão definitiva acerca do envolvimento dos tRNAs na progressão tumoral. O aumento da expressão do tRNA de Serina WT torna células tumorais mais resistentes ao tratamento com cisplatina. De um modo geral, os nossos resultados sugerem que a desregulação de tRNAs e o aumento dos erros da síntese proteica são importantes para a biologia dos tumores.

keywords

Protein Synthesis Errors, Unfolded Protein Response, tRNA deregulation, misreading tRNAs, cancer, local invasion, cisplatin resistance.

abstract

Deregulation of various components of the protein synthesis machinery, including tRNAs, aminoacyl-tRNA synthetases and tRNA modifying enzymes, are common in tumors, raising the hypothesis that protein synthesis accuracy is compromised in cancer.

To clarify this hypothesis, we determined the relative error rate of protein synthesis and observed that tumors mistranslate at higher levels than normal tissue. To understand the role of mistranslation in tumor biology, we expressed mutant Ser-tRNAs that misincorporate Ser-at-Ala (frequent error) and Ser-at-Leu (infrequent error) sites in NIH3T3 cells. The tRNA that misincorporated Ser-at-Ala codon sites induced tumor growth with similar kinetics of K-ras^{V12} expressing tumors. Upregulation of the AKT pathway and differential activation of the UPR, depending on the tRNA being expressed, were also observed. However, these studies did not clarify the role of tRNA deregulation or tRNA misreading in tumor initiation or progression. For this, a WT-Ser tRNA and a tRNA that misincorporates Ser-at-Ala codon sites were expressed in cells derived from normal bronchial epithelium (BEAS-2B) and in cells derived from a Large cell lung carcinoma (H460). The BEAS-2B cell lines studies showed that increased cell proliferation *in vitro*, increased protein synthesis rate and activation of UPR biomarkers, which were dependent on the recombinant tRNA being expressed. Both tRNA constructs increased colony formation capacity *in vitro.* Interestingly, the data suggest that upregulation of the WT Ser-tRNA is sufficient to trigger tumor formation, albeit with very slow growth kinetics. When the same tRNAs were expressed in H460 cells, tumor growth kinetics and local invasion potential of the cells increased. Finally, upregulation of the WT-Ser tRNA decreases tumor cell sensitivity to cisplatin treatment. The overall study highlights new features of tRNA function in tumor biology and open new avenues to explore the role of protein synthesis in cancer.

Contents

List of Figures

List of Tables

List of abbreviations

A

A – Alanine
aaRS – Aminoacyl tRNA synthetase
ALK – Anaplastic Lymphoma Kinase
Ala – Alanine
AlaRS – Alanyl-tRNA synthetase
AMP – Adenosine Monophosphate
Arg – Arginine
Asn – Asparagine
Asp – Aspartic acid
ATF4 – Activating Transcription Factor 4
ATF6 – Activating Transcription Factor 6
ATP – Adenosine Triphosphate

B

BAK1 – Bcl-2 homologous antagonist/killer
BAX – BCL-2 Associated X
BCL-2 – B-cell lymphoma 2
Bcl-xl – B-cell lymphoma-extra large
BiP – Binding immunoglobulin Protein
bp – Base pair

C

C – Cystein
cMET - Mesenchymal-epithelial transition factor
Cys – Cystein

D

D – Aspartic Acid
DNA – Deoxyribonucleic Acid

E

E – Glutamic Acid
EARS – Glutamyl-prolyl-tRNA synthetases
eEF – Eucaryotic Elongation Factor
EGFR - Epidermal growth factor receptor
eIF – Eukaryotic Initiation Factor
EMT - Epithelial-Mesenchymal Transition
ER – Endoplasmic Reticulum
ERAD – Endoplasmic Reticulum Associated Degradation
ERK - Extracellular signal–regulated kinase

G

G – Glycine
GADD34 – Growth arrest and DNA damage-inducible protein
GAPDH – Glyceraldehyde 3-phosphate dehydrogenase
GCN2 – General control nonderepressible 2
Glu - Glutamic acid
Gly – Glycine
GRP78 – 78 kDa glucose-regulated protein

H

H – Histidine
HSP – Heat Shock Protein

I
I – Isoleucine
Ile – Isoleucine
IRE1α – Inositol Requiring kinase 1
IRES- Internal Ribosome Entry Sites

K
K – Lysine
K-ras - Ki-ras2 Kirsten rat sarcoma viral oncogene homolog

L
L – Leucine
LARS – Leucyl-tRNA Synthetase
Leu – Leucine
Lys – Lysine

M
M – Metionine
MAPK – Mitogen-Activated Protein Kinase
Met – Metionine
MRS – Metionyl-tRNA synthetase
mRNA – Messenger RNA
mtDNA – Mitochondrial DNA
mTOR – Mammalian Target Of Rapamycin

N
N – Asparagine
NSCLC – Non-Small Cell Lung Cancer

P
P – Proline
PERK – PKR-like Endoplasmic Reticulum Kinase
Phe – Phenilalanine
PI3K – Phosphoinositide 3-kinase
PQC – Protein quality control

Q
Q – Glutamine

R
R – Arginine
RB – Retinoblastoma protein
RNA – Ribonucleic Acid
ROS – Reactive Oxygen Species
rRNA – Ribosomal RNA

S
S – Serine
SARS – Seryl-tRNA synthetase
Ser – Serine

T
T - Threonine
TFIIIB - RNA polymerase III-specific transcription factor B
TFIIIB - RNA polymerase III-specific transcription factor C
Thr - Threonine
tRNA – transfer RNA

Tyr – Tyrosine

U
U – Uridine
UPR – Unfolded Protein Response
UPS – Ubiquitin-Proteasome System

V
V – Valine
Val - Valine
VEGF - Vascular Endothelial Growth Factor

W
W – Triptophane
WARS – Triptophanyl-tRNA synthestase

X
XBP1 - X-box binding protein 1

Y
Y – Tyrosine
YARS – Tyrosyl-tRNA synthetase

Other abbreviations will be explained when used in the text.

1. Rational and objectives

Cancer is a multifactorial disease driven by the accumulation of DNA mutations, chromosomal aberrations and epigenetic alterations. As a consequence, transcriptional and post-transcriptional deregulation occur in most tumors types. Although, and despite the great effort to clarify the molecular profile of all tumors, a significant percentage of them that cannot be explained by known driver genetic or epigenetic events. For instance, approximately 40% of Non-Small Cell Lung Cancer (NSCLC) tumors have unknown etiology. There is increasing evidence for deregulation of tRNAs, aminoacyl-tRNA synthetases and tRNA modifying enzymes in tumors, but the consequences of such deregulation for tumor biology are poorly understood. A possibility is that protein mutations without corresponding changes in the DNA sequence explain the etiology of a certain fraction of human cancers.

Supporting this hypothesis, recent works show major differences in the tRNA pool of tumors and normal tissue, with specific enrichment of tRNAs that stabilize transcripts associated with cell cycle progression and cell proliferation. Deregulation of tRNA expression and processing may then lead to misreading of near-cognate codons and protein synthesis errors (PSE), however this has not been addressed in cancer so far. The characteristics of the tumor microenviroment, such as amino acid starvation, may also potentiate the occurrence PSE, leading to the upregulation of molecular chaperones, activation of the ubiquitin-proteasome system and the Unfolded Protein Response (UPR) in tumors. Increased PSE levels have also been associated with antibiotic and antifungal resistance in *Candida albicans* and *Mycobacteria,* raising the hypothesis that they may also play a role in cancer therapy resistance.

In this thesis we addressed the hypothesis that PSE increase in tumors, creating a phenotype that is advantageous for tumour cells. Its main objective is to understand whether PSE are increased in tumors, and if so, to characterize the impact of a mutant proteome in cancer cell initiation, growth kinetics and resistance to chemotherapy. To address this objective we developed a method to quantify PSEs and created cell line models of tRNA imbalance and/or misreading. With these tools in our hands, we designed the following specific aims:

1. Quantify the error rate of protein synthesis in tumors and normal tissue and identify the most and least common PSE in tumors using Mass Spectrometry (Chapter 3);

2. Elucidate whether tRNA deregulation and PSE may confer advantageous features to tumour cells (Chapter 3 and 5);

3. Understand if and how PSE and tRNA deregulation, *per se,* have a role in tumor initiation and growth kinetics (Chapter 3, 4 and 5).

4. Understand whether activation of the Unfolded Protein Response influences the impact of a statistical proteome in cell lines and tumour xenografts (Chapter 3, 4 and 5);

5. Assess the relevance of tRNA deregulation and PSE to chemotherapy (Chapter 6).

2. Introduction

Disclosure of interests: The introduction of this thesis will soon be submitted to Trends in Molecular Medicine.

2.1. Abstract

The proteome of cancer cells is seldom different from its transcriptome, once imbalances in translation components are frequent and the increased demand of protein synthesis also comes with a cost on fidelity. The deregulation of transfer RNAs has been poorly studied so far in cancer biology, however, recent evidences suggest that these molecules have a far more important function than anticipated, once they are able to modulate gene expression and induce metabolism changes in cells. In this Introduction, we summarize not only the direct evidences implying tRNAs as major players in cancer biology, but also the indirect evidences that open new insights into their role in tumor heterogeneity and the possibility of modulating tRNAs to target resistance to therapy.

2.2. Overview of tRNA structure and biology

Transfer RNAs (tRNAs) are small conserved RNA molecules (73–90 nucleotides) that connect genes and proteins [1]. In humans, there are 506 tRNA genes that are transcribed into primary transcripts by the RNA polymerase III. These pre-tRNAs are then processed post-transcriptionally to acquire their mature 5' and 3′ ends, modified nucleosides and the typical cloverleaf secondary structure. The latter has 4 domains organized in unpaired and paired regions: acceptor-arm, D-arm, anticodon-arm and TΨC-arm. The 3' CCA of the acceptor arm is added post-transcriptionally and accepts the amino acids. The anticodon-arm has a three nucleotide sequence in the unpaired region (anticodon) that interacts with mRNA codons. Mature tRNAs acquire a L-shape tertiary structure through base stacking and non-Watson-Crick base pairing between the acceptor and TΨC, D and anticodon arms (**Fig.2-1**).

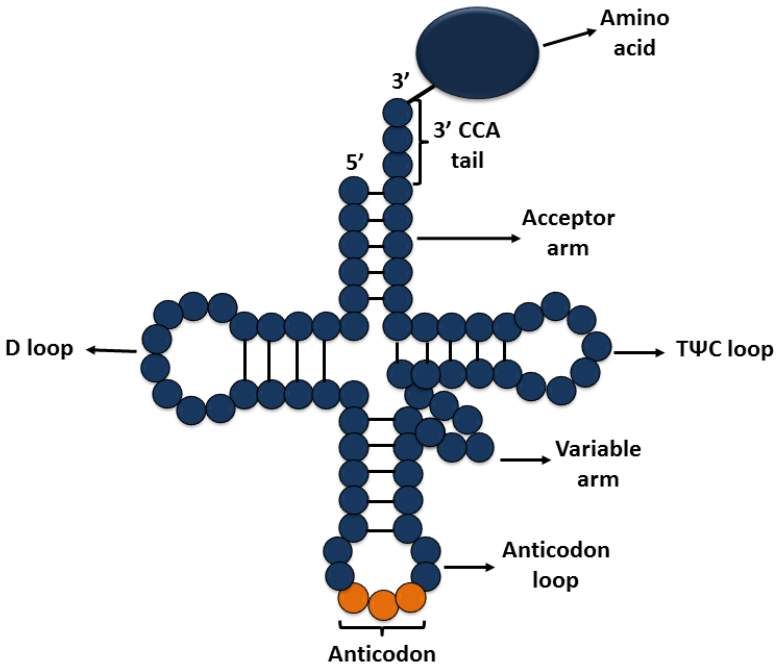

Figure 2-1: tRNA structure. tRNAs have a cloverleaf shape derived from a single nucleotide chain with 73 to 90 nucleotides in length and 4 domains organized in unpaired and paired regions: acceptor arm, D arm, anticodon arm and TΨC arm. The acceptor arm has a 3' CCA tail that links the cognate amino acid, and the anticodon arm has a three nucleotide sequence in the unpaired region, the anticodon loop, that interacts with the mRNA codon. Unpaired regions also mold loops in the D and the TΨC arms and an unpaired region between the anticodon and the TΨC arms represents the variable arm, also known as extra arm. The size of the variable arm can range from 3 to 21 bases and dictates tRNA grouping in class I or II.

tRNAs are charged with amino acids by aminoacyl-tRNA synthetases (aaRS). There is only one aaRS for each amino acid, but each aaRS charges multiple tRNA isoacceptors belonging to the same amino acid family [2]. The aminoacylation of tRNAs involves a two step reaction where the amino acid is activated with ATP forming an aminoacyl-AMP which is then connected to the 3'-end of tRNAs. aaRSs are subdivided in two classes according to the structure of their catalytic domains: Class I aaRSs are usually monomeric or dimeric and aminoacylates the tRNAs in the 2-OH, whereas Class II aaRSs are generally di- or tetrameric and aminoacylate tRNAs in the 3'-OH. Some of these enzymes possess an editing domain that corrects misactivated amino acids and mischarged tRNAs, which is essential for translational fidelity [3]. The abundance of tRNAs is tightly regulated and matches codon usage (**Box 1**) for the correct expression of proteins [4]. Deregulation of tRNA expression, mutations that lead to misacylation of tRNAs by aaRS and aberrant tRNA modification by tRNA modifying enzymes (tRNAmods) alter gene expression and have been associated with cancer, neurodegenerative and metabolic diseases [5–9]. We review here recent data that highlight tRNA contributions to tumor biology.

Box 1 – Codon Usage Bias

Most amino acids are encoded by several synonymous codons, which are not used with the same frequency in the genome. Highly expressed genes tend to be enriched in codons that match the tRNA pool. This codon usage bias has been associated with increased translation accuracy, efficiency, modulation of translation speed, protein folding and stability of secondary structures. Poor correlation between codon usage and the tRNA pool may result in incorrect allocation of resources, namely the increase of ribosome sequestration due to a decrease in translation speed, reducing the global cellular fitness.

2.3. tRNA expression in tumors

The first study suggesting that tRNAs may play a role in cancer was published in 2009 by Pavon and colleagues [10]. These authors observed upregulation of both cytoplasmatic and mitochondrial tRNAs in breast cancer, in particular of tRNA isoacceptors of the Serine (Ser), Threonine (Thr) and Tyrosine (Tyr) families. Since these tRNAs belong to amino acid families that regulate most of the cancer signaling cascades through phosphorylation, it was suggested that tRNA expression deregulation impacts on cancer signaling pathways [10]. Gingold and colleagues discovered a subset of tRNAs that are differentially expressed in several types of cancer, but are downregulated in differentiating or senescent cells. These tRNAs decode codons that are abundant in transcripts encoding proteins related to cell growth and proliferation, indicating that they may modulate gene expression at the translational level in those tumors [11]. Another study showed that overexpression of the initiator $tRNA^{iMet}$ *in vitro* can alter the entire tRNA expression landscape and increase cellular metabolic activity and proliferation rates *in vitro* [12]. The specific role of $tRNA^{iMet}$ overexpression in tumorigenesis is not yet clear since the observed global tRNA deregulation may alter global protein expression, induce the acquisition of traits that could be relevant to tumor growth and may even constitute a novel tumor initiation mechanism.

Recent works show that $tRNA^{Glu}UUC$ and $tRNA^{Arg}CCG$ are specifically upregulated in metastatic breast cancer cell lines, providing a link between tRNA pool deregulation and cancer progression [13]. How tRNA upregulation contributes to cancer biology is poorly understood, but it is likely that the upregulated tRNAs increase the translation efficiency of specific disease-promoting genes that are enriched in the codons recognized by these anticodons, shifting the proteome landscape towards a pro-metastatic state [13]. Alteration of the tRNA landscape may also modify the cellular microenvironment to favor tumor progression. Indeed, upregulation of $tRNA^{iMet}$ in

support fibroblasts induces secretion of collagen type II, favoring endothelial cell migration, angiogenesis and tumor growth [14]. In addition, the overexpression of $tRNA^{iMet}$ is sufficient to promote migration and invasion of melanoma cells, through mechanisms that are dependent on the α5β1 integrin, resulting in an increased metastatic potential without affecting proliferation and growth of the primary tumor [15].

Moreover, recent NGS works identified 76 tRNAs that are upregulated in breast tumors. This tRNA set is sufficient to discriminate normal and tumor samples, showing that tumors have tRNA populations that are distinct from those of normal cells. Fourteen of these tRNAs were associated with decreased overall survival and augmented risk of recurrence in a case-only approach. Of these, only chr6.tRNA5-SerAGA, chr6.tRNA50-SerAGA and chr6.tRNA51-SerTGA correlated with these biological features in a case-control approach [9].

Publicly available small non-coding RNA data (sncRNA) (YM500v3 database) provide systematic data of sncRNAs expression profiles in different tissues, types of cancer and on the influence in cancer patients overall survival. The stratification of tumors based on the expression levels of the sncRNAs showed that increased expression of several tRNAs consistently associate with bad prognosis in kidney renal clear cell carcinoma, adrenocortical carcinoma and breast invasive carcinoma (**Fig.2-2**) [16]. Moreover, increased expression of the tRNAs mentioned above is generally associated with bad prognosis in several types of cancer (**Fig.2-2**), suggesting that deregulation of tRNAs in tumors or tumor-support cells imposes important cellular reprogramming events that may sustain tumor growth and disease progression.

2.4. The molecular basis of differential tRNA deregulation in tumors

The traditional view of tRNA abundance was that it depends mainly on tRNA gene copy number [17], however, recent data suggest that regulation of tRNA expression is far more complex [10,11,13]. RNA polymerase III (PolIII) has increased activity in cancer likely to provide sufficient tRNA to sustain the increased protein synthesis rate observed in tumors [18]. PolIII transcription relies on the transcription factor IIIC (TFIIIC), a six subunit complex that binds to the A and B boxes of the tRNA genes internal promoters [19]. The TFC4 subunit of the TFIIIC then interacts with Brf1 and Bdp1 to recruit the TFIIIB factor [20], which recognizes upstream regions of tRNA genes and directs the recruitment of PolIII to the tRNA gene promoters [19]. Since the subunits of TFIIIB, Bdp1 and Brf1 [21], have multiple isoforms that are generated by alternative

splicing in a tissue-specific-manner [22], they may permit differential regulation of tRNA expression.

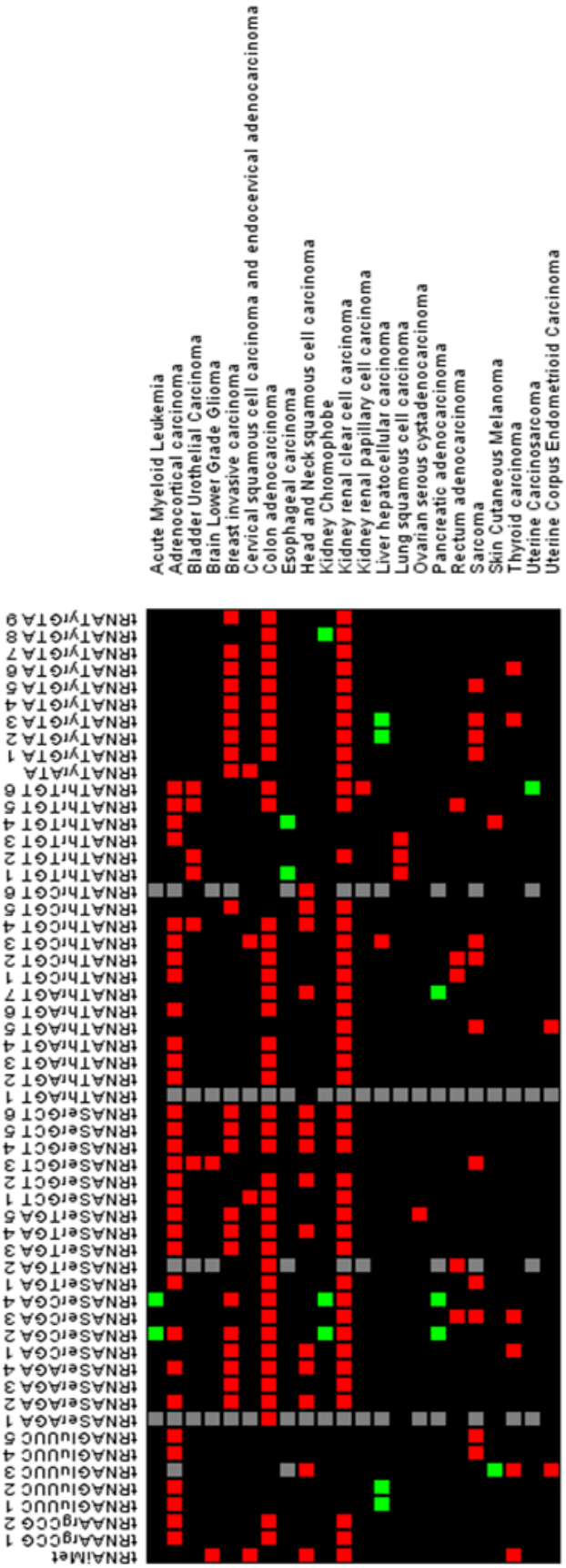

Figure 2-2: tRNA association with prognosis. tRNAs that were previously described in the literature to be associated with cancer were browsed on YM500v3 database for association with prognosis. Overall high expression of tRNAs is usually associated with bad prognosis. Legend: **Red** – Bad Prognosis; **Green** – Good Prognosis **Black** – No difference; **Grey** – Data not available.

RNA PolIII is also positively regulated by oncogenes, namely c-Myc, Ras/ERK, PI3K/Akt, mTOR and TERT whereas tumor suppressors (RB and p53) tend to downregulate its activity [23–25]. The c-Myc transcription factor which modulates cell growth, proliferation and apoptosis, also upregulates RNA polymerases I, II and III [26,27]. In the case of PolIII, c-Myc recruits the histone acetyltransferase GCN5 and the cofactor TRRAP to target tRNAs genes. This transcription factor also recruits the Brf1 and Bdp1 subunits of TFIIIB, dually contributing to PolIII transcription activation [27]. On the other hand, the Cytoskeletal filamin A (FLNA) which has an ambiguous role in cancer depending on its isoform and location, can repress PolIII by interacting with its actin-binding domain; its ablation upregulates some, but not all, tRNA genes in a tissue specific manner [28]. It is not yet clear if the transcription of specific tRNAs is due to regulation of PolIII alone or if it involves a more complex mechanism, but those data indicate that tRNA expression does not dependent on tRNA gene copy number alone and that different isoforms of Brf1 or Bdp1 and oncogenes may stabilize the binding of TFIIIB in different tRNA promoters, differentially regulating tRNA expression in different tissues and tumors [11,13].

2.5. Deregulation of tRNA-interacting partners in cancer

Transfer RNAs are highly modified post-transcriptionally by tRNA modifying enzymes (tRNAmods). These nucleoside modifications are crucial for the acquisition of the 3D L-shaped structure and stability, interaction with other translational factors, namely aaRS and the ribosome and for decoding efficiency and fidelity [29–31]. Hypomodified tRNAs become unstable and are normally degraded [32,33], in particular, hypomodification of the anticodon wobble position (N34), is normally deleterious and has been associated with several diseases [6,31,34–36]. Upregulation of the enzymes that catalyze modifications at N34 is also associated with translational control of gene expression. For example, ELP3 and CTU1/2 tRNA modifying enzymes, which catalyze the modification of U34 to mcm^5s^2-U34, are upregulated in breast cancer and this is apparently necessary to support translation of specific mRNAs required for breast

cancer progression, namely, the proinvasive transcription factor LEF1 [37]. Moreover, the modification of G26 to dimethyil-guanine-26 (m^2_2G26), carried out by the enzyme Trm1, limits the availability of a specific set of tRNAs for translation when PolIII transcription occurs at high rate, as in cancer, contributing to the regulation of the functional tRNA pool [38].

Another class of tRNA-interacting proteins that are deregulated in tumors is the aaRS protein family. These enzymes can activate or suppress several cancer hallmarks and impact in the outcome of therapy, through non-translation related interactions with other cellular and extracellular molecules. This topic as been extensively reviewed elsewhere [39,40], and we will only highlight some of the most relevant features for cancer. Various aaRS respond to inflammatory stimuli, are pro-angiogenic and are frequently upregulated in tumors. These aaRS include the Threonyl-, Tyrosyl- and Seryl-tRNA synthetases (TARS, YARS and SARS, respectively). Conversely, the Tryptophanyl or Glutamyl-prolyl-tRNA synthetases (WARS and EARS, respectively), are considered angiostatic and are typically downregulated [39,41]. The Lysyl-tRNA synthetases (KARS) promotes cancer cell migration and induces cytokine production by immune cells, thus increasing inflammatory stimuli in the tumor microenvironment [39]. Interestingly, the Leucyl-tRNA synthetase (LARS) acts as a Leucine (Leu) sensor, activating the PI-3-kinase Vps34 and mTORC1 signalling by regulating lysosomal translocation and activation of the phospholipase PLD1 [42]. Finally, upregulation of the Methionyl-tRNA synthetase (MRS) is associated with advanced stage and poor prognosis in Non-Small Cell Lung Cancer (NSCLC) [43].

2.6. Protein synthesis errors are increased in tumors

Tumors are characterized by the capacity of sustained proliferation signaling, evasion of apoptosis and unrestrained growth [44]. Protein synthesis rate is normally upregulated in cancer to sustain increased proliferation. This is achieved by upregulating tRNAs, aaRS, ribosome biogenesis and tRNAmods [10,45–48], but it is unclear whether such metabolic alterations increase translational error rate leading to aberrant protein synthesis in tumors [49–51]. It is known that increased translation speed comes with a cost on translational accuracy [51] and indirect evidences such as activation of the unfolded protein response (UPR), frequent upregulation of molecular chaperones, increased proteasome activity and autophagy, show that this may also occur in tumors [52–56]. Increased proteasome activity, mitigates the accumulation of misfolded proteins in

tumors and is required for apoptosis evasion, which makes this organelle an useful therapeutic target [55,57,58]. Additionally, in a tumor context, autophagy promotes cell survival under the conditions of metabolic stress created by the tumor microenvironment, through elimination of damaged mitochondria, reactive oxygen species (ROS) and protein aggregates derived from misfolded proteins [59,60].

The tumor microenvironment has a profound effect on protein homeostasis (proteostasis) as it is usually acidic, hypoxic and poor in nutrients, due to low vascularization. Nutrient starvation directly influences protein glycosylation and ATP production, triggering synthesis of misfolded proteins, an event also supported by the lack of oxygen that is crucial for disulfide bond formations and proper protein folding [61,62]. Amino acid depletion may increase protein synthesis errors through tRNA mischarging and accumulation of uncharged tRNAs [63]. The latter may trigger a cell surviving program through activation of GCN2, which phosphorylates the translation initiation factor eIF2α, and blocks cap-dependent translation initiation. This induces the translation of ATF4, which activates stress response genes transcription and autophagy to increase amino acid supply [64]. ATF4 will also induce the transcription of VEGF to enhance angiogenesis to restore the proper amino acid supply to cells (**Fig.2-3**) [65].

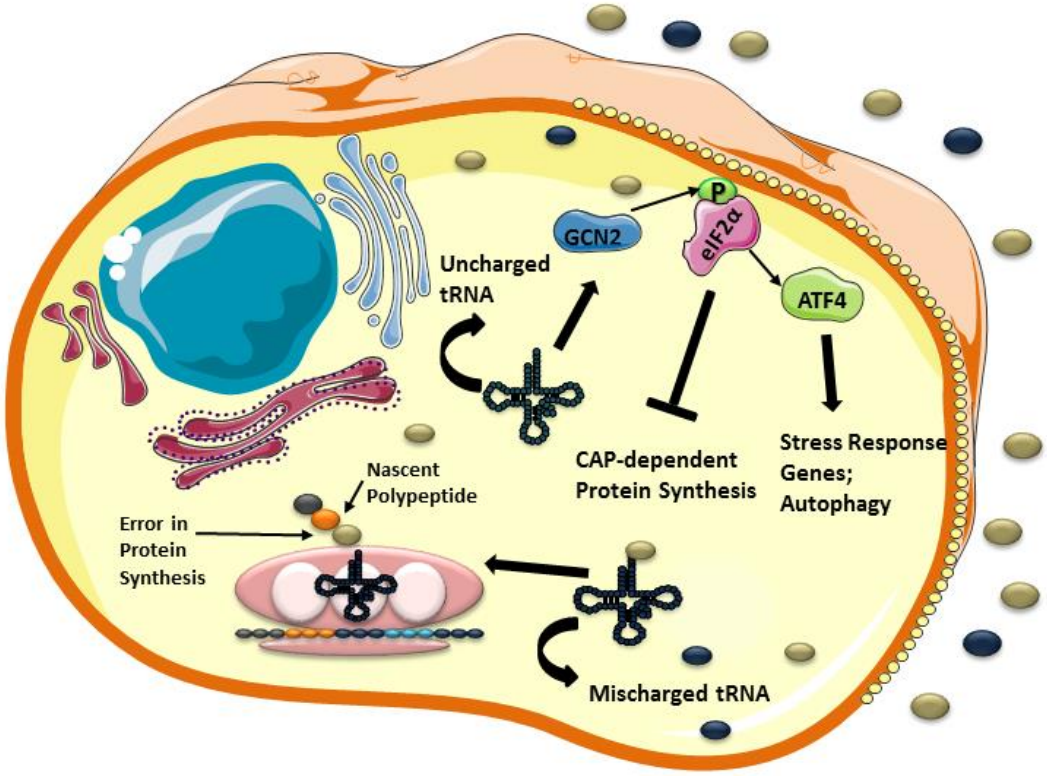

Figure 2-3: Amino acid starvation consequences. Amino acid starvation increases protein synthesis errors by inducing tRNA mischarging. Uncharged tRNAs will also be present due to lack of amino acids. The latter will trigger a cell surviving program through activation of GCN2, which phosphorylates the translation initiation factor eIF2α, blocking cap-dependent translation initiation, but inducing translation of ATF4 which is responsible for the transcription of stress response genes and activating autophagy to increase free amino acid supply in cells.

Inflammation triggered by innate immune cells, designed to fight infections and wound-healing, can support multiple tumor hallmark capabilities [44]. There is a crosstalk between inflammation and protein misfolding since one can induce the other. Misfolded proteins activate the Unfolded Protein Response (UPR), which relies on the activation its three effectors: the inositol requiring kinase 1 (IRE1α), the double-stranded RNA-activated protein kinase (PKR)-like endoplasmic reticulum kinase (PERK) and the activating transcription factor 6 (ATF6) (reviewed in [66]). These UPR effectors contribute to tumor growth and aggressiveness, microenvironment remodeling and resistance to treatment [52,67–70]. Regarding the microenvironment remodeling, the UPR can induce inflammation by increasing the release of pro-inflammatory cytokines which also contribute to tumor cell survival. Remarkably, tumor cells can induce the UPR in cells of the immune system, which further increases tumor-promoting inflammation [71]. The tumor microenvironment is also characterized by oxidative stress caused by increased ROS, which can also originate misfolded proteins. The UPR can also help to boost the antioxidant defenses through upregulation of the NFR2 [53].

Furthermore, the deregulation of the tRNA pool, especially that of near-cognate tRNAs can also result in protein synthesis errors [72]. Cognate and near-cognate tRNAs compete for mRNA codons and upregulation of near-cognate tRNAs, may lead to mistranslation events and protein structural instability. **(Fig.2-4A)** [73]. For example, the upregulation of the $tRNA^{Ser}AGA$ may allow it to decode the Ala GCT codon, incorporating Ser at Alanine (Ala) sites, on a proteome scale **(Fig.2-4A)**.

Mischarging of tRNAs also results in protein mistranslation **(Fig.2-4B)** [5,74]. The estimated error rate associated with the amino acylation of tRNAs is 10^{-4} to 10^{-5}, which is similar to global protein synthesis rate [75]. These errors are particularly relevant in the case of tRNAs that are charged with similar amino acids. Indeed, Valine (Val) tRNAs are often mischarged with Thr or Isoleucine (Ile) and Leu tRNAs with Ile or Val. Mischarging of Ala tRNAs with either Ser or Glycine (Gly) and the mischarging of Lysine (Lys) tRNAs with Arginine (Arg), Ala, Thr, Metionine (Met), Leu, Cysteine (Cys) or Ser are also frequent [75].

Mistranslation is normally viewed as being deleterious, as 10–50% of random substitutions result in the production of dysfunctional or misfolded proteins. However, these often accumulate in toxic aggregates or become degraded by the Proteasome **(Fig.2-5)** [76,77]. The remaining errors introduce protein mutations (epimutations) that can generate phenotypic diversity and may even contribute to adaptation to cellular stress or

changing physiological conditions (Adaptive mistranslation). For instance, under oxidative stress, the Methionyl-tRNA synthetase (MRS) is phosphorylated, loses its specificity and charges non-cognate tRNAs with Met, increasing the incorporation of Met into the proteome [78]. Interestingly, this is advantageous, since Met is a scavenger of ROS that protects proteins from oxidation, which may be particularly important for tumor cells to thrive, since tumors have high levels of ROS [43,79]. Importantly, it has also been recognized that a more accurate translation slows down cellular growth, which is not compatible with most types of cancer [80].

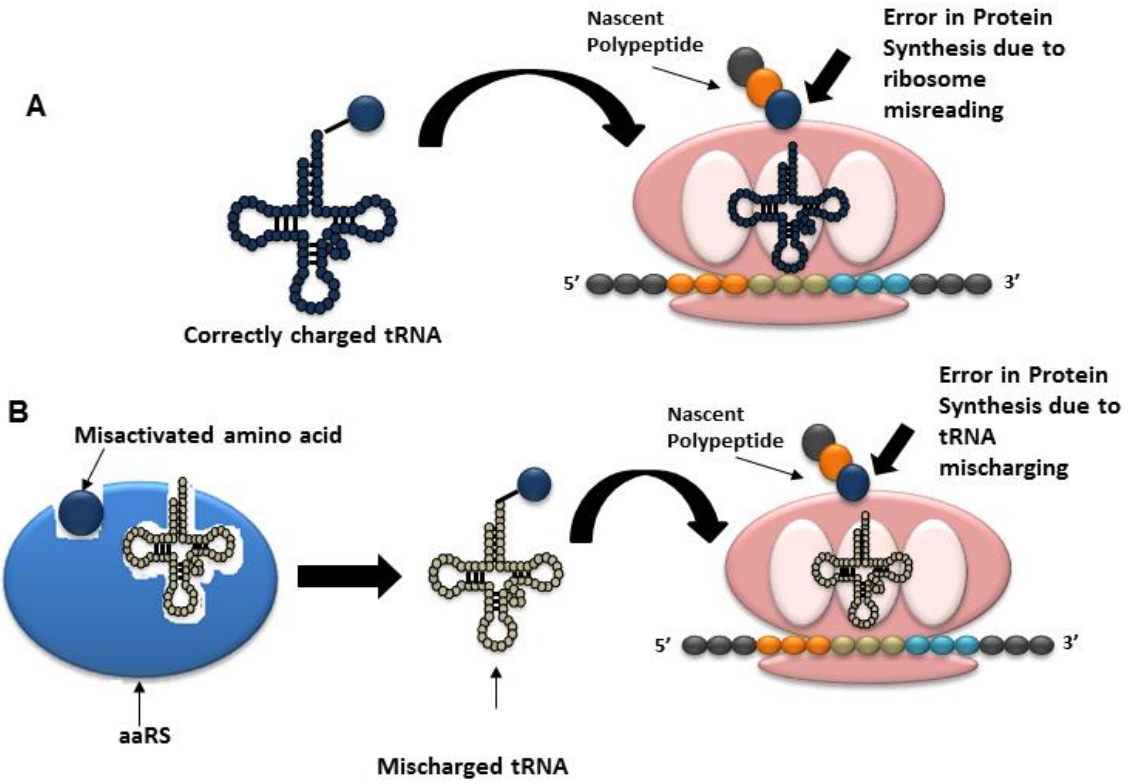

Figure 2-4: tRNAs are essential for translation accuracy. A) tRNA pool deregulation may cause ribosomes to choose overrepresented near-cognate tRNAs to read a codon in the mRNA, instead of underrepresented cognate tRNAs, thus incorporating the wrong amino acid in a polypeptide chain. **B)** tRNAs may be misacylated by aminoacyl-tRNA synthethases. If tRNAs carry the wrong amino acid, a missence error will be generated.

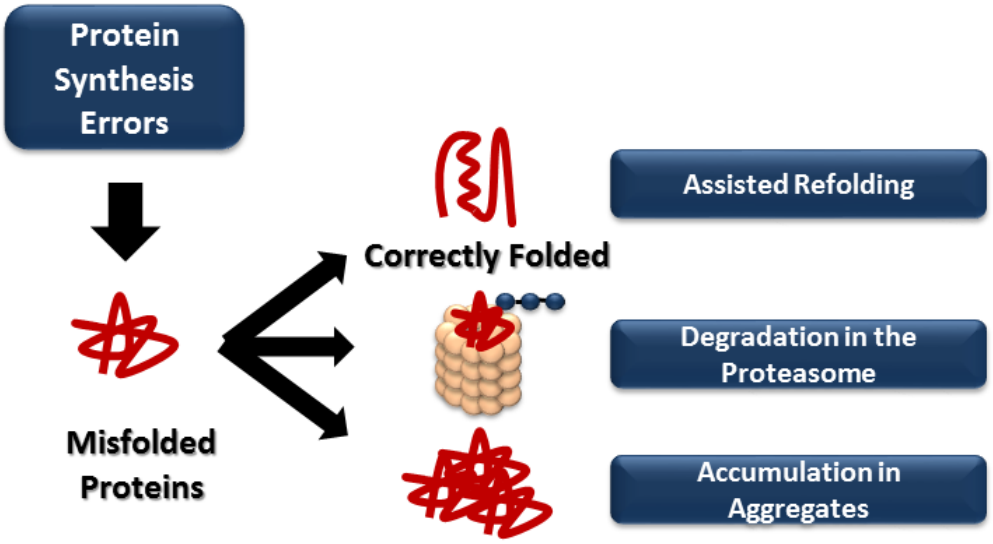

Figure 2-5: Protein Biosynthesis Errors' fate. Missence errors in proteins can be originated by several processes. These errors create misfolded or dysfunctional proteins. Misfolded proteins may then be degraded by the proteasome or accumulate in toxic aggregates. However, the majority of these proteins are refolded and may represent a gain-of-function to the cell, contributing to the adaptation to cellular

2.7. Implications of mistranslation for tumor heterogeneity and drug resistance

There is little information about the role of tRNA deregulation and mistranslation in tumor heterogeneity and drug resistance. Studies in microorganisms have shown that mistranslation contributes to increase their adaptive potential to stressful environments through diversification of the proteome and population heterogeneity [81–83]. In yeast, increased translational errors driven by tRNA misreading enables yeast to colonize hostile environments and to resist classical drug treatments. Also, mistranslation can help *Mycoplasma* to evade the host's immune system and *E.coli* are more resistant to antibiotics when its MRS is able to misacylate other tRNAs with Met [84]. Therefore, mutations in proteins that occur during mRNA decoding by the ribosome, produce statistical proteins, that destabilize the proteome and produce cell population heterogeneity. Interestingly, such protein mutations also destabilize the genome, increase DNA mutation rate and to reprogram the transcriptome (**Fig.2-6**) [83,85–87]. The role of mistranslation in tumor heterogeneity has not yet been proven, however, these data provide strong evidence for a pivotal role of mistranslation in genome instability, mutation rate, drug resistance and phenotypic diversification through population heterogeneity. Some works also shows that tRNAs are differentially expressed in tumors from different patients, which correlates positively with inter-tumor

heterogeneity (YM500v3 database). This has been linked to differences in risk of disease recurrence and overall survival time (**Fig.2-2**) [9].

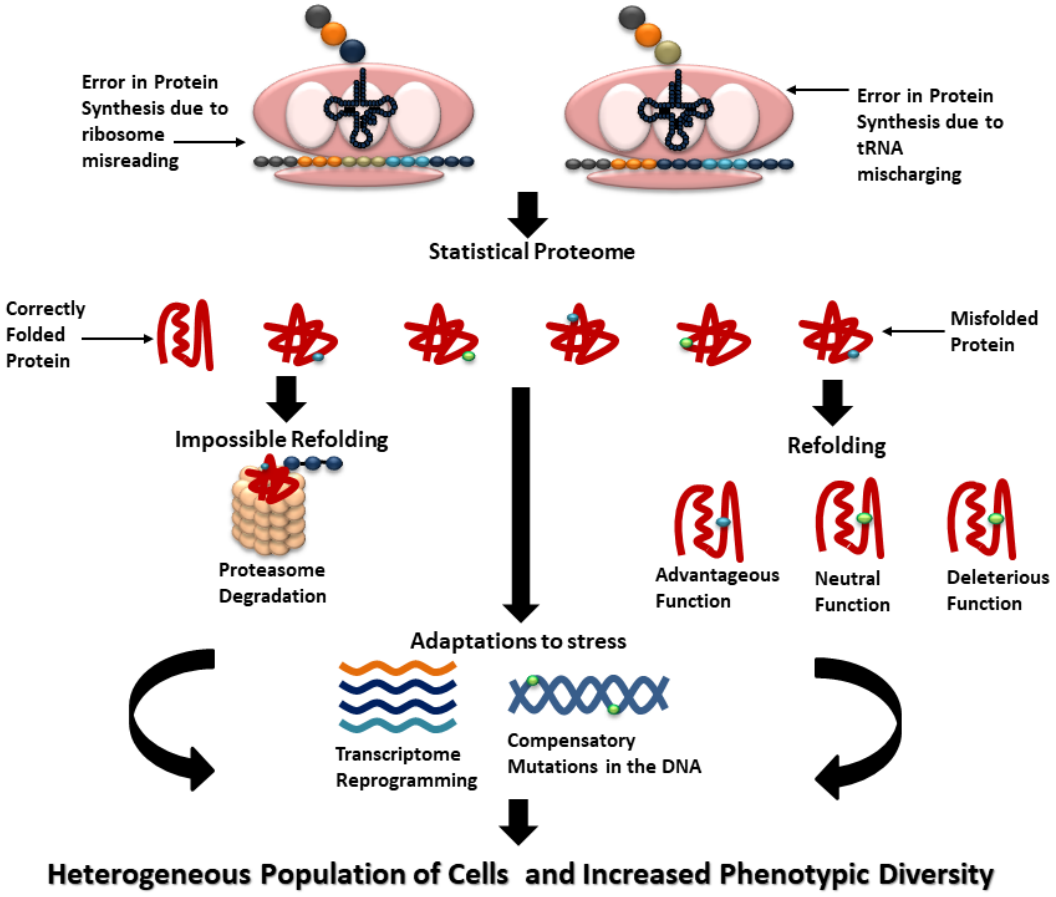

Figure 2-6: Consequences of mistranslation. Translational errors due to ribosome misreading or tRNA mischarging result in statistical proteomes composed by several protein isoforms. These statistical proteins can bestow cells with new advantageous or deleterious functions or they can be directly degraded by the proteasome with no further consequences to the cell. Additionally, they may impact on proteome homeostasis and phenotypic diversification, reprogramming the transcriptome and are able to flow back to DNA as compensatory mutations to mitigate proteome destabilization and loss of proteostasis.

Tumor heterogeneity is also one of the major problems regarding resistance to therapy. Resistance to therapy can be classified as intrinsic or acquired. Intrinsic resistance refers to preexisting characteristics of the cells which allow them to resist the drug treatments, whereas acquired resistance is induced by the treatment itself [88]. Tumor cells normally acquire drug resistance through drug inactivation, drug target alteration, drug efflux, DNA damage repair, cell death inhibition, epithelial-mesenchymal transition (EMT) and epigenetic modifications [89]. The most recent data on tRNAs imply that they may contribute to attenuate cell sensitivity to conventional chemotherapy [90]. For instance, the increased load of tRNAs in tumor cells can aid on apoptosis inhibition, since tRNAs can bind to cytochrome c and inhibit caspase activation, independently of their charging state [91,92]. It was also demonstrated that overexpression of specific tRNAs

may play a role in TGFβ-induced EMT progression or regulation [93]. Furthermore, conventional chemotherapy increases ROS levels in tumor cells, and misacylation of non-methionyl-tRNAs by MRS helps to mitigate this stress in tumor cells [78,94]. Also, imbalances in tumor cell tRNA pool can increase errors in protein synthesis [72], which will activate the PQC system. Activation of the PQC includes upregulation of molecular chaperones that will help to refold the misfolded proteins or direct them to one of the cellular degradation systems; upregulation of the ubiquitin-proteasome system (UPS) to increase protein turnover; activation of the UPR and autophagy. The concomitant activation of all these pathways has been observed in tumors and is often correlated with tumor progression, metastasis and also drug resistance [54,55,95].

tRNAs have the ability to modulate gene expression, increasing the translation efficiency of transcripts that have a codon usage bias towards them [13]. Thus, we can hypothesize that among these transcripts, some may bestow tumor cells with phenotypic advantages which will confer them the ability to resist to therapy. As a matter of fact, a set of tRNAs has been associated with increased probability of disease recurrence, indicating that they may be directly involved in acquisition of drug resistance [9]. The pool of tRNAs has also been shown to be very plastic, able to change in response to cellular stress [96]. Chemotherapy induces changes in the tRNA landscape, depending on the genetic background of tumor cells, possibly allowing cells to translate more efficiently transcripts which confer them the ability to adapt to the new conditions [97].

Therefore, despite lacking direct evidences of tRNA deregulation and mistranslation in tumor heterogeneity and drug resistance, the evidences provided by other model organisms and the activation of the PQC system supports the idea that their role is far more significant than previously anticipated.

2.8. Concluding Remarks

There are still many answered questions regarding the full role of tRNAs in tumor biology, mainly because until recently their deregulation was acknowledged as a strategy to meet the metabolism requirements. Transfer RNA transcription by PolIII is controlled by oncogenes but further studies are needed to demonstrate that they can bind to the promoter of a specific set of tRNAs and thus induce the translation of specific transcripts enriched in matching codons. Besides their ability to drive gene expression in cancer cells, tRNAs have shown to be able to protect proteins from oxidative stress by random insertion of methionine and misincorporations enable cells to resist to drug

treatments in other biological models. Their deregulation can support disease progression through upregulation of cell migration, invasion and metastasis and also promote tumor heterogeneity and therapy resistance, thus contributing to poor patient prognosis (**Fig.2-7**).

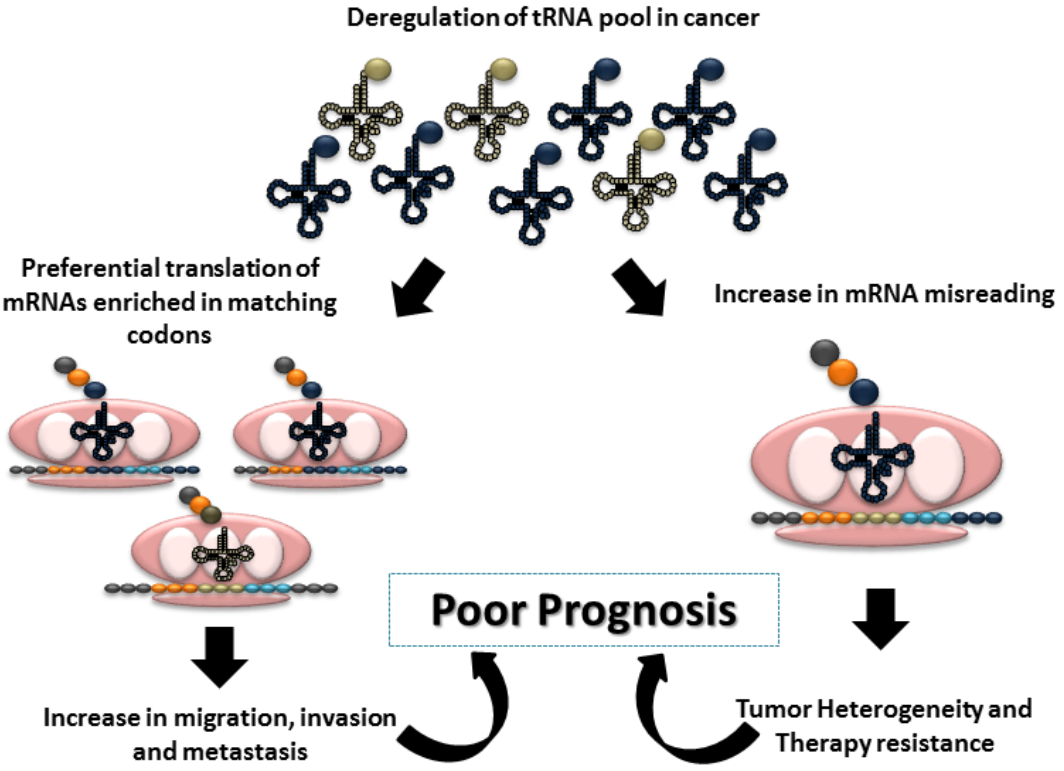

Figure 2-7: Deregulation of tRNA pool in cancer contributes to poor patient prognosis. The deregulation of tRNA pool in tumors has been associated to increased cell migration, invasion and metastasis due to preferential translation of mRNAs enriched in matching codons. On the other hand, this imbalance may cause an increase in tRNA misreading, which may contribute to tumor heterogeneity and therapy resistance. Altogether these data show that imbalances in the tRNA pool may contribute to poor patient prognosis.

3. Codon misreading tRNAs promote tumor growth in mice

Disclosure of Interests: This work was initiated by Patrícia Pereira. The author of this thesis has contributed to the following experiments of this work:
1) Development of the technique that allowed for the detection of tRNAs (SNaPshot) in both cell lines and tumors; 2) All the Mass Spectrometry data; 3) TNF alpha assay; 4) Dissection of the molecular pathways involved in tumor formation; 5) Analysis of all the data. The author of this thesis has also constructed the figures and wrote the manuscript.

3.1. Abstract

Deregulation of tRNAs, aminoacyl-tRNA synthetases and tRNA modifying enzymes, are common features of cancer, raising the hypothesis that protein synthesis accuracy is compromised in tumors. To clarify this hypothesis, we determined the relative error rate of protein synthesis in normal tissue and in tumors, and confirmed that tumors mistranslate at higher levels than normal tissue. To understand the involvement of mistranslation in tumor biology, we expressed mutant Ser-tRNAs that misincorporate Ser-at-Ala (frequent error) and Ser-at-Leu (infrequent error) in NIH3T3 cells. There was high tolerance to both misreading tRNA, but the Ser-to-Ala misincorporating tRNA induced high cell transformation capacity, stimulated angiogenesis and produced fast growing tumors in mice. Upregulation of the Akt pathway and the UPR were also observed. Most surprisingly, the relative expression of misreading tRNAs increased during tumor growth, suggesting that mistranslation is advantageous to cancer cells. These data highlight new features of protein synthesis in tumor biology.

3.2. Introduction

Cancer is a multifactorial disease driven by the accumulation of DNA mutations, chromosomal aberrations and epigenetic alterations [98]. Transcriptional, post-transcriptional and translational deregulation is also well established, however little is known about the contribution of translational errors to tumor initiation and growth. Eukaryotic cells translate mRNA with average basal error levels of 10^{-3} to 10^{-4} amino acid misincorporations per codon, resulting in at least one misincorporated amino acid in 15% of average length proteins [99–101]. Cells cope relatively well with this level of aberrant protein synthesis and it is controversial whether such errors play any role in cell degeneration, aging or disease [101–104].

However, recent mistranslation works in model organisms show that translational error rates marginally above the normal background level lead to accumulation of misfolded proteins [87,101,105,106], saturation of protein quality control (PQC) systems, proteotoxic stress, re-wiring of chaperone-clients interaction networks and to wide deregulation of cellular functions [87]. Whether mistranslation is elevated and produces similar phenotypes in tumors is not yet clear, but translational fidelity depends on tight regulation of tRNAs, aminoacyl-tRNA synthetases (aaRSs), RNA modifying enzymes (RNAmod), translation elongation factors (eEFs), ribosomal RNA (rRNA) processing, ribosome assembly and amino acid supply, which are frequently deregulated in tumors [10,12,107–112]. Considering the direct impact of mistranslation on proteome mutational load and protein stability it is likely that elevation of mistransaltion would have significant impact in tumor biology.

Other indirect links between tRNA deregulation, protein synthesis errors and cancer are provided by the activation of the unfolded protein response (UPR) [113]. In general, mistranslated proteins sequester BiP, activate the UPR sensors PERK, IRE-1 and ATF6, upregulate molecular chaperones and the ubiquitin-proteasome system. Tumor cells highjack these endoplasmic reticulum (ER) adaptive measures to thrive [114], explaining, at least in part, the UPR association with malignancy and aggressiveness of several types of cancer [69,115,116].

In this work, we have investigated the relevance of protein mistranslation to tumor biology. We show that: 1) tumors mistranslate at higher level than normal tissue; 2) codon misreading tRNAs are selected during tumor evolution, and; 3) translational errors alone increase cell transformation, activate the UPR and promote tumor growth. To achieve these results, we have determined the relative level of amino acid misincorporations in tumors and engineered NIH3T3 cell lines that misincorporate Ser at both Ala (frequent mistranslation event in tumors) and Leu (infrequent mistranslation event in tumors) codon sites. *In vitro* data showed no visible effects on cell viability, but cell transformation, angiogenesis, tumor growth, activation of the UPR and other cancer-related pathways, were evident *in vivo* in chicken and mouse models.

3.3. Results

3.3.1. Tumors mistranslate at higher rates than normal tissues

To clarify whether translational fidelity is deregulated in tumors, we carried out a

detailed analysis of the relative amino acid misincorporation frequencies, in both normal and cancer human samples, as well as in mouse xenograft tumors derived from two human epithelial cancer cell lines (NCI-H460 and MKN74). For this, we have implemented a mass spectrometry data analysis pipeline to identify peptides containing amino acid misincorporations in complex MS/MS label free raw data sets of normal colon, colon adenocarcinoma (COAD) and xenograft tumor samples. We used MS/MS data sets produced by the National Cancer Institute Clinical Proteomic Tumor Analysis Consortium (CPTAC) (https://cptac-data-portal.georgetown.edu/cptacPublic/) and our own MS/MS data sets produced with xenograft tumors. Normal colon samples were randomly selected, while COAD samples were selected to represent advanced stages of the disease. All MS/MS datasets were analyzed using the same bioinformatics pipeline.

We started by analyzing independently the global error rate of normal colon samples and tumor samples from COAD patients. The global error rate of normal samples was $1.97 \times 10^{-3} \pm$ SEM per amino acid decoded, while that of COAD samples was $6.49 \times 10^{-3} \pm$ SEM, indicating that COAD tumors are 3-fold more prone to translational errors than normal tissue. There was high dispersion of error values among the COAD samples, probably due to the high heterogeneity in cell type composition of tumor tissues, which normally include tumor, stromal, support and immune cells in different proportions. To clarify whether tumor cells were the main contributors to the global error rate detected, and whether the error values obtained for COAD tumors could be extrapolated to other tumors, we determined the error rate of tumors derived from two different human cancer cell lines grown in mice, namely MKN-74 (Gastric tubular adenocarcinoma) and H460 (Non-Small Cell Lung Cancer), in which more than 90% of the tumor mass is composed of tumor cells. The mistranslation rate of the MKN74-derived tumor was 6.85×10^{-3} and that of H460-derived tumors was 7.81×10^{-3}; i.e., 3.4-fold ($p<0.05$) and 4.2-fold ($p<0.01$) higher that the average error observed in normal tissue samples **(Fig.3-1A)**. We also determined the frequency of misincorporation of different amino acids at the protein sites corresponding to each codon family and there was a clear error elevation at all but Asn (N) codon family sites in COAD samples relative to normal tissue (**Fig.3-1B**). Interestingly, Asn sites were the most error prone sites in both tumors and normal tissue (**Fig.3-1B**).

We next analyzed the frequency of specific misincorporations in MKN74- and H460-derived tumors where more than 90% of the tumor mass is composed of tumor cells. As the complexity of the mistranslation MS/MS data space was very high, we

focused our efforts on the identification of a sub-group of errors associated with tRNA misacylation by Class II aaRS (probable errors) and in errors that cannot be explained by tRNA misacylation, near-cognate codon decoding nor other genetic code rules (improbable errors). Our expectation was that the theoretically probable errors predicted by genetic code rules would occur in proteins at much higher frequency than the theoretically improbable errors. We verified that, among errors associated with tRNA misacylation by Class II aaRS, Ser misincorporations at Ala codon sites were the most frequent errors found in proteins from xenograft tumors **(Fig.3-1C).** On the other hand, misincorporations of Phe at Ser and Ser at Leu codon sites, that do not conform with genetic code rules, were present at much lower level in the proteins of our dataset (rare misincorporations). These data are in line with previous data showing that mistranslation rates are amino acid and codon specific [2,117].

We then evaluated the relevance of both frequent (probable) and infrequent (improbable) errors in cancer. Since evolutionary optimization of the genetic code minimizes the impact of mistranslation on protein structure [101], we reasoned that theoretically probable misincorporations should be less deleterious (involving chemically similar amino acids), than those involving theoretically unlikely errors (involving chemically distinct amino acids). To address this hypothesis, we altered the anticodon of a Ser-tRNA to produce mutant Ser tRNAs that incorporate Ser at Ala (frequent) and Ser at Leu (infrequent) codon sites on a proteome wide scale. The Ser-tRNA was chosen as proof of concept since its anticodon can be mutated to read multiple codons, without affecting its acylation specificity by the SerRS [118].

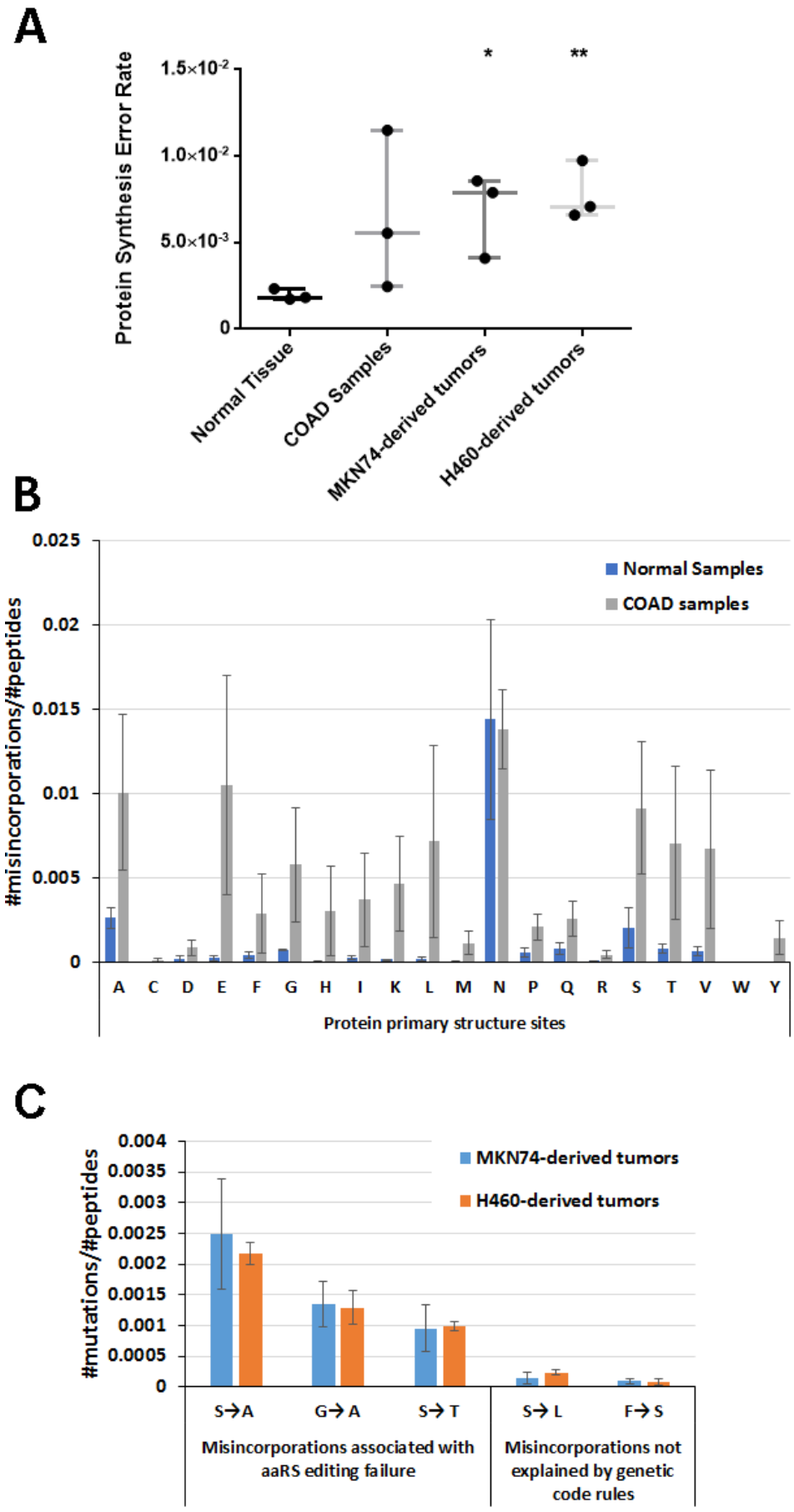
A
Protein Synthesis Error Rate
1.5×10-2
1.0×10-2
5.0×10-3
0
*
**
Normal Tissue
COAD Samples
MKN74-derived tumors
H460-derived tumors
B
#misincorporations/#peptides
0.025
0.02
0.015
0.01
0.005
0
Normal Samples
COAD samples
A C D E F G H I K L M N P Q R S T V W Y
Protein primary structure sites
C
#mutations/#peptides
0.004
0.0035
0.003
0.0025
0.002
0.0015
0.001
0.0005
0
MKN74-derived tumors
H460-derived tumors
S→A
G→A
S→T
S→L
F→S
Misincorporations associated with aaRS editing failure
Misincorporations not explained by genetic code rules

Figure 3-1: Tumors mistranslate at higher rates than normal tissue. A) Normal colon samples and colon adenocarcinoma (COAD) samples from patients and xenograft tumors derived from two epithelial cancer cell lines H460 and MKN74 cell lines were analysed. For each sample we counted the total number of mutations in the proteome, obtained using a blind search approach with the SPIDER tool in PEAKS8 software against Homo sapiens reference proteome. The misincorporation count was normalized for the total number of amino acids in the sample. The data show that these tumors have higher error rates, than the normal samples analysed. Data was analysed by two-tailed unpaired Student's t-test. Significant p-values are shown (*$p<0.05$; ** $p<0.01$). Graphics depicts average +/- SEM (n=3). Normal Colon Samples and COAD samples raw MS/MS data was generated by the CPTAC consortium. **B)** Analysis of amino acids misincorporated at protein primary structure sites (codon/amino acid family sites) showing that COAD tumors misincorporate higher number of amino acids than the normal samples, except for Asparagine site (N) where both normal and tumor tissue misincorporate similar levels of the different amino acids. The total number of amino acids misincorporated at each protein site was normalized to the total number of peptides present in each sample dataset (proteome space). Letters in the X axis represent the 20 amino acids and errors correspond to the total number of non-cognate amino acids misincorporated. For example N= total number of Asn sites present in the proteome space that contain at least one misincorporation. **C)** Misincorporations of Serine at Alanine sites were the most frequent found in tumor xenograft samples and misincorporations of Serine at Leucine sites were among the least common. We determined the number of specific misincorporations and normalized them to the total number of peptides present in each sample data set. Graphics B and C depict average +/- SEM (n=3).

3.3.2. Mammalian cell lines are highly tolerant to codon misreading tRNAs

We constructed mutant tRNAs that decode Ala-GCU/GCC ($tRNA^{Ser}$Ala), and Leu-CUU/CUC ($tRNA^{Ser}$Leu) codons **(Fig.3-2A, left panel)** as Ser. These Ser misincorporating tRNA genes were then cloned into the pIRE1-10-DsRed and were transfected into NIH3T3 cells. Cell lines stably expressing the engineered tRNAs and the wild-type $tRNA^{Ser}_{AGA}$ ($tRNA^{Ser}$ WT) were then selected for phenotypic characterization **(Fig.3-2A, right panel)**. Cells transfected with the empty vector (Mock) were used as controls. The transfection efficiency was determined by Real-Time PCR, using the pIRE1-10 *DsRed* gene as a readout probe and the data showed 100% transfection efficiency for the Mock, $tRNA^{Ser}$(WT) and $tRNA^{Ser}$(Ala) cell lines, and 72% for the $tRNA^{Ser}$(Leu) cell line. The integration of the misreading tRNA genes in the genome of the transfected cells was further confirmed by PCR and Sanger sequencing (**Fig.3-9A**). tRNA expression was determined using a primer extension assay (SNaPshot analysis) that permitted the detection of each mutant misreading tRNA and also the WT $tRNA^{Ser}$ gene. The cellular level of the endogenous WT $tRNA^{Ser}$ was 19.4-fold higher than the mutant $tRNA^{Ser}$(Ala) and 49.5-fold higher than the mutant $tRNA^{Ser}$(Leu) (**Fig.3-2B**).

We used cell viability, proliferation and apoptosis assays to evaluate the phenotypic consequences of expression of the mutant misreading tRNAs in the NIH3T3

cells. Trypan Blue staining showed no impact on viability (**Fig.3-9B**) and the Annexin V Apoptosis assay showed a basal necrosis level (≤1% of cells) and low percentage of cells in late (ca. 5% of cells) and early apoptosis (7-8% of cells) (Fig.1-2**C)**. Cell proliferation was also not significantly affected (**Fig.3-9C**), and cell cycle progression demonstrated a similar pattern in all cell lines (**Fig.3-9D**), indicating that NIH3T3 cells tolerated well the mutant misreading tRNAs. However, these mutant tRNAs increased the production of foci *in vitro* (**Fig.3-2D**), raising the hypothesis that they have the potential to transform NIH3T3 cells.

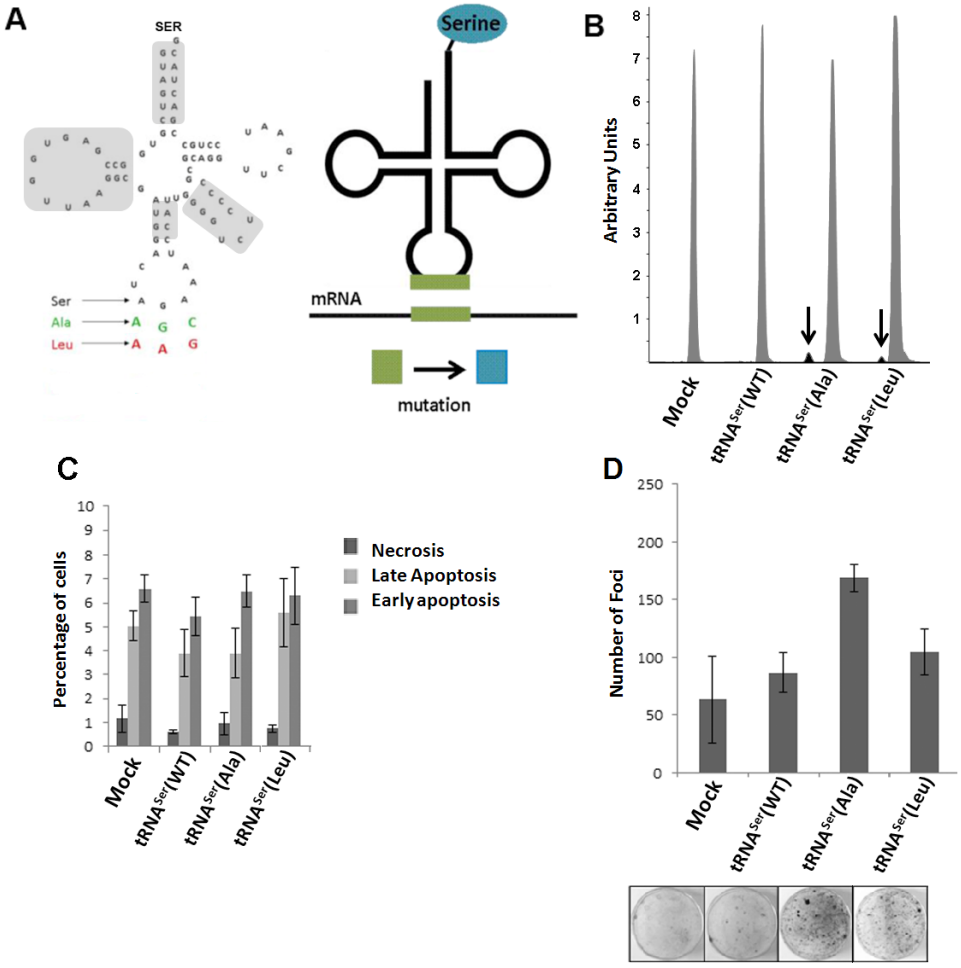

Figure 3-2: In vitro phenotypic effects induced by misreading tRNAs. A) Schematic tRNA model. Left panel) The human $tRNA^{Ser}_{AGA}$ gene (Chr6 tRNA#5), was cloned into pIRES2-DsRed plasmid and misreading constructs were generated by site-directed mutagenesis (green: Ala(AGC) and red: Leu(AAG)). Domains highlighted in grey are important for $tRNA^{Ser}$ recognition by SerRS. Right panel) Serylated misreading tRNAs misincorporate Ser at the non-cognate codons indicated. **B)** Expression of misreading tRNAs on stably expressing cells was confirmed using SNaPshot. Samples were sequenced and analysed using Peak Scanner software. The endogenous copies of $tRNA^{Ser}$ were 32 and 49.5-fold more expressed than $tRNA^{Ser}$(Ala) and $tRNA^{Ser}$(Leu) respectively. Grey: Non-mutated Serine tRNA; Black: Misreading Serine tRNA. **C)** Percentage of cells in necrosis, early and late apoptosis were determined by flow cytometry using AnnexinV-FITC (1:100) and Propidium iodide (2.5µg/ml) staining. **D)** The number of foci arising from NIH3T3 cells was counted after 13-21 days after transfection. Data represents average ± SEM (n=2-3) and was analysed with One-way ANOVA with Dunnett's post-test using Mock cell line as control. There are no significant differences among cell lines ($p>0.05$).

3.3.3. Phenotypic traits induced by misreading tRNAs are exposed by cancer microenvironment stimuli.

Previous works carried out in our laboratory, using yeast as a mistranslation model, showed that mistranslation is mostly deleterious under normal growth conditions, but can be advantageous if cells are exposed to environmental stress [119]. Since both the mutant misreading and the WT $tRNA^{Ser}$ were well tolerated and did not produce advantageous or deleterious phenotypes *in vitro*, we reasoned that external stimuli could be necessary to reveal putative phenotypic variation. To clarify this issue, we exposed the NIH3T3 cell lines expressing Mock, $tRNA^{Ser}$(WT) and the mutant misreading tRNAs to the pro-inflammatory tumor necrosis factor alpha (TNF-α) for different time periods, and used Akt and p38 phosphorylation as phenotypic readouts (Akt-P/Akt and p38-P/p38) (**Figs.3-3 and 3-10**). The p38 pathway was activated in $tRNA^{Ser}$(Leu) cells after 30 minutes and persisted up to 4 hours of exposure (3.43 and 2.1-fold change, respectively). A slight activation was also observed in $tRNA^{Ser}$(Ala) expressing cells at 30 minutes, but was lost after 4h (**Fig.3-3**). The Akt pathway was only significantly activated in $tRNA^{Ser}$(Ala) expressing cells after 30 minutes (2.6-fold change) (**Fig.3-3A**). This responsiveness to external stimuli and the tendency to increase transformation ability *in vitro*, lead us to hypothesize that cells expressing misreading tRNAs could have a growth advantage if inoculated *in vivo*.

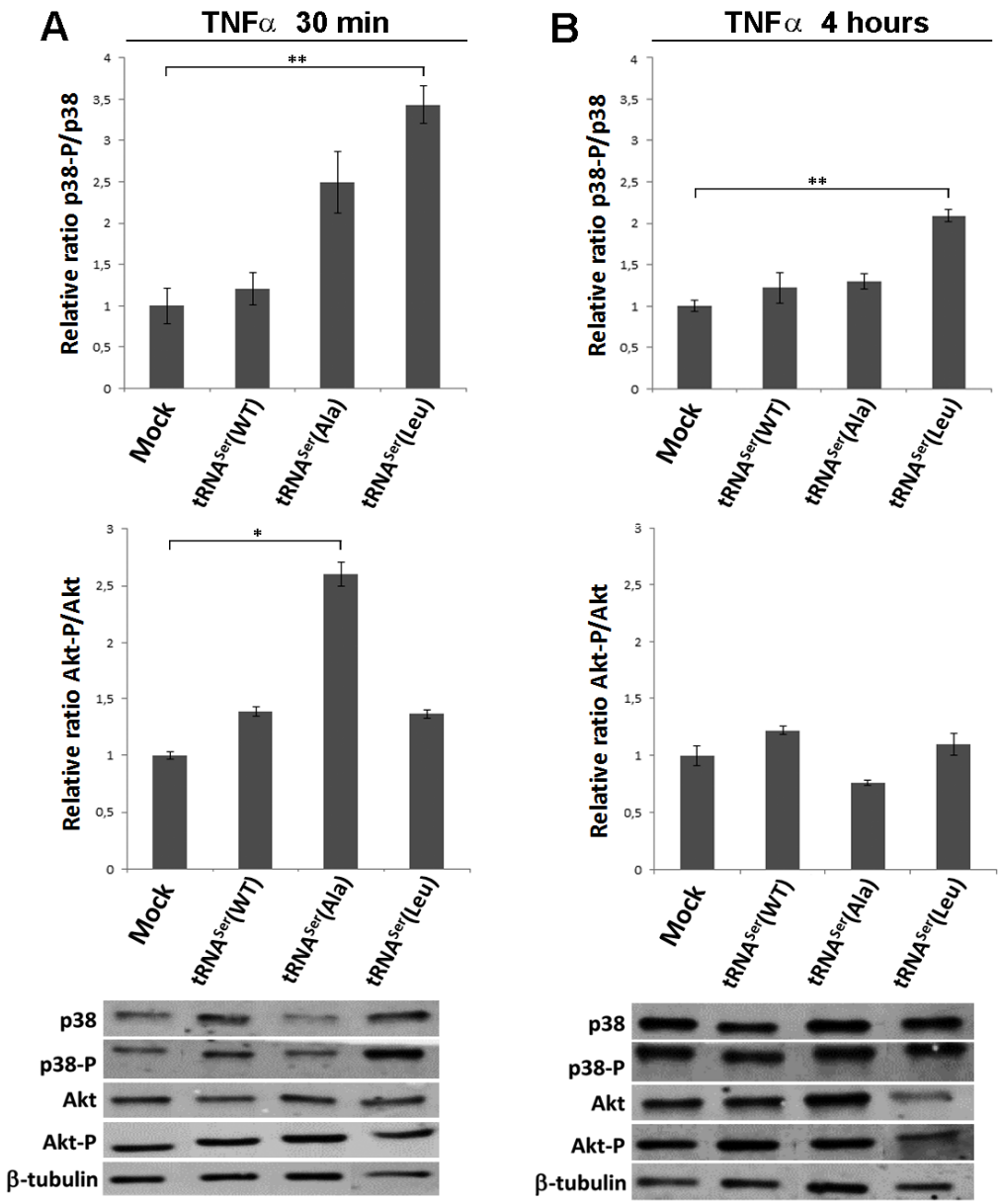

Figure 3-3: Pathways activated by TNFα induction. A) Treatment of cells misexpressing the tRNA^{Ser}(WT) and misreading tRNAs with TNFα (30ng/ml) for 30 minutes. **Upper panel)** Relative activation ratios of p38 in cell lines exposed to TNFα. **Middle panel)** Relative activation ratios of Akt in cell lines exposed to TNFα. **Lower panel)** Representative immunoblots of p38-P, total p38, Akt-P and total Akt in cell lines. β-tubulin was used as a loading control. **B) Treatment of misexpressing tRNA^{Ser}(WT) and misreading tRNAs expressing cell lines with TNFα (30ng/ml) for 4 hours. Upper panel)** Relative activation ratios of p38 in cell lines exposed to TNFα. **Middle panel)** Relative activation ratios of Akt in cell lines exposed to TNFα. **Lower panel)** Representative Immunoblots of p38-P, total p38, Akt-P and total Akt in cells lines. β-tubulin was used as a loading control. Data represents average ± SEM (n=3) and was analysed using One-way ANOVA with Dunnett's post-test and relevant p-values are displayed (*p<0.05; **p<0.01).

3.3.4. Expression of misreading tRNAs promotes tumor growth in vivo

We tested the behavior of the cells expressing the mutant misreading tRNAs in the *in vivo* chick chorioallantoic membrane assay (CAM) and took particular attention

to their effect in angiogenesis and growth (tumorigenic potential) relative to Mock cells. Only cells expressing $tRNA^{Ser}$Ala produced larger tumors and had stronger angiogenic response in the CAM assay **(Fig.3-4A)**. These results were further confirmed by inoculating cells expressing $tRNA^{Ser}$(WT), $tRNA^{Ser}$(Ala), $tRNA^{Ser}$(Leu) or K-ras^{V12} on the left dorsal flank of at least five mice (for each cell line) and control cells (Mock) on the corresponding right dorsal flank of every mice. Within 14 to 21 days post-inoculation (p.i.), tumors were produced by cells expressing K-ras^{V12} (5/5 mice), $tRNA^{Ser}$(Ala) (6/6 mice) and $tRNA^{Ser}$(Leu) (5/5 mice) (**Fig.3-4B, upper panel**). At day 27 p.i., 12/21 (57.1%) mice inoculated with Mock cells and 5/5 mice inoculated with $tRNA^{Ser}$(WT) cells developed equivalent smaller sized tumors. At this stage (day 27 p.i.), tumors produced by cells expressing $tRNA^{Ser}$(Ala) were the largest. At day 31 p.i., the experiment was terminated; $tRNA^{Ser}$(Ala) and K-ras^{V12} tumors were similar in size distribution and were statistically different from Mock tumors (p<0.01) (**Fig.3-4B, upper and middle panel**). Therefore, the mutant $tRNA^{Ser}$(Ala) accelerated significantly tumor growth, while Ser misincorpoartion at Leu codons and misexpression of WT $tRNA^{Ser}$ resulted in tumors that were marginally larger than those produced by control Mock cells.

Histological characterization of resected tumors unveiled high grade sarcomas with high proliferative index, as determined by Ki67 labeling (**Fig.3-4B, lower panel, Fig.3-11C**). Histopathological analysis of murine organs (ganglion, lung, kidney, liver, bladder, pleura and stomach), collected at day 31 p.i., revealed the presence of lung metastases in K-ras^{V12} expressing tumors, and no metastases in all other mice.

DNA extracted from tumors, from both CAM and mice experiments, was sequenced and genomic incorporation of all plasmids was validated (**Fig.3-11A,B**). tRNA expression in mice tumors was determined using the primer extension assay described above. Surprisingly, expression levels of misreading tRNAs was much higher in tumors than in the corresponding cell lines, i.e., 8- and 8.4-fold higher for the $tRNA^{Ser}$(Ala) and $tRNA^{Ser}$(Leu), respectively when compared to the endogenous WT tRNA genes **(Fig.3-4C)**. In other words, expression of misreading tRNAs increased during tumor evolution, suggesting that codon misreading is advantageous for tumor cells growing *in vivo* (**Fig.3-2B,4C**).

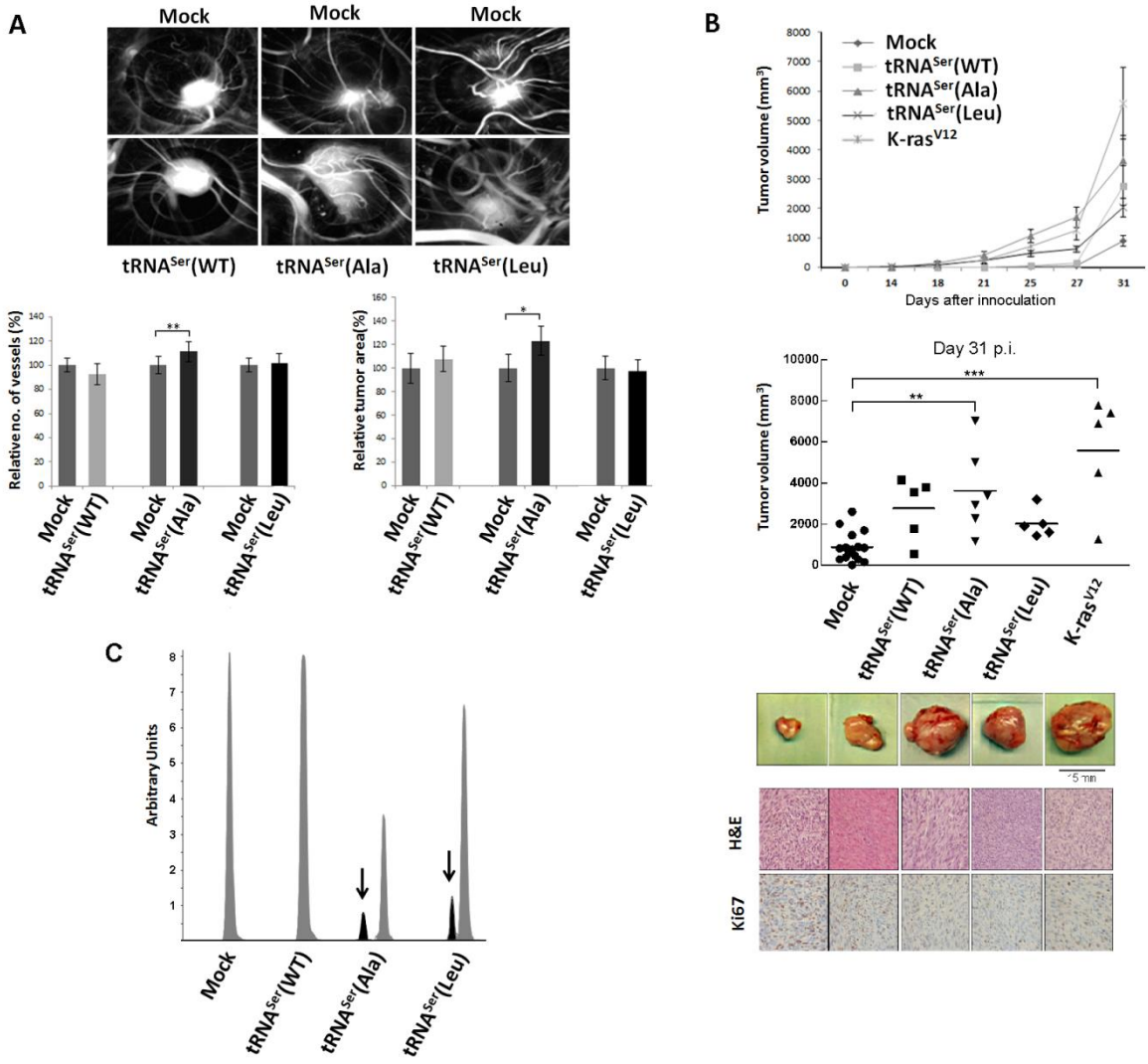

Figure 3-4: Impact of mistranslation on angiogenesis and tumor formation in vivo. A) CAM assay. Upper panel) Representative images of tumors and vessels produced by cell lines expressing Mock, tRNA^{Ser}(Ala), tRNA^{Ser}(Leu) and misexpressing tRNA^{Ser}(WT). **Lower panel, left)** Quantitative evaluation of new vessels' formation. **Lower panel, right)** Relative tumor area. Data is presented as the percentage relative to Mock. Graphics depict average ± SEM (n=12-14). Data was analysed by two-tailed paired Student's t test (*p<0.05; **p<0.01). **B) Tumorigenic capacity of misreading tRNAs in mice. Upper panel)** Kinetics of tumor growth determined after inoculation of cells expressing Mock plasmid, the tRNA^{Ser}(WT), tRNA^{Ser}(Ala), tRNA^{Ser}(Leu) and K-ras^{V12} (positive control) constructs. **Middle panel)** Quantitative evaluation of tumor area at 31 days p.i.. Graphics depict the average ± SEM (n=5-10). Data was analysed by One-way ANOVA with Dunnett's post-test (**p<0.01; ***p<0.001). **Lower panel)** Photographs of representative tumors, H&E and Ki67 staining (40x amplification) from each condition. **C)** Expression of misreading tRNAs in mice tumors measured by SNaPshot. Samples were sequenced and analysed using Peak Scanner software. Expression of the misreading tRNA^{Ser}(Ala) and tRNA^{Ser}(Leu) were 4 and 5.9-fold lower than the endogenous tRNA^{Ser}, respectively. Grey: Non-mutated Serine tRNA; Black: Misreading Serine tRNA.

To confirm that the mutant misreading tRNAs mediated the elevation of Ser misincorporation into proteins, we analyzed the soluble protein fraction (SF) of tumors derived from our cell lines, resourcing to the MS/MS data analysis approaches used before. To further validate our methodology, we investigated whether Ser was

misincorporated at the codon sites decoded by our mutant tRNAs. As theoretically expected, the data confirmed the increase in the incorporation of Ser at Ala sites (GCU codon) in the cell line containing the misreading $tRNA^{Ser}$(Ala) (**Fig.3-5, Upper panel)**. But, we could only detect a small increase of Ser-to-Leu misincorporation at the near-cognate codon CUC. Since Ser (polar amino acid) misincorporation at Leu sites (hydrophobic amino acid) is much more disruptive to protein structure than Ser-to-Ala mutations, we postulate that Ser-Leu mistranslated proteins are mainly degraded by the proteasome, making it harder to detect Ser-to-Leu misincorporations by MS/MS (**Fig.3-5, Lower panel)**. The inability to detect Ser-to-Leu mutations at the CUU cognate codon may be related to differences in Leu tRNA isoacceptor abundances and codon usage in the human transcriptome. Indeed, the CUC codon has no specific isoacceptor tRNA to decode it and is read by the near cognate tRNA isoacceptor that decodes the CUU codon. It is also used more frequently than the CUU codon (http://www.kazusa.or.jp/codon/). In other words, the mutant misreading Ser-tRNA may read the CUC codon more frequently than the CUU codon. Interestingly, the G-ending Leu CUG and UUG codon are much more prone to translational error than the CUU or CUC codons (**Fig.3-5, lower panel**), but the reasons for such differences in translational accuracy need to be clarified in future studies.

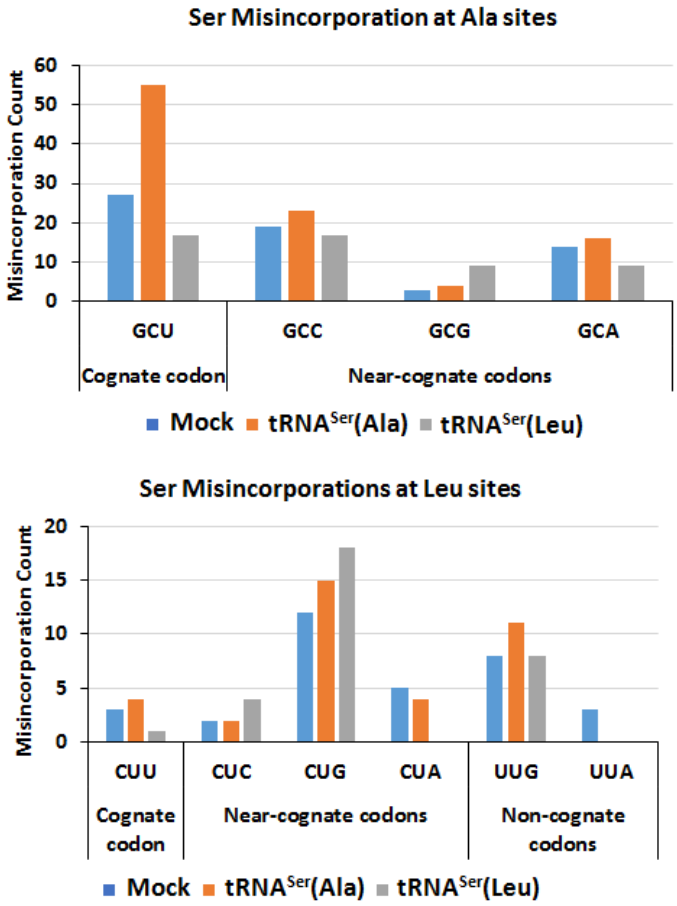

Figure 3-5: Misreading tRNAs misincorporate Ser at Ala and Leu codon sites. Upper Panel) Graphic depicts the absolute number of misincorporations of Ser detected at Ala sites in the soluble fraction of proteins extracted from tumors derived from our cell lines. There was a relative increase in the incorporation of Ser at Ala sites in the cell line expressing the misreading $tRNA^{Ser}$(Ala) at the cognate codon GCT only. $tRNA^{Ser}$(Leu) expressing cell line was used as a negative control to show that the increase in misincorporations is induced by $tRNA^{Ser}$(Ala). **Lower Panel)** Graphic depicts the absolute number of misincorporations of Ser detected at Leu sites in the soluble fraction of proteins extracted from tumors derived from our cell lines. We detected an increase of Ser to Leu misincorporations at the near-cognate codon CTC. $tRNA^{Ser}$(Ala) expressing cell line was used as a negative control to show that the increase in misincorporations is induced by $tRNA^{Ser}$(Leu).

3.3.5. Expression of misreading tRNAs activates the UPR

Since the UPR is frequently activated in cancer and is also an endpoint of protein mistranslation [87,120], we have tested whether it was also activated in our models. For this, we monitored the three UPR branches: IRE-1, PERK and ATF6. Activation of the IRE-1 pathway was evaluated by determining splicing levels of the XBP-1 transcription factor, using RT-PCR. The data showed activation of the IRE-1 pathway by 7% and 14% in tumors expressing $tRNA^{Ser}$(Ala) and $tRNA^{Ser}$(Leu), respectively (**Fig.3-12**). ATF6 activation was higher in tumors expressing $tRNA^{Ser}$(Ala) and the

tRNA^{Ser}(WT) than in Mock tumors (3.1- and 2.15-fold, respectively) (**Fig.3-6A,C**). We next assessed the phosphorylation status of eIF2α, the downstream target of PERK, to confirm UPR activation and also to clarify whether these tRNAs affected translation initiation rate. The levels of eIF2α-P (the inactive form of eIF2α) were 77% lower in tRNA^{Ser}(Ala) tumors relative to Mock controls, and did not change in other tumors (**Fig.3-6B,C**), raising the hypothesis that PERK could be downregulated or that the catalytic subunit of the PP1α phosphatase could be upregulated. Western blot analysis showed 6-fold upregulation of the PP1α catalytic subunit (**Fig.3-6B,C**), indicating that the fast growth rate of tRNA^{Ser}(Ala) tumors was likely due to upregulation of protein synthesis rate, through dephosphorylation of eIF2α by the PP1α-GADD34 phosphatase complex.

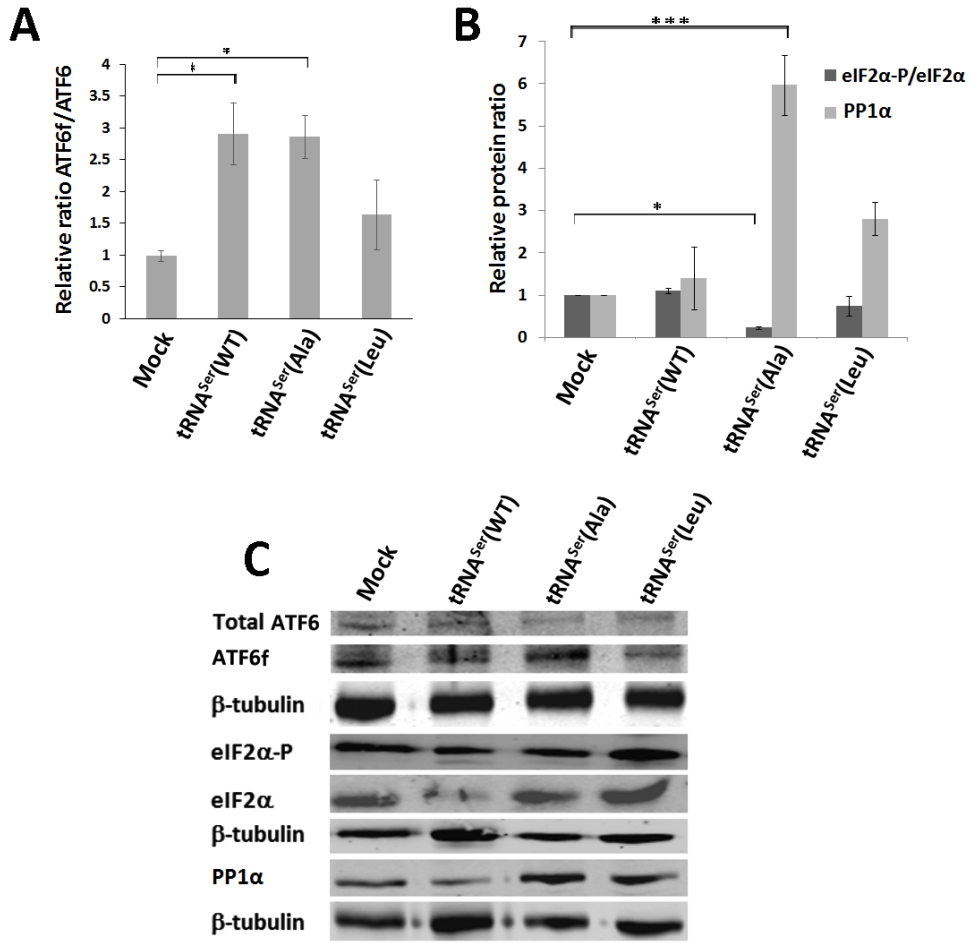

Figure 3-6: Activation of the UPR by misreading tRNAs in vivo. A) Activation of ATF6 in tumors harbouring the wild-type and misreading tRNAs. Total ATF6 and ATF6 fragment were detected by immunoblotting. **B)** eIF2α-P and PP1A catalytic subunit levels in each tumor lysate were analysed by immunoblotting and relative expression values are shown. β-tubulin levels served as protein loading control. **C)** Representative immunoblots for total ATF6, ATF6 fragment, total eiF2α, eIF2α-P, PP1α catalytic subunit and β-tubulin for each membrane. Graphics depict average ± SEM (n=3). Data was analysed by One-way ANOVA with Dunnett's post-test and significant p-values are shown (*p<0.05; ***p<0.001).

3.3.6. Expression of misreading tRNAs influences cancer-associated signaling pathways

Serine, Threonine and Tyrosine tRNAs are among the most overexpressed tRNAs in breast cancer [10]. The respective amino acids can be phosphorylated and their misincorporation at non-cognate sites may cause aberrant phosphorylation and alteration of signaling transduction pathways [10]. This lead us to hypothesize that the Ras/Raf/MEK/ERK and the Ras/PI3K/PTEN/Akt signaling pathways could be affected in our model of Ser misincorporation, promoting unrestrained cellular growth, proliferation and tumor formation [121]. Indeed, global Ser phosphorylation was increased in $tRNA^{Ser}$(Ala) and $tRNA^{Ser}$(Leu) expressing tumors (1.53 and 1.71-fold, respectively) (**Fig.3-7A**), confirming that cell signaling could be deregulated. We then analyzed the activation of Akt, ERK1/2 and p38 in the same tumors and observed activation of the Akt pathway in all tRNA misreading tumors (**Fig.3-7B**) and downregulation of the ERK1 (64%) and ERK2 (54%) pathways in tumors expressing $tRNA^{Ser}$(Leu) (**Fig.3-13A,C**). p38 was downregulated 82% in $tRNA^{Ser}$(WT) relative to Mock, but was unchanged in the other tumors (**Fig.3-13B,C**). Therefore, tumorigenesis induced by misreading tRNAs is likely associated with activation of the Akt pathway, while growth rate differences between tumors could be linked to differential activation of the ERK1/2 pathways.

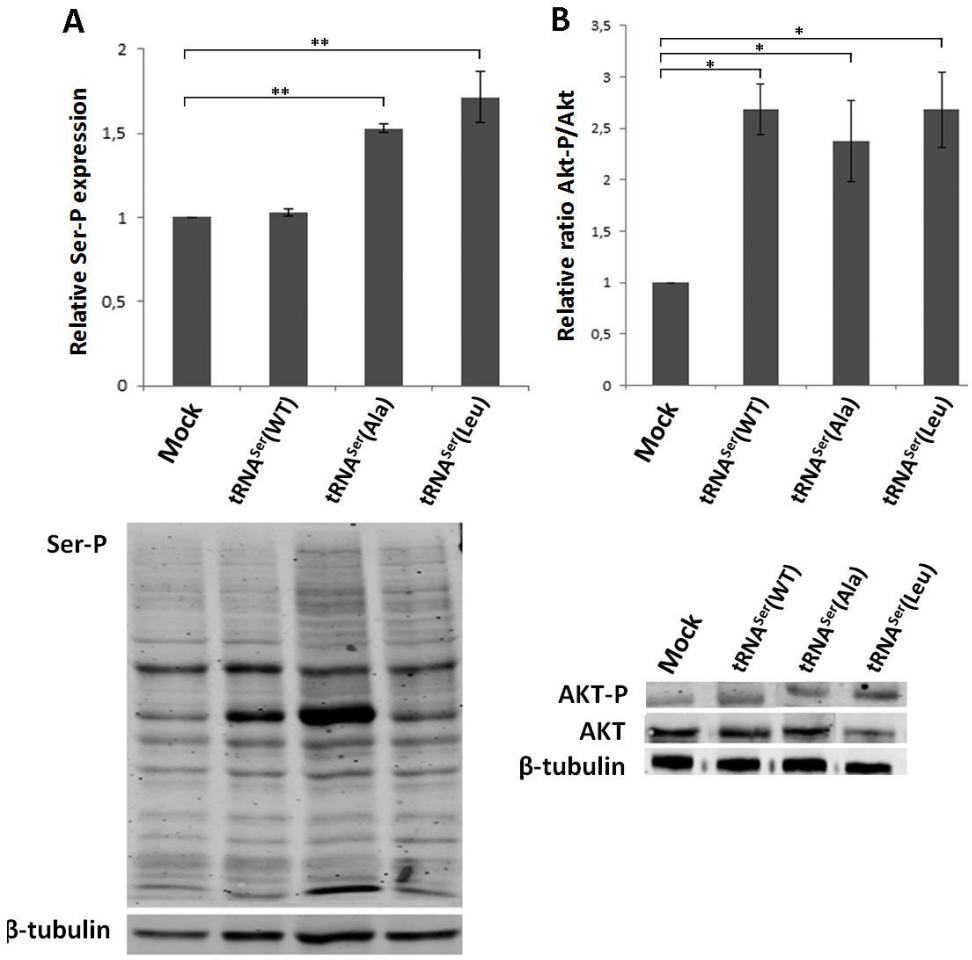

Figure 3-7: Classical cancer-associated pathways activated in mice tumors. A) Evaluation of total phosphoserine levels in tissue lysates from mice tumors. **B)** Relative activation ratio of Akt in tumor lysates compared to the Mock and representative immunoblots of Akt-P, total Akt and β-tubulin (loading control) from tumor lysates. Graphics depict average ± SEM (n=3). Data was analysed by One-way ANOVA with Dunnett's post-test and significant p-values are shown (*p<0.05; **p<0.01).

3.4. Discussion

Imbalance of tRNA pools promotes the formation of non-cognate tRNA-aaRS pairs and tRNA mischarging [122]. Pavon *et al*. reported increased expression of certain tRNAs associated with malignant phenotypes and Gingold *et al.* reported enrichment of tRNAs required for fast translation of proliferation genes in cancer [10–12], suggesting that protein synthesis accuracy could be deregulated in tumors. Since mistranslation impacts proteostasis and produces important phenotypic diversification, drug tolerance and resistance in other biological models [85,123,124], we have hypothesized that it may also interfere with tumor growth, heterogeneity and response to therapy. In this first attempt to tackle these issues, we have expressed mutant misreading tRNAs that recapitulate both frequent and rare amino acid misincorporations detected in tumors of human patients and in near-normal NIH3T3 cell lines.

Our mutant misreading tRNAs were well tolerated *in vitro* and did not produce visible effects on cell viability, apoptosis, proliferation and cell cycle progression, but induced foci formation, promoted angiogenesis and tumor growth *in vivo.* In particular, the mutant misreading tRNA that misincorporated Ser at Ala codon sites ($tRNA^{Ser}Ala$), produced tumors that grew as fast as K-ras^{V12} tumors in nude mice. Previous studies have shown that Ser misincorporation at Ala codon sites, due to an inactivating mutation of the editing site of the AlaRS, induces rapid loss of purkinge cells, ataxia and premature death in mice [5], contradicting our tumor results. Therefore, it is likely that tRNA misreading effects are cell type dependent, i.e., they may lead to apoptosis in purkinge cells and to transformation and neoplasia in other cell types.

The selection and increased expression of the mutant misreading tRNAs in mice tumors (**Fig.3-4C**) indicates that tRNA misreading is adaptive in tumor contexts and depends on the tumor microenvironment. These data are in agreement with previous works showing that mistranslation increases yeast tolerance to stress and allows for growth in the presence of lethal doses of drugs and chemicals [81,82]. Yeast mistranslating cells adapt to the deleterious effects of mistranslation by altering genomic architecture, increasing protein synthesis, protein degradation and glucose uptake rates [106]. In other words, the deleterious effects of tRNA misreading are rapidly mitigated through genomic, metabolic and proteomic changes, raising the hypothesis that mistranslation may have consequences for tumor biology that go beyond the expected proteome instability.

The impressive growth rate of the tumors expressing the $tRNA^{Ser}$(Ala) is likely due to decreased levels of eIF2α-P (**Fig.3-6B**) since the relative increase of eIF2α levels alone is sufficient to transform NIH3T3 cells [125]. This requires up-regulation of the PP1α catalytic activity by cancer signaling pathways, namely the MAPK pathway or recruitment of active PP1α to its eIF2α-P substrate by the regulatory subunit GADD34 [66,126]. Since there was no difference in the activation status of the ERK1/2 downstream effectors of the MAPK it is likely that eIF2α-P dephosphorylation is mediated by the UPR through activation of the ATF4 transcription factor which upregulates GADD34. The observed activation of the other UPR mediators ATF6 and IRE-1 may also contribute to that fast growth of those tumors as they are associated with cellular protection and growth stimulation [115,127,128]. Moreover, UPR coupled with induced tumor dormancy protects neoplasic cells from apoptosis and permits recurrence once favorable growth conditions are restored [129].

It is well established that tumor development needs genetic and epigenetic changes as well as cooperation of microenvironment components to promote adaptation and growth [130]. Common adaptive responses include enhanced plasticity, cell motility, resistance to apoptosis and survival in hostile environments where hypoxia, acidity, amino acid deprivation, inflammatory cytokines and induction of the UPR are common [131,132]. Importantly, PERK activity and eIF2α-P levels are reduced in mouse breast tumors, where Akt is activated [133]. In line with these results, tumors expressing both types of misreading tRNAs showed concomitant activation of the Akt pathway and UPR induction. We postulate that this conjugation of factors may drive apoptosis evasion, cell survival and potentiation of tumor growth (**Fig.3-8**).

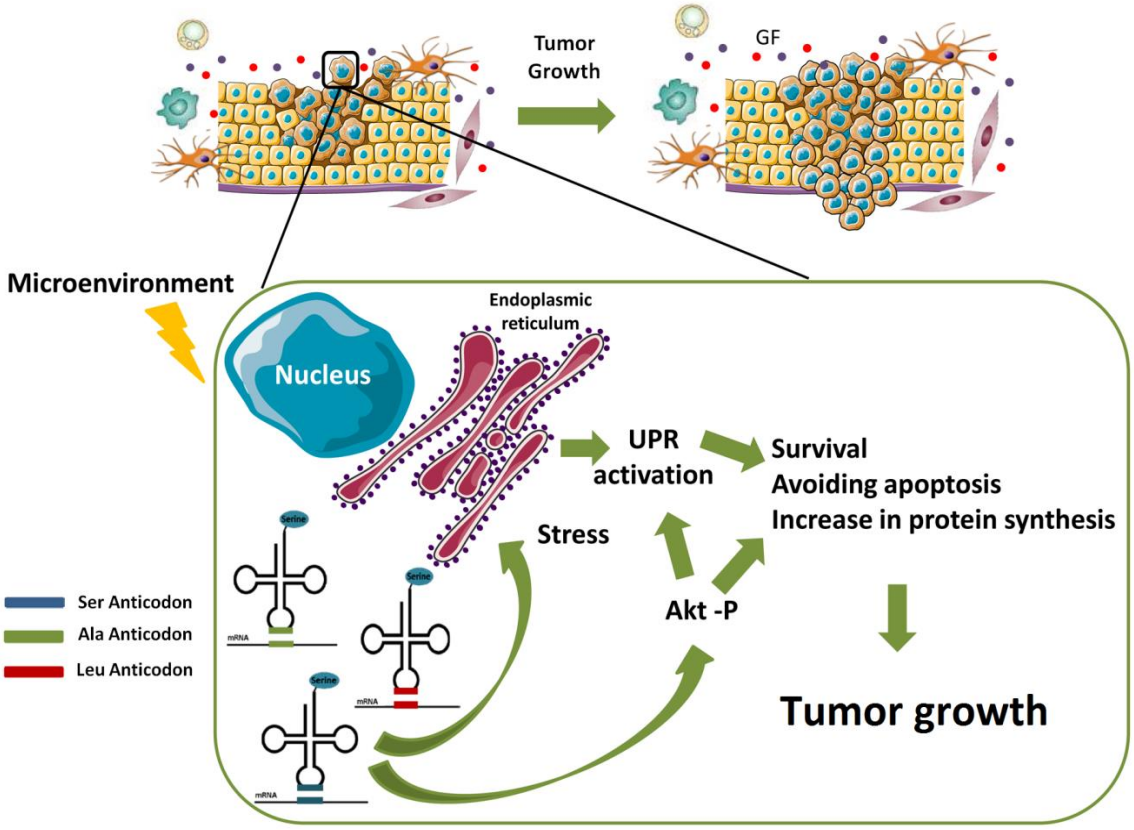

Figure 3-8: Representation of the stress response induced by misreading tRNAs. The mutant misreading tRNAs expressed in NIH3T3 cells exposed to microenvironment stimuli in vivo induce ER stress and activation of the Akt pathway. These events lead to UPR activation, increasing the cells capacity to survive, evade apoptosis and upregulate protein synthesis, especially in $tRNA^{Ser}$(Ala) expressing cells where eIF2α-P is downregulated by upregulation of PP1α catalytic subunit. Overall these molecular mechanisms accelerate in tumor growth. Adapted from Servier Medical Art collection (http://www.servier.com).

Although remarkable progress has been made on the elucidation of the molecular basis of cancer, the etiology of most cancers is still unknown. In the past few years, new molecular links between cancer and translation deregulation have been unraveled, highlighting this setting as etiopathogenic [134]. Our model supports and

extends this link by disclosing unexpected selection and up-regulation of mutant misreading tRNAs in tumors and that mistranslation alone is sufficient to accelerate tumor growth. It will be fascinating to clarify in future studies if the proteome instability and heterogeneity produced by mistranslation generates tumor heterogeneity and increases resistance to anti-cancer drugs, as is the case in yeast.

3.5. Materials and Methods

3.5.1. Construction of misreading tRNA plasmids

A DNA fragment of 248kb corresponding to part of the gene encoding human wild type tRNASerAGA (Chr6 tRNA#5) and it's flanking region were amplified by PCR from genomic DNA using the primers: forward 5'-GCCGAATTCAGCTATTATTAAATCCCTAATAAAAGG-3' and reverse 5'-CGCCTCGAGTTGTAAAAGATCGAAAGCCTTTTTA-3'. The amplified region has the sequence: 5'-AGCTATTATTAAATCCCTAATAAAAGGAGTACAATATGTGATGTATGGAAA CATGTAAGACATTTAATAAGGTTTTTGGTATCTGTAGTCGTGGCCGAGTGGT TAAGGCGATGGACTAGAAATCCATTGGGGTCTCCCCGCGCAGGTTCGAATC CTGCCGACTACGGCAGTGGGTTTTTGCATCTTCAAGCAGGTTTCATCCGACC GATCGATATTTCACGTGTAAAAAGGCTTTCGATCTTTTACAA-3'. The amplified region was cloned into modified vector pIRE1-10-DsRed with new MCS, using the enzymes EcoRI (Thermo Scientific,#ER0275), XhoI (Thermo Scientific,#ER0695) and T4 DNA ligase (Thermo Scientific,#EL0011). Site-directed mutagenesis was carried out to change the anticodon of the tRNASerAGA by other anticodons. The primers used for site-directed mutagenesis of human tRNASerAGA were the following: forward to tRNASerAAG(Leu) 5'-GGTTAAGGCGATGGACTAAGAATCCATTGGGGTCTCCC-3'; reverse to tRNASerAAG(Leu) 5'-GGGAGACCCCAATGGATTCTTAGTCCATCGCCTTAACC-3'; forward to tRNASerAGC(Ala) 5'-GTTAAGGCGATGGACTAGCAATCCATTGGGGTCTCCC-3'; and reverse to tRNASerAGC(Ala) 5'-GGGAGACCCCAATGGATTGCTAGTCCATCGCCTTAAC-3'.

3.5.2. Cell culture

Mouse Embryo Fibroblast cell line (NIH3T3) was obtained from the American Type Culture Collection (ATCC® CRL-1658™). The cell line was grown in DMEM (Gibco,#11965092) supplemented with 10% fetal bovine serum (FBS; Hyclone,#SH30088.03HI) and 1% penicillin–streptomycin (Invitrogen,#15140122) in a humidified atmosphere at 37ºC in the presence of 5% CO2.

3.5.3. Generation of mistranslating cell lines

Cells with 60–80% confluency were transfected with 1µg DNA of plasmid using Lipofectamine 2000 (Invitrogen,#11668019), following the manufacturer's instructions. Stably transfected cell lines were established with 1000 µg/ml G418, after 72 h transfection, for 1 month before being used to perform assays. Cells were transfected with the empty vector (Mock) or the plasmid containing the wild type tRNASerAGA (WT) or the misreading tRNAs: tRNASerAGC(Ala) and tRNASerAAG(Leu).

3.5.4. Polymerase chain reaction analysis

To prove the incorporation of the plasmid in the generated cell lines, genomic DNA was used as template for PCR amplification across the fragment of pIRE1-10-DsRed plasmid containing the tRNA insert. Primers used were: 5'-CAATACGCCCGCGTTTCTT-3' and 5'-TTATCCAAAAAGGATCTTCACCTAGA-3'. PCR conditions were: 95°C for 15 min; 95°C for 30 sec; 54°C for 1min 30 sec; 72°C for 1 min 30 sec with 35 cycles of amplification and a final step of extension at 72°C for 10 min. A 297 bp amplicon was generated, which corresponds to part of the pIRE1-10-DsRed vector without the tRNA insert (Mock) and a 547 bp amplicon, which corresponds to part of the pIRE1-10-DsRed plasmid with the tRNA inserted [tRNASer(WT), tRNASer(Ala) and tRNASer(Leu)]. We analyzed the PCR product in a 1% agarose gel and PCR product was analyzed via Sanger sequencing (Supplementary figure 1). This technique was also performed using genomic DNA extracted from the tumors to prove that our cells were indeed the origin of the tumor.

3.5.5. Confirmation of misreading tRNA expression in cell lines and tumors

The RNA extraction was followed by purification with the standard protocol of DNaseI Amplification Grade kit (Invitrogen,#18068015). RNA was then precipitated with a standard Phenol/Chlorophorm extraction and conserved at -80ºC. cDNA was obtained with Ncode™ VI20™ miRNA cDNA synthesis kit (Invitrogen,#A11193050), using 200ng of RNA. Amplification of the cDNA or DNA of interest was done by PCR with the following primers: 5'-CGTAGTCGGCAGGATTCGAA-3' and 5'-GTCGTGGCCGAGTGGTTAAG-3'. PCR conditions were: 95ºC for 15min, (95ºC for 30 sec, 62ºC for 1 min and 30 sec, 72ºC for 1 min and 30 sec, 3 cycles) (95ºC for 30 sec, 60ºC for 1 min and 30 sec, 72ºC for 1 min and 30 sec, 3 cycles); (95ºC for 30 sec, 58ºC for 1 min and 30 sec, 72ºC for 1 min and 30 sec, 30 cycles) and a final step of extension at 72°C for 10 min. Due to the similarity among serine tRNA bodies, our primers will not only amplify the recombinant tRNAs, but also other endogenous copies of serine tRNAs (tRNA-Ser-AGA-2-6; tRNA-Ser-AGA-2-5; tRNA-Ser-AGA-2-4; tRNA-Ser-AGA-2-3; tRNA-Ser-AGA-2-2; tRNA-Ser-AGA-2-1; tRNA-Ser-TGA-2-2 and tRNA-Ser-TGA-2-1 isoforms). PCR product was run on a 2% agarose gel and the band (~90bp) was excised and purified using Ilustra™ GFX™ PCR DNA and Gel Band Purification Kit (GE,#28-9034-71). Reamplification of the fragment was performed using the same primers used before and PCR conditions were: 95ºC for 15min, (95ºC for 30 sec, 62ºC for 1 min and 30 sec, 72ºC for 1 min and 30 sec, 3 cycles) (95ºC for 30 sec, 60ºC for 1 min and 30 sec, 72ºC for 1 min and 30 sec, 3 cycles); (95ºC for 30 sec, 58ºC for 1 min and 30 sec, 72ºC for 1 min and 30 sec, 25 cycles) and a final step of extension at 72°C for 10 min. 3 µl of PCR product were run on a 2% agarose gel to confirm the presence of just one band and 10 µl of the product were purified with 1µl of ExoI (Thermo Scientific,#EN0581) and 1µl of FastAp (Thermo Scientific,#EF0651) for 1 hour at 37ºC and 15 min at 85ºC. SNaPshot reaction was performed with the following primer: 5'-GGGAGACCCCAATGGATT-3' and using SNaPshot Multiplex Ready Reaction Mix (Applied Biosystems,#4323151). The reaction was preformed with the following temperature cycles: 96ºC for 10 sec, 54ºC for 5 seconds and 60ºC for 30 sec, 15 cycles. The snapshot product was purified adding 1µL of FastAp (Thermo Scientific,#EF0651) and the samples were incubated for 1h at 37ºC and 85ºC for 15 min (inactivation step). Samples were then sequenced and analysed on Peak Scanner software (Applied Biosystems,#4381867).

3.5.6. Viability and proliferation cell assays

To measure cell viability, 1x106 stable cells were plated in T25 cm2 flasks in the presence 1000 µg/ml G418 for 48 h. Number of viable cells was counted after trypan blue staining (0.4%) (Gibco,#15250061).

To access cell proliferation, 2x105 stable cells were plated in the presence 1000 µg/ml G418 in 6-well plates containing 10 mm cover slips for 48 h and incubated with Bromodeoxyuridine (BrdU) for 1 h. Afterwards, medium was aspirated and cells were washed twice with PBS and fixed with paraformaldehyde 4% for 30 min and then stored in 4ºC until used. On the day of analysis, cover slips were washed three times with PBS, treated with HCl 2M for 20 min at room temperature and washed again twice with PBS and twice with PBS-0.5%-Tween 20-0.05% BSA. Subsequently, cover slips were incubated with 1:10 mouse anti-BrdU (Roche,#11170376001) and 1:500 goat anti-mouse Ig Alexa Fluor 488 (Invitrogen,#A-11001). Fluorescence images were digitally recorded in 5 randomly chosen fields (200x magnification) and positive cells were scored. Total number of cells was counted by staining with DAPI.

For cell-cycle analysis, stable cells were plated at a density of 105 cells in 6-well plates and cultured for 48h before in the presence 1000 µg/ml G418, washed twice in PBS and harvested with trypsin (Gibco,#25200056). Cells were centrifuged at 1200 rpm for 5 min, washed three times in PBS, and then fixed by adding 2 ml of ice-cold absolute ethanol in a drop-wise fashion, with gentle agitation. Cells were stored at 4ºC in the dark until used. On the day of analysis, fixed cells were washed once with PBS, re-suspended in RNase A (Sigma, 100 mg/ml) and propidium iodide (PI; Sigma,1 mg/ml,#P4864), and incubated in the dark at room temperature for 15 min before flow cytometry analysis (BD Immunocytometry Systems FACS Calibur).

For cell death assay, cells were seeded in the presence 1000 µg/ml G418 in 6-wells plates, at a final concentration of 1x105cells/ml, for 24h. The procedure up to the centrifugation step of the cell suspension was the same as in the cell cycle analysis. After the centrifugation, the supernatant was discharged, and cells were resuspended in 500µl of 1x binding buffer. After, 1:100 of Annexin V-FITC and 2.5 µg/ml of propidium iodide (Invitrogen) were added, and the cells were incubated for 5 minutes at room temperature in the dark. Then, the cells were analyzed by flow cytometry (BD Immunocytometry Systems FACS Calibur). All flow cytometry results were analyzed using the FlowJo software.

3.5.7. Focus formation assay

Low-passage NIH3T3 cells seeded on 6-well plates at 60%–80% confluence were transfected using Lipofectamine 2000 (Invitrogen) with a total of 1 µg of plasmid DNA, according to the manufacturer's instructions. Seventy-two hours later, cells were trypsinized, and 1x105 cells were plated in three 100mm dishes and maintained in DMEM plus 5% (v/v) FBS (Hyclone) and 1% penicillin–streptomycin (Invitrogen). The medium was renewed every 3 days thereafter. After 13 (for the cells expressing the K-RasV12 vector) and 21 days (for the cells expressing our vectors), cells were fixed with ice-cold methanol and stained with 0.5% crystal violet in methanol to count the foci and photograph the dishes. The pEGFP vector containing K-RasV12 was used as positive control 1. The results were confirmed by two independent experiments.

3.5.8. TNFα induction assay

3.45 x 105 cells were plated in 6-well plates the day before the induction. Cells were then incubated with 30ng/ml for 30 minutes and 4 hours. The concentration of TNFα (PeproTech,#300-01A) as well as time points were chosen according to information in literature and previous protocol optimization [4,5]. After incubation cells were recovered for protein extraction.

3.5.9. Chick embryo CAM assay

The chicken embryo chorioallantoic membrane (CAM) model was used to evaluate the angiogenic response and growth capability of cells containing the empty vector (Mock) in comparison with tRNASer(WT) and misreading tRNASer(Ala) and tRNASer(Leu) expressing cells. Briefly, fertilized chick (Gallus gallus) eggs obtained from commercial sources were incubated horizontally at 37.8°C in a humidified atmosphere and referred to embryonic day (E). On E3 a square window was opened in the shell after removal of 1.5-2ml of albumin to allow detachment of the developing CAM. The window was sealed with a transparent adhesive tape and the eggs returned to the incubator. Cells, re-suspended in 10µl of complete medium, were placed on top of E10 growing CAM (1x106 cells per ring) into 3mm nylon rings under sterile conditions. Two rings were placed in each CAM, one was filed with Mock cell suspension and the second with one of the tRNA's transfected cells (WT, Ala or Leu; N=14 for each paired group). The eggs were re-sealed and returned to the incubator for additional 3 days

incubation. After removing the rings, the CAM was excised from the embryos and photographed *ex ovo* under a stereoscope (Olympus, SZX16 coupled with a DP71 camera) at 20x magnification. The number of new vessels (with less than 15 µm diameter) growing radially towards the ring area was counted in a blind fashion manner. The area of CAM tumors was determined using the Cell A (Olympus) program. Some of the tumors were frozen in liquid nitrogen and stored at –80ºC until used.

A two-tailored paired Student's t test (for samples with unequal variance) was used to calculate significance in an interval of 95% confidence level (values of $p<0.05$ were considered to be statistically significant) between each group (tRNASer(WT), tRNASer(Ala), tRNASer(Leu)) and their respective control (Mock).

3.5.10. Tumor induction assay

Six-week-old male N:NIH(s)II:nu/nu nude mice were obtained previously from the Medical School, University of Cape Town in 1991 and then reproduced, maintained and housed at IPATIMUP Animal House at the Medical Faculty of the University of Porto, in a pathogen-free environment under controlled conditions of light and humidity. Male nude mice, aged 6-8 weeks, were used for in vivo experiments. Animal experiments were carried out in accordance with the Guidelines for the Care and Use of Laboratory Animals, directive 2010/63/EU. To measure tumorigenic potential in vivo, NIH3T3 cell lines harboring the empty vector (Mock), the tRNASer(WT) and the misreading tRNASer(Ala) and tRNASer(Leu) were subcutaneously injected in the dorsal flanks using a 25-gauge needle with 1x106 of each cell line. A total of 5 mice per group were used. Each mouse was injected in the right flank with the Mock variant and in the left flank with the cells misexpressing the Wt variant or misreading variants of each previously described clone. Mice were weighed, and tumor width and length were measured with calipers three times per week. Tumor volumes were calculated assuming ellipsoid growth patterns. Mice were humanely euthanized when tumors reached a median volume of 2000-4000mm3 or whenever any signs of disease were detected. Due to exponential pattern of growth some mice had larger tumors as seen on Fig.3B. Tumors, lungs, liver, kidney, bladder, stomach, pleura and lymph nodes were collected, fixed in 10% buffered formalin, paraffin embedded and then sectioned for histopathological examination. A part of each tumor was frozen in liquid nitrogen for microarray analysis and stored at –80ºC until used.

3.5.11. RNA and DNA isolation

Total RNA was isolated from mouse frozen tumors and genomic DNA was extracted from mouse and CAM frozen tumors and stable cell lines using the AllPrep DNA/RNA/Protein Mini Kit (Qiagen,#8004) according to the manufacturer's protocol. RNA quantity and integrity were assessed using the Nanodrop 1000 Spectrophotometer (Thermo Scientific) and Agilent 2100 bioanalyser system, respectively. Total RNA fraction was used to determine its RIN, which were in the range of 7.5 to 10. DNA quantity and integrity were assessed using Nanodrop 1000 Spectrophotometer and agarose gel, respectively.

3.5.12. Isolation of protein fractions for mass spectrometry analysis

25 mg of tumor tissue (H460-, MKN74-, and NIH3T3-derived tumors) were homogenized in Protein Lysis Buffer (0.5% Triton X-100, 50mM HEPES, 250mM NaCl, 1mM DTT, 1mM NaF, 2mM EDTA, 1mM EGTA, 1mM PMSF, 1mM Na_3VO_4 supplemented with a cocktail of protease inhibitors (Complete, EDTA-free, Roche). Cells were sonicated with a probe sonicator in 5 pulses of 5 seconds, incubated on ice for 30min and centrifuged at 5000rpm for 15min at 4ºC. 10µL of the supernatant (total protein fraction) were stored to measure protein concentration with BCA assay (Thermo Fisher Scientific). 300µg of total protein were centrifuged again at 12000rpm for 20min at 4ºC to isolate the Soluble Fraction of the protein extract present in the supernatant. The supernatant was concentrated under vacuum (SpeedVac®, Thermo Savant, USA) until a volume of 20µL was reached. The total volume was then resolved in a 10% SDS-PAGE gel.

3.5.13. Protein identification and characterization by mass spectrometry

Complete lanes of were manually cut out of the SDS-PAGE gel and sliced into 8 sections, destained with 25 mM ammonium bicarbonate/50% acetonitrile and dried under vacuum (SpeedVac®, Thermo Savant, USA). The dried gel pieces were rehydrated with 25 µL of 10 µg/mL trypsin (Promega V5111) in 50 mM ammonium bicarbonate and digested overnight at 37 °C. Tryptic peptides were extracted from the gel with 10% formic acid/ 50% acetonitrile and were then dried in a vacuum concentrator and re-suspended in 10 µL of a 50% acetonitrile/0.1% formic acid solution. Separation of tryptic peptides by nano-HPLC was performed on the module

separation Proexeon EASY-nLC 1000 from Thermo equipped with a 50-cm EASY C18 column with particle size 2-µm. Each sample was separated over a gradient of 5-32 % ACN in 90 at 250 nl/min. Peptide cations were converted to gas-phase ions by electrospray ionization and analyzed on a Thermo Orbitrap Fusion Lumos mass spectrometer. Precursor scans were performed from 300 to 1,500 m/z at 120K resolution (at 445 m/z) using a 1 x 105 AGC target. Precursors selected for tandem MS were isolated at 1 Th with the quadrupole, fragmented by HCD with a normalized collision energy of 30, and analyzed using rapid scan in the ion trap. The maximum injection time for M1-10 analysis was 50 ms, with an AGC target of 1 x 10^4. Precursors with a charge state of 2-5 were sampled for M1-10. Dynamic exclusion time was set at 60 seconds, with a 5 ppm tolerance around the selected precursor.

We used MS/MS data sets produced by the National Cancer Institute Clinical Proteomic Tumor Analysis Consortium (CPTAC) (https://cptac-data-portal.georgetown.edu/cptacPublic/) and our own MS/MS data sets produced using xenograft tumors, prepared as described above. Normal colon samples were randomly selected (Sample codes: JX0008, JX0025A, JX0030A) while COAD samples were selected to represent advanced stages of the disease by analyzing the metadata available (Sample codes: TCGA-AA-3695-01A-22-2150-27, TCGA-AA-A02E-01A-23-A20O-27, TCGA-AA-A02H-01A-32-A20O-27). Normal samples MS/MS raw data was downloaded from https://cptac-data-portal.georgetown.edu/cptac/s/S019 and COAD samples MS/MS raw data downloaded from https://cptac-data-portal.georgetown.edu/cptac/s/S016. All MS/MS datasets were analyzed using the same bioinformatics pipeline.

The raw files were searched directly against the *Mus musculus* or *Homo sapiens* reference proteomes obtained from UniprotKB, using PEAKS8 software and mutations in the proteome were found using the SPIDER tool [135]. Searches were carried using a precursor search tolerance of 5 ppm. Search criteria included a static modification of +57.0214 Da on cysteine residues, variable modification of +15.9949 Da on oxidized methionine to reduce false positives; some misincorporations and amino acid modifications may produce similar spectra. Searches were performed with semi-tryptic digestion and allowed a maximum of three missed cleavages on peptides analyzed by the sequence database. False discovery rates (FDR) were estimated with decoy-fusion and then set to 1% for each analysis, as previously reported [136]. The sequences of the mutated peptides observed in this analysis were used to generate a modified database,

containing new entries with the proteins harboring those mutations; to rule out false positives. These samples were re-analyzed using the PEAKS software, but this time against the modified databases, validating only the mutated peptides which aligned with the mutated sequence. Data was filtered so that each protein was represented by a single entry to avoid overestimation of protein mistranslation events. The number of spectra for each peptide was taken into account to calculate the total number of misincorporations in the samples.

3.5.14. Reverse transcriptase PCR and quantitative real-time PCR

Poly A mRNA from tumors was reverse-transcribed using the SuperScript II RT system (Invitrogen,#18064014). cDNA was used as template for PCR amplification across the fragment of the Xbp-1 cDNA bearing the intron target of IRE1α ribonuclease activity. Primers used were: murine Xbp-1, 5'-TTACGGGAGAAAACTCACGGC-3' and 5'-GGGTCCAACTTGTCCAGAATGC-3'. PCR conditions were: 95°C for 15 min; 94°C for 30 sec; 57°C for 30 sec; 72°C for 2 min with 35 cycles of amplification and a final extension step at 72°C for 10 min. A 289 bp amplicon was generated from unspliced Xbp-1 (Xbp-1un); a 263 bp amplicon was generated from spliced Xbp-1 (Xbp-1s) and a 315 bp amplicon was generated from hybrid Xbp-1 (Xbp-1H). PCR products were resolved on on QIAxcel DNA Fast Screening Kit (20-50 bp resolution) and agarose gel 4%. As previously reported, a minor hybrid amplicon species consisting of unspliced Xbp-1 annealed to spliced Xbp-1 was also produced through the PCR reaction and appeared above the unspliced amplicon 2. Quantification of Xbp-1 activation (in percentage) was performed using the following formula: 100 x [Xbp-1s + 0.5 Xbp-1H] / [Xbp-1s + Xbp-1H + Xbp-1un], as previously described 3.

TaqMan assays were performed to determine the expression of the mRNA by quantitative real-time PCR (qRT-PCR). The primers used to evaluate the expression of mouse DsRED and Gapdh mRNAs were obtained commercially from Integrated DNA Technologies. All assays including no template controls were carried out in triplicate. The threshold cycle data (CT) and baselines were determined using auto settings. Gapdh mRNA levels served as an internal normalization standard for to determine expression levels of DsRED in each sample. The 2-ΔΔCT analysis method was applied in all experiments.

3.5.15. Immunoblot analysis

Tissue lysates were homogenized using the tissue homogenizer Precellys • 24 (Precellys) in RIPA lysis buffer, containing phosphatase (Sigma-Aldrich) and protease (Roche) inhibitor cocktails. Whole tissue protein lysates were loaded onto 10-12% SDS-PAGE and blotted onto nitrocellulose membranes according to standard procedures. For our analysis we used antibodies against phoshoserine (1:500; Invitrogen); eIF2α (1:1000; Cell signalling); phospho-eIF2α (1:1000; Abcam); ATF6 (1:400; Stressgen); PP1α catalytic subunit (1:400; ThermoFisher Scientific); Akt (1:1000; Cell signaling); phospho-Akt (1:1000; Cell signaling); ERK1/2 (1:1000; Cell signaling); phospho-ERK1/2 (1:1000; Cell signaling); phosphor-p38 (1:1000; Cell signaling); p38 (1:1000; Cell signaling) and β-tubulin (1:1000; Invitrogen). Bound antibody was visualized by incubating membranes with an IRDye680 goat anti-rabbit or IRDye800 goat anti-mouse secondary antibodies (Li-cor Biosciences, Lincoln, NE, USA) at 1:10000 dilution. Detection was carried out using an Odyssey Infrared Imaging system (Li-cor Biosciences). The amount of β-tubulin was used to normalize the amount of the loaded proteins. Lysates from TNFα induction assay were analyzed for p38 and Akt antibodies (phosphorylated and total forms).

3.5.16. Ki67 immunohistochemistry

Tumor sections obtained from mice tumors were de-paraffinized, re-hydrated with graded ethanol and washed in distilled water followed by PBS. Heat induced antigen retrieval was performed using 0.01M citrate buffer, pH 6.0, for 40 min. To block endogenous peroxidase activity, slides were treated with 0.5% H2O2 in methanol, for 20 min at room temperature (RT). To block non-specific binding, slides were exposed to large volume of ultra V block solution (LabVision), for 30 min at RT. Slides were subsequently incubated with rabbit monoclonal antibody against Ki67 (clone SP6; Thermo Scientific) at 1:400 in large volume ultra Ab dilution (Lab Vision), for 2h at RT. After washing, sections were incubated with Envision detection system peroxidase/DAB (Dako) followed by hematoxilin staining using the standard protocol.

3.5.17. Statistical analysis

For all the assays, except for the *in vivo* experiments, our data represents 3

replicates and 2-3 independent experiments. Data are reported as the average values + SEM (standard error of the mean). Statistical significance was determined using One-way ANOVA with Dunnett's post-test. The CAM experiments were analyzed using paired two-tailored Student's t-test.

3.6. Supplementary Figures

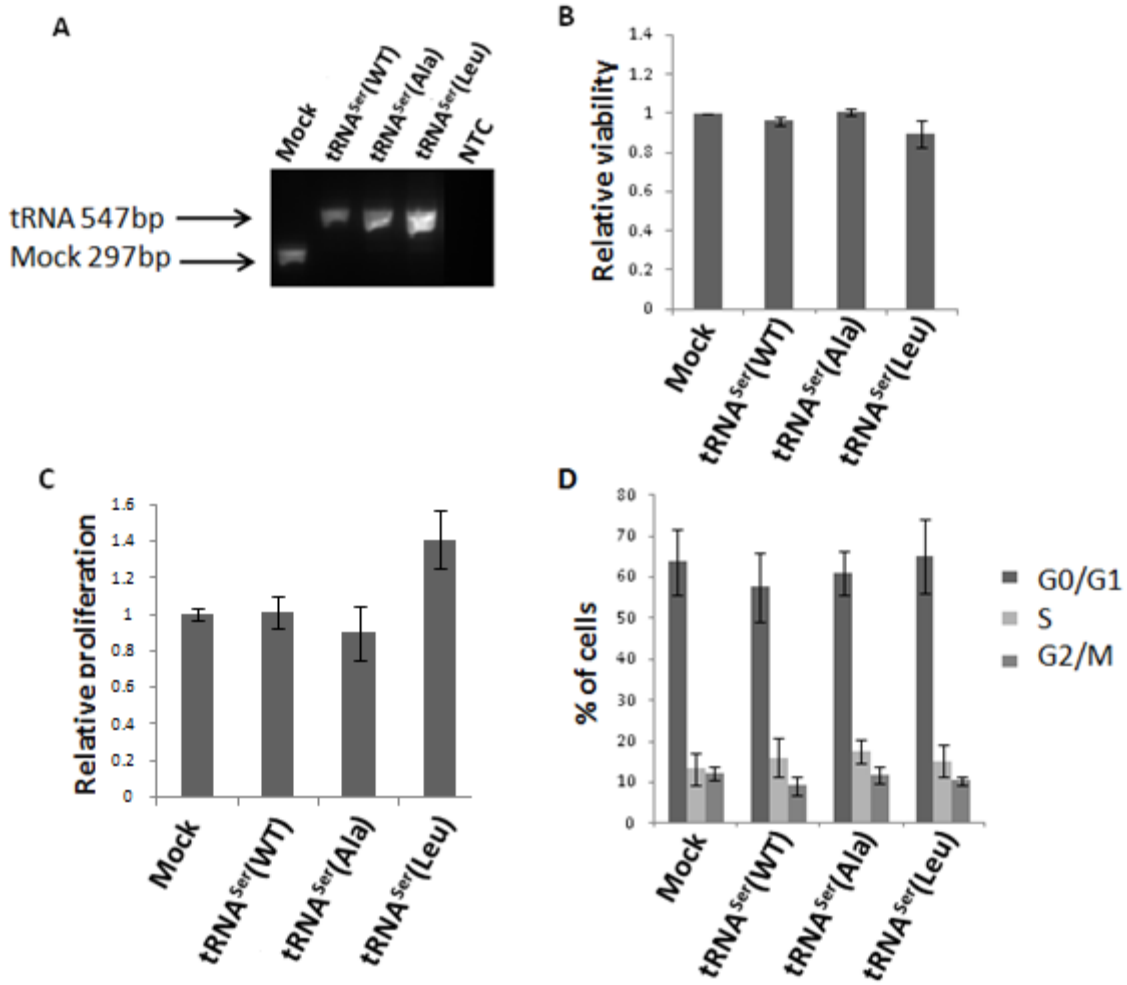

Figure 3-9: **Integration of pIRES2-DsRed and recombinant tRNAs in the cell lines and its phenotypic effects. A)** Agarose gel (1%) of the PCR product obtained by amplification of genomic DNA from cell lines across the fragment of pIRES2-DsRed plasmid containing the tRNA insert. NTC represents the negative control. **B)** To access the cell viability, cells were grown for 48h and then stained with trypan blue (0.4%). Number of viable cells was then registered and then normalized to the Mock cell line. **C)** To check if there were differences in proliferation, stable cell lines were grown in 10 mm cover slips for 48h and then incubated with BrdU for 1h. Cover slips were incubated with1:10 mouse anti-BrdU and 1:500 goat anti-mouse Ig Alexa Fluor® 488. Total number of cells was counted by staining with DAPI. Number of proliferating cells was determined and normalized to the Mock cell line. **D)** For cell-cycle analysis we performed flow cytometry (Propidium Iodide (1mg/ml) staining). The percentage of cells detected in each phase of the cell cycle (G0/G1; S; G2/M) is shown. Data represents average ± SEM (n=3). Statistical significance was determined using unpaired two-tailored Student's t-test. Results are not statistically significant ($p > 0.05$).

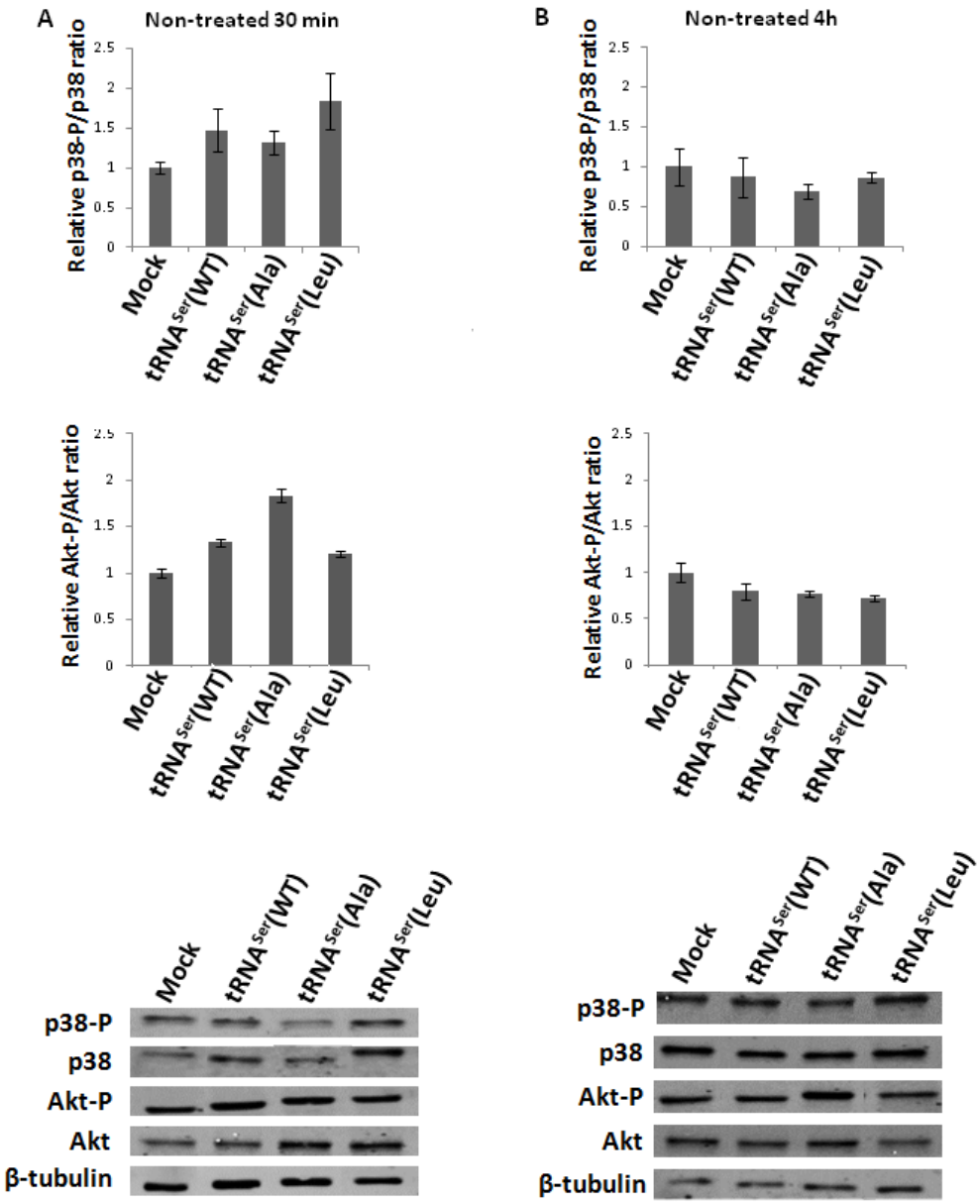

Figure 3-10: Negative Controls of TNFα induction assay. A) Negative controls of cells treated with TNFα for 30 minutes**. Upper panel)** Relative activation ratios of p38 in the cell lines not exposed to TNFα. **Middle panel)** Relative activation ratios of Akt in the cell lines not exposed to TNFα. **Lower panel)** Representative immunoblots of phosphorylated p38, p38, phosphorylated Akt and total Akt in cells lines that were not treated with TNFα. β-tubulin was used as a loading control. **B)** Negative controls of cells treated with As with TNFα for 4 hours. **Upper panel)** Relative activation ratios of p38 in the cell lines not exposed to TNFα. **Middle panel)** Relative activation ratios of Akt in the cell lines not exposed to TNFα. **Lower panel)** Representative immunoblots of phosphorylated p38, p38, phosphorylated Akt and total Akt in cells lines that were not treated with TNFα. β-tubulin was used as a loading control. Data represents average ± SEM (n=3). Statistical significance was determined using unpaired two-tailored Student's t-test. Results are not statistically significant ($p > 0.05$), showing that there are no differences among cell lines when they are not exposed to any stimuli *in vitro*.

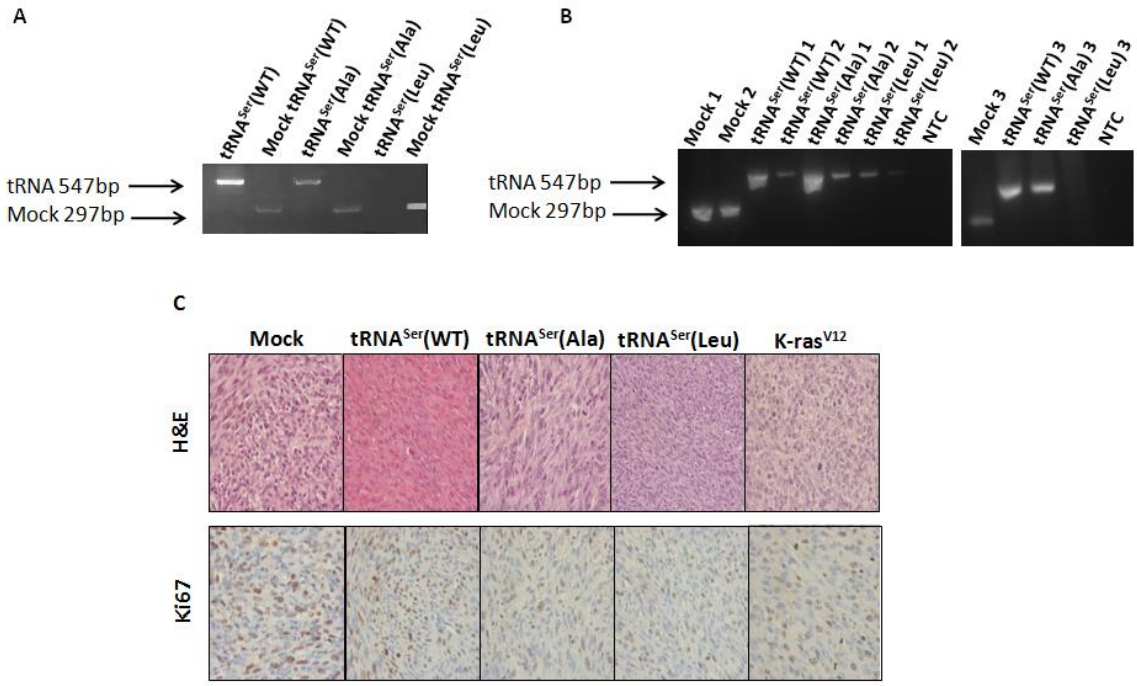

Figure 3-11: Presence of the plasmid pIRES2-DsRed and recombinant tRNAs in the tumors CAM and mice) and histological analysis of representative tumors. A) Agarose gel of the PCR product obtained by amplification of genomic DNA from tumors, extracted from chicken embryo chorioallantoic membrane (CAM) model, across the fragment of pIRES2-DsRed plasmid containing the tRNA insert. NTC represents the negative control. **B)** Agarose gel of the PCR product obtained by amplification of genomic DNA from tumors, extracted from mice model, across the fragment of pIRES2-DsRed plasmid containing the tRNA insert. NTC represents the negative control. **C)** Histological analysis. **Upper panel)** Hematoxylin and eosin staining (H&E) on paraffin-embedded tumor tissues showing high grade sarcomas (40x amplification). **Lower panel)** Immunohistochemical analysis with anti-Ki67 antibody (1:400) on paraffin-embedded tumor tissues presenting high level of proliferation in all tumors (40x amplification).

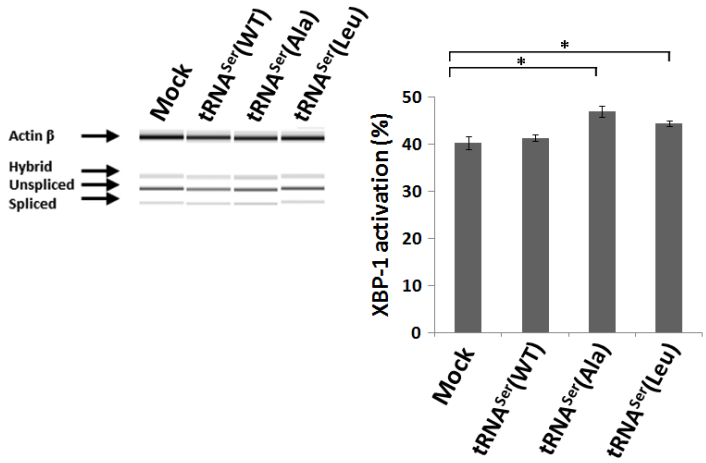

Figure 3-12: Activation of XBP-1 in tumors expressing misreading tRNAs. Left panel) The presence of unspliced (un), hybrid (H) and spliced (s) XBP-1 forms was checked by RT-PCR. Actin β served as a loading control. **Right panel)** Activation of XBP-1 was determined using the formula: 100x[XBP-1s+0.5 XBP-1H]/[XBP-1s+XBP-1H+XBP-1un]. Graphics depict average ± SEM (n=3). Data was analysed by One-way ANOVA with Dunnett's post-test and significant p-values are shown (*p<0.05).

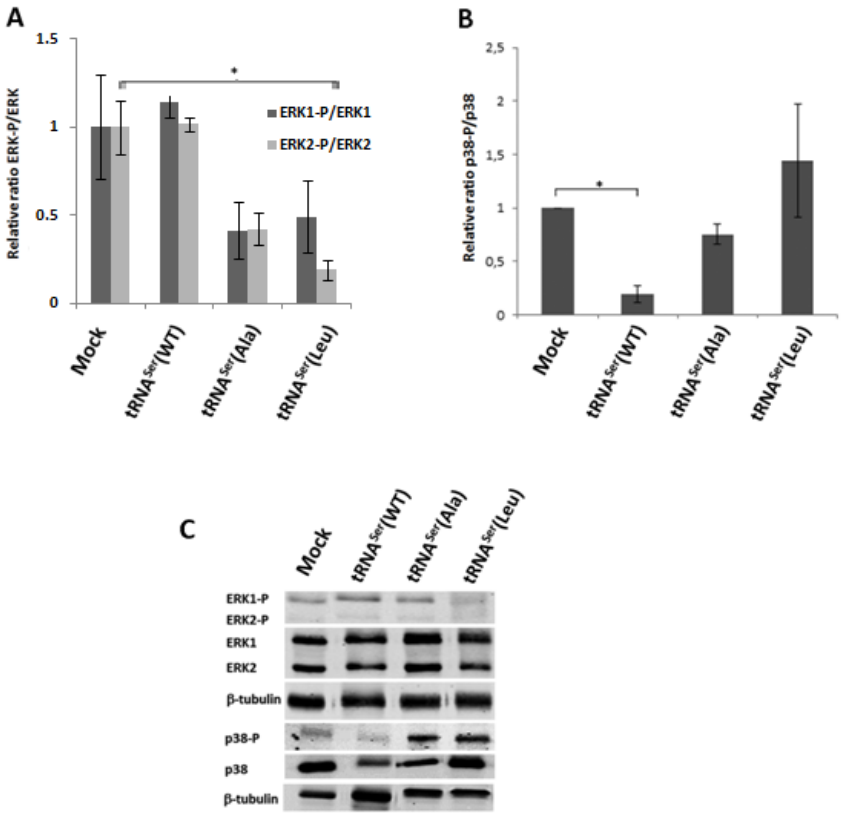

Figure 3-13: Classical cancer-associated pathways modulated in mice tumors. A) ERK1/2 relative activation ratio among tumor lysates. **B)** Relative activation ratios of p38 in tumor lysates. **C)** Representative immunoblots of ERK1/2-P, ERK1/2, p38-P, total p38 and the respective β-tubulin (loading control) from tumor lysates. Graphics depict average ± SEM (n=3). Data was analyzed by One-way ANOVA with Dunnett's post-test and significant *p-values* are shown (*p<0.05; **p<0.01).

4. tRNA deregulation may drive tumor initiation

4.1. Abstract

Although tRNAs are often overexpressed in tumors, their role in tumor biology and specially in tumor initiation is unknown. In normal breast cells, upregulation of specific tRNAs can increase metabolic activity and cell proliferation, but the contribution of tRNA overexpression to tumor initiation has not yet been addressed. tRNA deregulation may cause protein misincorporation at near-cognate codon sites and, depending on the level of protein misfolding, may also activate the protein quality control (PQC) system. There are evidences that the PQC and specifically the unfolded protein response (UPR) are activated in tumors, but the role of amino acid misincorporations in tumorigenesis is also unexplored. In order to tackle these questions, we have overexpressed both a Wild Type (WT) Ser tRNA, which was found to be upregulated in tumors, and a misreading tRNA that misincorporates Ser at Ala codons in near-normal cells BEAS-2B. We found that stable expression of these tRNAs increases cellular proliferation, accompanied by increased protein synthesis and activation of the PERK branch of the UPR. Both tRNA constructs were able to increase *in vitro* colony formation, indicating increased tumorigenic capacity. Our preliminary data further suggests that overexpression of the WT Ser tRNA may be enough to initiate tumor formation with slow growth kinetics.

4.2. Introduction

The expression levels of tRNAs belonging to families of amino acids that can be phosphorylated are often elevated in tumors [10,11]. Additionally, tRNA profiles alone are sufficient to discriminate tumor samples from normal tissue [9]. The role of tRNA deregulation in cancer remains elusive, however, it has been associated with increased translation of specific transcripts that are enriched in codons that are decoded by the deregulated tRNAs [13]. Overexpression of $tRNA_iMet$ was also associated with increased metabolic activity and cell proliferation of a normal breast cell line; features that are associated with cell transformation [12]. Moreover, the overexpression of Ser tRNAs has been associated with poor prognosis in several types of cancer and also with increased risk of recurrence in breast cancer [9]. Whether these tRNAs play a role in tumor initiation and how they may do so, remains elusive. It is possible that the over-representation of Ser tRNAs can lead to misreading of near-cognate codons, such as the Ala (AGC) codon [51]. In line with this, we observed that misincorporation of Ser at Ala sites is one of the most abundant mistranslation events in tumor cells (previous chapter).

Mistranslation can induce the formation of aberrant misfolded proteins, which in turn activate the proteome quality control (PQC) system, consisting of several molecular chaperones and degradation systems that work together to ensure a healthy and functional proteome [137]. We observed that tumors with high mistranslation rates activate the different branches of the Unfolded Protein Response (UPR) (Chapter 3).

When misfolded proteins accumulate in the Endoplamic Reticulum (ER) they sequester the molecular chaperone BiP (or GRP78) [138]. This chaperone releases the UPR effectors PERK, ATF6 and IRE1α. PERK and IRE1α autophosphorylate themselves and ATF6 migrates to the Golgi where it is cleaved and activated [113]. Together, these branches activate a pro-survival cellular response, but when the stress is prolonged they switch into a pro-apoptotic signaling mode [139]. Cancer cells can hijack the UPR and profit from its pro-survival measures, to increase tumor aggressiveness, tumor-promoting inflammation, survival during hypoxia and tumor resistance to treatment [140–143]. The PERK branch of the UPR is responsible for controlling the protein synthesis rate to prevent ER overloading with misfolded proteins [144,145]. PERK directly phosphorylates the initiation factor eIF2α, thus inhibiting the assembly of the translation initiation complex. Nevertheless, selective translation of stress response transcripts, such as the transcription factor ATF4, CHOP and BiP, occurs to counteract the stressful cellular conditions [146]. ATF4 induces the transcription of stress response genes, such as GADD34, which directs PP1α to dephosphorylate eIF2α and restore global protein synthesis rate [147]. Decreased levels of eIF2α phosphorylation are sufficient to trigger transformation on a near-normal *Mus musculus* cell line [125]. PERK can also activate known oncogenes such as Akt, mTOR and MAPK through phosphorylation of diacylglycerol (DAG) and generation of phosphatidic acid [148,149]. Furthermore, PERK is able to phosphorylate the transcription factor Nrf2, which is responsible for transcription of antioxidant cellular defences [150]. This branch of the UPR is essential for tumor establishment and growth [151]. Moreover, ER stress and UPR activation were detected in pre-malignant lesions that precede hepatocellular carcinoma (HCC), and when combined with hypernutrition their activation leads to HCC development [152].

In this chapter, we clarify the role of Ser-tRNA deregulation and tRNA misreading in tumor initiation and unveil the contribution of the PERK branch of the UPR to this phenotype. To do so, we overexpressed both a Ser WT tRNA and a

misreading Ser tRNA (which reads Ala codons) in a normal cell line derived from normal bronchial epithelium, BEAS-2B. We found that overexpression of the WT Ser-tRNA and expression of the misreading Ser tRNA can increase protein synthesis rate and proliferation in a normal cell line. Increased expression of this WT Ser-tRNA is likely sufficient to initiate the formation of slow growing tumors. Modulation of the UPR was similar in both cell lines, however the factors that contribute to the decreased phosphorylation of eIF2α in the cell line expressing the misreading tRNA have to be identified in the future.

4.3. Results

4.3.1. Misreading and WT tRNAs have a positive impact on cellular fitness

Our previous results showed that tRNAs are involved in tumor growth, but it is unclear whether tRNA misreading or deregulation of WT tRNA expression or both are involved in tumor initiation and/or in tumor progression. To elucidate if tRNAs are involved in tumor initiation, we expressed a $tRNA^{Ser}$(Ala) misreading tRNA and overexpressed the Ser WT tRNA, selected from our previous work (Chapter 3), in a normal cell line (BEAS-2B). To exclude the hypothesis that the phenotypes observed were transfection specific, we established three independent stable cell lines for each condition (**Fig.4-1A,B**). Regarding the expression of the recombinant tRNAs, in the BEAS $tRNA^{Ser}$(WT) the expression of the WT Ser tRNA was upregulated by 1.6-fold ($p<0.05$), when comparing to the Mock cell line (**Fig.4-1C**), and in the BEAS $tRNA^{Ser}$(Ala) cell line the misreading $tRNA^{Ser}$(Ala) was 16-fold less expressed than the endogenous WT Ser tRNA (**Fig.4-1C**).

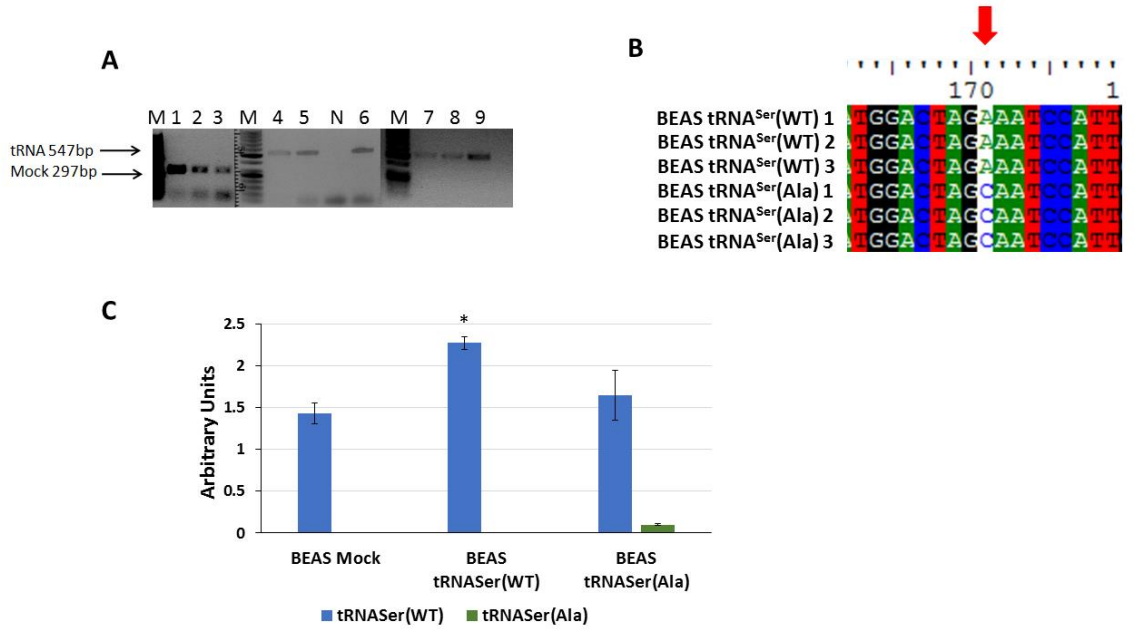

Figure 4-1: Integration of pIRES2-DsRed and recombinant tRNAs in the cell lines. A) Agarose gel (1%) of the PCR product obtained using gDNA. DNA bands correspond to the fragment of pIRES2-DsRed plasmid containing the tRNA gene insert. Legend: M – Molecular Marker; 1, 2, 3 – BEAS Mock 1, 2 and 3, respectively; 4, 5, 6 – BEAS tRNA^{Ser}(WT) 1, 2 and 3, respectively; 7, 8 and 9 BEAS tRNA^{Ser}(Ala) 1, 2 and 3, respectively; N -Negative control. **B)** Sanger sequencing of the PCR products showing the mutation in the anticodon of the tRNA from AGA in tRNA^{Ser}(WT) cell lines to AGC in the tRNA^{Ser}(Ala) cell lines, indicated by the red arrow. **(C)** Quantification of tRNA expression by Snapshot sequencing. tRNAs were quantified based on a primer extension assay and values were normalized for the expression of GAPDH. tRNA^{Ser}(WT) expression was upregulated 1.6-fold increase relative to the Mock cell line. The graph confirms that tRNA^{Ser}(Ala) was also expressed in BEAS tRNA^{Ser}(Ala) cell line. Graphic depict average ± SEM (n=3). Data was anlalysed with unpaired, two-tailed Student´s t-test with Welch correction and significant p-values are shown (*p<0.05)

Similarly to other published results, upregulation of the WT Ser tRNA and the expression of the misreading tRNA^{Ser}(Ala), did not affect the viability of BEAS-2B, once stable cell lines were achieved (**Fig.4-2**).

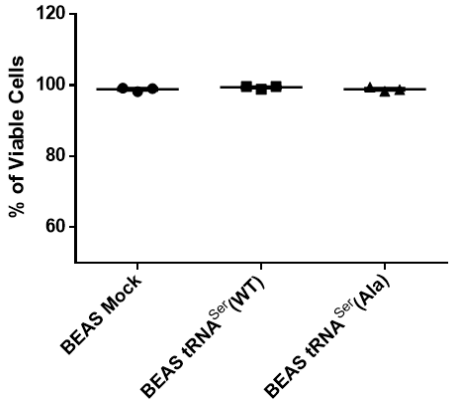

Figure 4-2: Stable expression of recombinant tRNAs do not impact cell viability. Cells grown for 48h were stained with trypan blue (0.4%) to determine the cell viability of BEAS-2B derived cell lines (n=3, with 3 technical replicates). Graphic depicts the percentage of viable cells ±SEM. Data was analyzed with One-way ANOVA and Holm Sidak's post-test (p>0.05).

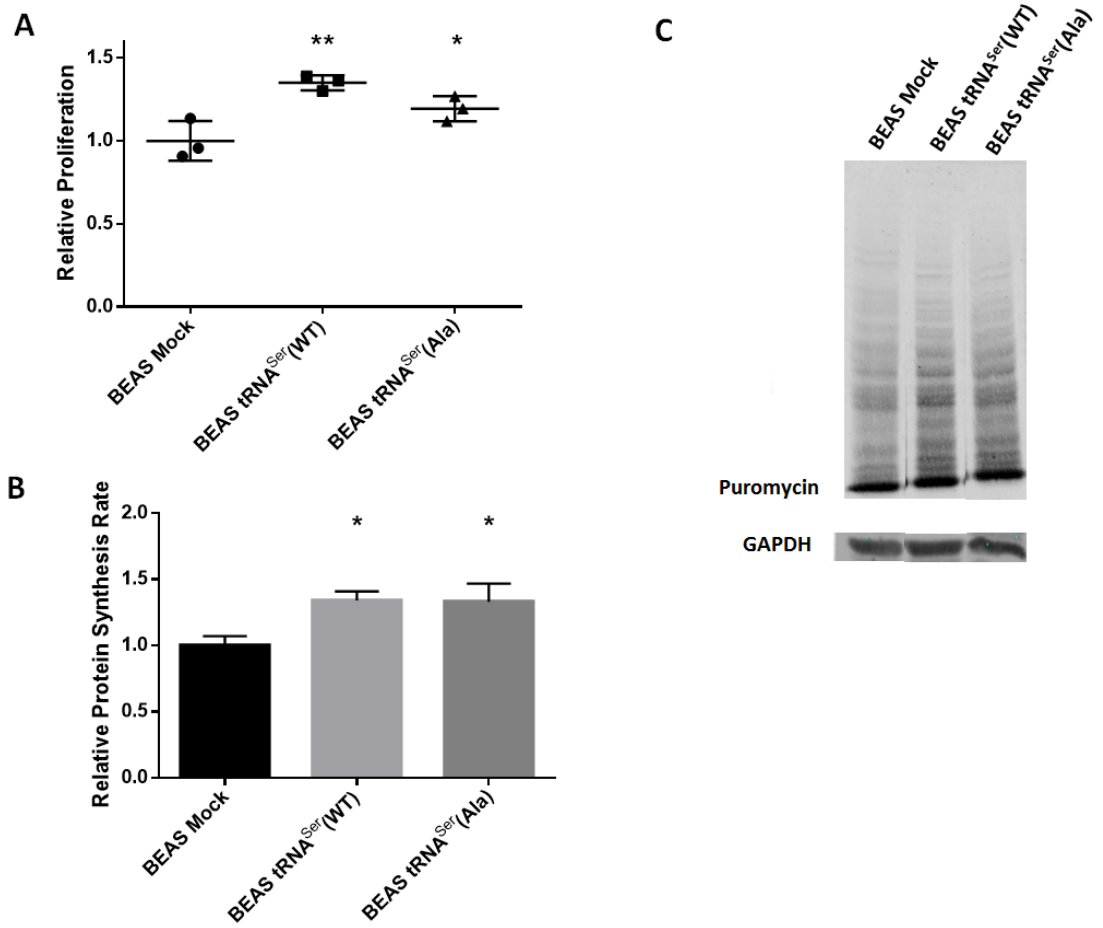

Figure 4-3: Expression of recombinant tRNAs increase cell proliferation and protein synthesis rate. **(A)** To evaluate cellular proliferation, $5x10^3$cells/well were plated in 96-well plates and incubated for 48h prior to measuring BrdU incorporation during DNA synthesis, using a colorimetric immunoassay. Relative proliferation of BEAS-2B derived cell lines – The expression of $tRNA^{Ser}$(WT) and $tRNA^{Ser}$(Ala) increased cellular proliferation capacity in vitro. **(B)** The $tRNA^{Ser}$(WT) and $tRNA^{Ser}$(Ala) increased protein synthesis rate in BEAS-2B-derived cell lines. **(C)** Protein synthesis rate was estimated by immunoblot against puromycin. GAPDH served as a protein loading control. Graphics depict average ±SEM of n=3, with 3 technical replicates. Data was analyzed with One-way ANOVA and Holm Sidak's post-test and significant p values are shown (*p<0.05; **p<0.01).

In BEAS-2B derived cell lines expression of $tRNA^{Ser}$(WT) and $tRNA^{Ser}$(Ala) increased proliferation by 1.35-fold (p<0.01) and e 1.14-fold (p<0.05), respectively (**Fig.4-3A**). Since cell proliferation was increased by the expression of both tRNAs, we investigated if protein synthesis rate was also changed. We did so by measuring the incorporation of puromycin into proteins, using the SunSET technique. There was an increase of 1.34- and 1.37-fold in protein synthesis rate in the cell lines expressing the $tRNA^{Ser}$(WT) and $tRNA^{Ser}$(Ala), respectively (p<0.05 in both cases) (**Fig.4-3B,C**). Therefore, the increased cell proliferation is accompanied by an increase in protein synthesis rate in these cells.

4.3.2. Expression of misreading and WT tRNAs induce the Unfolded Protein Response in BEAS-2B cells

We have investigated the activation of the PERK branch of the UPR and BiP deregulation in BEAS-2B cells. We observed that BiP was upregulated in the cell line overexpressing the $tRNA^{Ser}$(WT) by 1.54-fold ($p<0.05$), but its levels were unchanged in the cell line expressing the misreading $tRNA^{Ser}$(Ala) (**Fig.4-4A**,**E**). Phosphorylation levels of eIF2α were decreased by 0.21- and 0.31-fold in $tRNA^{Ser}$(WT) and $tRNA^{Ser}$(Ala) expressing cell lines, respectively, relative to the Mock cell line ($p<0.05$) (**Fig.4-4B**,**E**), which is in agreement with our previous results (Chapter 3). These results are positively correlated with the increased protein synthesis rate observed in Fig.4-3. eIF2α dephosphorylation is often preceded by increased ATF4 activity, which starts a negative feedback loop to restore global levels of protein synthesis rate. We observed that $tRNA^{Ser}$(WT) and $tRNA^{Ser}$(Ala) expressing cell lines have increased activity of ATF4 (1.49-fold ($p<0.01$) and 1.23-fold ($p<0.05$), respectively (**Fig.4-4C**,**E**). Additionally, the cell line overexpressing the $tRNA^{Ser}$(WT) upregulates the GADD34 regulatory subunit that directs PP1α to eIF2α, by 6.86-fold ($p<0.05$). However, its levels in $tRNA^{Ser}$(Ala) expressing cells were unchanged (**Fig.4-4D**,**E**), suggesting that GADD34 is not involved in modulating eIF2α–P levels in this cell line.

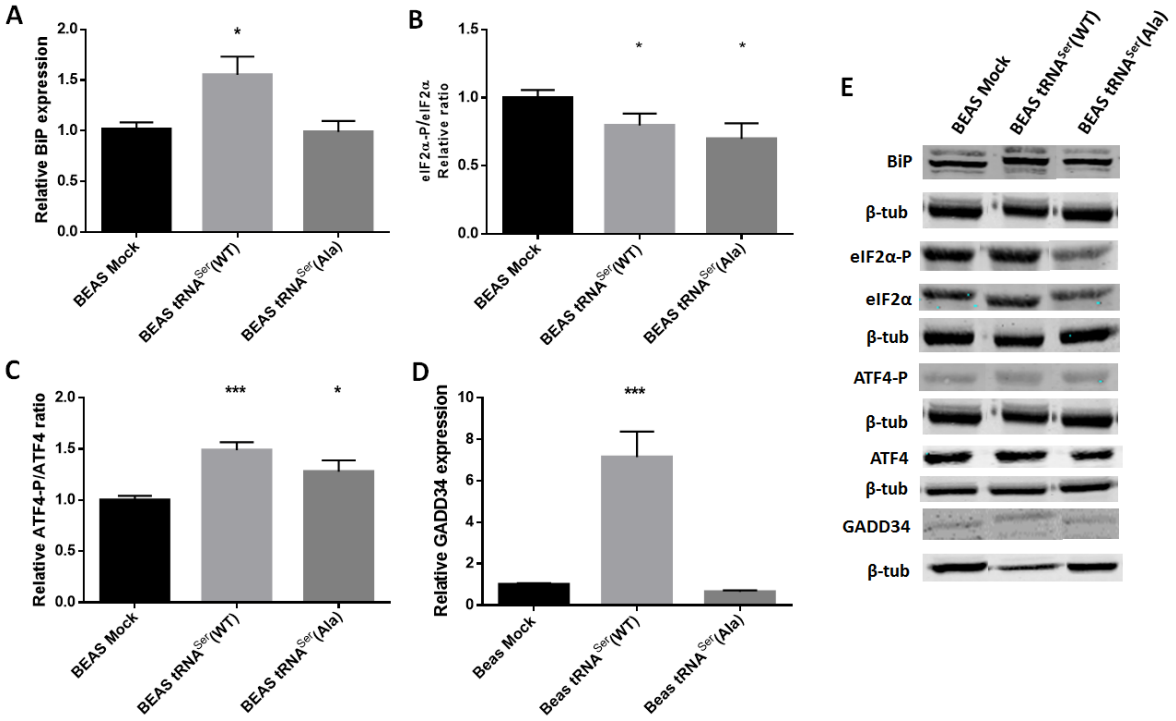

Figure 4-4: UPR deregulation induced by recombinant tRNAs. (A) Expression of tRNA^{Ser}(WT) but not tRNA^{Ser}(Ala) increases BiP expression on BEAS-2B cells. **(B)** Both tRNA constructs reduced the levels of eIF2α-P. **(C)** tRNA^{Ser}(WT) and tRNA^{Ser}(Ala) expression in BEAS2B cell line increased the activation of ATF4 transcription factor. **(D)** Expression of GADD34 was only increased in BEAS-2B tRNA^{Ser}(WT) cell line. **(E)** Immunoblots against BiP, eIF2α-P, eIF2α, ATF4-P, ATF4 and GADD34. B-tub served as protein loading control. Graphics depict average ± SEM (n=3), with 3 technical replicates. Data was analyzed with One-way ANOVA and Holm Sidak's post-test and significant p values are shown(*p<0.05; ***p<0.001).

4.3.3. Recombinant tRNAs increase in vitro transformation ability of BEAS-2B-derived cell lines

Regarding modulation of transformation ability, both constructs were able to increase the number of colonies of BEAS-2B, in an anchorage-dependent colony formation assay. Upregulation of the tRNA^{Ser}(WT) increased colony formation by 1.43-fold (p<0.01) and expression of the misreading tRNA^{Ser}(Ala) increased it by 1.52-fold (p<0.01) (**Fig.4-5**). Interestingly, the number of colonies obtained with this assay for BEAS tRNA^{Ser}(WT) and BEAS tRNA^{Ser}(Ala) different transfections was very similar, indicating that this phenotype is not transfection-specific (**Fig.4-5**). These results suggest that deregulation of tRNA expression or mistranslation alone are sufficient to transform normal immortalized cell, and are likely to induce tumorigenesis in the same normal cell lines.

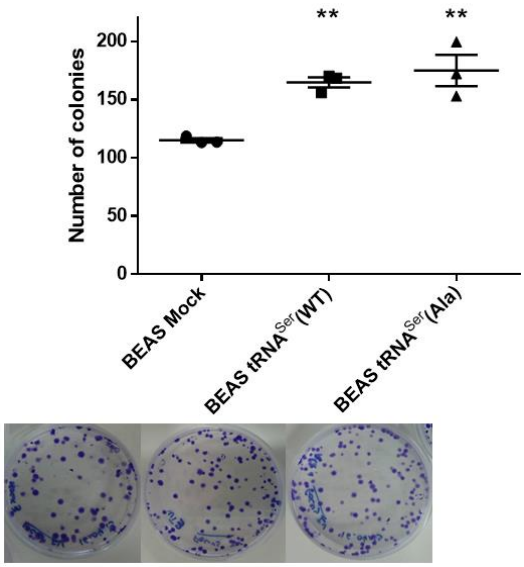

Figure 4-5: Deregulation of WT tRNA expression and mistranslation increase tumorigenic capacity of normal cells *in vitro*. Overexpression of $tRNA^{Ser}$(WT) and expression of the misreading $tRNA^{Ser}$(Ala) increases anchorage-dependent colony formation in BEAS-2B-derived cell lines, indicating that they may bestow these cells with increased tumorigenic capacity.

4.3.4. The impact of tRNA deregulation in tumor initiation

To assess the impact of tRNA deregulation in tumor initiation, we inoculated $4.5x10^6$ cells of BEAS 2B-derived cell lines harboring our tRNA constructs in the right dorsal flank of four mice (for each tRNA construct) and control cells (Mock) on the corresponding left dorsal flank of every mice. After 3 months, the experiment was terminated because tumors were growing very slowly and were still hard to measure accurately. In the BEAS $tRNA^{Ser}$(WT) experimental arm, all mice developed tumors for the cell line expressing the $tRNA^{Ser}$(WT) construct, whereas only two animals developed tumors expressing the Mock construct. These tumors were much smaller than the $tRNA^{Ser}$(WT) expressing tumors (**Fig.4-6, 4-7A**). Regarding the BEAS $tRNA^{Ser}$(Ala) experimental arm, the results were variable: one mouse died of causes non-related to the experiment; one mouse developed a tumor expressing the Mock construct; one mouse developed a tumor expressing the $tRNA^{Ser}$(Ala) construct and a tumor expressing the Mock construct; and one mouse only developed a tumor expressing the $tRNA^{Ser}$(Ala) construct (**Fig.4-6, 4-7B**). Despite the inconclusiveness of results from the last arm, in the first arm, overexpression of the WT Ser tRNA could trigger tumor formation with slow kinetics, since all mice developed tumors expressing this construct, as opposed to controls. In any case, this experiment need to be repeated with greater numbers (more animals) and with a greater number of injected cells per mice.

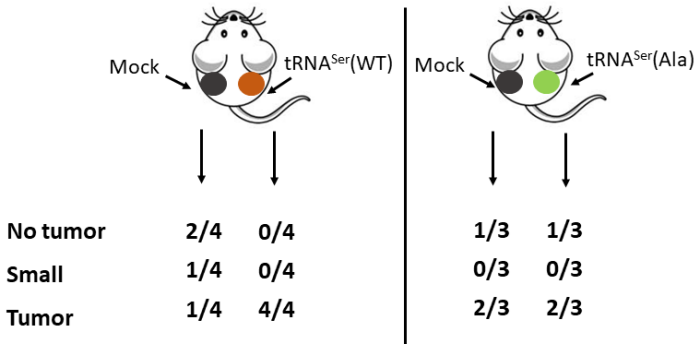

Figure 4-6: Effect of tRNA deregulation in tumor initiation. All animals inoculated with BEAS tRNA^{Ser}(WT) developed a tumor, whereas BEAS Mock tumors only developed in 2/4 mice and had a small size. In the tRNA^{Ser}(Ala) arm, one mouse only developed a BEAS Mock derived tumor, one mouse developed tumors derived from both cell lines and one mouse only developed a tumor derived from BEAS tRNA^{Ser}(Ala) cell line.

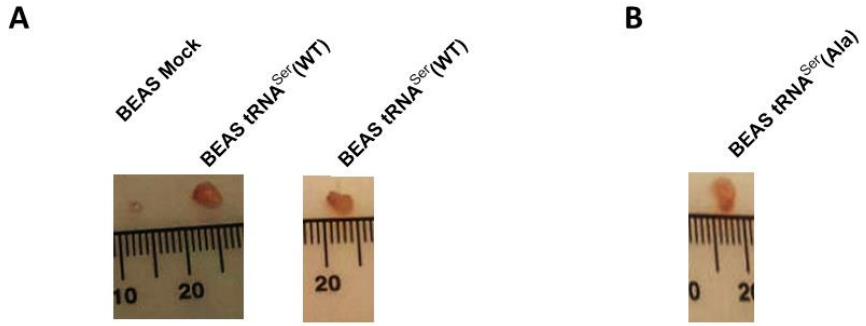

Figure 4-7: Tumors developed by BEAS-2B-derived cell lines. **A)** Tumors derived from BEAS tRNA^{Ser}(WT) and BEAS Mock cells inoculated in the same animal. Left panel shows an example of an animal that developed tumors derived from both cell lines where the size of the Mock tumor is almost negligible relative to the tRNA^{Ser}(WT) expressing tumor; the right panel shows the tumor of an animal that only developed a tumor expressing the tRNA^{Ser}(WT) construct. **B)** Tumor of the animal that only developed a tumor expressing the tRNA^{Ser}(Ala) construct.

4.4. Discussion

In agreement with previous reports, of Pavon and colleagues showing that mild overexpression of tRNAiMet is sufficient to increase metabolic activity and proliferation rates, we observed that increased expression of tRNA^{Ser}(WT) and expression of a misreading tRNA^{Ser}(Ala) boosted protein synthesis rates in normal epithelial cells, and increased cellular proliferation rates when stably expressed [12]. In the present study, we have gone beyond previous observations and studied the effect of increasing the expression of WT Ser tRNA overexpression and expressing a mutant tRNA^{Ser}(Ala) in tumorigenic initiation. Both tRNAs increased colony formation capacity in an anchorage-dependent colony formation assay, which is an indicator of increased tumorigenic ability [153]. We also studied the activation of the PERK branch of the UPR and found that in both conditions the levels of phosphorylated eIF2α were

lower than the control, which has been associated to cellular transformation [125]. In the cell line overexpressing the WT Ser tRNA, there was upregulation of GADD34, which explains the decrease in eIF2α-P levels, but GADD34 was not upregulated in the cell line expressing the misreading tRNA. In other words, those cell lines achieved the same eIF2α phosphorylation outcome through different molecular mechanisms. This cell line may instead increase CReP expression levels, an homolog of GADD34, which can also bind and direct PP1α towards eIF2α [154], but this hasn't been confirmed. The reduced levels of eIF2α-P are also positively correlated with the increased protein synthesis rate observed in both cell lines. Activation of the transcription factor ATF4 was also increased, suggesting that transcription of GADD34 and genes that are relevant for adaptation under hypoxic conditions, oxidative stress and nutrient deprivation, which are hallmarks of tumors, were upregulated as well [155–157]. Moreover, BiP was upregulated in the $tRNA^{Ser}$(WT) cell line, which have been detected in head and neck cancer initiating cells and in lung pre-malignant lesions [158,159].

The low number of mice used in our *in vivo* pilot assay and the erratic nature of the results prevented us to demonstrate that those tRNAs contribute to tumor initiation. In the mice harboring $tRNA^{Ser}$(WT) tumors, the data indicate that overexpression of the $tRNA^{Ser}$(WT) may indeed trigger formation of slow growing tumors. This experiment need to be repeated to clarify the role of those tRNAs in tumor initiation.

4.5. Materials and Methods

4.5.1. Cell Culture

BEAS-2B cell line was kindly provided by Professor Maria Carmen Alpoim, from IBILI, University of Coimbra. BEAS-2B cells were cultured in LHC-9 medium (Gibco, Life Technologies) supplemented with 1% of Penicillin-Streptomycin (Pen/Strep) (Gibco, Life Technologies). Cells were maintained in an incubator at 37ºC with 5% CO_2 and 95% relative humidity. To execute the following procedures, cells were detached using Tryple Xpress (Gibco, Life Technologies). Cells were regularly tested for mycoplasma contamination.

4.5.2. Generation of stable cell lines

BEAS-2B stable cell lines were generated through electroporation (three independent times). BEAS-2B cells were seeded in 100mm dishes and cultured until 70-90% of confluence was reached. Cells were detached and the pellet was resuspended in Hepes Buffered Saline (HBS) solution to improve the transfection efficiency. Then, 4mm electroporation cuvettes were prepared with 10µg of plasmid and 0.5ml of cell suspension was added, mixing carefully. For each sample, the voltage applied was 230V, with capacitance of 1500µF and resistance of 125Ω. This step was performed using ECM Electro Cell Manipulator (BTX, Harvard Apparatus). Immediately after the electroporation, 1ml of LHC-9 culture medium was added to the cuvette, cells were then carefully homogeneized and transferred to 60mm dishes. Stable cell lines were obtained by selection with 200µg/ml of G418 for three weeks.

4.5.3. Extraction and Quantification of gDNA

To ensure the plasmid did not acquire mutations when integrated in the genome, gDNA was extracted for Sanger sequencing. The NZY Tissue gDNA Isolation Kit was used following instructions recommended by the manufacturer. gDNA concentration was determined using a NanoDrop.

4.5.4. Cellular Viability Assay

$1.5x10^5$ cells/well (BEAS-2B and NCI-H460 derived cell lines) were seeded in a 24-well plate. After 48h, cells were detached and equal volumes of cell suspension and trypan blue were mixed. Finally, cell viability (%) was obtained by counting the live and death cells using a TC10Tm Automated Cell Counter (Bio-Rad). This assay was performed with triplicates and repeated three times.

4.5.5. Cellular Proliferation Assay

To evaluate cellular proliferation, we used a colorimetric immunoassay ELISA, based on the measurement of BrdU incorporation during DNA synthesis (Roche, Cat.11647229001), following the manufacturer's instructions. $5x10^3$cells/well (BEAS-2B and NCI-H460 derived cell lines) were plated in a 96-well and analysis was performed after 48h.

4.5.6. Anchorage-Dependent Colony Formation Assay

300 cells per condition were seeded in 60mm dishes and maintained in culture for two weeks (BEAS-2B derived cell lines) or 9 days (NCI-H460 derived cell lines). The colonies were then fixed using ice cold methanol and incubated at -30ºC for 30min. Methanol was removed and a solution of 0.1% crystal violet in 20% methanol was added and the plates were incubated at room temperature for 30min. Plates were washed with H_2O milliQ to remove excess dye and the colonies were counted. This assay was performed in triplicates and repeated four times.

4.5.7. Protein synthesis rate determination

To determine protein synthesis rate, we used a non-reactive fluorescence-activated cell sorting-based assay called SUnSET, with few modifications. $1x10^6$cells were plated in 60mm petri dishes and after 48h, 10% v/v puromycin (Sigma Aldrich) was added to each plate. Cells were then incubated for 15 min. Total protein lysates were obtained from cells with Lysis Buffer (0.5% Triton X-100, 50mM HEPES, 250mM NaCl, 1mM DTT, 1mM NaF, 2mM EDTA, 1mM EGTA, 1mM PMSF, 1mM Na3VO4 supplemented with a cocktail of protease inhibitors (Roche). Cells were sonicated with a probe sonicator in 5 pulses of 5 seconds. After centrifugation at 16000g for 30min, protein in the supernatants was quantified using the BCA assay (Thermo Fisher Scientific). 100 µg of protein was denaturated with loading buffer (6x) at 95ºC for 5 min, resolved in 10% SDS-PAGE and blotted onto nitrocellulose membranes (0.2µm) (GE Healthcare Life Sciences). Anti-puromycin, clone 12D10 (kindly given by Philippe Pierre) was used (1:2500) to detect the incorporation of puromycin in proteins. IRDye800 goat anti-mouse secondary antibody (Li-cor Biosciences, Cat.400-33) was used (1:10000 dilution) and detected in an Odyssey Infrared Imaging System (Licor Biosciences). Membranes were also probed with Anti-GAPDH (Santa Cruz Biotechnology) (1:1000) as a loading control.

4.5.8. Immunoblots

Total protein lysates were obtained with the same extraction method used with the SUnSET assay. 40µg of protein were immunoblotted onto nitrocellulose membranes with antibodies against eIF2α (1:1000; Cell signalling); phospho-eIF2α (1:1000; Abcam); ATF6 (1:400; Stressgen); GADD34 (1:1000 ThermoFisher Scientific);

phospho-ATF4 (1:1000; tebu-bio); ATF4 (1:1000; tebu-bio) and β-tubulin (1:1000; Invitrogen). IRDye680 goat anti-rabbit or IRDye800 goat anti-mouse secondary antibodies (1:10000, Li-cor Biosciences) were used and the signal was detected using an Odyssey Infrared Imaging system (Li-cor Biosciences).

4.5.9. Tumor induction assay

Six-week-old male N:NIH(s)II:nu/nu nude mice were obtained previously from the Medical School, University of Cape Town in 1991 and then reproduced, maintained and housed at IPATIMUP Animal House at the Medical Faculty of the University of Porto, in a pathogen-free environment under controlled conditions of light and humidity. Male nude mice, aged 6-8 weeks, were used for *in vivo* experiments. Animal experiments were carried out in accordance with the Guidelines for the Care and Use of Laboratory Animals, directive 2010/63/EU. To measure tumorigenic potential *in vivo*, BEAS-2B cell lines harboring the empty vector (Mock), the $tRNA^{Ser}$(WT) and the misreading $tRNA^{Ser}$(Ala) were subcutaneously injected in the dorsal flanks using a 25-gauge needle with $4.5x10^6$ (BEAS-2B) of each cell line. A total of 4 mice per group were used. Each mouse was injected in the left flank with the Mock variant and in the right flank with the cells misexpressing the WT or the misreading variants of each previously described clone. Mice were weighed, and tumor width and length were measured with calipers three times per week. Tumor volumes were calculated assuming ellipsoid growth patterns. Mice were humanely euthanized when tumors reached a median volume of $2000mm^3$ or whenever any signs of disease were detected. Tumors and lungs, were collected, fixed in 10% buffered formalin, paraffin embedded and then sectioned for histological examination. A part of each tumor was frozen in liquid nitrogen and stored at –80ºC until used.

4.5.10. Statistical analysis

For all the assays, except for the *in vivo* experiments, our data represents 3 independent biological replicates and 3-4 independent experiments. Average values are usually shown and error bars represent the standard error of the mean (SEM). Statistical significance was determined using One-way ANOVA with Dunnet's post-test; Kruskal-Walis with Dunnet's post-test or Two-Way ANOVA for the *in vivo* experiments.

5. tRNA deregulation modulates cell migration and increases cell invasion potential

5.1. Abstract

Overexpression of certain tRNAs has been associated with increased migration potential and metastization, through differential translation of mRNAs enriched in specific codon sets. However, overexpression of some tRNAs may cause amino acid misincorporation into proteins, creating high proteome heterogeneity, whose consequences for cancer biology are poorly understood. In previous works, we observed that elevated expression of Wild Type (WT) Ser tRNAs or misincorporation of Ser at Ala codon sites influence tumor behavior. To further clarify the role of this phenomena in tumor biology, we expressed these tRNAs in Non-Small Cell Lung Cancer (NSCLC) cells and characterized their potential to modulate cell migration, invasion and metastization. Upregulation of $tRNA^{Ser}$(WT) but not expression of $tRNA^{Ser}$(Ala) increased cell proliferation *in vitro*. Both tRNA constructs accelerated tumor growth kinetics, however $tRNA^{Ser}$(Ala) expressing tumors grew slightly faster than $tRNA^{Ser}$(WT) expressing tumors, which can partially be explained by reduced levels of eIF2α-P and upregulation of GADD34. Also, tumors expressing both tRNA constructs showed upregulation of BiP and activation of ATF4, which has been correlated with high grade NSCLC tumors. Expression of the misreading $tRNA^{Ser}$(Ala) increased cell migration potential, whereas overexpression of $tRNA^{Ser}$(WT) impaired cell migration potential, showing that these tRNA constructs may have different impacts on cell biology. Despite the fact that both tRNA constructs increased the local invasion potential of H460 cells, the results obtained in the *in vivo* metastization assay were inconclusive due to high dispersion of data.

5.2. Introduction

Deregulation of tRNAs in tumors or tumor-support cells imposes important cellular reprogramming events that sustain tumor growth and disease progression [13,15]. This has been associated with increased translation of specific transcripts which are enriched in codons matching the anticodons of such tRNAs [13]. For instance, $tRNA^{Glu}$UUC and $tRNA^{Arg}$CCG upregulation occurs in metastatic breast cancer cell lines relatively to their non-metastatic counterparts. The upregulation of these tRNAs increase the translational efficiency of disease-promoting transcripts, shifting the proteome towards a pro-metastatic state [13]. Also, upregulation of $tRNA_iMet$ in support or tumor cells can favor disease progression through different molecular mechanisms. In support fibroblasts, the upregulation of this tRNA induces secretion of collagen type II,

which favors endothelial cell migration, angiogenesis and tumor growth [14], whereas its upregulation in melanoma cells promotes cell migration, invasion and increased metastatic potential without affecting proliferation and growth of the primary tumor [15].

The upregulation of Ser tRNAs has been associated with poor prognosis in several types of cancer (YM500v3 database)[9], suggesting that such tRNAs are important to achieve disease progression. The over-representation of some tRNAs can induce near-cognate codon misreading, originating protein missense errors (mistranslation) [51] that increased in tumor samples relative to normal tissue (Chapter 3). Interestingly, misincorporation of Ser at Ala protein sites is one of the most abundant missense errors in the proteome of tumor cells (Chapter 3). Such mistranslation can result in the accumulation of aberrant misfolded proteins, which in turn activate the proteome quality control (PQC) system, increasing protein refolding capacity, protein degradation or protein delivery to distinct quality control compartments that sequester potentially harmful misfolded species [137]. Accumulation of misfolded proteins in the Endoplasmic Reticulum (ER) they sequester the molecular chaperone BiP (or GRP78) [138], activating the Unfolded Protein Response (UPR) effectors PERK, ATF6 and IRE1α [113], and inducing a pro-survival signaling program that can be used by cancer cells cancer cells to survive and thrive [139–142]. The PERK branch of the UPR is specially interesting because it can modulate protein synthesis rate, induce the transcription of stress response genes and activate protein degradation systems, such as the proteasome or autophagy [144,145,150,160,161]. Increased ability to degrade misfolded proteins is essential for tumor initiation and maintenance. This involves the upregulation of the proteasome through PERK-dependent Nrf2 activation [150,160]. Furthermore, ATF4 activation through phosphorylation of eIF2α, activates autophagy [161]. This transcription factor induces the transcription of various autophagy genes, including *Atg16l1, Map1lc3B, Atg12, Atg3, Atg7, Becn1, Gabarapl2*. The latter alone or in combination with one of its targets, CHOP, also induces the transcription of *p62, Nbr1 and Atg7* [161]. Autophagy is essential for cancer cells to recycle damaged organelles, macromolecules and protein aggregates that may originate from misfolded proteins [162]. However, its role in cancer is highly context dependent, as it is required for Ras-mediated tumorigenesis, but it can delay disease onset in a pancreatic cancer model [163,164]. In pancreatic cancer it is instead required for tumor maintenance and progression [164]. Autophagy regulates the metastization process from its initial steps (cell migration and local invasion) and also promotes the survival of disseminating tumor cells in circulation, as well as the survival

of stem-like subpopulations of tumor cells, which drive the colonization at distant sites [165–167]. Hence, we can conclude that the PERK branch of the UPR is relevant for disease progression.

In this work, we tried to clarify the role of deregulating a WT Ser-tRNA and inducing Ser misincorporation at Ala codons in tumor progression and also studied the contribution of the PERK branch of the UPR in this context. To do so, we increased the expression of a WT Ser tRNA and also expressed a mutant Ser tRNA that misreads Ala codons in a large cell carcinoma cell line, NCI-H460. We found that elevated expression of the WT Ser-tRNA increased cellular proliferation *in vitro*, which did not happen in cells expressing the misreading $tRNA^{Ser}$(Ala). Both tRNAs increased tumor growth kinetics *in vivo,* but presented differential modulation of the PERK branch of the UPR. tRNA misreading showed positive impact on cell migration and local invasion, but the results from the metastization assay were inconclusive.

5.3. Results

5.3.1. Deregulation of the tRNA pool increases cell proliferation

Our previous results showed that tRNAs are involved in tumor growth, and possibly in tumor initiation, but their effect on tumor progression was not clarified. For this, we expressed the misreading $tRNA^{Ser}$(Ala), and overexpressed the Ser tRNA in a cell line derived from a large cell carcinoma, NCI-H460 (henceforth H460). To exclude transfection specific effects, we established three independent stable cell lines for each condition (**Fig.5-1A,B**).

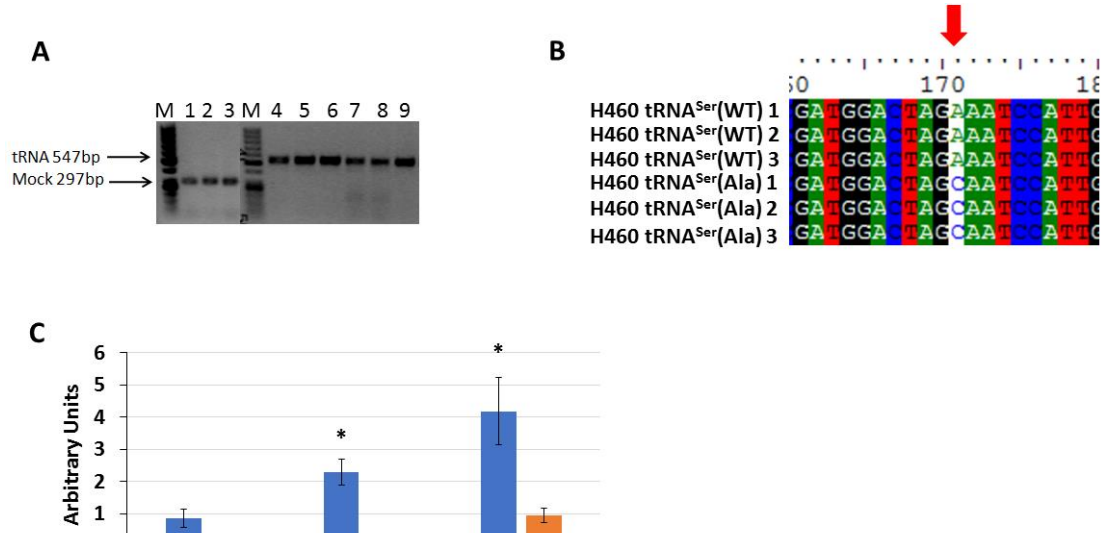

Figure 5-1: Integration of the pIRES2-DsRed and recombinant tRNA genes in the cell lines. (A) Agarose gel (1%) of the PCR product obtained by amplification of genomic DNA from cell lines across the fragment of pIRES2-DsRed plasmid containing the tRNA gene insert. Legend: M – Molecular Marker; 1, 2, 3 – H460 Mock 1, 2 and 3, respectively; 4, 5, 6 – H460 tRNA^{Ser}(WT) 1, 2 and 3, respectively; 7, 8 and 9 H460 tRNA^{Ser}(Ala) 1, 2 and 3, respectively. **(B)** Sanger sequencing of the PCR products showing the WT anticodon of the tRNA (AGA) in tRNA^{Ser}(WT) cell lines and the mutated anticodon (AGC) in the tRNA^{Ser}(Ala) cell lines, indicated by the red arrow. **(C)** Quantification of tRNA expression by Snapshot sequencing. tRNAs were quantified based on a primer extension assay and values were normalized for the expression of GAPDH. tRNA^{Ser}(WT) expression increased 2.63-fold respective to the Mock cell line, and the expression of tRNA^{Ser}(Ala) was also detected. Interestingly expression of the WT Ser tRNA also increased in the tRNA^{Ser}(Ala) cell line by 4-fold. Graphic depict average ± SEM (n=3). Data was analysed with unpaired, two-tailed Student´s t-test with Welch correction and significant p-values are shown (*p<0.05).

Expression of the WT Ser tRNA was increased by 2.63-fold in H460 tRNA^{Ser}(WT) cell line when comparing to the Mock cell line (**Fig.5-1C**). The expression of the WT Ser tRNA expression was also increased in the H460 tRNA^{Ser}(Ala) cell line, suggesting that the expression of a specific tRNA can affect the expression levels of the others (**Fig.5-1C**). The misreading tRNA^{Ser}(Ala) was also successfully expressed in H460 cells and its expression levels are similar to that of the WT Ser tRNA in the Mock cell line (**Fig.5-1C**). Similarly to other published results, the viability of H460 cell lines stably expressing the recombinant tRNAs was not altered (**Fig.5-2**).

Elevated expression of the WT Ser tRNA increased cellular proliferation rates by 1.34-fold (p<0.05), but expression of the misreading tRNA^{Ser}(Ala) had no impact on cellular proliferation (**Fig.5-3A**). Since overexpression of the WT Ser tRNA increased cell proliferation, we checked if protein synthesis rate was also upregulated, but no difference was observed, suggesting that other mechanisms may be involved in this phenotype (**Fig.5-3B,C**).

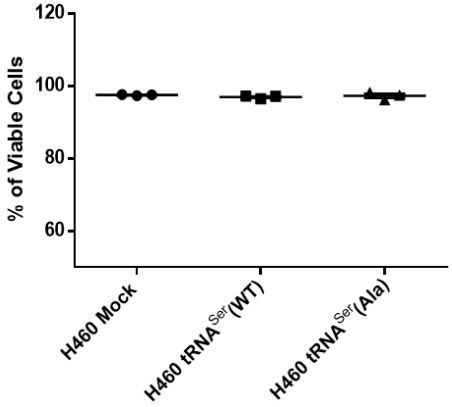

Figure 5-2: Stable expression of recombinant tRNAs do not impact on cell viability. Cells were grown for 48h and then stained with trypan blue (0.4%). Cell viability of H460 derived cell lines (n=3, with 4 technical replicates) did not change in the three conditions tested. Graphics depict the percentage of viable cells ±SEM. Data was analyzed with One-way ANOVA and Holm Sidak's post-test ($p>0.05$).

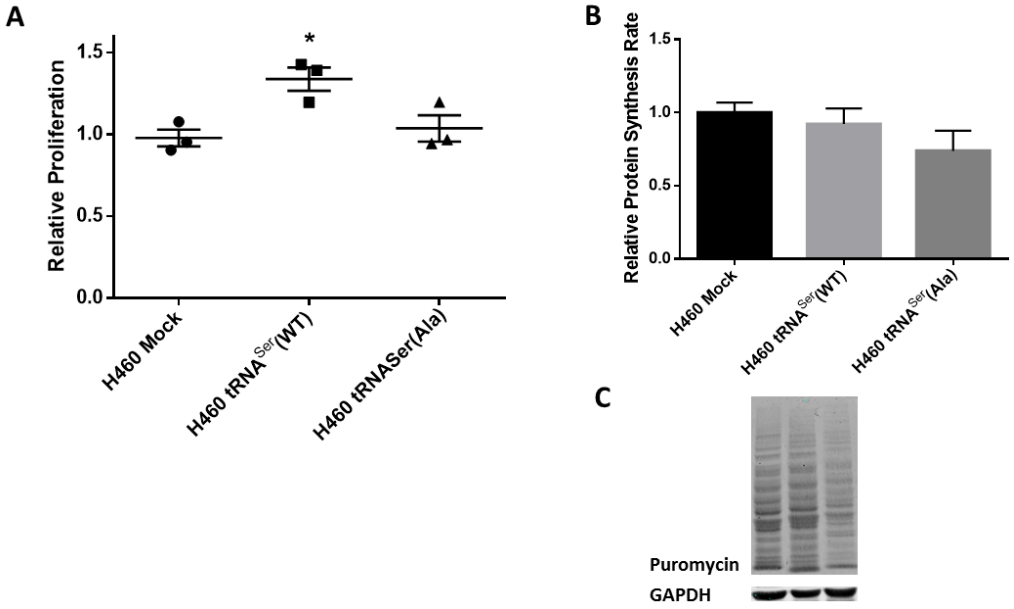

Figure 5-03: Expression of tRNA^{Ser}(WT) increases cell proliferation without altering protein synthesis rate. (A) To evaluate cellular proliferation, $5x10^3$cells/well were plated in a 96-well plate and BrdU incorporation during DNA synthesis was measured using a colorimetric immunoassay after 48h of incubation. Relative proliferation of H460 derived cell lines – Only expression of tRNA^{Ser}(WT) increased proliferation of a tumorigenic cell line in vitro. **(B)** Expression of recombinant tRNAs did not influence protein synthesis rate in H460-derived cell lines **(C)** Protein synthesis rate was estimated by immunoblot against puromycin. From left to right, H460 Mock, H460 tRNA^{Ser}(WT) and H460 tRNA^{Ser}(Ala). GAPDH was used as a protein loading control. Graphics depict average ±SEM of n=3, with 3 technical replicates. Data was analyzed with One-way ANOVA and Holm Sidak's post-test and significant p values are shown (*$p<0.05$).

5.3.2. Recombinant tRNA expression did not alter in vitro transformation ability of H460-derived cell lines

Regarding modulation of transformation ability *in vitro*, no changes were observed in the H460-derived cell lines expressing the recombinant tRNAs. This may be explained by the fact that this cell line is already tumorigenic and has high colony formation efficiency (**Fig.5-4**).

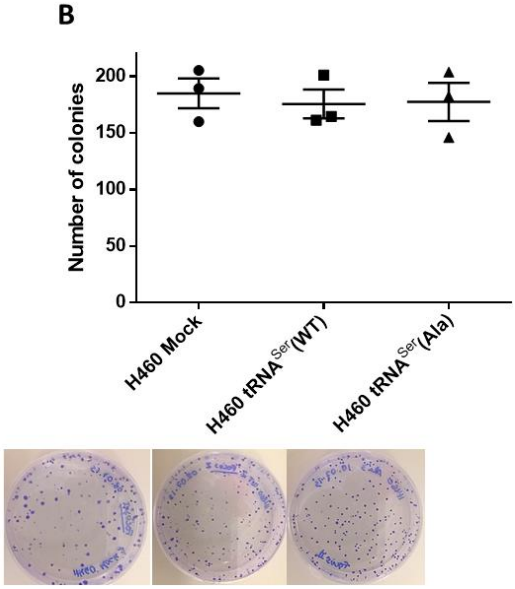

Figure 5-4: Expression of recombinant tRNAs did not produce any effects on colony formation on H460-derived cell lines. Graphic depict average ±SEM of n=3, with 3 technical replicates. Data was analyzed with One-way ANOVA and Holm Sidak's post-test ($p>0.05$).

5.3.3. Recombinant tRNAs accelerate tumor growth kinetics in an already tumorigenic cell line

To clarify whether the recombinant tRNAs influenced tumor growth kinetics in a tumorigenic cell line, we inoculated H460-derived cell lines expressing our tRNA genes in the right dorsal flank of nude mice. Four mice were injected in the left flank with the Mock variant and in the right flank with cells overexpressing the WT or the misreading tRNA variants. Three mice were double inoculated with the same cell line in both flanks to rule out influence of one tumor over the other. Both tRNA constructs accelerated tumor growth kinetics (**Fig.5-5A**) and the experiment was humanely terminated 14 days after inoculation, since the combined volume of both tumors in most mice had reach 2000mm^3. tRNA^{Ser}(Ala) expressing tumors started growing sooner that the other tumors and were the most homogeneous group of tumors of the experiment. At the end of the experiment these tumors were 1.7-fold bigger than the Mock tumors ($p<0.001$). Also, at

day 14 tRNA^{Ser}(WT) expressing tumors were 1.35-fold bigger than the Mock tumors and (p<0.05) (**Fig.5-5A,B**).

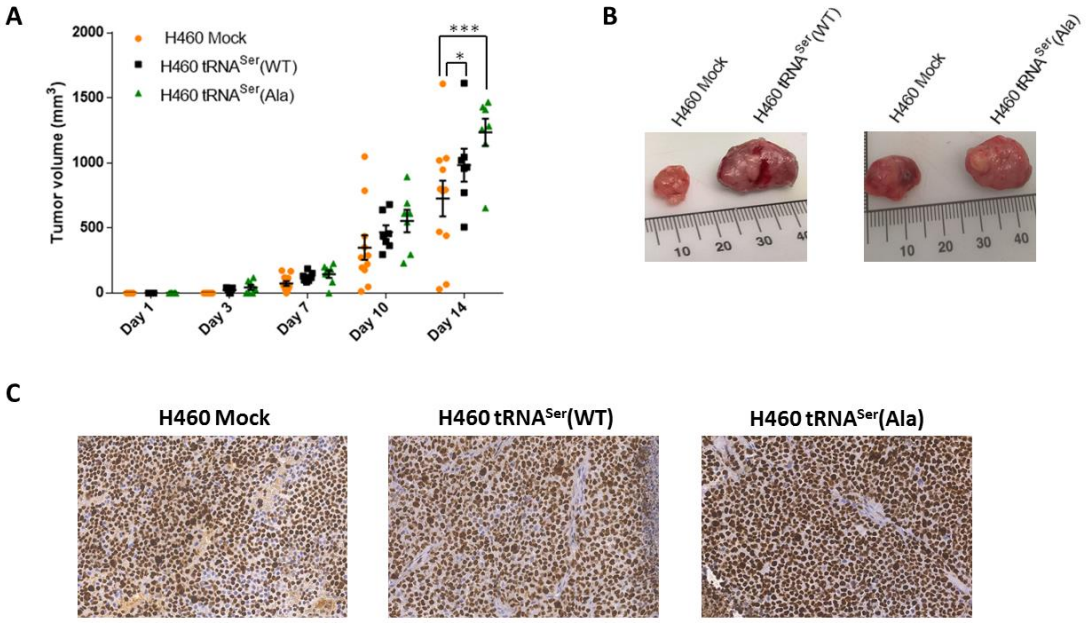

Figure 5-5: Impact of mistranslation on tumor growth kinetics in vivo. A) Kinetics of tumor growth determined after inoculation of cells expressing Mock plasmid, the tRNA^{Ser}(WT) and tRNA^{Ser}(Ala) constructs. At day 14 post-inoculation both tRNA constructs increased tumor kinetics of a tumorigenic cell line. In the graphic each point represents the volume of an individual tumor and the error bar depicts the average ± SEM. Data was analyzed by Two-way ANOVA and significant p values are shown (n=7-11) (*p<0.05; **p<0.01) **B)** Representative photographs of paired tumors derived from the same animal. **C)** Photographs of representative Ki67 staining (40x amplification) from each condition.

Histological analysis revealed that the tumors from each condition are very similar with epithelial-like cell morphology, present rare vascular invasion and have identical mitotic indexes. Ki67 staining demonstrated that the tumors are very proliferative in all conditions, with more than 95% of the cells being labeled (**Fig.5-5C**). Neither condition produced distant metastasis, which may be related to the short duration of the experiment. Therefore, both tRNA deregulation and mistranslation can influence tumor cell behavior *in vivo*, producing tumors that grow faster than those produced by the control cells.

5.3.4. Tumors expressing heterologous tRNAs show differences in UPR activation

Our previous studies showed that tumors derived from a near-normal cell line expressing the same heterologous tRNAs differentially activated the UPR. Here, we assessed the expression levels of BiP in these tumors and observed a 2-fold increase in both the tumors expressing the tRNA^{Ser}(WT) and the tRNA^{Ser}(Ala) constructs (p<0.05)

(**Fig.5-6A**). Similarly to previous results, the levels of eIF2α-P decreased by 24% (p<0.05), only in the tumors harboring the $tRNA^{Ser}$(Ala) construct relative to Mock tumors (**Fig.5-6B,E**). We hypothesized that the differences in the phosphorylation of eIF2α observed in the different tumors could be due to differential activation of the ATF4 transcription factor or its downstream targets. The ATF4 transcription factor was activated by 1.23- and 1.29-fold in $tRNA^{Ser}$(WT) and $tRNA^{Ser}$(Ala) expressing tumors (p<0.05), respectively, relative to the Mock tumors (**Fig.5-6C,E**). Since ATF4 was activated in tumors expressing both tRNA constructs, we studied the expression of GADD34, the regulatory subunit of PP1α, and direct target of ATF4. Its expression was increased in $tRNA^{Ser}$(Ala) expressing tumors by 5.34-fold relative to Mock tumors (p<0.01) (**Fig.5-6D,E**), supporting the results for the results obtained for eIF2α phosphorylation observed in these tumors (**Fig.5-6B,E**).

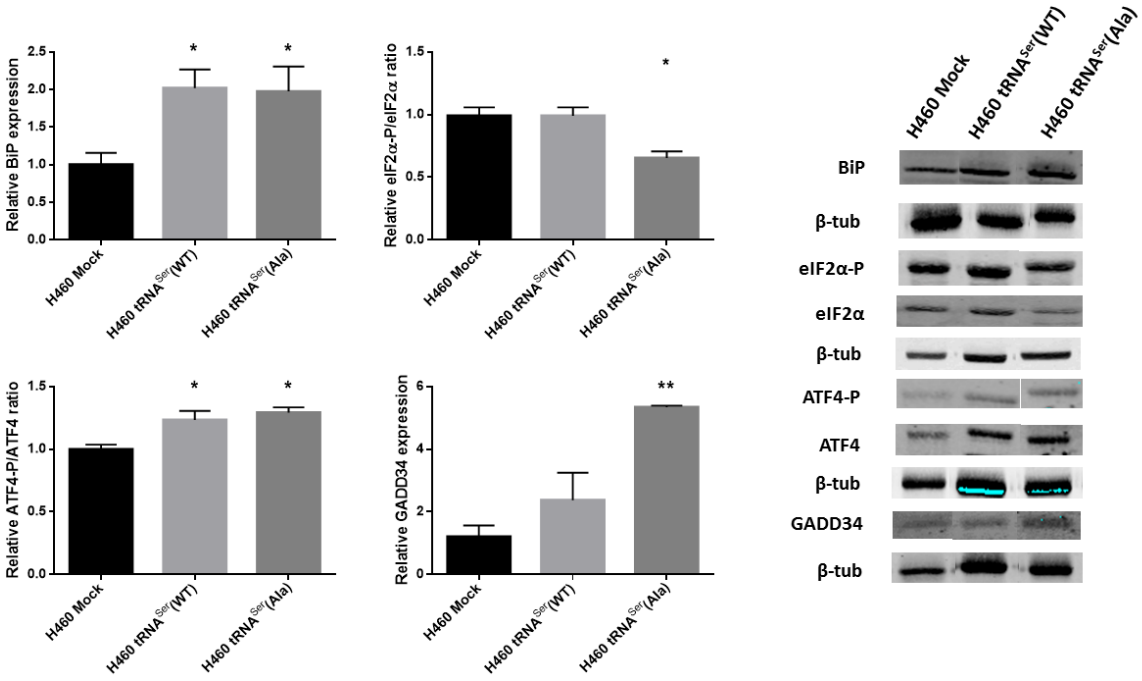

Figure 5-6: UPR modulation in H460 tumors. (A) Expression of tRNA^{Ser}(WT) and tRNA^{Ser}(Ala) increases BiP expression on H460 tumors. **(B)** Levels of eIF2α-P were reduced in tRNA^{Ser}(Ala) expressing tumors. **(C)** tRNA^{Ser}(WT) and tRNA^{Ser}(Ala) expression in H460 tumors increased the activation of ATF4 transcription factor. **(D)** Expression of GADD34 was only increased in H460 tRNA^{Ser}(Ala) tumors. **(E)** Immunoblots against BiP, eIF2α-P, eIF2α, ATF4-P, ATF4 and GADD34. β-tub served as protein loading control. Graphics depict average ± SEM (n=3), with 3 technical replicates. Data was analyzed with One-way ANOVA and Holm Sidak's post-test and significant p values are shown (*p<0.05; **p<0.01).

5.3.5. Local invasion is affected by heterologous tRNA expression

Since expression of certain tRNAs induces cell migration, we wanted to clarify if this phenotype was induced by mistranslation or by tRNA upregulation. We evaluated the migration potential of these cells with a wound healing assay and determined the area covered by cells in 12h intervals up to 48h after removing the wound insert. For the tRNA^{Ser}(Ala) expressing cell line, we observed an increase in cell migration from 12h after the insert was removed until the end of the assay (p<0.001) (**Fig.5-7A,B**). However, upregulation of the tRNA^{Ser}(WT) reduced the migration potential of H460 cells after 24h (p<0.01) (**Fig.5-7A,B**), showing a clear difference between the misreading tRNA and the upregulation of the WT tRNA. Concerning the extracellular matrix invasion, there was increased invasion potential in both cell lines, with 2.88- and 5.58-fold increase in tRNA^{Ser}(WT) (p<0.01) and tRNA^{Ser}(Ala) (p<0.001) expressing cell lines, respectively (**Fig.5-7C,D**).

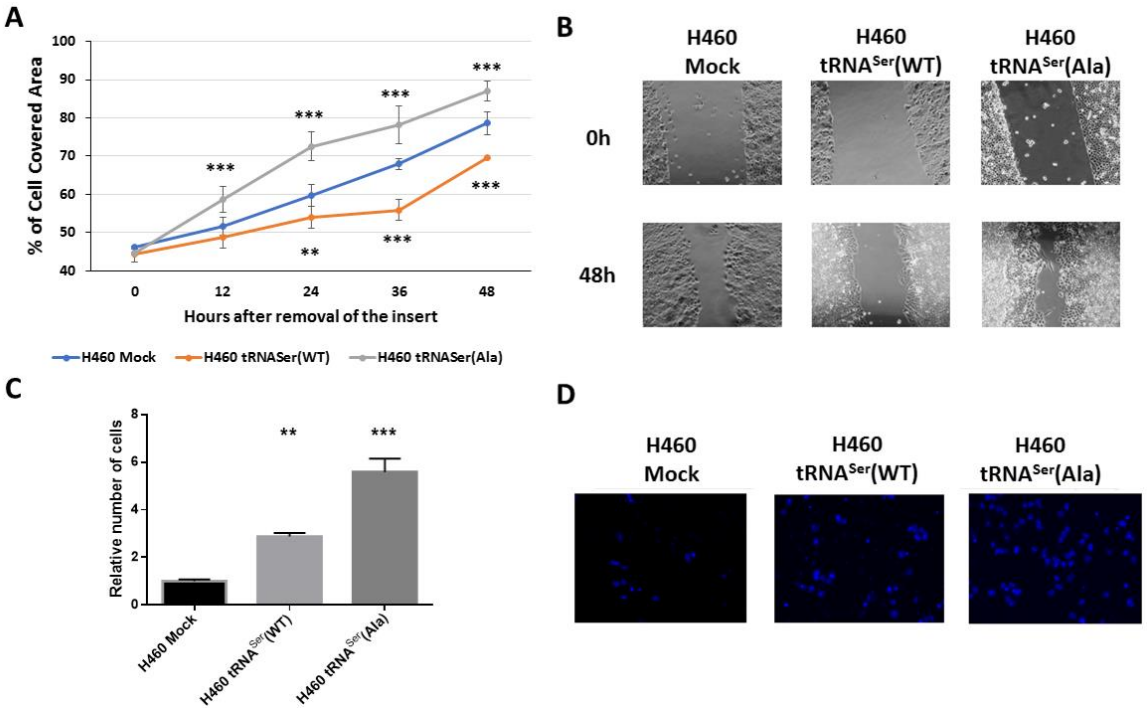

Figure 5-7: Expression of recombinant tRNAs increase local invasion potential of H460 cells. (A) Migration potential of cells was assessed by a Wound healing assay. The area covered by cells was evaluated at 12h intervals. Cell lines expressing $tRNA^{Ser}$(Ala) show increased migration potential, whereas cells expressing $tRNA^{Ser}$(WT) have decreased migration potential. Graph depicts average ± SEM of n=3, with 3 technical replicates. Data was analyzed by Two-way ANOVA and significant p values are shown (**p<0.01; ***p<0.001). **(B)** Representative pictures of the wounds at time of removal of the insert and 48h later for all cell lines (10x amplification). **(C)** The extracellular invasion capacity of the cell lines was evaluated by their capacity to invade matrigel-coated transwell inserts. Cells on the bottom of the insert were stained with DAPI and counted. Both $tRNA^{Ser}$(WT) and $tRNA^{Ser}$(Ala) constructs increased the invasion potential of H460 cells. **(D)** Representative photos of areas of the insert (20x magnification). Graph depict average ± SEM (n=3), with 2-3 technical replicates. Data was analyzed with One-way ANOVA and Holm Sidak's post-test and significant p values are shown (**p<0.01; ***p<0.001).

To clarify if our tRNAs affected disease progression, we performed a classic metastization assay by injecting $1x10^6$ cells in the tail vein of 5 nude mice per cell line. After 5 weeks the mice were humanely euthanized and lungs, lymph nodes and liver samples were collected for histological analysis. The lung data was highly dispersed for all the groups, with some mice having high metastization area and others showing little metastization in the lungs, among the mice from the same group (**Fig.5-8**). Therefore, this experiment needs to be repeated with higher number of mice and analysis of the liver and lymph nodes which were recovered from these mice.

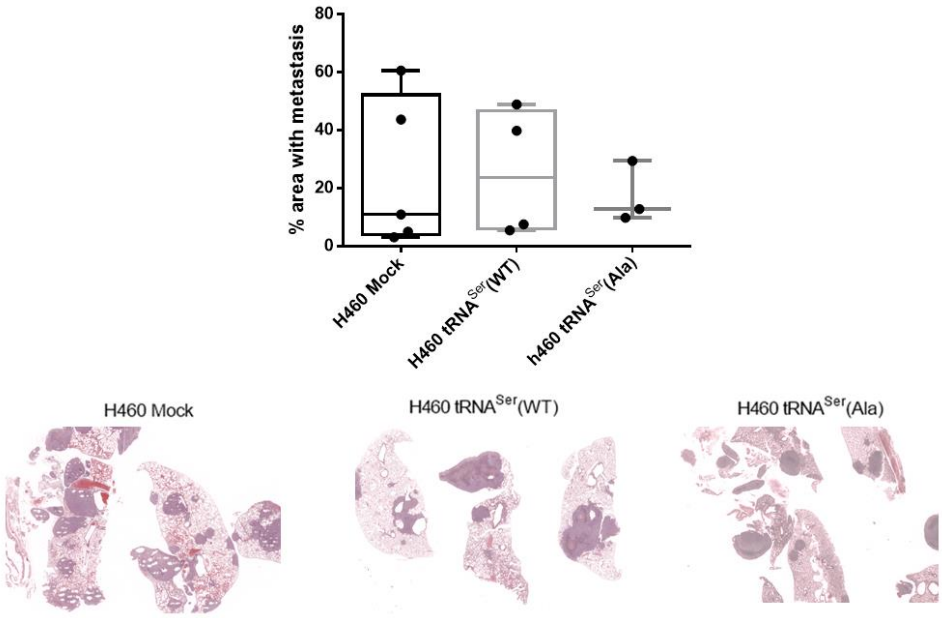

Figure 5-8 Impact of tRNA upregulation and misreading in tumor progression. (Upper panel) Graph depicts the area of the lung with metastasis. Each dot represents one animal. Box and whiskers represents min to max distribution and median is also represented in the box (n=3-5). Data was analysed with the Kruskal Wallis assay with Dunnett's post-test ($p>0.05$). **(Lower Panel)** Representative pictures of the lungs of the mice in each group.

5.4. Discussion

Our data show that deregulation of a WT Ser tRNA and expression of a misreading tRNA, increases tumor growth kinetics *in vivo*. The tumors expressing the misreading $tRNA^{Ser}$(Ala) appeared earlier and grew faster than $tRNA^{Ser}$(WT) tumors, likely due to dephosphorylation of the initiation factor eIF2α. As NIH3T3 cells expressing the same tRNAs, when inoculated in mice presented a similar behavior, we hypothesized that this may be caused by overexpression of GADD34 regulatory subunit (Chapter 3). The data presented in this chapter confirm this hypothesis since H460-derived tumors expressing $tRNA^{Ser}$(Ala), overexpressed GADD34 (5-fold upregulation), relative to the Mock tumors. The upregulation of the BiP chaperone was observed in tumors expressing the tRNA constructs and this was correlated in other studies with high grade NSCLC tumors [168], implying that tumors expressing the tRNA constructs may have a more aggressive phenotype. Additionally, activation of ATF4 suggests that autophagy is increased in tumors harboring both tRNA constructs [161]. Autophagy has been shown to be important not only for tumor maintenance, but also for disease progression [164,165].

We studied the early stages of the metastization process and observed that cells expressing the misreading $tRNA^{Ser}$(Ala) had increased migration and local invasion potential, relative to Mock cells. On the other hand, $tRNA^{Ser}$(WT) expressing cells showed impaired migration ability, but increased invasion potential, showing that these tRNAs induce different phenotypes in H460 cells. There are also similar phenotypes, but the pathways involved in these phenotypic alterations may be distinct and need to be clarified in future studies. The differences that we observed in cell migration also need to be clarified, but it is likely that they are related with differences in the transcripts that are decoded by these tRNAs. Indeed, upregulation of some tRNAs increases translation of transcripts that are enriched in their matching codons [13]. In other words, transcripts enriched in TCT codons, matching the AGA anticodon in the $tRNA^{Ser}$(WT), may be translated more efficiently, leading to alterations in cell migration.

Alanine residues mimic non-phosphorylated status of proteins [169]. Although phosphorylation is context specific [170], the insertion of Ser at Ala sites has the potential to activate signaling pathways that were otherwise silent and may affect cell migration ability. Interestingly, both tRNA constructs were able to increase extracellular matrix invasion in these cells. To clarify these mechanisms we will have to identify the proteins that contain amino acid misincorporations and map them to specific biological processes. Ribosome profiling coupled with ribo-seq may also provide clues about the fraction of the translatome that is affected in these cells. Potential targets will then be validated by decreasing their expression with siRNAs. Additionally, other branches of the UPR should also be monitored since IRE1α has also been implicated in cell invasion and its activation may help to further characterize our cell models [171]. The proteasome activity and autophagy are likely altered and should also be monitored in future studies.

5.5. Materials and Methods

5.5.1. Cell Culture

NCI-H460 were obtained from the American Type Culture Collection (ATCC) and were cultured in RPMI 1640 medium (Gibco, Life Technologies), supplemented with 10% Fetal Bovine Serum (FBS) (Sigma) and 1% Pen/Strep. Cells were maintained in an incubator at 37ºC with 5% CO_2 and 95% relative humidity. To execute the following procedures, cells were detached using Tryple Xpress (Gibco, Life Technologies). Cells were regularly tested for the presence of mycoplasma.

5.5.2. Generation of stable cell lines

5.0 x 10^4 NCI-H460 cells were plated in MW24 plates, incubated for 48h and then were transfected using 1.5µg of plasmid DNA and 0.75µL of Lipofectamine® 3000 (Invitrogen). Three independent transfections were carried out for the empty vector (Mock), the plasmid containing an extra copy of the wild WT $tRNA^{Ser}_{AGA}$(WT) or the misreading $tRNA^{Ser}_{AGC}$(Ala). Stably transfected cells were obtained after three weeks of selection in 800µg/ml of G418.

5.5.3. Extraction and Quantification of gDNA

To ensure the plasmid did not acquire mutations when integrated in the genome, gDNA was extracted and Sanger sequenced. For that, the NZY Tissue gDNA Isolation Kit was used, following the recommended instructions. gDNA concentration was determined using the NanoDrop.

5.5.4. Cellular Viability Assay

1.5x10^5 cells/well were seeded in a 24-well plate. After 48h, cells were detached and equal volumes of cell suspension and trypan blue were mixed. Finally, cell viability (%) was obtained by counting the live and death cells using a TC10Tm Automated Cell Counter (Bio-Rad). This assay was performed in triplicates and repeated three times.

5.5.5. Cellular Proliferation Assay

To evaluate cellular proliferation, we used a colorimetric immunoassay ELISA, based on the measurement of BrdU incorporation during DNA synthesis (Roche, Cat.11647229001), following manufacturer's instructions. 5x10^3cells/well were plated in a 96-well and analysis was performed 48h later.

5.5.6. Anchorage-Dependent Colony Formation Assay

300 cells per condition were seeded in 60mm dishes and maintained in culture for 9 days. The colonies were then fixed using ice cold methanol and incubated at -30ºC for 30min. Methanol was removed and a solution of 0.1% crystal violet in 20% methanol was added and the plates were incubated at room temperature for 30min. Plates were washed with milliQ H_2O to remove excess dye and the colonies were counted. This assay was performed with triplicates and repeated four times.

5.5.7. Determination of Protein synthesis rate

To determine protein synthesis rate, we used a non-reactive fluorescence-activated cell sorting-based assay, called SUnSET with few modifications. $1x10^6$cells were plated in 60mm petri dishes and after 48h, 10% v/v puromycin (Sigma Aldrich) was added to each plate. Cells were then incubated for 15 min. Total protein lysates were obtained from cells with Lysis Buffer (0.5% Triton X-100, 50mM HEPES, 250mM NaCl, 1mM DTT, 1mM NaF, 2mM EDTA, 1mM EGTA, 1mM PMSF, 1mM Na3VO4) supplemented with a cocktail of protease inhibitors (Roche). Cells were sonicated with a probe sonicator in 5 pulses of 5 seconds. After centrifugation at 16000g for 30min, protein in the supernatants was quantified using the BCA assay (Thermo Fisher Scientific). 100 µg of protein was denaturated with loading buffer (6x) at 95ºC for 5 min, resolved in 10% SDS-PAGE and blotted onto nitrocellulose membranes (0.2µm) (GE Healthcare Life Sciences). Anti-puromycin, clone 12D10 (kindly given by Philippe Pierre) was used (1:2500) to detect the incorporation of puromycin in proteins. IRDye800 goat anti-mouse secondary antibody (Li-cor Biosciences, Cat.400-33) was used (1:10000 dilution) and detected in an Odyssey Infrared Imaging System (Licor Biosciences). Membranes were also probed with Anti-GAPDH (Santa Cruz Biotechnology) (1:1000) as a loading control.

5.5.8. Immunoblots

Total protein lysates were obtained with the same extraction method used with the SUnSET assay. 40µg of protein were immunoblotted onto nitrocellulose membranes with antibodies against eIF2α (1:1000; Cell signalling); phospho-eIF2α (1:1000; Abcam); ATF6 (1:400; Stressgen); GADD34 (1:1000 ThermoFisher Scientific); phospho-ATF4 (1:1000; tebu-bio); ATF4 (1:1000; tebu-bio) and β-tubulin (1:1000;

Invitrogen). IRDye680 goat anti-rabbit or IRDye800 goat anti-mouse secondary antibodies (1:10000, Li-cor Biosciences) were used and the signal was detected using an Odyssey Infrared Imaging system (Li-cor Biosciences).

5.5.9. Tumor induction assay

Six-week-old male N:NIH(s)II:nu/nu nude mice were previously obtained from the Medical School, University of Cape Town in 1991 and then reproduced, maintained and housed at IPATIMUP Animal House, at the Medical Faculty of the University of Porto, in a pathogen-free environment under controlled conditions of light and humidity. Male nude mice, aged 6-8 weeks, were used in the *in vivo* experiments. Animal experiments were carried out in accordance with the Guidelines for the Care and Use of Laboratory Animals, directive 2010/63/EU. To measure tumorigenic potential *in vivo*, H460 cell lines harboring the empty vector (Mock), the $tRNA^{Ser}$(WT) and the misreading $tRNA^{Ser}$(Ala) were subcutaneously injected with $1x10^6$ cells in the dorsal flanks using a 25-gauge needle. A total of 7 mice per group were used. Four mice were injected in the left flank with the Mock variant and in the right flank with the cells misexpressing the WT or the misreading variants of each previously described clone. Three mice were double inoculated with the same cell line in both flanks to rule out influence of one tumor over the other. Mice were weighed, and tumor width and length were measured with calipers three times per week. Tumor volumes were calculated assuming ellipsoid growth patterns. Mice were humanely euthanized when tumors reached a median volume of $2000mm^3$ or whenever any signs of disease were detected. Tumors and lungs, were collected, fixed in 10% buffered formalin, paraffin embedded and then sectioned for histological examination. A part of each tumor was frozen in liquid nitrogen and stored at –80ºC until used.

5.5.10. Ki67 immunohistochemistry

Tumor sections obtained from mice tumors were de-paraffinized, re-hydrated with graded ethanol and washed in distilled water followed by PBS. Heat induced antigen retrieval was performed using 0.01M citrate buffer, pH 6.0, for 40 min. To block endogenous peroxidase activity, slides were treated with 0.5% H_2O_2 in methanol, for 20 min at room temperature (RT). To block non-specific binding, slides were exposed to large volume of ultra V block solution (LabVision), for 30 min at RT. Slides

were subsequently incubated with rabbit monoclonal antibody against Ki67 (clone SP6; Thermo Scientific) at 1:400 in large volume ultra Ab dilution (Lab Vision), for 2h at RT. After washing, sections were incubated with the Envision detection system peroxidase/DAB (Dako) followed by hematoxilin staining using the standard protocol.

5.5.11. Wound Healing Assay

2 well Culture-inserts (ibidi) were fixed in the bottom surface of 24-well plates. A cell suspension of 2.5 $x10^5$/ml was added to each well and after 24h, when cells were forming a confluent monolayer, the insert was removed leaving a gap of approximately 500µM between the cells. Fresh medium was added and photos were taken every 12h to monitor cell migration.

5.5.12. Invasion Assay

$1x10^5$ cells were ressuspended in RPMI 1640 without supplements and then seeded on top of a transwell insert (8µM pores, Corning) coated with Matrigel. Media supplemented with 10% FBS was added to the bottom of the transwell insert to act as chemoattractant. After 24h the matrigel and the cells on top of the membrane were removed with a cotton swab. The cells on the bottom of the membrane were fixed with methanol and the nuclei were stained with DAPI. The number of cells present in 5 fields/chamber were then counted in a fluorenscence microscope.

5.5.13. in vivo Metastization

$1x10^6$ cells of H460-derived cell lines were injected in the tail vein of six-week-old male N:NIH(s)II:nu/nu nude mice. A total of 5 five mice were randomized and used in each group in a total of 3 groups. Each group was injected with a different cell line (H460 Mock, H460 $tRNA^{Ser}$(WT) or H460 $tRNA^{Ser}$(Ala)). We monitored the weight of the animals at least twice a week and after 5 weeks we humanely euthanized the animals. Lungs, liver and lymph nodes were collected, fixed in 10% buffered formalin, paraffin embedded and then sectioned for histological analysis where the total metastization area was evaluated.

5.5.14. Statistical analysis

For all the assays, except for the *in vivo* experiments, our data represents 3 independent biological replicates and 3-4 independent experiments. Average values are usually shown and error bars represent the standard error of the mean (SEM). Statistical significance was determined using One-way ANOVA with Holm's Sidak post-test; Kruskal-Wallis with Dunnet's post-test or Two-Way ANOVA for the *in vivo* experiments.

6. tRNA deregulation reduces tumor sensitivity to cisplatin

6.1. Abstract

Non-Small Cell Lung Cancer is responsible for many cancer-related deaths worldwide, due to late stage diagnosis and disease recurrence after therapy. Although novel therapies have been developed recently, patients are normally treated with platinum-based drugs. The resistance mechanisms to cisplatin involve several non-overlapping molecular pathways that allow cancer cells to reduce the amount of drug in the cell, inhibit apoptosis, and upregulate pro-survival pathways, such as the Akt-pathway. Alterations in the unfolded-protein response (UPR), levels of molecular chaperones and autophagy mediators, also reduce tumor cell sensitivity to cisplatin effects. Mistranslation is a phenotype that has been associated with cellular adaptation to stressful environments, as well as antibiotic and antifungal resistance in *Candida albicans* and *Mycobacteria*, raising the hypothesis that it may also play a role in cancer therapy resistance. In the previous chapters of this thesis, we observed that a non-small cell lung cancer cell line (H460), known to be resistant to conventional chemotherapy, displayed UPR deregulation (Chapter 5) and increased misincorporation of Serine at Alanine sites (Chapter 3), suggesting that resistance to cisplatin (CDDP) may be correlated with UPR dysfunction, amino acid misincorporation or tRNA-pool deregulation. In fact, the mistranslating cells (expressing $tRNA^{Ser}$(Ala)) showed reduced sensitivity to both cisplatin and carboplatin *in vitro*, while cells with upregulation of the $tRNA^{Ser}$(WT) were only resistant do carboplatin, relative to Mock control cells. Our *in vivo* data demonstrate that tumors overexpressing the $tRNA^{Ser}$(WT) were more resistant to CDDP *in vivo* than Mock tumors, and that $tRNA^{Ser}$(Ala) expressing tumors also did not respond to CDDP treatment. This chapter highlights a new putative mechanism of CDDP resistance mechanism mediated by tRNAs.

6.2. Introduction

Cancer mortality is mainly fueled by tumor heterogeneity and by the acquisition of mechanisms that enable tumor cells to resist therapy over time. The known mechanisms by which tumor cells acquire drug resistance are drug inactivation, drug target alteration, drug efflux, DNA damage repair, cell death inhibition, epithelial-mesenchymal transition and epigenetic modifications [89]. However, in the vast majority of the patients treated with chemotherapy, the mechanisms through which tumor cells develop multi-drug resistance is still unclear [172]. Resistance to therapy is generally classified as intrinsic if the tumor does not respond to the first line of treatment,

indicating pre-existing resistance mechanisms in tumor cells; or acquired, if the disease progresses after an initial response [173].

Non-Small Cell Lung Cancer (NSCLC) is usually diagnosed in advanced stages and the 5-year overall survival of the patients is just 10-15%, still being the non-gender specific cancer responsible for the majority of cancer-related deaths worldwide [174]. NSCLC pathogenesis is not yet fully understood and further efforts are needed to characterize the disease from a molecular point of view to identify novel potential targets for therapy. Patients diagnosed with NSCLC normally undergo surgery to remove the primary tumor and receive adjuvant chemotherapy, because 30-55% of patients relapse after curative resection due to the presence of undetectable micrometastasis or circulating tumor cells [175]. Cytotoxic chemotherapy regiments in NSCLC normally combine two different drugs: usually one platinum derived drug (most often cisplatin) and paclitaxel, etoposide, vinblastine, gemcitabine, pemetrexed, vinorelbine, or docetaxel [176–181].

Several targeted therapies were developed to improve patient Overall Survival (OS), in subsets of patients which have tumors with specific mutations, most often mutations in the epidermal growth factor receptor (*EGFR*). EGFR is overexpressed in up to 40-80% of NSCLC and can be activated by either increased expression of the receptor, production of excess ligand or activating mutations of *EGFR* within malignant cells. EGFR activates the PI3K/AKT and RAS/RAF/MAPK pathways, inducing the expression of genes responsible for increased cell survival, proliferation, angiogenesis, invasion and metastasis [182,183]. The activating mutations can be targeted by small Tyrosine Kinase Inhibitors (TKI) (gefitinib or erlotinib) or using antibodies (cetuximab) [184]. Although the tumors initially respond to these drugs, most patients will relapse either through secondary *EGFR* mutations (most common mechanism) or activation of EGFR-independent pathways to circumvent EGFR inhibition [185]. However, 30% of the mechanisms which lead to resistance are still unknown [186].

Other targeted therapies to specific gene alterations in NSCLC were also developed. Rearrangements, activating point mutations or gene amplification of anaplastic lymphoma kinase (*ALK*) were identified in 2% to 7% of NCSLC, in the absence of *KRAS* and *EGFR* mutations and are targeted with small TKIs (crizotinib, ceritinib and alectinib) [187,188]. The overexpression of the vascular endothelial growth factor (VEGFA) is related to poor prognosis and targeting this protein with a monoclonal antibody (Bevacizumab) improved progression free survival in NSCLC

patients in combination with cisplatin [182,184,189]. Also, alteration of mesenchymal-epithelial transition factor (MET) expression is also relevant in NSCLC and has been targeted with small multikinase TKIs, such as crizotinib, cabozantinib and golvatinib; spefic TKIs like capmatinib, tepotinib and tivantinib; or monoclonal antibody therapy with onartuzumab and emibetuzumab [190].

However, the most prevalent mutations in NSCLC are *KRAS* gene mutations, which are present in 20-30% of the tumors, representing 90% of all *RAS* mutations in adenocarcinomas. These mutations are common in smokers and patients that were exposed to asbestos, being more prevalent in women, and there is no currently approved targeted therapy for this set of patients [191,192]. Therefore, despite the progress achieved in many targeted therapies that have been developed to improve disease outcomes, platinum-based chemotherapy still remains the therapeutic choice for most patients [193].

Cisplatin (CDDP), the most used cytotoxic drug in NSCLC, is able to crosslink with the purine bases on the DNA, interfere with DNA repair mechanisms, cause DNA damage and induce apoptosis in cancer cells [194]. Yet, only ~1% of CDDP interacts with DNA. The molecular mechanisms through which CDDP acts are poorly understood, but may involve: i) accumulation of ROS and nitric oxide (NO), which exacerbate CDDP genotoxicity and favour the opening of the permeability transition pore complex (PTPC); ii) transduction of mitochondrial outer membrane permeabilization (MOMP)-stimulatory signal via the PTPC component voltage-dependent anion channel 1 (VDAC1) and the pro-apoptotic BCL-2 family members BAK1 and BAX; iii) activation of cytoplasmic p53 which promotes MOMP via various mechanisms and iv) trigger ER stress response [94].

Carboplatin is the only platinum derived drug which has some advantages over CDDP, as it induces fewer side effects [195]. It has a bidentate dicarboxylate (CBDCA) ligand instead of the two chloride ligands, which are the leaving groups in cisplatin [196]. It has lower reactivity and slower DNA binding kinetics, which limits excretion of the drug. The lower excretion rate of carboplatin results in higher drug availability, for a longer period of time, but 90% of carboplatin can be recovered in urine compared to 50% of cisplatin [197,198]. The half-lives of carboplatin and CDDP are 30h and 1.5-3.6h, respectively. Nevertheless, carboplatin is less effective than cisplatin and usually a four times higher dose is needed to achieve the same result [194]. Therefore, carboplatin regimens are only used when patients have co-morbidities or display a high toxicity to cisplatin [199].

Although the majority of patients follow a platinum based chemotherapy, most patients develop resistance during sequential cycles of treatment with CDDP. CDDP-resistant cells show decreased CDDP accumulation, and the identification of the proteins responsible for drug resistance is necessary to identify new therapy targets to circumvent or decrease CDDP resistance [200].

Resistance to CDDP is frequently multifactorial and relies on simultaneous activation of multiple, non-redundant molecular pathways [94]. First, the vast majority of CDDP is uptaken by the cells through copper transporters, namely CTR1, and is exported from the cell through ATP7B. Alterations in the expression level, subcellular localization and functionality of these transporters have already been linked to CDDP resistance, as they can reduce the amount of CDDP available in the cytoplasm [201,202]. The sensitivity of cancer cells to CDDP is limited by the robustness of DNA repair mechanisms. The mismatch repair (MMR) machinery is mainly responsible for detecting the DNA adducts formed by CDDP, whereas the nucleotide excision repair (NER) system resolves the majority of damages caused by this drug [203]. The upregulation of genes involved in NER are positively correlated with CDDP resistance, risk of progression and death [204]. Interestingly, the MMR activation recognizes the CDDP adducts but is unable to resolve them. This triggers a cytotoxic response that leads to apoptosis [203]. Therefore, the main effectors of the MMR pathway, MLH1 and MSH2 are usually downregulated or mutated in tumors that are resistant to CDDP [205–207]. CDDP can also cause single or double-strand breaks (SSB and DSB, respectively) in the DNA that are repaired by the base excision repair (BER) pathway and the homologous recombinantion (HR) system, respectively. CDDP resistant tumors seem to rely on these systems to survive, as they often upregulate PARP1 (BER pathway) and BRCA1 (HR system) and are sensitive to targeted therapies, such as the treatment with PARP1 inhibitors [204,208].

Tumor cells also have to circumvent the activation of the pro-apoptotic signals upon CDDP-based therapy. CDDP can cause mitochondrial-DNA (mtDNA) mutations, which result in partial mitochondrial dysfunction and have been linked to chemotherapy resistance [209,210]. Tumor cells often impair pro-apoptotic signal transducers, such as p53, to overcome CDDP cytotoxic effects [211,212], and upregulate BCL-2 anti-apoptotic proteins, BCL-2, Bcl-xL and MCL-1 [213–215].

The susceptibility of cancer cells to CDDP can also be limited by molecular pathways that are not directly activated by CDDP, but induce compensatory survival

signals. Tumors can activate pathways that induce strong proliferation signals, such as the AKT or the mTOR pathways and activate antioxidant defences to counteract ROS levels induced by CDDP [216–218]. Finally, resistance to CDDP can also be achieved by upregulating the PQC system. Activation of the UPR, induced by mild ER-stress prior to treatment with CDDP, inhibits cancer cell sensitivity to the treatment through regulation of autophagy [143]. Moreover, increased expression of the UPR master regulator, BiP, in NSCLC, is correlated with shorter OS and contributes to the optimal activation of the AKT pathway, leading to CDDP resistance [95,219]. The heat shock proteins (HSPs) are not only essential to regulate posttranslational folding, stability and function of oncoproteins that are often mutated, but also regulate tumor development, progression, metastasis and drug resistance (not only CDDP), therefore their overexpression is an indicator of poor prognosis [54].

Several reports indicate that protein mistranslation, which often leads to protein misfolding, induces growth advantages and phenotypic drug resistance to antibiotics in bacteria and fungi [104]. In *Mycobacteria*, substitutions of glutamate for glutamine and aspartate for asparagine caused by tRNA mischarging, increase phenotypic resistance to rifampicin, whereas decreasing mistranslation produces increased susceptibility to the antibiotic [124]. In *Candida albicans*, mistranslation is controlled by the environment and high levels of mistranslation correlate with phenotypic diversity and fluconazole resistance [119,123,220]. Mistranslation can also help *Mycoplasma* to evade the host's immune system in a manner similar to antigenic variation and in *E.coli* resistance to stress and antibiotics increases if the MetRS misacylates other tRNAs with Met [84].

We have previously observed that deregulation of the tRNA pool and expression of misreading $tRNA^{Ser}$(Ala) were beneficial to tumor growth, local invasion and activated the UPR. Given that UPR activation has been linked to CDDP resistance and that mistranslation has been associated with drug resistance, we hypothesized that deregulation of the tRNA pool or tRNA mischarging could also induce resistance to platinum-based drugs. To test this hypothesis, we exposed H460- and A549-derived cell lines expressing $tRNA^{Ser}$(WT) and $tRNA^{Ser}$(Ala) to CDDP and carboplatin both *in vitro* and *in vivo.* We observed that cells expressing the mistranslating $tRNA^{Ser}$(Ala) were more resistant to cisplatin and carboplatin *in vitro*, but cells with upregulation of the $tRNA^{Ser}$(WT) were only resistant to carboplatin, relative to Mock control cells. We also demonstrated that tumors overexpressing the $tRNA^{Ser}$(WT) were more resistant to CDDP *in vivo* than Mock tumors, and that $tRNA^{Ser}$(Ala) expressing tumors did not

respond to CDDP treatment. This data shows that tRNA pool deregulation and tRNA misreading are sufficient to induce resistance to platinum-based chemotherapy.

6.3. Results

6.3.1. Mistranslating cells are more resistant to conventional therapy

We observed in Chapter 5 that mistranslation has an impact on tumor growth and local invasion, indicating that the role of tRNAs in tumorigenesis goes beyond what was anticipated. In this chapter, we focused on the hypothesis that mistranslation could enhance the ability of cancer cells to resist chemotherapy, as it increases drug resistance in other organisms. We used our previously established H460-derived cell lines expressing $tRNA^{Ser}$(WT) and $tRNA^{Ser}$(Ala) constructs to test this hypothesis. As the H460 parental cell line has an activating mutation in the *KRAS* gene (Q61R), we chose to test their resistance to platinum-based drugs, which would be the therapy of choice for patients with this mutation [221].

The colony formation assay assessed the ability of individualized cells exposed to treatment to resist the treatment itself and to proliferate and form colonies. The H460-derived cell lines expressing the misreading $tRNA^{Ser}$(Ala) were more resistant to CDDP than the control, showing an increase in colony formation of 1.48-fold (p<0.01) (**Fig.6-1**). On the other hand, either cell lines expressing the misreading $tRNA^{Ser}$(Ala) or overexpressing the $tRNA^{Ser}$(WT), were resistant to the treatment with Carboplatin, with an increase in colony formation of 1.35-fold (p<0.05) and 1.45-fold (p<0.05), respectively (**Fig.6-2**).

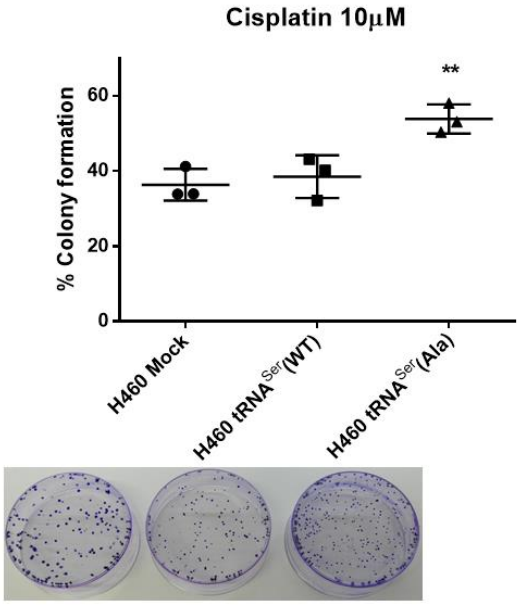

Figure 6-1: *In vitro* resistance to cisplatin of H460-derived cell lines. Misreading $tRNA^{Ser}$(Ala) were more resistant to CDDP than the control, showing an increase in colony formation of 1.48-fold. Graph depicts average ± SEM (n=3). Data was analyzed with One-way ANOVA, with Dunnet's post-test and signicant p-values are shown (**p<0.01).

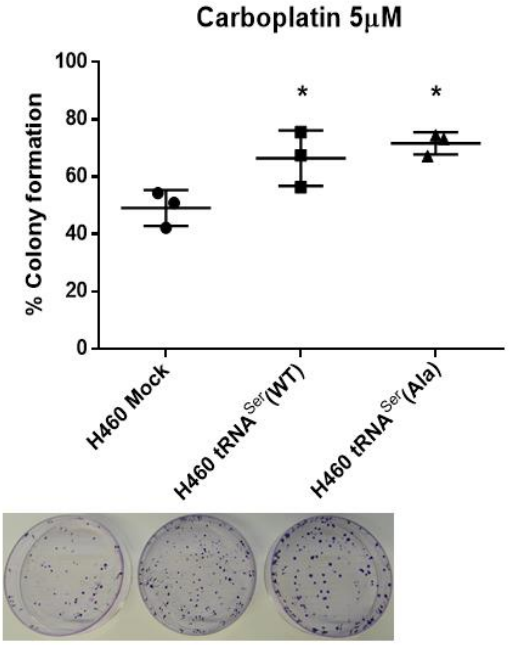

Figure 6-2: *In vitro* resistance to carboplatin of H460-derived cell lines. Expression of either $tRNA^{Ser}$(WT) or misreading $tRNA^{Ser}$(Ala) diminished the sensitivity of H460 cells to treatment with carboplatin, showing an increase in colony formation of 1.35-fold and 1.45-fold, respectively. Graph depicts average ± SEM (n=3). Data was analyzed with One-way ANOVA, with Dunnet's post-test and signicant p-values are shown (*p<0.01).

To exclude the hypothesis that these data could be cell line-specific, we stably expressed our tRNA constructs in A549 cells (Lung adenocarcinoma). After verifying the integration (**Fig.6-3, Upper panel**) and sequence integrity of the plasmids (**Fig.6-3, Lower panel**) in the genome of these cells, we used them to confirm the results obtained with the H460-derived cell lines.

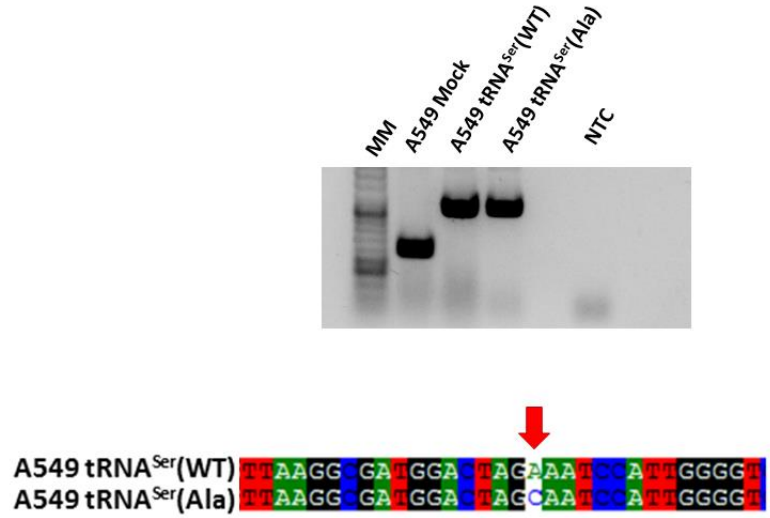

Figure 6-3: Integration of pIRES2-DsRed and recombinant tRNAs in the cell lines. (Upper panel) Agarose gel (1%) of the PCR product obtained by amplification of genomic DNA from cell lines across the fragment of pIRES2-DsRed plasmid containing the tRNA insert. NTC represents the negative control. **(Lower panel)** Sanger sequencing of the PCR products showing the AGA to AGC anticodon mutation of the tRNA tRNA^{Ser}(WT), creating the misreading tRNA^{Ser}(Ala) in the A549 cell line.

The drug resistance pattern of the A549-derived cell lines was very similar to that of the H460-derived cell lines (**Fig.6-4**). Treatment of A549-derived cell lines with 15 µM of CDDP, showed that only cells that expressed the misreading tRNA^{Ser}(Ala) were more resistant than the control with a 1.55-fold increase in colony formation (p<0.05) (**Fig.6-4, Left panel**). Also, upon treated with 10 µM of Carboplatin, both the cell lines harboring the recombinant tRNAs showed increased colony formation of 1.21-fold (p<0.001) and 1.32-fold (p<0.001), for tRNA^{Ser}(WT) and tRNA^{Ser}(Ala) cell lines, respectively (**Fig.6-4, Right panel**).

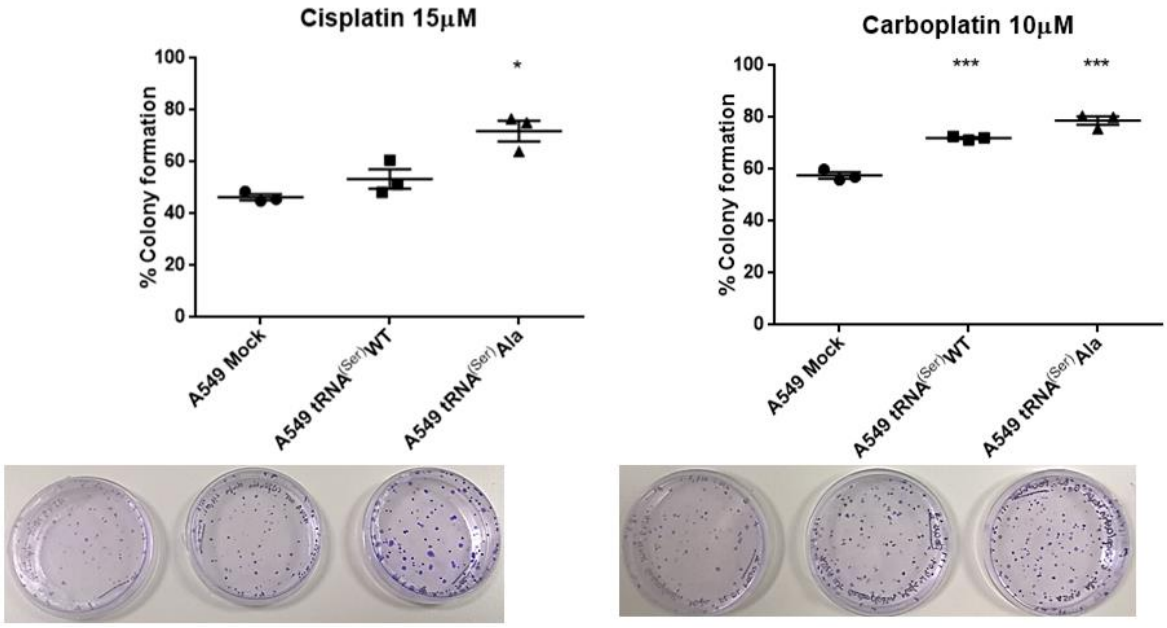

Figure 6-4: **In vitro resistance to platinum-based drugs of H460-derived cell lines. (Left panel)** Misreading $tRNA^{Ser}$(Ala) were more resistant to CDDP than the control, showing an increase in colony formation of 1.55-fold. **(Right panel)** Expression of both $tRNA^{Ser}$(WT) and misreading $tRNA^{Ser}$(Ala) decreased the sensitivity of H460 cells to treatment with carboplatin, showing an increase in colony formation of 1.21-fold and 1.32-fold, respectively. Graphics depicts average ± SEM (n=3). Data was analyzed with One-way ANOVA, with Dunnet's post-test and signicant p-values are shown (*p<0.05;***p<0.001).

These results confirm that both the upregulation of the WT-Ser tRNA and the expression of the misreading $tRNA^{Ser}$(Ala) increase resistance of NSCLC cancer cells to conventional chemotherapy, independently of the parental cell line where the recombinant tRNAs were expressed.

We further studied if tumors expressing these tRNAs were resistant to CDDP treatment *in vivo*. We chose CDDP for the *in vivo* treatments, since it was the drug that produced the biggest fold change in terms of colony formation in cells expressing the misreading $tRNA^{Ser}$(Ala). We inoculated nude mice with H460-derived cell lines in their dorsal flanks and allowed them to grow until they reached ~100mm^3, before initiating the treatment with cisplatin. We did bilateral injections in each mouse and randomized them in 4 groups, presented in Table 6-1.

Groups	Cells injected in the left flank	Cells injected in the right flank	Treatment
Group 1	Mock	$tRNA^{Ser}$(WT)	CDDP
Group 2	Mock	$tRNA^{Ser}$(WT)	Vehicle
Group 3	Mock	$tRNA^{Ser}$(Ala)	CDDP
Group 4	Mock	$tRNA^{Ser}$(Ala)	Vehicle

Table 6-1: Groups of mice used in the in vivo experiment. In this table the information about the cell lines that were injected in each flank of the mice and the treatment that they received is represented.

The results obtained *in vivo* were slightly different from those observed *in vitro*. The mice from groups 1 and 2 that harbored the Mock and tRNA^{Ser}(WT) variants, showed similar tumor kinetics in the mice that received vehicle. When we treated the mice with CDDP, Mock tumors were much more sensitive to the drug after the second treatment. Conversely, the tumors expressing tRNA^{Ser}(WT) were resistant to treatment and grew slightly slower than the tumors expressing the same vector that were treated with the vehicle (p>0.05) **(Fig.6-5)**.

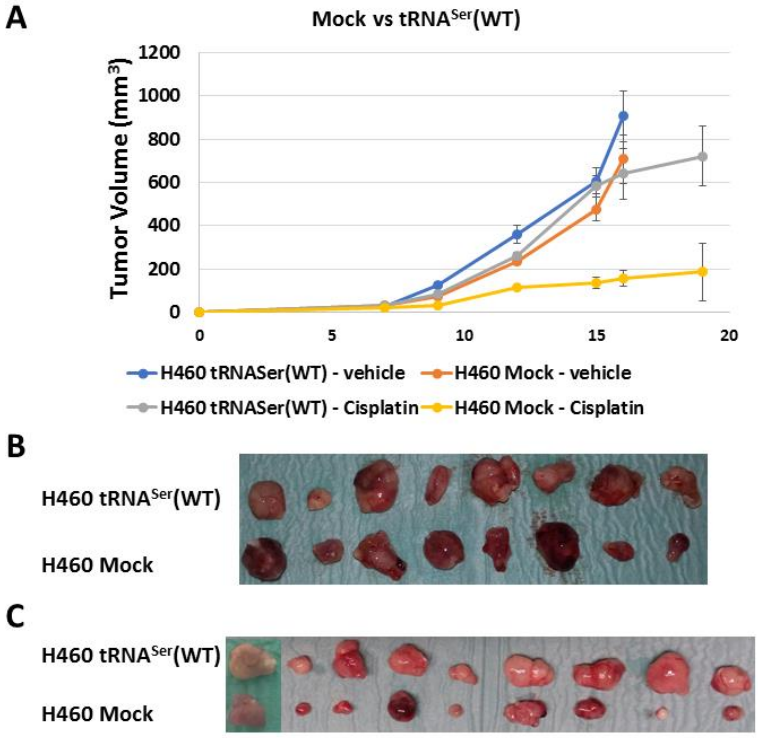

Figure 6-5: tRNA^{Ser}(WT) tumors resistance to cisplatin in vivo. (A) Upregulation of the tRNA^{Ser}(WT) inhibits sensitivity of H460-derived tumors to systemic treatment with cisplatin (p<0.01, from day 15 post-inoculation). **(B)** Group 1 tumors, treated with vehicle. Tumors derived from the same animal are aligned vertically. Mock tumors are slightly smaller than the tumors expressing tRNA^{Ser}(WT). **(C)** Group 2 tumors, treated with 4mg/kg of CDDP. Tumors derived from the same animal are aligned vertically. We can observe that Mock tumors are slightly smaller than the tumors expressing tRNA^{Ser}(WT).

On the other hand, the Mock tumors that were paired with tRNA^{Ser}(Ala) expressing tumors, did not grow when mice were treated with the vehicle or cisplatin **(Fig.6-6A, B)**. The reasons for this phenotype are difficult to understand and the experiment should be repeated in the near future. In fact, tumors harboring the tRNA^{Ser}(Ala) vector grew faster in the mice that were treated with CDDP relative to Mock tumors that grew on the left flank of the same mice **(Fig.6-6A,C)**. However, the Mock tumors that were treated with cisplatin grew similarly to those that received the vehicle **(Fig.6-6)**. Therefore, it is not clear if the tRNA^{Ser}(Ala) expressing tumors are

more resistant to cisplatin that the control tumors; despite the differences in growth kinetics. In any case, these tumors were not responsive to CDDP treatment.

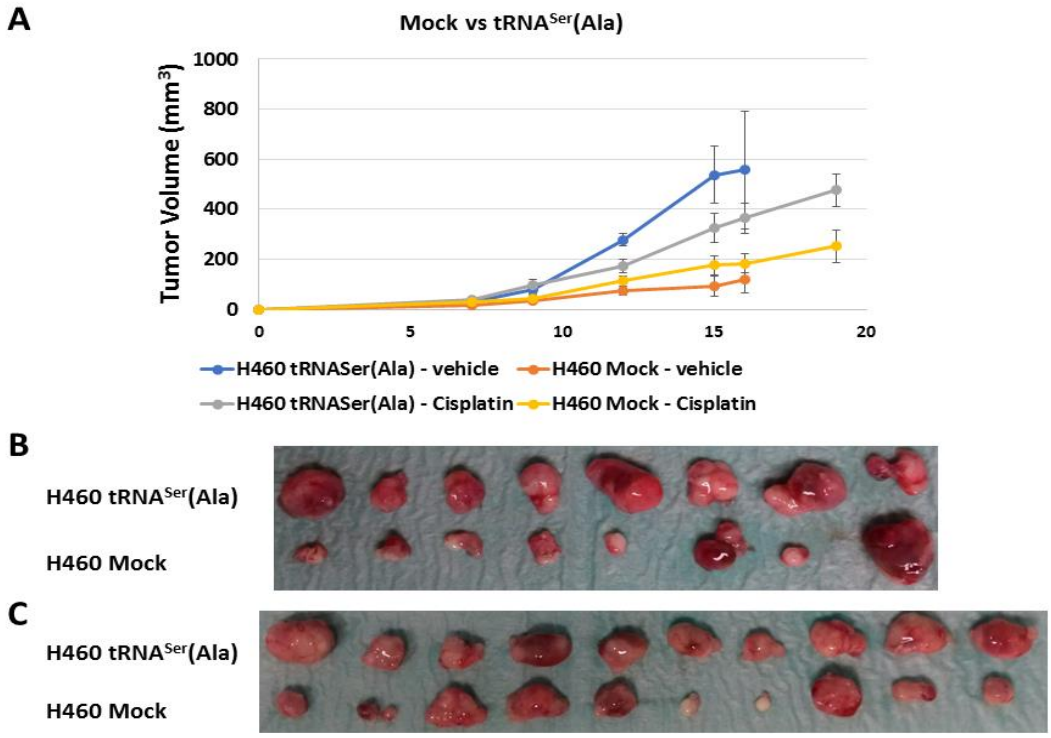

Figure 6-6: tRNA^{Ser}(Ala) tumors resistance to cisplatin in vivo. (A) Cisplatin treatment has little effect on Mock and tRNA^{Ser}(Ala) expressing tumors, although the latter had faster growth kinetics ($p<0.01$, from day 15 post-inoculation) than the former. **(B)** Group 3 tumors, treated with vehicle. Tumors derived from the same animal are aligned vertically. We can observe that Mock grew very little when relative to tumors expressing tRNA^{Ser}(Ala). **(C)** Group 4 tumors, treated with 4mg/kg of CDDP. Tumors derived from the same animal are aligned vertically. We can observe that Mock tumors are slightly smaller than the tumors expressing tRNA^{Ser}(Ala).

In conclusion, the treatment response observed in isolated cells *in vitro* was not correlated with tumor growth *in vivo*, when the drug is given systemically. We are unable to explain these differences at present, but lower drug availability in a tumor mass when compared to that of individualized cells *in vitro*, may contribute to those differences.

6.4. Discussion

Our data show that deregulation of the tRNA pool alone is sufficient to reduce tumor sensitivity to cytotoxic chemotherapy with cisplatin. Expression of a misreading tRNA^{Ser}(Ala) also decreases the sensitivity of tumor cells to CDDP and carboplatin *in vitro* and inhibit the response to cisplatin treatment *in vivo*. The molecular mechanisms that support these phenotypes still need to be clarified, but it is likely that activation of the UPR by the recombinant tRNAs prior to treatment may be involved. The fact that

cells with upregulation of the $tRNA^{Ser}$(WT) were resistant to carboplatin *in vitro* only, may be explained by the higher reactivity and faster DNA binding kinetics of cisplatin. Also, mistranslation in $tRNA^{Ser}$(Ala) expressing cells is expected to increase the proteomic and phenotypic diversity, enhancing adaptation capacity to stress [83,85]. Therefore, we hypothesize that cisplatin induces rapid and acute stress to cells, whereas the lower reactivity of carboplatin gives $tRNA^{Ser}$(WT) expressing cells the time to adapt and thrive under such conditions.

The overexpression of the Ser tRNA (chr6.tRNA5-SerAGA) has been associated to reduced OS in Breast invasive carcinoma, adrenocortical carcinoma, colon adenocarcinoma, head and neck squamous carcinoma and kidney renal clear cell carcinoma (YM500v3 database). Moreover, this tRNA has been associated with augmented risk of recurrence, which may indicate that it can influence therapy outcome [9]. Indeed, our *in vivo* results show that the upregulation of this tRNA is sufficient to increase resistance to cisplatin in NSCLC tumors.

Considering our previous results (Chapter III), we could not anticipate that Mock tumors, paired with $tRNA^{Ser}$(Ala) tumors, would not grow *in vivo*. To eliminate the hypothesis of $tRNA^{Ser}$(Ala) tumors affecting the growth of Mock tumors and confirm that tRNA misreading reduces tumor sensitivity to CDDP, further experiments with mice injected with only one of the cell lines need to be carried out. Mice from the same litter were randomly distributed to different groups in our experiment, to ensure that each group had mice with different genetic backgrounds, ages and weights, so these would not be interfering factors. The subcutaneous injections were also made in no specific order. Therefore, it seems unlikely that the effect observed in this group of mice results from experimental biases that we were not aware off.

Careful molecular profiling of the tumors should be carried out to understand the mechanisms through which resistance to cisplatin is achieved. One hypothesis is that pre-activation of the UPR in these cells reduces their sensibility to cisplatin. Our Chapter III data show that tumors expressing these tRNA constructs active the UPR, especially BiP, which has been related to decreased OS in NSCLC and resistance to CDDP [95,219]. However, given that the UPR activation can be a double-edged sword for tumors, depending on the duration of the activation and factors that are still unknown other mechanisms cannot be excluded [143,222]. For example, the level of pre-adaptive mutations in the genome may also increase due to proteome instability generated by the recombinant tRNAs [83]. Therefore exome sequencing should be used to map such

mutations. Monitoring the translatome using ribosome profiling coupled with ribo-seq could also provide clues about the genes that effectively translated in those tumors [13]. Finally, proteomic alterations should also be monitored since the misreading $tRNA^{Ser}$(Ala) increases misincorporations of Ser at Ala (Chapter 3) and some of these misincorporations may induce phenotypic mutations important for the establishment of the resistant phenotype.

6.5. Materials and Methods

6.5.1. Cell Culture

NCI-H460 and A549 cell lines were obtained from American Type Culture Collection (ATCC). Both cell lines were cultured in RPMI 1640 medium (Gibco, Life Technologies), supplemented with 10% Fetal Bovine Serum (FBS) (Sigma) and 1% Pen/Strep. During the assays, cells were cultured without Pen/Strep. Cells were maintained in an incubator at 37ºC with 5% CO_2 and 95% relative humidity. To execute the following procedures, cells were detached using Tryple Xpress (Gibco, Life Technologies). Cells were regularly tested for mycoplasma presence.

6.5.2. Generation of stable cell lines

5.0 x 10^4 NCI-H460 or A549 cells were plated in MW24 plates and after 48h were transfected using 1.5µg of plasmid DNA and 0.75µL of Lipofectamine® 3000 (Invitrogen). NCI- H460 cells were transfected three independent times with the empty vector (Mock), the plasmid containing an extra copy of the wild type $tRNA^{Ser}_{AGA}$(WT) or the misreading $tRNA^{Ser}_{AGC}$(Ala). Stably transfected cells were obtained after three weeks of selection with 800µg/ml or 1000 µg/ml of G418 for NCI-H460 and A549, respectively.

6.5.3. Extraction and Quantification of gDNA

To ensure that the plasmid did not acquire mutations when integrated in the genome, gDNA was extracted and sequenced. The NZY Tissue gDNA Isolation Kit was used, following the recommended instructions, and gDNA concentration was quantified using a NanoDrop.

6.5.4. Anchorage-Dependent Colony Formation Assay

300 cells per condition were seeded in 60mm dishes. 24h later, cells were treated with 10µM (H460) or 15µM (A549) of cisplatin for one hour or 5µM (H460) or 10µM (A549) of carboplatin for two hours. Drug concentration was optimized in order to inhibit approximately 50% of colony formation in the cells harbouring the empty plasmid. Other plates were also with the respective vehicles (0.9% of NaCl for cisplatin and DMSO for carboplatin) as controls. After the treatment, cells were washed with 1x PBS and fresh medium was added to each plate. After 9 days, the colonies were fixed using ice cold methanol and incubated at -30ºC for 30min. Methanol was removed and a solution of 0.1% crystal violet in 20% methanol was added and the plates were incubated at room temperature for 30min. Plates were washed with H_2O milliQ to remove excess dye and colonies with more than 50 cells were counted. This assay was performed with triplicates and repeated three times. Data was analyzed by calculating the percentage of colonies that were formed in the plates that were treated either with cisplatin or carboplatin, when compared to the plates that were treated with the respective vehicles.

6.5.5. Tumor induction assay

Six-week-old male N:NIH(s)II:nu/nu nude mice were obtained previously from the Medical School, University of Cape Town in 1991 and then reproduced, maintained and housed at IPATIMUP Animal House at the Medical Faculty of the University of Porto, in a pathogen-free environment under controlled conditions of light and humidity. Male nude mice, aged 6-8 weeks, were used for *in vivo* experiments. Animal experiments were carried out in accordance with the Guidelines for the Care and Use of Laboratory Animals, directive 2010/63/EU and had the ethical approval of the Direcção Geral de Veterinária (Project: CO_2016_01). To verify if deregulation of the tRNAs could result in tumors that were more resistant to treatment *in vivo*, H460 cell lines harboring the empty vector (Mock), the $tRNA^{Ser}$(WT) and the misreading $tRNA^{Ser}$(Ala) were subcutaneously injected in the dorsal flanks using a 25-gauge needle with $1x10^6$ (H460) of each cell line. 39 mice were randomized in four groups: Group 1 – Mice harboring Mock cell line in the left dorsal flank and $tRNA^{Ser}$(WT) in the right dorsal flank, that were treated with 4mg/kg of cisplatin via Intraperitoneal (IP) ; Group 2 – Mice harboring Mock cell line in the left dorsal flank and $tRNA^{Ser}$(WT) in the right

dorsal flank, that received 0.9% NaCl (vehicle) via IP; Group 3 – Mice harboring Mock cell line in the left dorsal flank and $tRNA^{Ser}$(Ala) in the right dorsal flank, that were treated with 4mg/kg of cisplatin via IP ; Group 4 – Mice harboring Mock cell line in the left dorsal flank and $tRNA^{Ser}$(Ala) in the right dorsal flank, that received 0.9% NaCl (vehicle) via IP. Groups 1 and 3 had 9 mice, Group 2 had 10 mice and Group 4 was constituted by 11 mice. The treatment began when tumors reached ~100mm^3 and mice were treated 2 times per week. Before each treatment, mice were weighted, and tumor width and length were measured with calipers. Tumor volumes were calculated assuming ellipsoid growth patterns. We monitored the mice between treatments, giving them 500µL of 0.9% NaCl, subcutaneously, when mice presented signs of dehydration. Mice were humanely euthanized when tumors reached a median volume of 2000mm^3 or whenever any signs of disease were detected. Tumors, were collected, fixed in 10% buffered formalin, paraffin embedded and then sectioned for histological examination. A part of each tumor was frozen in liquid nitrogen and stored at –80ºC.

7. General discussion

7.1. Protein Synthesis Errors in cancer

Cancer is a multifactorial disease seldom associated with the accumulation of DNA mutations, chromosomal aberrations, epigenetic alterations and transcriptional deregulation [98]. Despite the remarkable efforts to characterize the molecular profile of tumors, the etiology of a significant percentage of tumors is still unknown [184]. Deregulation of the tRNA pool, tRNA interacting enzymes, other translational factors, amino acid starvation and activation of protein quality control systems are common features of tumors, raising the hypothesis that protein synthesis accuracy is compromised in cancer [11,46,65,160,223,224]. Specifically, the tRNA pool of tumors is different from that of normal tissue, with specific enrichment of tRNAs that stabilize transcripts which promote cancer hallmarks [11]. tRNA deregulation may also lead to misreading of near-cognate codons, inducing errors in protein synthesis and destabilizing the proteome, however this

has not yet been addressed in cancer [72]. It is possible that mutations in proteins caused by errors in protein synthesis, explain the etiology of a certain fraction of human cancers, since proteome instability also destabilizes the genome [83]. Working under the hypothesis that tRNA deregulation increases protein synthesis errors creating a phenotype that is advantageous for tumour cells, we established a method to determine protein synthesis error rate in the proteome of tumors and normal tissue and constructed cell lines to investigate the effects of the most common types of error in near-normal and tumor cells.

Available methods for quantification of amino acid misincorporation in proteins rely on the use of radioactive amino acids, chemiluminescence and fluorescence probes, however these methods can only detect specific amino acid misincorporations and underestimate global error rates [2,83,87,119,225,226]. Mass spectrometry (MS) has also been used to search for specific types of amino acids mutations and, at least in theory, should permit the determination of error rates at the proteome scale [227]. However, this is difficult due to the low abundance of mistranslated peptides in complex proteome samples, but recent technology developments both in MS instruments and software are gradually overcoming the technical difficulties. In this thesis, we have developed a label free methodology for the determination of the frequency of protein synthesis errors in tumors and in normal tissue using a Thermo Orbitrap Fusion Lumos mass spectrometer. We implemented a mass spectrometry data analysis pipeline to identify peptides containing amino acid misincorporations (mutations) in raw data sets of normal colon,

colon adenocarcinoma (COAD) and xenograft tumor samples. The SPIDER tool of the PEAKS8 software platform allowed us to deep search the proteome of our cells and detect the mutant peptides that occur at very low level. The SPIDER algorithm calculates the probability of a mutation to occur in a given place, relative to other possible mutations or amino acid modifications [135], creating a database of putative mutated peptides. To reduce the number of false positives, the results obtained were then validated by running the raw files again against modified databases containing the sequences of the mutated proteins. Our results show that the data analysis pipeline is robust, but sample preparation should be optimized to increase the number of peptides detected. Spike-in internal controls using synthetic peptides of known concentration should also be used to better infer the level of mutant peptides in our samples [85]. Samples run on SDS-PAGE should be fractioned to increase the depth of analysis and detect rare amino acid misincorporation events. Regarding the samples of the CPTAC database that we also used in our study, the number of samples analyzed should be increased to improve the robustness of the statistical analysis (**Fig.3-1A**).

Although the difference between COAD and normal samples was not statistically significant, likely due to high cell type heterogeneity in tumors [228], there was a clear trend for increased error levels in tumor samples. This first attempt to quantify global protein synthesis errors in tumors showed increased error rate for all amino acids, but Asn (N) in the COAD samples. The Ser-at-Ala misincorporation, which is likely associated with tRNA misacylation by Class II aaRS, was the most common misincorporation identified in our xenograft tumors. The observation that misincorporations that do not comply with genetic code rules were present at much lower level in these samples, strongly supports our methodology for detecting rare misincorporation events in complex proteomes.

7.2. The role of frequent and rare protein synthesis errors in cancer

In this work, we have studied the role of one frequent and one rare amino acid misincorporation in tumors. The SerRS recognizes specific elements in the acceptor stem, D-arm, extra arm and the anticodon stem of Ser tRNAs, but does not depend on anticodon recognition, allowing for the alteration of the anticodon without affecting the aminoacylation specificity [229,230]. Geslain and colleagues, produced 10 mutant Ser-tRNAs which were aminoacylated with Ser, but decoded codons complementary to the mutated anticodon, and successfully introduced random mutations in the proteome [118].

We chose the Ser-tRNA as proof of concept and mutated its anticodon to decode and incorporate Ser at Ala ($tRNA^{Ser}$(Ala); frequent event) or Leu ($tRNA^{Ser}$(Leu); infrequent event) codons. These mutant tRNAs were stably expressed in a *Mus musculus* near-normal cell line, but relevant phenotypes were not observed *in vitro*, unless the cells were stimulated with a pro-inflammatory cytokine (**Figs.3-2; 3-3**). These data support previous results from our lab showing that mistranslation is mainly advantageous when cells are challenged with external stimuli [85,119,123]; under physiologic conditions it is mainly detrimental in other model organisms. Given that cells expressing the misreading $tRNA^{Ser}$(Ala) responded to TNFα treatment activating the Akt pathway also showed a slight increase in colony formation *in vitro* (**Figs.3-2; 3-3**), we hypothesized that the molecular changes induced by this mutant tRNA could impact the tumorigenic capacity of these cells. Supporting this hypothesis, the $tRNA^{Ser}$(Ala) expressing tumors demonstrated increased angiogenesis and a tumor growth rate that was comparable to that of NIH3T3 cells expressing K-ras^{V12} (**Fig.3-4**). These tumors differed from Mock, $tRNA^{Ser}$(WT) and $tRNA^{Ser}$(Leu) expressing tumors, by showing concomitant activation of all the UPR branches and the Akt-pathway (**Figs.3-6; 3-7; 3-12**). Decreased phosphorylation of eIF2α observed in $tRNA^{Ser}$(Ala) expressing tumors, likely contributed to increased protein synthesis rate and faster growth rate of these tumors [231]; this is in line with transformation of NIH3T3 cells by modulation of eIF2α-P levels, which were previously described [125]. Tumors expressing $tRNA^{Ser}$(Ala) also activated the ATF6 and IRE1α branches of the UPR (**Figs. 3-6; 3-12**), which are associated with cellular protection and growth stimulation [115,127,128]. The $tRNA^{Ser}$(WT) expressing tumors only showed activation of the ATF6 UPR branch and downregulation of the p38 MAPK, which is important to sustain tumor cell survival and proliferation [232], justifying the slower growth of these tumors relative to $tRNA^{Ser}$(Ala) expressing tumors. The difference in growth rate between $tRNA^{Ser}$(Ala) and $tRNA^{Ser}$(Leu) may be, at least in part, explained by the decreased activation of the ERK1/2 pathway in tumors expressing the mutant $tRNA^{Ser}$(Leu) (**Fig.3-13**). The activation of this pathway is linked to G1/S cell cycle progression and tumor cell survival and its downregulation may lead to cell cycle arrest and decreased survival of tumor cells [233].

Overall, we demonstrated that protein synthesis errors are increased in tumors and that frequent and infrequent errors trigger different molecular pathways in NIH3T3 cells. Interestingly, the frequent Ser-at-Ala misincorporation, increased angiogenesis

and produced tumors that grew as fast as K-ras^{V12} expressing tumors, suggesting that frequent mistranslation events can indeed contribute to tumor development.

To study the effect tRNA deregulation and tRNA misreading in different tumor stages, we expressed the tRNA^{Ser}(WT) and tRNA^{Ser}(Ala) in two human cell lines derived from the same organ, namely in cells derived from normal bronchial epithelium (BEAS-2B) and in cells derived from a large cell carcinoma, H460. This paired model has been successfully used before to prove the oncogenic role of a miRNA in NSCLC [234].

The expression levels of both tRNAs was higher in the H460 than in the BEAS-2B cell lines (**Figs.4-1; 5-1**); this may be due to the difficulty of stably transfecting BEAS-2B cell line. BEAS-2B showed high sensitivity to the recombinant tRNA during the first week after electroporation, whereas H460 recovered shortly after transfection, suggesting that normal cell lines are more sensitive to changes in the tRNA pool and tRNA misreading than tumor cell lines. Interestingly, in the H460 tRNA^{Ser}(Ala) cell line, the expression of the WT Ser-tRNA increased (**Fig.5-1**). How the former affects the latter is not clear, but the WT-Ser tRNA may dilute the effect of tRNA^{Ser}(Ala) expression, which reached similar expression levels to those observed for WT Ser-tRNA in Mock cell lines.

The expression of both the recombinant tRNA^{Ser}(WT) and the misreading tRNA^{Ser}(Ala) in BEAS-2B increased cell proliferation, protein synthesis rate and decreased the levels of eIF2α-P. The PP1α regulatory subunit GADD34, which is responsible for eIF2α-P dephosphorylation, was also upregulated in BEAS tRNA^{Ser}(WT) cells and was unaltered in BEAS tRNA^{Ser}(Ala) cells (**Fig.4-4**). The low levels of eIF2α-P in this cell line should be clarified in the future by studying the activation levels of eIF2α kinases, namely PERK and GCN2, the levels of the PP1α phosphatase and also the expression of CReP, an homolog of GADD34 which can also bind and direct PP1α to eIF2α [154,235]. Expression of our recombinant tRNAs increased colony formation in BEAS-2B, which is an indicator of increased tumorigenic ability. Moreover, BiP was upregulated in the BEAS cells expressing the tRNA^{Ser}(WT) (**Fig.4-4**), similarly to what has been observed in pre-malignant lesions of lung cancer [159]. Therefore, the decreased levels of eIF2α-P, the overexpression of BiP and the increase in colony formation, suggest that expression of the recombinant Ser-tRNAs could influence tumor initiation. In fact, we observed an advantage of tRNA^{Ser}(WT) expressing tumors over Mock tumors grown in the same animal (**Fig.4-6;4-7**): only 2/4

Mock minimal size tumors developed, whereas larger 4/4 $tRNA^{Ser}$(WT) expressing tumors developed (**Fig.4-6;4-7**), indicating that overexpression of this WT-Ser tRNA may be sufficient to trigger tumor formation with slow growth kinetics. This experiment should be repeated with more animals to increase its statistical significance.

Although expression of the recombinant tRNAs in H460 did not increase the number of colonies formed *in vitro*, it increased tumor growth kinetics *in vivo*. Similarly to what happened in the NIH3T3-derived tumors expressing the misreading $tRNA^{Ser}$(Ala), the H460 tumors had lower levels of eIF2α-P, likely due to GADD34 upregulation (**Figs.3-6;5-6**). Both tumors had higher BiP levels which is associated with increased aggressiveness in NSCLC tumors (**Fig. 3-6**) [168].

The only common response observed in BEAS-2B-derived cell lines and H460-derived tumors expressing the recombinant tRNAs, was the activation of the ATF4 transcription factor (**Figs.4-4;5-6**). This transcription factor regulates the expression of many stress response genes, including GADD34 and autophagy-related genes [147,161]. The role of autophagy in cancer is context dependent; in pancreatic cancer it is associated with late onset of tumor development, but is important for tumor maintenance and progression [164]. Whether autophagy is relevant in our model remains to be clarified, but the slow growth kinetics of tumors derived from BEAS-2B cells expressing the recombinant tRNAs, and the increased growth kinetics of tumors derived from the H460 cells expressing the same tRNAs, which are already tumorigenic, suggest that it may be important. ATF4 activation has also been associated with high grade tumors and metastization in NSCLC tumors [236], further suggesting that deregulation of the tRNA pool and tRNA misreading may increase the metastization capacity of those cells.

The metastization process is divided into various stages: local invasion, intravasation, survival in the circulation, extravasation, survival at a second site and finally outgrowth at a second site [237]. We studied the early stages of metastization, by analysing cell migration, extracellular matrix invasion and also *in vivo* metastization. Upregulation of the Ser-tRNA reduced the migration capacity of H460 cells, while expression of the misreading $tRNA^{Ser}$(Ala) increased it (**Fig.5-7**). Both tRNA constructs significantly increased extracellular matrix invasion ability, but the metastization assay results were inconclusive, as mice injected with the same cell line displayed high and low metastization areas in the lungs (**Figs.5-7; 5-8**). Despite this, metastization should not be ruled out because, other groups observed that overexpression of $tRNA_iMet$

increases migration, invasion and metastization of melanoma cells [14]. Also, expression of $tRNA^{Glu}UUC$ and $tRNA^{Arg}CCG$ shifts the proteome towards a pro-metastatic state in breast cancer cells, through the stabilization of transcripts enriched in codons matching their anticodons [13], suggesting that different tRNAs can drive the same phenotype in tumors in different tissues. Since the tRNA pool differs among tissues to fulfill its specific translational requirements [238], it is likely that changes in the tRNA pool may have distinct impacts on tumor development depending on the tissue of origin. In our study, upregulation of $tRNA^{Ser}$(WT) in NSCLC cells may increase the translation efficiency of transcripts enriched in UCU codons (matching the AGA anticodon), which may impair cell migration ability without affecting extracellular matrix invasion. This needs to be clarified in future studies.

Altogether our results suggest that expression of the recombinant $tRNA^{Ser}$(WT) in BEAS-2B may drive tumor initiation, likely due to BiP upregulation and decreased levels of eIF2α-P; upregulation of ATF4 and most likely autophagy may be responsible for the late onset of these tumors. Additionally, expression of such tRNAs in a tumorigenic cell line, showed that cells expressing the misreading $tRNA^{Ser}$(Ala) have a more aggressive phenotype, since the expression of this tRNA increased tumor growth kinetics, cell migration and extracellular matrix invasion. These phenotypes may be partially explained by the concomitant upregulation of BiP and ATF4.

7.3. tRNA upregulation decreases tumor sensitivity to cisplatin

The overexpression of the Ser tRNA (chr6.tRNA5-SerAGA) has been linked to reduced Overall Survival of patients with breast invasive carcinoma, adrenocortical carcinoma, colon adenocarcinoma, head and neck squamous carcinoma and kidney renal clear cell carcinoma (YM500v3 database). The risk of recurrence is also augmented, suggesting that its overexpression can influence therapy outcomes [9]. This hypothesis is supported by the observation that protein mistranslation is beneficial in some microorganisms by bestowing them with growth advantages and phenotypic resistance to antibiotics [104]. For instance, in *Candida albicans*, high mistranslation levels are associated with phenotypic diversity and fluconazole resistance [119,123,220] and *E.coli* strains that misacylate various tRNAs with Met are more resistant to stress and antibiotics [84]. Interestingly, H460 tumors expressing the recombinant $tRNA^{Ser}$(WT) and the misreading $tRNA^{Ser}$(Ala), upregulated of BiP and activated ATF4. It is known that activation of the UPR, induced by mild ER-stress prior to treatment with cisplatin,

increases resistance to treatment through activation of autophagy [143], and that BiP overexpression in NSCLC is correlated with shorter overall survival and cisplatin resistance [95,219]. These data strongly suggest that expression of the recombinant tRNAs may also increase resistance to platinum-based drugs.

The *in vitro* results showed that only H460 cells expressing $tRNA^{Ser}$(Ala) were resistant to cisplatin, whereas H460 cells expressing $tRNA^{Ser}$(WT) and $tRNA^{Ser}$(Ala) were resistant to carboplatin (**Figs.6-1;6-2**). We confirmed the results obtained in another NSCLC cell line, A549, and observed a similar phenotype (**Fig.6-4**). However, the results from the *in vivo* experiments were surprising. We demonstrated that tumors overexpressing the $tRNA^{Ser}$(WT) were more resistant to CDDP *in vivo* than Mock expressing tumors, and that $tRNA^{Ser}$(Ala) expressing tumors did not respond to CDDP treatment (**Figs.6-5;6-6**). Regarding the $tRNA^{Ser}$(Ala) branch of the experiment, we could not anticipate that Mock tumors, paired with $tRNA^{Ser}$(Ala) tumors, would not grow (**Fig.6-6**). It is unlikely that we have unintentionally introduced an experimental bias, since the mice and the injections were randomized to ensure that genetic backgrounds, ages and weights would not interfere with results. Additional experiments with mice carrying tumors derived from only one cell line should be performed, to avoid cross-interactions between tumors expressing different constructs. Careful molecular profiling of these tumors should also be done to understand the mechanisms through which they achieve resistance to cisplatin.

7.4. Conclusions and future work

Our data show that tumors mistranslate at higher levels than normal tissue, but each type of tRNA produces different phenotypes likely due to activation of distinct signaling pathways. It is likely that the transcripts enriched in UCU codons, matching the AGA anticodon in the $tRNA^{Ser}$(WT) expressing cell lines, are more efficiently translated and the different phenotypes observed among cell lines are likely due to differences in their genetic background. The increased expression of WT tRNAs may increase misreading of near-cognate codons, increasing protein mistranslation in these cells [51]. Additionally, the transcripts enriched in GCU/GCC Ala codons are probably different from those enriched in UCU codons and their differential translation may explain in part the effects observed in cells expressing the $tRNA^{Ser}$(Ala) and the WT-Ser tRNA. Additionally, Alanine is often used to mimic non-phosphorylated forms of proteins and this may impact phenotypic diversity [169]. Although phosphorylation is

context specific [170], we cannot exclude that the insertion of Ser at Ala sites may activate some pathways that are otherwise silent.

Upregulation of the WT Ser tRNA and expression of the misreading $tRNA^{Ser}$(Ala) increased tumor cell growth rate, invasion potential, drug resistance and activation of the UPR. These phenotypes share several characteristics with the phenotypes induced by mistranslation in *Saccharomyces cerevisiae* and *Candida albicans* [82,83,85,87,102,119,220]. Increased fitness of mistranslating yeast has been associated with high proteome diversity leading to population heterogeneity. Tumor heterogeneity is thought to arise from genetic instability and phenotypic diversity, and mistranslation in yeast destabilizes the genome in a rather dramatic manner and also increases phenotypic diversity [83,85].

Although the phenotypes we observed need further clarification, tRNA deregulation and mistranslation in cancer are far more important than previously anticipated.

Future studies should focus on the following priorities:

1) Optimizing mass spectrometry analysis to identify higher nember of proteins with mutations and clarify how they may impact on the phenotypes observed;

2) Quantification of the distinct types of errors that occur in these samples and associating errors to codons to clarify if there are error prone codons.

3) Ribosome profiling coupled with RNA-seq to identify the transcripts that are more efficiently translated in the engineered cell lines;

4) Monitor in more detail the UPR to identify all the UPR branches that are induced in the recombinant cells;

5) Assess differences in proteasome activity and study if autophagy is activated by the expression of the recombinant tRNAs in NSCLC cells;

6) Sequence the exomes of the engineered cells to identify the mutations associated with resistance to cisplatin.

Regarding the experiments that will have to be repeated:

1) The number of mice used in the initiation and the metastization assays should be increased;

2) The number of cells used per inoculum in the initiation assay should also be increased;
3) Metastization in the other organs collected in the metastization experiment should be analyzed.
4) Mice should also be injected with only one type of cells to avoid cross-influence of one tumor over the other.

8. References

1. Gebetsberger J, Polacek N. Slicing tRNAs to boost functional ncRNA diversity. RNA Biol 2013; 10:1798–806.
2. Moghal A, Mohler K, Ibba M. Mistranslation of the genetic code. FEBS Lett 2014; 588:4305–10.
3. Smith TF, Hartman H. The evolution of Class II Aminoacyl-tRNA synthetases and the first code. FEBS Lett 2015; 589:3499–507.
4. Schmitt BM, Rudolph KLM, Karagianni P, Fonseca NA, White RJ, Talianidis I, Odom DT, Marioni JC, Kutter C. High-resolution mapping of transcriptional dynamics across tissue development reveals a stable mRNA-tRNA interface. Genome Res 2014; 24:1797–807.
5. Lee JW, Beebe K, Nangle LA, Jang J, Longo-Guess CM, Cook SA, Davisson MT, Sundberg JP, Schimmel P, Ackerman SL. Editing-defective tRNA synthetase causes protein misfolding and neurodegeneration. Nature 2006; 443:50–5.
6. Khan MA, Rafiq MA, Noor A, Hussain S, Flores JV, Rupp V, Vincent AK, Malli R, Ali G, Khan FS, et al. Mutation in NSUN2, which Encodes an RNA Methyltransferase, Causes Autosomal-Recessive Intellectual Disability. Am J Hum Genet 2016; 90:856–63.
7. Frye M, Dragoni I, Chin SF, Spiteri I, Kurowski A, Provenzano E, Green A, Ellis IO, Grimmer D, Teschendorff A, et al. Genomic gain of 5p15 leads to over-expression of Misu (NSUN2) in breast cancer. Cancer Lett 2010; 289:71–80.
8. Krokowski D, Han J, Saikia M, Majumder M, Yuan CL, Guan B-J, Bevilacqua E, Bussolati O, Bröer S, Arvan P, et al. A Self-defeating Anabolic Program Leads to β-Cell Apoptosis in Endoplasmic Reticulum Stress-induced Diabetes via Regulation of Amino Acid Flux. J Biol Chem 2013; 288:17202–13.
9. Krishnan P, Sunita G, Wang B, Heyns M, Li D, Mackey JR, Kovalchuk O, Damaraju S. Genome-wide profiling of transfer RNAs and their role as novel prognostic markers for breast cancer. Sci Rep 2016; 6.
10. Pavon-Eternod M, Gomes S, Geslain R, Dai Q, Rosner MR, Pan T. tRNA over-expression in breast cancer and functional consequences. Nucleic Acids Res 2009; 37:7268–80.
11. Gingold H, Tehler D, Christoffersen NR, Nielsen MM, Asmar F, Kooistra SM, Christophersen NS, Christensen LL, Borre M, Sørensen KD, et al. A Dual Program for Translation Regulation in Cellular Proliferation and Differentiation.

Cell 2015; 158:1281–92.

12. Pavon-Eternod M, Gomes S, Rosner MR, Pan T. Overexpression of initiator methionine tRNA leads to global reprogramming of tRNA expression and increased proliferation in human epithelial cells. RNA 2013; 19:461–6.
13. Goodarzi H, Nguyen HCB, Zhang S, Dill BD, Molina H, Tavazoie SF. Modulated Expression of Specific tRNAs Drives Gene Expression and Cancer Progression. Cell 2016; :1416–1427.
14. Clarke CJ, Berg TJ, Birch J, Ennis D, Mitchell L, Cloix C, Campbell A, Sumpton D, Nixon C, Campbell K, et al. The Initiator Methionine tRNA Drives Secretion of Type II Collagen from Stromal Fibroblasts to Promote Tumor Growth and Angiogenesis. Curr Biol 2016; 26:755–65.
15. Birch J, Clarke CJ, Campbell AD, Campbell K, Mitchell L, Liko D, Kalna G, Strathdee D, Sansom OJ, Neilson M, et al. The initiator methionine tRNA drives cell migration and invasion leading to increased metastatic potential in melanoma. Biol Open 2016;
16. Chung I-F, Chang S-J, Chen C-Y, Liu S-H, Li C-Y, Chan C-H, Shih C-C, Cheng W-C. YM500v3: a database for small RNA sequencing in human cancer research. Nucleic Acids Res 2016;
17. Mahlab S, Tuller T, Linial M. Conservation of the relative tRNA composition in healthy and cancerous tissues. RNA 2012; 18:640–52.
18. Haurie V, Durrieu-Gaillard S, Dumay-Odelot H, Da Silva D, Rey C, Prochazkova M, Roeder RG, Besser D, Teichmann M. Two isoforms of human RNA polymerase III with specific functions in cell growth and transformation. Proc Natl Acad Sci U S A 2010; 107:4176–81.
19. Schramm L, Hernandez N. Recruitment of RNA polymerase III to its target promoters. Genes Dev 2002; 16:2593–620.
20. Male G, von Appen A, Glatt S, Taylor NMI, Cristovao M, Groetsch H, Beck M, Müller CW. Architecture of TFIIIC and its role in RNA polymerase III pre-initiation complex assembly. Nat Commun 2015; 6:7387.
21. Moqtaderi Z, Wang J, Raha D, White RJ, Snyder M, Weng Z, Struhl K. Genomic binding profiles of functionally distinct RNA polymerase III transcription complexes in human cells. Nat Struct Mol Biol 2010; 17:635–40.
22. Zhang G, Lukoszek R, Mueller-Roeber B, Ignatova Z. Different sequence signatures in the upstream regions of plant and animal tRNA genes shape distinct

modes of regulation. Nucleic Acids Res 2011; 39:3331–9.

23. White RJ. RNA polymerases I and III, growth control and cancer. Nat Rev Mol Cell Biol 2005; 6:69–78.
24. Arimbasseri AG, Maraia RJ. RNA Polymerase III Advances: Structural and tRNA Functional Views. Trends Biochem Sci 2016; 41:546–59.
25. Khattar E, Kumar P, Liu CY, Akıncılar SC, Raju A, Lakshmanan M, Maury JJP, Qiang Y, Li S, Tan EY, et al. Telomerase reverse transcriptase promotes cancer cell proliferation by augmenting tRNA expression. J Clin Invest 2016; 126:4045–60.
26. Gomez-Roman N, Grandori C, Eisenman RN, White RJ. Direct activation of RNA polymerase III transcription by c-Myc. Nature 2003; 421:290–4.
27. Kenneth NS, Ramsbottom B a, Gomez-Roman N, Marshall L, Cole P a, White RJ. TRRAP and GCN5 are used by c-Myc to activate RNA polymerase III transcription. Proc Natl Acad Sci 2007; 104:14917–22.
28. Wang J, Zhao S, Wei Y, Zhou Y, Shore P, Deng W. Cytoskeletal Filamin A Differentially Modulates RNA Polymerase III Gene Transcription in Transformed Cell Lines. J Biol Chem 2016; 291:25239–46.
29. Torres AG, Batlle E, Ribas de Pouplana L. Role of tRNA modifications in human diseases. Trends Mol Med 2014; 20:306–14.
30. Giegé R, Eriani G. Transfer RNA Recognition and Aminoacylation by Synthetases. In: eLS. 2014.
31. Zinshteyn B, Gilbert W V. Loss of a conserved tRNA anticodon modification perturbs cellular signaling. PLoS Genet 2013; 9:e1003675.
32. Whipple JM, Lane EA, Chernyakov I, D'Silva S, Phizicky EM. The yeast rapid tRNA decay pathway primarily monitors the structural integrity of the acceptor and T-stems of mature tRNA. Genes Dev 2011; 25:1173–84.
33. Dewe JM, Whipple JM, Chernyakov I, Jaramillo LN, Phizicky EM. The yeast rapid tRNA decay pathway competes with elongation factor 1A for substrate tRNAs and acts on tRNAs lacking one or more of several modifications. Rna 2012; 18:1886–96.
34. Kirino Y, Goto Y-I, Campos Y, Arenas J, Suzuki T. Specific correlation between the wobble modification deficiency in mutant tRNAs and the clinical features of a human mitochondrial disease. Proc Natl Acad Sci U S A 2005; 102:7127–32.
35. Begley U, Sosa MS, Avivar-Valderas A, Patil A, Endres L, Estrada Y, Chan

CTY, Su D, Dedon PC, Aguirre-Ghiso JA, et al. A human tRNA methyltransferase 9-like protein prevents tumour growth by regulating LIN9 and HIF1-α. EMBO Mol Med 2013; 5:366–83.

36. Kirino Y, Yasukawa T, Marjavaara SK, Jacobs HT, Holt IJ, Watanabe K, Suzuki T. Acquisition of the wobble modification in mitochondrial tRNALeu(CUN) bearing the G12300A mutation suppresses the MELAS molecular defect. Hum Mol Genet 2006; 15:897–904.
37. Delaunay S, Rapino F, Tharun L, Zhou Z, Heukamp L, Termathe M, Shostak K, Klevernic I, Florin A, Desmecht H, et al. Elp3 links tRNA modification to IRES-dependent translation of LEF1 to sustain metastasis in breast cancer. J Exp Med 2016; 213:2503 LP-2523.
38. Arimbasseri AG, Blewett NH, Iben JR, Lamichhane TN, Cherkasova V, Hafner M, Maraia RJ. RNA Polymerase III Output Is Functionally Linked to tRNA Dimethyl-G26 Modification. PLoS Genet 2015; 11.
39. Kim D, Kwon NH, Kim S. Association of aminoacyl-tRNA synthetases with cancer. Top. Curr. Chem.2014; 344:207–45.
40. Guo M, Schimmel P. Essential Non-Translational Functions of tRNA Synthetases. Nat Chem Biol 2013; 9:145–53.
41. Wellman TL, Eckenstein M, Wong C, Rincon M, Ashikaga T, Mount SL, Francklyn CS, Lounsbury KM. Threonyl-tRNA synthetase overexpression correlates with angiogenic markers and progression of human ovarian cancer. BMC Cancer 2014; 14:620.
42. Yoon M-S, Son K, Arauz E, Han JM, Kim S, Chen J. Leucyl-tRNA Synthetase Activates Vps34 in Amino Acid-Sensing mTORC1 Signaling. Cell Rep 2017; 16:1510–7.
43. Kim EY, Jung JY, Kim A, Kim K, Chang YS. Methionyl-tRNA synthetase overexpression is associated with poor clinical outcomes in non-small cell lung cancer. BMC Cancer 2017; 17:467.
44. Hanahan D, Weinberg RA. Hallmarks of cancer: The next generation. Cell2011; 144:646–74.
45. Lee JH, You S, Hyeon DY, Kang B, Kim H, Park KM, Han B, Hwang D, Kim S. Comprehensive data resources and analytical tools for pathological association of aminoacyl tRNA synthetases with cancer. Database 2015; 2015.
46. Frye M, Watt FM. The RNA Methyltransferase Misu (NSun2) Mediates Myc-

Induced Proliferation and Is Upregulated in Tumors. Curr Biol 2006; 16:971–81.

47. Kim TW, Kim B, Kim JH, Kang S, Park S-B, Jeong G, Kang H-S, Kim SJ. Nuclear-encoded mitochondrial MTO1 and MRPL41 are regulated in an opposite epigenetic mode based on estrogen receptor status in breast cancer. BMC Cancer 2013; 13:502.
48. Dolfi SC, Chan LL-Y, Qiu J, Tedeschi PM, Bertino JR, Hirshfield KM, Oltvai ZN, Vazquez A. The metabolic demands of cancer cells are coupled to their size and protein synthesis rates. Cancer Metab 2013; 1:20.
49. Conn CS, Qian S-B. Nutrient signaling in protein homeostasis: an increase in quantity at the expense of quality. Sci Signal 2013; 6:ra24.
50. Zaher HS, Green R. Fidelity at the molecular level: lessons from protein synthesis. Cell 2009; 136:746–62.
51. Yang J-R, Chen X, Zhang J. Codon-by-Codon Modulation of Translational Speed and Accuracy Via mRNA Folding. PLOS Biol 2014; 12:e1001910.
52. Dadey DYA, Kapoor V, Khudanyan A, Urano F, Kim AH, Thotala D, Hallahan DE. The ATF6 pathway of the ER stress response contributes to enhanced viability in glioblastoma. Oncotarget 2016; 7:2080–92.
53. Salaroglio IC, Panada E, Moiso E, Buondonno I, Provero P, Rubinstein M, Kopecka J, Riganti C. PERK induces resistance to cell death elicited by endoplasmic reticulum stress and chemotherapy. Mol Cancer 2017; 16:91.
54. Wu J, Liu T, Rios Z, Mei Q, Lin X, Cao S. Heat Shock Proteins and Cancer. Trends Pharmacol Sci 2017; 38:226–56.
55. Walerych D, Lisek K, Sommaggio R, Piazza S, Ciani Y, Dalla E, Rajkowska K, Gaweda-Walerych K, Ingallina E, Tonelli C, et al. Proteasome machinery is instrumental in a common gain-of-function program of the p53 missense mutants in cancer. Nat Cell Biol 2016; 18:897–909.
56. Kenific CM, Debnath J. Cellular and metabolic functions for autophagy in cancer cells. Trends Cell Biol 2015; 25:37–45.
57. Mairinger FD, Walter RFH, Theegarten D, Hager T, Vollbrecht C, Christoph DC, Worm K, Ting S, Werner R, Stamatis G, et al. Gene expression analysis of the 26S proteasome subunit PSMB4 reveals significant upregulation, different expression and association with proliferation in human pulmonary neuroendocrine tumours. J Cancer 2014; 5:646–54.
58. Arlt A, Sebens S, Krebs S, Geismann C, Grossmann M, Kruse M-L, Schreiber S,

Schafer H. Inhibition of the Nrf2 transcription factor by the alkaloid trigonelline renders pancreatic cancer cells more susceptible to apoptosis through decreased proteasomal gene expression and proteasome activity. Oncogene 2013; 32:4825–35.

59. Glick D, Barth S, Macleod KF. Autophagy: cellular and molecular mechanisms. J Pathol 2010; 221:3–12.
60. Yang Z, Klionsky DJ. Eaten alive: a history of macroautophagy. Nat Cell Biol 2010; 12:814–22.
61. Koritzinsky M, Levitin F, van den Beucken T, Rumantir RA, Harding NJ, Chu KC, Boutros PC, Braakman I, Wouters BG. Two phases of disulfide bond formation have differing requirements for oxygen. J Cell Biol 2013; 203:615–27.
62. Kamphorst JJ, Cross JR, Fan J, de Stanchina E, Mathew R, White EP, Thompson CB, Rabinowitz JD. Hypoxic and Ras-transformed cells support growth by scavenging unsaturated fatty acids from lysophospholipids. Proc Natl Acad Sci 2013; 110:8882–7.
63. Pan T. Adaptive translation as a mechanism of stress response and adaptation. Annu Rev Genet 2013; 47:121–37.
64. Ye J, Palm W, Peng M, King B, Lindsten T, Li MO, Koumenis C, Thompson CB. GCN2 sustains mTORC1 suppression upon amino acid deprivation by inducing Sestrin2. Genes Dev 2015; 29:2331–6.
65. Wang Y, Ning Y, Alam GN, Jankowski BM, Dong Z, Nör JE, Polverini PJ. Amino Acid Deprivation Promotes Tumor Angiogenesis through the GCN2/ATF4 Pathway. Neoplasia 2013; 15:989–97.
66. Urra H, Dufey E, Avril T, Chevet E, Hetz C. Endoplasmic Reticulum Stress and the Hallmarks of Cancer. Trends in Cancer 2017; 2:252–62.
67. de Ridder GG, Ray R, Pizzo S V. A murine monoclonal antibody directed against the carboxyl-terminal domain of GRP78 suppresses melanoma growth in mice. Melanoma Res 2012; 22.
68. Pytel D, Seyb K, Liu M, Ray SS, Concannon J, Huang M, Cuny GD, Diehl JA, Glicksman MA. Enzymatic Characterization of ER Stress-Dependent Kinase, PERK, and Development of a High-Throughput Assay for Identification of PERK Inhibitors. J Biomol Screen 2014; 19:1024–34.
69. Papandreou I, Denko NC, Olson M, Van Melckebeke H, Lust S, Tam A, Solow-Cordero DE, Bouley DM, Offner F, Niwa M, et al. Identification of an Ire1alpha

endonuclease specific inhibitor with cytotoxic activity against human multiple myeloma. Blood 2011; 117:1311–4.

70. Atkins C, Liu Q, Minthorn E, Zhang S-Y, Figueroa DJ, Moss K, Stanley TB, Sanders B, Goetz A, Gaul N, et al. Characterization of a Novel PERK Kinase Inhibitor with Antitumor and Antiangiogenic Activity. Cancer Res 2013; 73:1993 LP-2002.
71. Rufo N, Garg AD, Agostinis P. The Unfolded Protein Response in Immunogenic Cell Death and Cancer Immunotherapy. Trends in Cancer 2017; 3:643–58.
72. Shah P, Gilchrist MA. Effect of Correlated tRNA Abundances on Translation Errors and Evolution of Codon Usage Bias. PLoS Genet 2010; 6:e1001128.
73. Ogle JM, Murphy F V., Tarry MJ, Ramakrishnan V. Selection of tRNA by the Ribosome Requires a Transition from an Open to a Closed Form. Cell 2002; 111:721–32.
74. Guo M, Chong YE, Shapiro R, Beebe K, Yang X-L, Schimmel P. Paradox of mistranslation of serine for alanine caused by AlaRS recognition dilemma. Nature 2009; 462:808–12.
75. Jakubowski H. Quality control in tRNA charging. Wiley Interdiscip. Rev. RNA2012; 3:295–310.
76. Guo HH, Choe J, Loeb LA. Protein tolerance to random amino acid change. Proc Natl Acad Sci U S A 2004; 101:9205–10.
77. Drummond DA, Wilke CO. Mistranslation-Induced Protein Misfolding as a Dominant Constraint on Coding-Sequence Evolution. Cell 2008; 134:341–52.
78. Lee JY, Kim DG, Kim B-G, Yang WS, Hong J, Kang T, Oh YS, Kim KR, Han BW, Hwang BJ, et al. Promiscuous methionyl-tRNA synthetase mediates adaptive mistranslation to protect cells against oxidative stress. J Cell Sci 2014; 127:4234–45.
79. Kondoh M, Ohga N, Akiyama K, Hida Y, Maishi N, Towfik AM, Inoue N, Shindoh M, Hida K. Hypoxia-Induced Reactive Oxygen Species Cause Chromosomal Abnormalities in Endothelial Cells in the Tumor Microenvironment. PLoS One 2013; 8:e80349.
80. Ruusala T, Andersson D, Ehrenberg M, Kurland CG. Hyper-accurate ribosomes inhibit growth. EMBO J 1984; 3:2575–80.
81. Santos M a S, Cheesman C, Costa V, Moradas-Ferreira P, Tuite MF. Selective advantages created by codon ambiguity allowed for the evolution of an

alternative genetic code in Candida spp. Mol Microbiol 1999; 31:937–47.

82. Silva RM, Paredes JA, Moura GR, Manadas B, Costa TL, Rocha R, Miranda I, Gomes AC, Koerkamp MJ, Perrot M, et al. Critical roles for a genetic code alteration in the evolution of the genus Candida. EMBO J 2007; 26:4555–65.
83. Bezerra AR, Simões J, Lee W, Rung J, Weil T, Gut IG, Gut M, Bayés M, Rizzetto L, Cavalieri D, et al. Reversion of a fungal genetic code alteration links proteome instability with genomic and phenotypic diversification. Proc Natl Acad Sci U S A 2013; 110:11079–84.
84. Schwartz MH, Pan T. Function and origin of mistranslation in distinct cellular contexts. Crit Rev Biochem Mol Biol 2017; 52:205–19.
85. Gomes AC, Miranda I, Silva RM, Moura GR, Thomas B, Akoulitchev A, Santos MA. A genetic code alteration generates a proteome of high diversity in the human pathogen Candida albicans. Genome Biol 2007; 8.
86. Miranda I, Rocha R, Santos MC, Mateus DD, Moura GR, Carreto L, Santos MAS. A genetic code alteration is a phenotype diversity generator in the human pathogen Candida albicans. PLoS One 2007; 2:e996.
87. Paredes JA, Carreto L, Simões J, Bezerra AR, Gomes AC, Santamaria R, Kapushesky M, Moura GR, Santos MAS. Low level genome mistranslations deregulate the transcriptome and translatome and generate proteotoxic stress in yeast. BMC Biol 2012; 10:55.
88. Meena AS, Sharma A, Kumari R, Mohammad N, Singh SV, Bhat MK. Inherent and Acquired Resistance to Paclitaxel in Hepatocellular Carcinoma: Molecular Events Involved. PLoS One 2013; 8:e61524.
89. Housman G, Byler S, Heerboth S, Lapinska K, Longacre M, Snyder N, Sarkar S. Drug Resistance in Cancer: An Overview. Cancers (Basel) 2014; 6:1769–92.
90. Wang X, Chow CR, Ebine K, Lee J, Rosner MR, Pan T, Munshi HG. Interaction of tRNA with MEK2 in pancreatic cancer cells. 2016; 6:28260.
91. Mei Y, Yong J, Liu H, Shi Y, Meinkoth J, Dreyfuss G, Yang X. tRNA Binds to Cytochrome c and Inhibits Caspase Activation. Mol Cell 2010; 37:668–78.
92. Gorla M, Sepuri NB V. Perturbation of apoptosis upon binding of tRNA to the heme domain of cytochrome c. Apoptosis 2014; 19:259–68.
93. Grelet S, McShane A, Geslain R, Howe PH. Pleiotropic Roles of Non-Coding RNAs in TGF-β-Mediated Epithelial-Mesenchymal Transition and Their Functions in Tumor Progression. Cancers (Basel).2017; 9.

94. Galluzzi L, Vitale I, Michels J, Brenner C, Szabadkai G, Harel-Bellan A, Castedo M, Kroemer G. Systems biology of cisplatin resistance: past, present and future. Cell Death Dis 2014; 5:e1257.
95. Ma X, Guo W, Yang S, Zhu X, Xiang J, Li H. Serum GRP78 as a tumor marker and its prognostic significance in non-small cell lung cancers: A retrospective study. Dis Markers 2015; 2015.
96. Pang YLJ, Abo R, Levine SS, Dedon PC. Diverse cell stresses induce unique patterns of tRNA up- and down-regulation: tRNA-seq for quantifying changes in tRNA copy number. Nucleic Acids Res 2014; 42:e170–e170.
97. Zhou Y, Goodenbour JM, Godley LA, Wickrema A, Pan T. High levels of tRNA abundance and alteration of tRNA charging by bortezomib in multiple myeloma. Biochem Biophys Res Commun 2009; 385:160–4.
98. You JS, Jones PA. Cancer genetics and epigenetics: two sides of the same coin? Cancer Cell 2012; 22:9–20.
99. Jakubowski H, Goldman E. Editing of errors in selection of amino acids for protein synthesis. Microbiol Rev 1992; 56:412–29.
100. Loftfield R, Vanderjagt D. The frequency of errors in protein biosynthesis. Biochem J 1972; 128:1353–6.
101. Allan Drummond D, Wilke CO. The evolutionary consequences of erroneous protein synthesis. Nat Rev Genet 2009; 10:715–24.
102. Silva RM, Duarte ICN, Paredes JA, Lima-Costa T, Perrot M, Boucherie H, Goodfellow BJ, Gomes AC, Mateus DD, Moura GR, et al. The Yeast PNC1 longevity gene Is up-regulated by mRNA mistranslation. PLoS One 2009; 4:e5212.
103. Pan T. Adaptive translation as a mechanism of stress response and adaptation. Annu Rev Genet 2013; 47:121–37.
104. Ribas de Pouplana L, Santos M a S, Zhu JH, Farabaugh PJ, Javid B. Protein mistranslation: Friend or foe? Trends Biochem Sci 2014; 39:355–62.
105. Bloom JD, Labthavikul ST, Otey CR, Arnold FH. Protein stability promotes evolvability. Proc Natl Acad Sci U S A 2006; 103:5869–74.
106. Kalapis D, Bezerra AR, Farkas Z, Horvath P, Bódi Z, Daraba A, Szamecz B, Gut I, Bayes M, Santos MAS, et al. Evolution of Robustness to Protein Mistranslation by Accelerated Protein Turnover. PLoS Biol 2015; 13.
107. Bjornsti MA, Houghton PJ. Lost in translation: Dysregulation of cap-dependent

translation and cancer. Cancer Cell2004; 5:519–23.

108. Mamane Y, Petroulakis E, Rong L, Yoshida K, Ler LW, Sonenberg N. eIF4E--from translation to transformation. Oncogene 2004; 23:3172–9.
109. Pandolfi PP. Aberrant mRNA translation in cancer pathogenesis: an old concept revisited comes finally of age. Oncogene 2004; 23:3134–7.
110. Park SG, Schimmel P, Kim S. Aminoacyl tRNA synthetases and their connections to disease. Proc Natl Acad Sci U S A 2008; 105:11043–9.
111. Ruggero D, Pandolfi PP. Does the ribosome translate cancer? Nat Rev Cancer 2003; 3:179–92.
112. White RJ. RNA polymerase III transcription and cancer. Oncogene 2004; 23:3208–16.
113. Clarke HJ, Chambers JE, Liniker E, Marciniak SJ. Endoplasmic Reticulum Stress in Malignancy. Cancer Cell 2014; 25:563–73.
114. Maas NL, Diehl JA. The PERKs and Pitfalls of Targeting the Unfolded Protein Response in Cancer. Clin Cancer Res 2015; 21:675–9.
115. Schewe DM, Aguirre-Ghiso JA. ATF6alpha-Rheb-mTOR signaling promotes survival of dormant tumor cells in vivo. Proc Natl Acad Sci U S A 2008; 105:10519–24.
116. Bi M, Naczki C, Koritzinsky M, Fels D, Blais J, Hu N, Harding H, Novoa I, Varia M, Raleigh J, et al. ER stress-regulated translation increases tolerance to extreme hypoxia and promotes tumor growth. EMBO J 2005; 24:3470–81.
117. Mohler K, Ibba M. Translational fidelity and mistranslation in the cellular response to stress. 2017; 2:17117.
118. Geslain R, Cubells L, Bori-Sanz T, Alvarez-Medina R, Rossell D, Martí E, de Pouplana LR. Chimeric tRNAs as tools to induce proteome damage and identify components of stress responses. Nucleic Acids Res 2010; 38:e30.
119. Simões J, Bezerra AR, Moura GR, Araújo H, Gut I, Bayes M, Santos MAS. The fungus Candida albicans tolerates ambiguity at multiple codons. Front Microbiol 2016; 7.
120. Wang S, Kaufman RJ. The impact of the unfolded protein response on human disease. J Cell Biol 2012; 197:857–67.
121. Chappell WH, Steelman LS, Long JM, Kempf RC, Abrams SL, Franklin RA, Bäsecke J, Stivala F, Donia M, Fagone P, et al. Ras/Raf/MEK/ERK and PI3K/PTEN/Akt/mTOR inhibitors: rationale and importance to inhibiting these

pathways in human health. Oncotarget 2011; 2:135–64.

122. Dittmar KA, Sørensen MA, Elf J, Ehrenberg M, Pan T. Selective charging of tRNA isoacceptors induced by amino-acid starvation. EMBO Rep 2005; 6:151–7.
123. Bezerra AR, Simões J, Lee W, Rung J, Weil T, Gut IG, Gut M, Bayés M, Rizzetto L, Cavalieri D, et al. Reversion of a fungal genetic code alteration links proteome instability with genomic and phenotypic diversification. Proc Natl Acad Sci U S A 2013; 110:11079–84.
124. Javid B, Sorrentino F, Toosky M, Zheng W, Pinkham JT, Jain N, Pan M, Deighan P, Rubin EJ. Mycobacterial mistranslation is necessary and sufficient for rifampicin phenotypic resistance. Proc Natl Acad Sci 2014; 111:1132–7.
125. Perkins D, Barber G. Defects in Translational Regulation Mediated by the Subunit of Eukaryotic Initiation Factor 2 Inhibit Antiviral Activity and Facilitate the Malignant Transformation of Human Fibroblasts. Mol Cell Biol 2004; 24:2025–40.
126. Monick MM, Powers LS, Gross TJ, Flaherty DM, Barrett CW, Hunninghake GW. Active ERK Contributes to Protein Translation by Preventing JNK-Dependent Inhibition of Protein Phosphatase 1. J Immunol 2006; 177:1636 LP-1645.
127. Romero-Ramirez L, Cao H, Nelson D, Hammond E, Lee A-H, Yoshida H, Mori K, Glimcher LH, Denko NC, Giaccia AJ, et al. XBP1 is essential for survival under hypoxic conditions and is required for tumor growth. Cancer Res 2004; 64:5943–7.
128. Belmont PJ, Tadimalla A, Chen WJ, Martindale JJ, Thuerauf DJ, Marcinko M, Gude N, Sussman MA, Glembotski CC. Coordination of growth and endoplasmic reticulum stress signaling by regulator of calcineurin 1 (RCAN1), a novel ATF6-inducible gene. J Biol Chem 2008; 283:14012–21.
129. Dong D, Stapleton C, Luo B, Xiong S, Ye W, Zhang Y, Jhaveri N, Zhu G, Ye R, Liu Z, et al. A critical role for GRP78/BiP in the tumor microenvironment for neovascularization during tumor growth and metastasis. Cancer Res 2011; 71:2848–57.
130. Taddei ML, Giannoni E, Comito G, Chiarugi P. Microenvironment and tumor cell plasticity: An easy way out. Cancer Lett.2013; 341:80–96.
131. Clarke R, Cook KL, Hu R, Facey COB, Tavassoly I, Schwartz JL, Baumann WT, Tyson JJ, Xuan J, Wang Y, et al. Endoplasmic reticulum stress, the unfolded

protein response, autophagy, and the integrated regulation of breast cancer cell fate. Cancer Res.2012; 72:1321–31.

132. Fels DR, Koumenis C. The PERK/eIF2??/ATF4 module of the UPR in hypoxia resistance and tumor growth. Cancer Biol. Ther.2006; 5:723–8.
133. Mounir Z, Krishnamoorthy JL, Wang S, Papadopoulou B, Campbell S, Muller WJ, Hatzoglou M, Koromilas AE. Akt determines cell fate through inhibition of the PERK-eIF2α phosphorylation pathway. Sci Signal 2011; 4:ra62.
134. Sang Won L, Young Sun K, Kim S. Multifunctional Proteins in Tumorigenesis: Aminoacyl-tRNA Synthetases and Translational Componentse. Curr Proteomics 2006; 3:233–47.
135. Han Y, Ma B, Zhang K. SPIDER: software for protein identification from sequence tags with de novo sequencing error. Proc IEEE Comput Syst Bioinform Conf 2004; 3:206–15.
136. Zhang J, Xin L, Shan B, Chen W, Xie M, Yuen D, Zhang W, Zhang Z, Lajoie GA, Ma B. PEAKS DB: De Novo Sequencing Assisted Database Search for Sensitive and Accurate Peptide Identification. Mol Cell Proteomics 2012; 11.
137. Houck SA, Singh S, Cyr DM. Cellular Responses to Misfolded Proteins and Protein Aggregates. Methods Mol Biol 2012; 832:455–61.
138. Luo B, Lee AS. The critical roles of endoplasmic reticulum chaperones and unfolded protein response in tumorigenesis and anti-cancer therapies. Oncogene 2013; 32:10.1038/onc.2012.130.
139. Lu M, Lawrence DA, Marsters S, Acosta-Alvear D, Kimmig P, Mendez AS, Paton AW, Paton JC, Walter P, Ashkenazi A. Opposing unfolded-protein-response signals converge on death receptor 5 to control apoptosis. Science (80-) 2014; 345:98 LP-101.
140. Dejeans N, Barroso K, Fernandez-Zapico ME, Samali A, Chevet E. Novel roles of the unfolded protein response in the control of tumor development and aggressiveness. Semin Cancer Biol 2015; 33:67–73.
141. Tam AB, Mercado EL, Hoffmann A, Niwa M. ER Stress Activates NF-κB by Integrating Functions of Basal IKK Activity, IRE1 and PERK. PLoS One 2012; 7:e45078.
142. Mujcic H, Nagelkerke A, Rouschop KMA, Chung S, Chaudary N, Span PN, Clarke B, Milosevic M, Sykes J, Hill RP, et al. Hypoxic Activation of the PERK/eIF2α Arm of the Unfolded Protein Response Promotes Metastasis

through Induction of LAMP3. Clin Cancer Res 2013; 19:6126 LP-6137.

143. Chen R, Dai RY, Duan CY, Liu YP, Chen SK, Yan DM, Chen CN, Wei M, Li H. Unfolded protein response suppresses cisplatin-induced apoptosis via autophagy regulation in human hepatocellular carcinoma cells. Folia Biol (Praha) 2011; 57:87–95.
144. Scheuner D, Song B, McEwen E, Liu C, Laybutt R, Gillespie P, Saunders T, Bonner-Weir S, Kaufman RJ. Translational Control Is Required for the Unfolded Protein Response and In Vivo Glucose Homeostasis. Mol Cell 2001; 7:1165–76.
145. Harding HP, Zhang Y, Bertolotti A, Zeng H, Ron D. Perk Is Essential for Translational Regulation and Cell Survival during the Unfolded Protein Response. Mol Cell 2000; 5:897–904.
146. Harding HP, Novoa I, Zhang Y, Zeng H, Wek R, Schapira M, Ron D. Regulated Translation Initiation Controls Stress-Induced Gene Expression in Mammalian Cells. Mol Cell 2000; 6:1099–108.
147. Novoa I, Zeng H, Harding HP, Ron D. Feedback Inhibition of the Unfolded Protein Response by GADD34-Mediated Dephosphorylation of eIF2α. J Cell Biol 2001; 153:1011 LP-1022.
148. Bobrovnikova-Marjon E, Hatzivassiliou G, Grigoriadou C, Romero M, Cavener DR, Thompson CB, Diehl JA. PERK-dependent regulation of lipogenesis during mouse mammary gland development and adipocyte differentiation. Proc Natl Acad Sci U S A 2008; 105:16314–9.
149. Bu Y, Diehl JA. PERK Integrates Oncogenic Signaling and Cell Survival During Cancer Development. J. Cell. Physiol.2016; 231:2088–96.
150. Cullinan SB, Zhang D, Hannink M, Arvisais E, Kaufman RJ, Diehl JA. Nrf2 is a direct PERK substrate and effector of PERK-dependent cell survival. Mol Cell Biol 2003; 23.
151. Bobrovnikova-Marjon E, Grigoriadou C, Pytel D, Zhang F, Ye J, Koumenis C, Cavener D, Diehl JA. PERK promotes cancer cell proliferation and tumor growth by limiting oxidative DNA damage. Oncogene 2010; 29:3881–95.
152. Nakagawa H, Umemura A, Taniguchi K, Font-Burgada J, Dhar D, Ogata H, Zhong Z, Valasek MA, Seki E, Hidalgo J, et al. ER Stress Cooperates with Hypernutrition to Trigger TNF-Dependent Spontaneous HCC Development. Cancer Cell 2014; 26:331–43.
153. De Marco C, Malanga D, Rinaldo N, De Vita F, Scrima M, Lovisa S, Fabris L,

Carriero MV, Franco R, Rizzuto A, et al. Mutant AKT1-E17K is oncogenic in lung epithelial cells. Oncotarget 2015; 6:39634–50.

154. Boyce M, Yuan J. Cellular response to endoplasmic reticulum stress: a matter of life or death. Cell Death Differ 2006; 13:363–73.
155. Fels DR, Koumenis C. The PERK/eIF2α/ATF4 module of the UPR in hypoxia resistance and tumor growth. Cancer Biol Ther 2006; 5:723–8.
156. Lewerenz J, Maher P. Basal Levels of eIF2α Phosphorylation Determine Cellular Antioxidant Status by Regulating ATF4 and xCT Expression. J Biol Chem 2009; 284:1106–15.
157. Ye J, Kumanova M, Hart LS, Sloane K, Zhang H, De Panis DN, Bobrovnikova-Marjon E, Diehl JA, Ron D, Koumenis C. The GCN2-ATF4 pathway is critical for tumour cell survival and proliferation in response to nutrient deprivation. EMBO J 2010; 29:2082 LP-2096.
158. Wu M-J, Jan C-I, Tsay Y-G, Yu Y-H, Huang C-Y, Lin S-C, Liu C-J, Chen Y-S, Lo J-F, Yu C-C. Elimination of head and neck cancer initiating cells through targeting glucose regulated protein78 signaling. Mol Cancer 2010; 9:283.
159. Kim KM, Yu TK, Chu HH, Park HS, Jang KY, Moon WS, Kang MJ, Lee DG, Kim MH, Lee JH, et al. Expression of ER stress and autophagy-related molecules in human non-small cell lung cancer and premalignant lesions. Int J Cancer 2012; 131:E362-70.
160. Chen L, Brewer MD, Guo L, Wang R, Jiang P, Yang X. Enhanced Degradation of Misfolded Proteins Promotes Tumorigenesis. Cell Rep 2017; 18:3143–54.
161. B'chir W, Maurin A-C, Carraro V, Averous J, Jousse C, Muranishi Y, Parry L, Stepien G, Fafournoux P, Bruhat A. The eIF2α/ATF4 pathway is essential for stress-induced autophagy gene expression. Nucleic Acids Res 2013; 41:7683–99.
162. Mizushima N, Komatsu M. Autophagy: Renovation of Cells and Tissues. Cell 2011; 147:728–41.
163. Guo JY, Chen H-Y, Mathew R, Fan J, Strohecker AM, Karsli-Uzunbas G, Kamphorst JJ, Chen G, Lemons JMS, Karantza V, et al. Activated Ras requires autophagy to maintain oxidative metabolism and tumorigenesis. Genes Dev 2011; 25:460–70.
164. Rosenfeldt MT, O/'Prey J, Morton JP, Nixon C, MacKay G, Mrowinska A, Au A, Rai TS, Zheng L, Ridgway R, et al. p53 status determines the role of autophagy in pancreatic tumour development. Nature 2013; 504:296–300.

165. Peng Y-F, Shi Y-H, Ding Z-B, Ke A-W, Gu C-Y, Hui B, Zhou J, Qiu S-J, Dai Z, Fan J. Autophagy inhibition suppresses pulmonary metastasis of HCC in mice via impairing anoikis resistance and colonization of HCC cells. Autophagy 2013; 9:2056–68.
166. Qiang L, Zhao B, Ming M, Wang N, He T-C, Hwang S, Thorburn A, He Y-Y. Regulation of cell proliferation and migration by p62 through stabilization of Twist1. Proc Natl Acad Sci 2014; 111:9241–6.
167. Lock R, Kenific CM, Leidal AM, Salas E, Debnath J. Autophagy-Dependent Production of Secreted Factors Facilitates Oncogenic RAS-Driven Invasion. Cancer Discov 2014; 4:466 LP-479.
168. Wang Q, He Z, Zhang J, Wang Y, Wang T, Tong S, Wang L, Wang S, Chen Y. Overexpression of endoplasmic reticulum molecular chaperone GRP94 and GRP78 in human lung cancer tissues and its significance. Cancer Detect Prev 2005; 29:544–51.
169. Dissmeyer N, Schnittger A. Use of Phospho-Site Substitutions to Analyze the Biological Relevance of Phosphorylation Events in Regulatory Networks BT - Plant Kinases: Methods and Protocols. In: Dissmeyer N, Schnittger A, editors. . Totowa, NJ: Humana Press; 2011. page 93–138.
170. Patrick R, Horin C, Kobe B, Cao K-AL, Bodén M. Prediction of kinase-specific phosphorylation sites through an integrative model of protein context and sequence. Biochim Biophys Acta - Proteins Proteomics 2016; 1864:1599–608.
171. Auf G, Jabouille A, Guérit S, Pineau R, Delugin M, Bouchecareilh M, Magnin N, Favereaux A, Maitre M, Gaiser T, et al. Inositol-requiring enzyme 1α is a key regulator of angiogenesis and invasion in malignant glioma. Proc Natl Acad Sci 2010; 107:15553–8.
172. Moiseenko F, Volkov N, Bogdanov A, Dubina M, Moiseyenko V. Resistance mechanisms to drug therapy in breast cancer and other solid tumors: An opinion. F1000Research 2017; 6:288.
173. Maione P, Sacco PC, Sgambato A, Casaluce F, Rossi A, Gridelli C. Overcoming resistance to targeted therapies in NSCLC: current approaches and clinical application. Ther Adv Med Oncol 2015; 7:263–73.
174. Bilfinger T, Keresztes R, Albano D, Nemesure B. Five-Year Survival Among Stage IIIA Lung Cancer Patients Receiving Two Different Treatment Modalities. Med Sci Monit 2016; 22:2589–94.

175. Uramoto H, Tanaka F. Recurrence after surgery in patients with NSCLC. Transl Lung Cancer Res 2014; 3:242–9.
176. Eberhardt WEE, Gauler TC, LePechoux C, Stamatis G, Bildat S, Krbek T, Welter S, Grunenwald D, Fischer B, Rodrigo H de los R, et al. 10-year long-term survival (LTS) of induction chemotherapy with three cycles cisplatin/paclitaxel followed by concurrent chemoradiation cisplatin/etoposide/45Gy (1.5Gy bid) plus surgery in locally advanced non-small-cell lung cancer (NSCLC)—A multicenter . Lung Cancer 2013; 82:83–9.
177. Wu Y-L, Zhou C, Hu C-P, Feng J, Lu S, Huang Y, Li W, Hou M, Shi JH, Lee KY, et al. Afatinib versus cisplatin plus gemcitabine for first-line treatment of Asian patients with advanced non-small-cell lung cancer harbouring EGFR mutations (LUX-Lung 6): an open-label, randomised phase 3 trial. Lancet Oncol 2014; 15:213–22.
178. Paz-Ares LG, de Marinis F, Dediu M, Thomas M, Pujol J-L, Bidoli P, Molinier O, Sahoo TP, Laack E, Reck M, et al. PARAMOUNT: Final Overall Survival Results of the Phase III Study of Maintenance Pemetrexed Versus Placebo Immediately After Induction Treatment With Pemetrexed Plus Cisplatin for Advanced Nonsquamous Non–Small-Cell Lung Cancer. J Clin Oncol 2013; 31:2895–902.
179. Pignon J-P, Tribodet H, Scagliotti G V, Douillard J-Y, Shepherd FA, Stephens RJ, Dunant A, Torri V, Rosell R, Seymour L, et al. Lung Adjuvant Cisplatin Evaluation: A Pooled Analysis by the LACE Collaborative Group. J Clin Oncol 2008; 26:3552–9.
180. Santana-Davila R, Devisetty K, Szabo A, Sparapani R, Arce-Lara C, Gore EM, Moran A, Williams CD, Kelley MJ, Whittle J. Cisplatin and Etoposide Versus Carboplatin and Paclitaxel With Concurrent Radiotherapy for Stage III Non–Small-Cell Lung Cancer: An Analysis of Veterans Health Administration Data. J Clin Oncol 2015; 33:567–74.
181. Tabchi S, Blais N, Campeau M-P, Tehfe M. Single-center comparison of multiple chemotherapy regimens for concurrent chemoradiotherapy in unresectable stage III non-small-cell lung cancer. Cancer Chemother Pharmacol 2017; 79:381–7.
182. Raparia K, Villa C, DeCamp MM, Patel JD, Mehta MP. Molecular profiling in non-small cell lung cancer: a step toward personalized medicine. Arch Pathol Lab

Med 2013; 137:481–91.

183. Mello RA De. Epidermal growth factor receptor and K-Ras in non-small cell lung cancer-molecular pathways involved and targeted therapies. World J Clin Oncol 2011; 2:367.
184. Chan BA, Hughes BGM. Targeted therapy for non-small cell lung cancer: current standards and the promise of the future. Transl Lung Cancer Res 2015; 4:36–54.
185. Jakobsen KR, Demuth C, Madsen AT, Hussmann D, Vad-Nielsen J, Nielsen AL, Sorensen BS. MET amplification and epithelial-to-mesenchymal transition exist as parallel resistance mechanisms in erlotinib-resistant, EGFR-mutated, NSCLC HCC827 cells. Oncogenesis2017; 6:e307.
186. Sequist L V, Waltman BA, Dias-Santagata D, Digumarthy S, Turke AB, Fidias P, Bergethon K, Shaw AT, Gettinger S, Cosper AK, et al. Genotypic and Histological Evolution of Lung Cancers Acquiring Resistance to EGFR Inhibitors. Sci Transl Med 2011; 3:75ra26-75ra26.
187. Harris A, Sc M, Johnson DW, Ph D, Kesselhut J, Li JJ, Pharm B, Com B, Luxton G, Pilmore A, et al. Anaplastic Lymphoma Kinase Inhibition in Non–Small-Cell Lung Cancer. N Engl J Med 2010; 363:609–19.
188. Holla VR, Elamin YY, Bailey AM, Johnson AM, Litzenburger BC, Khotskaya YB, Sanchez NS, Zeng J, Shufean MA, Shaw KR, et al. ALK: a tyrosine kinase target for cancer therapy. Cold Spring Harb Mol Case Stud 2017; 3:a001115.
189. Kim M-S, Park T-I, Lee Y-M, Jo Y-M, Kim S. Expression of Id-1 and VEGF in non-small cell lung cancer. Int J Clin Exp Pathol 2013; 6:2102–11.
190. Drilon A, Cappuzzo F, Ou S-HI, Camidge DR. Targeting MET in Lung Cancer: Will Expectations Finally Be MET? J Thorac Oncol 2017; 12:15–26.
191. Bhattacharya S, Socinski MA, Burns TF. KRAS mutant lung cancer: progress thus far on an elusive therapeutic target. Clin Transl Med 2015; 4:35.
192. de Castro Carpeño J, Belda-Iniesta C. KRAS mutant NSCLC, a new opportunity for the synthetic lethality therapeutic approach. Transl Lung Cancer Res 2013; 2:142–51.
193. Fenchel K, Sellmann L, Dempke WCM. Overall survival in non-small cell lung cancer—what is clinically meaningful? Transl Lung Cancer Res 2016; 5:115–9.
194. Dasari S, Tchounwou PB. Cisplatin in cancer therapy: molecular mechanisms of action. Eur J Pharmacol 2014; 0:364–78.
195. Ardizzoni A, Boni L, Tiseo M, Fossella F V, Schiller JH, Paesmans M,

Radosavljevic D, Paccagnella A, Zatloukal P, Mazzanti P, et al. Cisplatin- Versus Carboplatin-Based Chemotherapy in First-Line Treatment of Advanced Non–Small-Cell Lung Cancer: An Individual Patient Data Meta-analysis. JNCI J Natl Cancer Inst 2007; 99:847–57.

196. Wysokiński R, Kuduk-Jaworska J, Michalska D. Electronic structure, Raman and infrared spectra, and vibrational assignment of carboplatin. Density functional theory studies††The authors dedicate this paper to Professor Henryk Chojnacki on the occasion of his 70th birthday. J Mol Struct THEOCHEM 2006; 758:169–79.
197. Hah SS, Stivers KM, De Vere White RW, Henderson PT. Kinetics of carboplatin-DNA binding in genomic DNA and bladder cancer cells as determined by accelerator mass spectrometry. Chem Res Toxicol 2006; 19:622–6.
198. Aggarwal SK, Fadool JM. Effects of Cisplatin and Carboplatin on Neurohypophysis, Parathyroid and their Role in Nephrotoxicity BT - Platinum and Other Metal Coordination Compounds in Cancer Chemotherapy: Proceedings of the Fifth International Symposium on Platinum and Other Metal. In: Nicolini M, editor. . Boston, MA: Springer US; 1988. page 235–47.
199. Fennell DA, Summers Y, Cadranel J, Benepal T, Christoph DC, Lal R, Das M, Maxwell F, Visseren-Grul C, Ferry D. Cisplatin in the modern era: The backbone of first-line chemotherapy for non-small cell lung cancer. Cancer Treat Rev 2016; 44:42–50.
200. Gao J, Meng Q, Zhao Y, Chen X, Cai L. EHD1 confers resistance to cisplatin in non-small cell lung cancer by regulating intracellular cisplatin concentrations. BMC Cancer 2016; 16:470.
201. Kim ES, Tang X, Peterson DR, Kilari D, Chow C-W, Fujimoto J, Kalhor N, Swisher SG, Stewart DJ, Wistuba II, et al. Copper transporter CTR1 expression and tissue platinum concentration in non-small cell lung cancer. Lung Cancer 2014; 85:88–93.
202. Yang T, Chen M, Chen T, Thakur A. Expression of the copper transporters hCtr1, ATP7A and ATP7B is associated with the response to chemotherapy and survival time in patients with resected non-small cell lung cancer. Oncol Lett 2015; 10:2584–90.
203. O'Grady S, Finn SP, Cuffe S, Richard DJ, O'Byrne KJ, Barr MP. The role of

DNA repair pathways in cisplatin resistant lung cancer. Cancer Treat Rev 2014; 40:1161–70.

204. Zhao H, Zhang H, Du Y, Gu X. Prognostic significance of BRCA1, ERCC1, RRM1, and RRM2 in patients with advanced non-small cell lung cancer receiving chemotherapy. Tumor Biol 2014; 35:12679–88.
205. Wu F, Lu M, Qu L, Li D-Q, Hu C-H. DNA methylation of hMLH1 correlates with the clinical response to cisplatin after a surgical resection in Non-small cell lung cancer. Int J Clin Exp Pathol 2015; 8:5457–63.
206. Kamal NS, Soria J-C, Mendiboure J, Planchard D, Olaussen KA, Rousseau V, Popper H, Pirker R, Bertrand P, Dunant A, et al. MutS Homologue 2 and the Long-term Benefit of Adjuvant Chemotherapy in Lung Cancer. Clin Cancer Res 2010; 16:1206 LP-1215.
207. Holohan C, Van Schaeybroeck S, Longley DB, Johnston PG. Cancer drug resistance: an evolving paradigm. Nat Rev Cancer 2013; 13:714–26.
208. Michels J, Vitale I, Galluzzi L, Adam J, Olaussen KA, Kepp O, Senovilla L, Talhaoui I, Guegan J, Enot DP, et al. Cisplatin Resistance Associated with PARP Hyperactivation. Cancer Res 2013; 73:2271 LP-2280.
209. Wang S-F, Chen M-S, Chou Y-C, Ueng Y-F, Yin P-H, Yeh T-S, Lee H-C. Mitochondrial dysfunction enhances cisplatin resistance in human gastric cancer cells via the ROS-activated GCN2-eIF2α-ATF4-xCT pathway. Oncotarget 2016; 7:74132–51.
210. Yao Z, Jones AWE, Fassone E, Sweeney MG, Lebiedzinska M, Suski JM, Wieckowski MR, Tajeddine N, Hargreaves IP, Yasukawa T, et al. PGC-1[beta] mediates adaptive chemoresistance associated with mitochondrial DNA mutations. Oncogene 2013; 32:2592–600.
211. Tung M-C, Lin P-L, Wang Y-C, He T-Y, Lee M-C, Yeh S-D, Chen C-Y, Lee H. Mutant p53 confers chemoresistance in non-small cell lung cancer by upregulating Nrf2. Oncotarget 2015; 6:41692–705.
212. Ma X, Le Teuff G, Lacas B, Tsao MS, Graziano S, Pignon J-P, Douillard J-Y, Le Chevalier T, Seymour L, Filipits M, et al. Prognostic and Predictive Effect of TP53 Mutations in Patients with Non–Small Cell Lung Cancer from Adjuvant Cisplatin–Based Therapy Randomized Trials: A LACE-Bio Pooled Analysis. J Thorac Oncol 2016; 11:850–61.
213. Nishioka T, Luo L-Y, Shen L, He H, Mariyannis A, Dai W, Chen C. Nicotine

increases the resistance of lung cancer cells to cisplatin through enhancing Bcl-2 stability. Br J Cancer 2014; 110:1785–92.

214. Williams J, Lucas PC, Griffith KA, Choi M, Fogoros S, Hu YY, Liu JR. Expression of Bcl-xL in ovarian carcinoma is associated with chemoresistance and recurrent disease. Gynecol Oncol 2005; 96:287–95.
215. Chen W, Bai L, Wang X, Xu S, Belinsky SA, Lin Y. Acquired Activation of the Akt/Cyclooxygenase-2/Mcl-1 Pathway Renders Lung Cancer Cells Resistant to Apoptosis. Mol Pharmacol 2010; 77:416 LP-423.
216. Liu L-Z, Zhou X-D, Qian G, Shi X, Fang J, Jiang B-H. AKT1 Amplification Regulates Cisplatin Resistance in Human Lung Cancer Cells through the Mammalian Target of Rapamycin/p70S6K1 Pathway. Cancer Res 2007; 67:6325 LP-6332.
217. Hu W, Jin P, Liu W. Periostin Contributes to Cisplatin Resistance in Human Non-Small Cell Lung Cancer A549 Cells via Activation of Stat3 and Akt and Upregulation of Survivin. Cell Physiol Biochem 2016; 38:1199–208.
218. Traverso N, Ricciarelli R, Nitti M, Marengo B, Furfaro AL, Pronzato MA, Marinari UM, Domenicotti C. Role of glutathione in cancer progression and chemoresistance. Oxid. Med. Cell. Longev.2013;
219. Gray MJ, Mhawech-Fauceglia P, Yoo E, Yang W, Wu E, Lee AS, Lin YG. AKT inhibition mitigates GRP78 (glucose-regulated protein) expression and contribution to chemoresistance in endometrial cancers. Int J Cancer 2013; 133:21–30.
220. Weil T, Santamaría R, Lee W, Rung J, Tocci N, Abbey D, Bezerra AR, Carreto L, Moura GR, Bayés M, et al. Adaptive Mistranslation Accelerates the Evolution of Fluconazole Resistance and Induces Major Genomic and Gene Expression Alterations in Candida albicans. mSphere 2017; 2.
221. Blanco R, Iwakawa R, Tang M, Kohno T, Angulo B, Pio R, Montuenga LM, Minna JD, Yokota J, Sanchez-Cespedes M. A Gene-Alteration Profile of Human Lung Cancer Cell Lines. Hum Mutat 2009; 30:1199–206.
222. VANDEWYNCKEL Y-P, LAUKENS D, GEERTS A, BOGAERTS E, PARIDAENS A, VERHELST X, JANSSENS S, HEINDRYCKX F, VAN VLIERBERGHE H. The Paradox of the Unfolded Protein Response in Cancer. Anticancer Res 2013; 33:4683–94.
223. Alain T, Morita M, Fonseca BD, Yanagiya A, Siddiqui N, Bhat M, Zammit D,

Marcus V, Metrakos P, Voyer L-A, et al. eIF4E/4E-BP ratio predicts the efficacy of mTOR targeted therapies. Cancer Res.2012;

224. Li X, Zhang K, Li Z. Unfolded protein response in cancer: the physician's perspective. J Hematol Oncol 2011; 4:8.
225. Netzer N, Goodenbour JM, David A, Dittmar KA, Jones RB, Schneider JR, Boone D, Eves EM, Rosner MR, Gibbs JS, et al. Innate immune and chemically triggered oxidative stress modifies translational fidelity. Nature 2009; 462:522–6.
226. Reverendo M, Soares AR, Pereira PM, Carreto L, Ferreira V, Gatti E, Pierre P, Moura GR, Santos MA. TRNA mutations that affect decoding fidelity deregulate development and the proteostasis network in zebrafish. RNA Biol 2014; 11:1199–213.
227. Li L, Boniecki MT, Jaffe JD, Imai BS, Yau PM, Luthey-Schulten ZA, Martinis SA. Naturally occurring aminoacyl-tRNA synthetases editing-domain mutations that cause mistranslation in Mycoplasma parasites. Proc Natl Acad Sci U S A 2011; 108:9378–83.
228. Chapman A, Fernandez del Ama L, Ferguson J, Kamarashev J, Wellbrock C, Hurlstone A. Heterogeneous Tumor Subpopulations Cooperate to Drive Invasion. Cell Rep 2014; 8:688–95.
229. Lenhard B, Orellana O, Ibba M, Weygand-Durašević I. tRNA recognition and evolution of determinants in seryl-tRNA synthesis. Nucleic Acids Res.1999; 27:721–9.
230. Cusack S, Yaremchuk A, Tukalo M. The crystal structure of the ternary complex of T.thermophilus seryl-tRNA synthetase with tRNA(Ser) and a seryl-adenylate analogue reveals a conformational switch in the active site. EMBO J 1996; 15:2834–42.
231. Moreno JA, Radford H, Peretti D, Steinert JR, Verity N, Martin MG, Halliday M, Morgan J, Dinsdale D, Ortori CA, et al. Sustained translational repression by eIF2α–P mediates prion neurodegeneration. Nature 2012; 485:507–11.
232. Koul HK, Pal M, Koul S. Role of p38 MAP Kinase Signal Transduction in Solid Tumors. Genes Cancer 2013; 4:342–59.
233. Balmanno K, Cook SJ. Tumour cell survival signalling by the ERK1/2 pathway. Cell Death Differ 2008; 16:368–77.
234. Guerriero I, D'Angelo D, Pallante P, Santos M, Scrima M, Malanga D, De Marco C, Weisz A, Laudanna C, Ceccarelli M, et al. Analysis of miRNA profiles

identified miR-196a as a crucial mediator of aberrant PI3K/AKT signaling in lung cancer cells. Oncotarget 2017; 8:19172–91.

235. Wek RC, Jiang H-Y, Anthony TG. Coping with stress: eIF2 kinases and translational control. Biochem Soc Trans 2006; 34:7 LP-11.
236. Fan C-F, Miao Y, Lin X-Y, Zhang D, Wang E-H. Expression of a phosphorylated form of ATF4 in lung and non-small cell lung cancer tissues. Tumor Biol 2014; 35:765–71.
237. Mowers EE, Sharifi MN, Macleod KF. Autophagy in cancer metastasis. Oncogene 2017; 36:1619–30.
238. Dittmar KA, Goodenbour JM, Pan T. Tissue-Specific Differences in Human Transfer RNA Expression. PLOS Genet 2006; 2:e221.

Annex A - Map of the plasmid

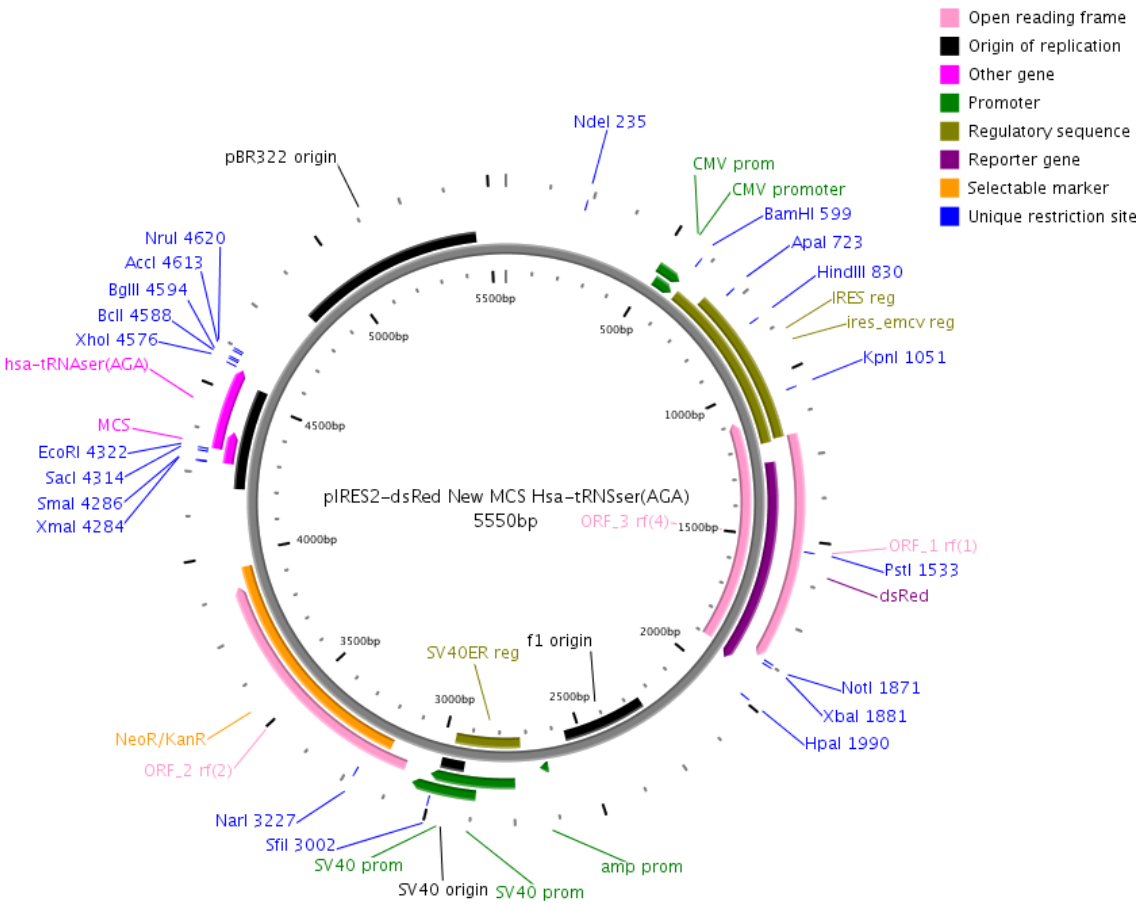

Annex B – (Manuscript) Adaptation of human cells to protein synthesis errors

Disclosure of interests: The author of this thesis, Mafalda Santos, has contributed to the following experiments of this work in collaboration with the first author of the manuscript, Sofia Varanda:

1) Development of the technique that allowed for the detection of tRNAs (SNaPshot);
2) Optimization of the Immunoblots against UPR biomarkers;
3) Revision of this manuscript.

Ana Sofia Varanda[1,2,3], Mafalda Santos[1,2,3], Ana Soares[1], Philippe Pierre[5,6,7], Carla Oliveira[2,3,4] and Manuel Santos[1]

[1]iBiMED & Medical Sciences Department; University of Aveiro; Portugal

[2]Expression Regulation in Cancer, Institute of Molecular Pathology and Immunology, University of Porto (IPATIMUP); Porto; Portugal, [3]Instituto de Investigação e InovaçãoemSaúde; University of Porto; Porto; Portugal, [4]Dept. Pathology and Oncology, Faculty of Medicine, University of Porto; Porto; Portugal

[5]Centre d'Immunologie de Marseille-Luminy; Aix-Marseille Université; Marseille; France

[6]INSERM; Marseille; France, [7]CNRS; Marseille, France

1.1 Abstract

Protein synthesis is a highly-regulated process and maintenance of its fidelity is essential to life. Alterations in the components of the protein synthesis machinery, namely tRNAs, aminoacyl-tRNA synthetases (aaRS) or tRNA modifying enzymes, increase the level of protein synthesis errors (PSE), and are associated with several conditions, from cancer to neurodegeneration. Still, the cause-effect mechanisms remain to be elucidated in many conditions. We hypothesized that accumulation of PSE in human cells activate different protein quality control (PQC) mechanisms depending on the type of error and the duration of the stress stimulus. To address this issue, we modified the anticodon of a human serine transfer RNA ($tRNA^{Ser}$), to incorporate the amino acid serine (Ser) at various non-cognate sites and overexpressed the wild type (Wt) $tRNA^{Ser}$ to evaluate the effects of tRNA misexpression. Stable HEK293 cell lines were produced and analyzed at different time points (cells passages). As expected, mutant tRNAs and tRNA pool deregulation led to accumulation of misfolded proteins. Activation of the ubiquitin-proteasome system (UPS) and the unfolded protein response (UPR) fully protected these cells from proteotoxic stress, maintaining viability intact. Evolution of these

cell lines showed differential adaptation responses to different types of tRNAs' misexpression. In some cases, adaption was mainly due to increased protein turnover, while in other cases, UPR activation with consequent protein synthesis inhibition was the main adaption mechanism. Our data provide new insight on how mammalian cells cope and adapt to proteotoxic stress induced by PSE.

1.2 Introduction

Tight control of protein synthesis is essential for cell functioning, nonetheless the high rate of ribosome decoding, which is required to maintain proteome homeostasis, affects the accuracy of mRNA translation and proteins are synthesized with some level of error. Indeed, lowering translation rate increases protein synthesis accuracy, but impacts negatively on growth rate and fitness [1, 2]. Protein synthesis errors (PSE) can arise during both aminoacylation of tRNAs and mRNA decoding by the ribosomes [3, 4]. The rate of eukaryotic protein synthesis error measured under normal experimental conditions, i.e., downstream of protein quality control (PQC) processes, is between 10^{-3} and 10^{-4} [4, 5]. Since most polypeptides containing erroneous amino acids are degraded, the real rate of amino acid misincorporation is much higher than those values, suggesting that defective PQC can have catastrophic consequences for the cell. Similarly, stress conditions, in particular amino acid starvation, and metabolic deregulation associated with pathology and aging increase error frequency [6]. In other words, a fraction of defective proteins is continually produced by cells making the existence of perfect proteomes an impossible task [7].

Not surprisingly, deregulation of protein synthesis factors that maintain translational accuracy has been associated with human diseases [8, 9]. For instance, mutations in genes encoding the glycyl-tRNA synthetase (GlyRS), have been found in patients with Charcot-Marie-Tooth neuropathy [10, 11]. Mutations in mitochondrial $tRNA^{Leu}$ are linked to mitochondrial encephalomyophathy, lactic acidosis, and stroke-like episodes (MELAS) [12, 13]. Deregulation of the tRNA pool and tRNA modifying enzymes have been observed in cancer [14–19]. In breast tumors there is strong upregulation (> 10 fold) of nuclear and mitochondrial encoded tRNAs [14]. The tRNA modifying enzyme TRMT12 (tRNA methyltransferase homolog 12, involved in the formation of wybutosine at position 37 on $tRNA^{Phe}$) is overexpressed in various breast tumors [17, 19]. Despite clear association with disease, how such deregulation and mutations causes disease are poorly understood. One possibility is that PSE may saturate PQC, leading to accumulation of misfolded and aggregated proteins [20–24]. For example, molecular chaperones

selectively recognize misfolded proteins and promote refolding or degradation via the ubiquitin-proteasome system (UPS) [6, 25]. Accumulation of misfolded proteins in the endoplasmic reticulum (ER) normally saturates ER chaperones (as GRP78/BiP), triggering the activation of the unfolded protein response (UPR) through its branches, namely ATF6, IRE1 or PERK [26]. These pathways, regulate protein synthesis, decrease ER load, increase ER folding capacity and increase the degradation of misfolded proteins [27]. In mice, a mutation in the editing domain of alanyl-tRNA synthetase (AlaRS), leads to the formation of toxic aggregates, an increase in protein ubiquitination, formation of autophagosomes, induction of molecular chaperones (members of Hsp70 family) and upregulation of the UPR (induction of BiP and CHOP). This ultimately leads to Purkinge cell death [21]. Some cancer cells have increased growth rate, regulated by signals related to proliferation, metabolism and protein synthesis, explaining the global upregulation of tRNAs and tRNA modifying enzymes [28]. This also induces ER stress and activation of UPR pathways [29, 30], suggesting that protein misfolding, and eventually PSE, may be prevalent in cancer.

The objective of this study was to clarify the poorly understood consequences of PSE in human cells. In particular, we wanted to elucidate how these cells cope and adapte to such errors and whether they affect cell viability, activate the UPR and produce phenotypes that are common in diseases associated with deregulation of protein synthesis factors. To address these questions, we have created HEK293 cell lines expressing mutant tRNAs that randomly misincorporate serine (Ser) at alanine (Ala), leucine (Leu) and histidine (His) codon sites, on a proteome wide scale. A cell line expressing extra copies of the wild type (Wt) $tRNA_{AGA}^{Ser}$ was also produced to gain insight on the cellular consequences of tRNA imbalances; often observed in tumors. Cellular responses were studied at different time points (cells passages) to clarify how these HEK293 cells adapt to PSE.

Our data show that immortalized cells cope relatively well with the presence of mutant tRNAs or overexpression of the Wt $tRNA^{Ser}$. We observed accumulation of aggregated and ubiquitinated proteins and activation of the UPS and UPR, as expected. Activation of PQC mechanisms is differential according to the type of error introduced in proteins and to the cell passage. Additionally, the expression of mutant tRNAs decreased as cell passage increase, suggesting that human cells modulate expression of mutant tRNAs to decrease their destabilizing effect on the proteome.

1.3 Results

1.3.1 Human cell line models of PSE

Previous studies from Geslain and colleagues reported a novel approach for the induction of stress responses to protein aggregation, based on engineered tRNAs in HEK293 cells [24]. This strategy allows the introduction of mutations of increasing severity randomly in the proteome. The decoding sequence (anticodon) of $tRNA^{Ser}$ was altered, not influencing the recognition by the seryl-tRNA synthetase (SerRS). The altered tRNA is aminoacylated with Ser, but will be used by the ribosome to translate codons complementary to the engineered anticodon. tRNAs produced by Geslain were tested for their ability to restore fluorescence of a GFP reporter, where the essential residue serine-65 (S65) had been substituted for the codons recognized by the engineered tRNAs, proving that mutant tRNAs are fully functional in HEK293 cells. Amino acid analysis of purified GFP from cells transfected with some of these tRNAs ($tRNA^{Ser}$(Lys), $tRNA^{Ser}$(His), $tRNA^{Ser}$(Ile)) showed that the mutable residues had been replaced by serine [24].

In the current study, and to induce PSE in HEK293 cells, we mutated the anticodon of the human Wt $tRNA_{AGA}^{Ser}$ to produce a set of tRNAs: $tRNA_{AGC}^{Ser}$, $tRNA_{AAG}^{Ser}$, $tRNA_{GTG}^{Ser}$ that misincorporate Ser at Ala, Leu and His codon sites, respectively (Figure 1-1).

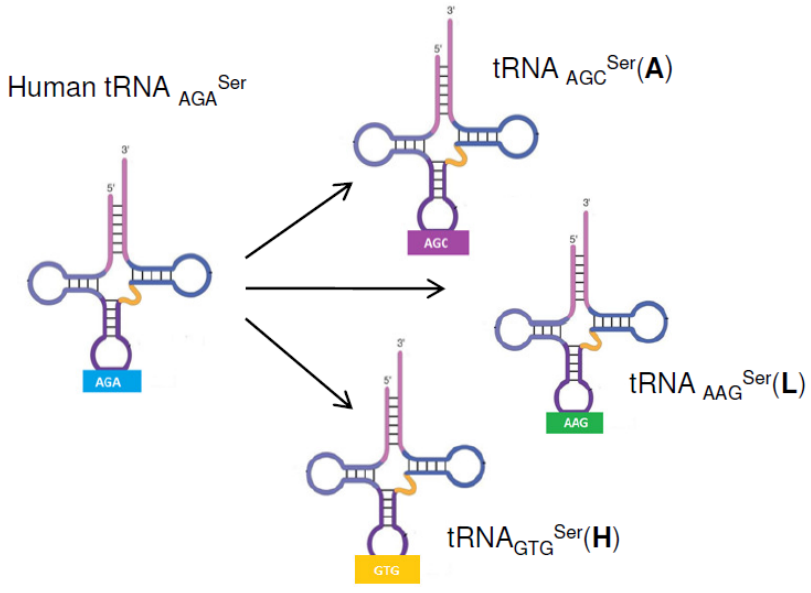

Figure 1-1. Representation of the human $tRNA_{AGA}^{Ser}$ and mutant tRNAs used in the study.

These mutations do not interfere with serylation of the tRNAs by the SerRS, because this enzyme recognizes the extra-arm and discriminator base, rather than the anticodon of $tRNA^{Ser}$ [31, 32]. Participation of these tRNAs in protein synthesis leads to random incorporation of Ser at non-cognate sites, synthesis, misfolding, aggregation and degradation of the faulty proteins (Figure 1-2) [22, 24].

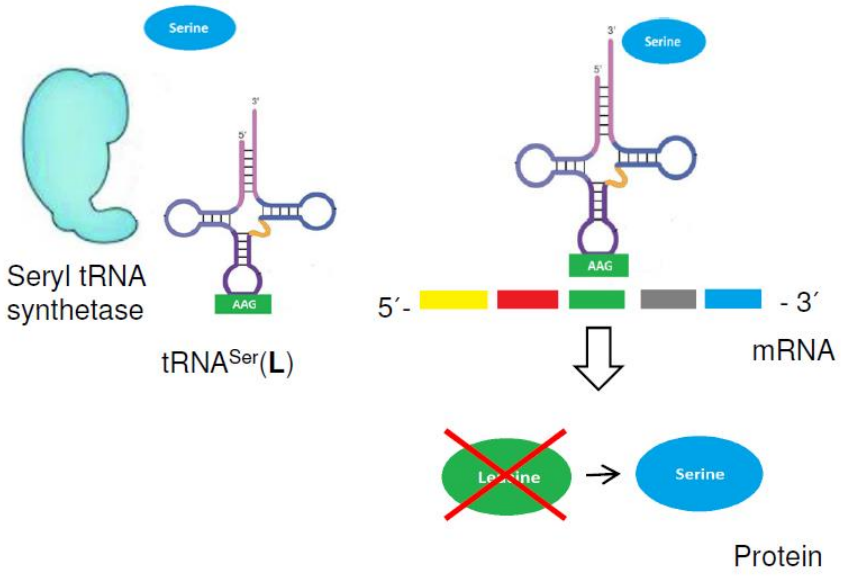

Figure 1-2. Schematic representation of PSE incorporation by the mutant $tRNA_{AAG}^{Ser}$. SerRS is not able to discriminate between endogenous $tRNA^{Ser}$ and mutant tRNAs and charges them equally, leading to Ser misincorporation at Leu codon sites.

We chose these alterations in the anticodon to have a broad spectrum of amino acid chemical differences. Ser is polar and hydrophilic and is normally present on protein surfaces, whereas Ala is nonpolar, hydrophobic and is found inside or outside proteins. Leu is hydrophobic and is generally buried in folded proteins, while His is a basic and polar residue [33]. Therefore, Ser misincorporation severity should be higher in the case of misincorporation at Leu codon sites and much lower at Ala codon sites, depending also on the usage of those codons, the competition between endogenous tRNAs ($tRNA_{AGC}^{Ala}$, $tRNA_{AAG}^{Leu}$, $tRNA_{GTG}^{His}$) in the ribosome, and the competition of endogenous $tRNA_{AGA}^{Ser}$ and mutant tRNAs for the SerRS.

HEK293 cells were transfected with the plasmid pIRES2-DsRed containing one copy of each mutant tRNA. The resulting cell lines were denominated: $tRNA^{Ser}$(A), $tRNA^{Ser}$(L), $tRNA^{Ser}$(H). Two additional cell lines were also produced: one was transfected with the empty plasmid; Mock (negative control) and another misexpressing the Wt $tRNA_{AGA}^{Ser}$ ($tRNA^{Ser}$(S)).

To gain insight on the long-term adaptation to PSE, three time points (P1, P15 and P30, corresponding to the number of cell passages after transfection and selection in geneticin containing media) were studied. Mutant tRNA expression in these cell lines was monitored by Sanger sequencing during evolution in culture. After P30, some of these cell lines presented additional mutations in the recombinant tRNA genes, namely in the acceptor arm, and for this reason cells were only studied till P30. Each cell line was compared with the control (Mock) of each passage, and for each cell line the values of the three passages (P1, P15 and P30) were compared among each other.

1.3.2 Expression and copy number of mutant tRNAs and tRNA^{Ser} in HEK293 cells

Exogenous tRNA expression was determined using a primer extension reaction (SNaPshot analysis), which allowed to specifically detect the tRNAs with the altered nucleotide in the anticodon. We were able to detect in all cell lines, both the expression of the endogenous tRNA^{Ser} (Figure 1-3 A) and each mutant tRNA (Figure 1-3 B). In the Mock cell line the expression of the endogenous tRNA^{Ser} did not change from P1 to P30 (values around 5 in arbitrary units (a.u.)), but the expression of tRNA^{Ser} in the tRNA^{Ser}(S) cell line (both the endogenous and the exogenous tRNA are detected) altered during our timeline (Figure 1-3 A). The expression of tRNA^{Ser} increased slightly from passage P1 (8.9 a.u.) to P15 (12.7 a.u.) and then decreased from P15 (12.7 a.u.) to P30 (2.9 a.u.) (Figure 1-3 A), suggesting that increasing the levels of the Wt tRNA^{Ser} may be slightly advantageous at the beginning of the evolution, but becomes deleterious in the long term. Expression of all mutant tRNAs decreased gradually from P1 to P30 (Figure 1-3 B). In P1, in tRNA^{Ser}(A) the levels of tRNA$_{AGC}^{Ser}$ were 0.58 a.u. (60% of the endogenous tRNA^{Ser} expression) and in P30 declined to 0.1 a.u. (10% of the endogenous tRNA^{Ser} expression). The relative levels of the tRNA$_{AAG}^{Ser}$(in tRNA^{Ser}(L) cells) and tRNA$_{GTG}^{Ser}$(in tRNA^{Ser}(H) cells) in P1 were 0.3 a.u. (30% of the endogenous tRNA^{Ser} expression) and declined to 0.05 a.u. and 0.03 a.u. (5% and 3% of the endogenous tRNA^{Ser} expression) in P30, respectively (Figure 1-3 B).

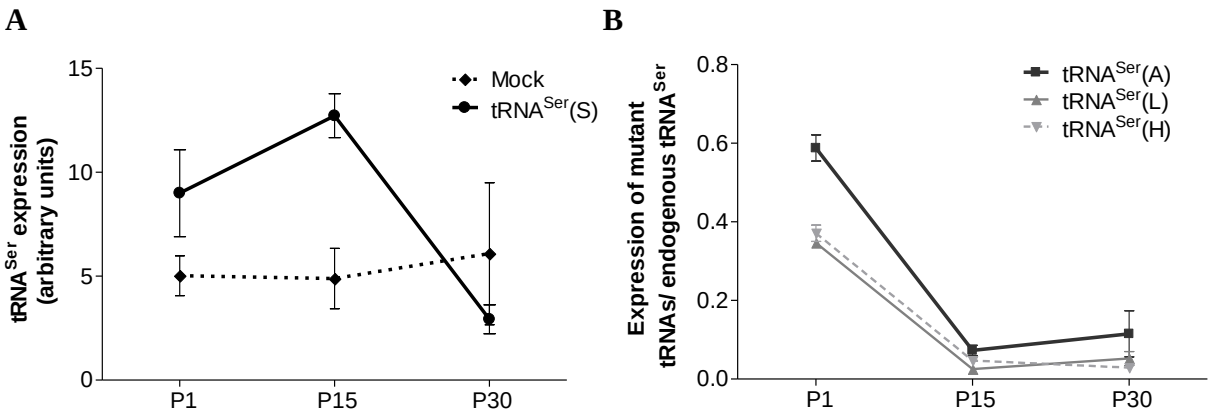

Figure 1-3. Quantification of tRNA^{Ser} and mutant tRNAs expression. A – Detection of tRNA$_{AGA}^{Ser}$ expression in Mock and tRNA^{Ser}(S) cell lines, assessed by the SNaPshot assay. **B –** Expression of mutant tRNAs relative to the Wt endogenous tRNA$_{AGA}^{Ser}$ determined by SNaPshot in tRNA^{Ser}(A), tRNA^{Ser}(L) and tRNA^{Ser}(H) cell lines. tRNA values were normalized to an endogenous control, GAPDH. Data represents Average±SEM of one biological replicate and at least two technical replicates.

To clarify if the gradual decrease in tRNA levels observed during the P1-P30 evolution were caused by differences in tRNA gene copy number we have also used the SNaPshot technique to detect tDNA insertion into the genome of HEK293 cells (Figure 1-4). The number of copies of the tRNA^{Ser} in the genome of Mock and tRNA^{Ser}(S) cell lines was not altered from P1 to P30. As expected, the copy number of tRNA^{Ser} was higher in tRNA^{Ser}(S) cells than in the Mock cell line, confirming incorporation of the plasmid into the genome (Figure 1-4 A). In the tRNA^{Ser}(A) cell line the number of copies of the tDNA decreased from P1 (0.26 a.u., 26% of tRNA^{Ser} copies) to P30 (0.15 a.u., 15% of tRNA^{Ser}copies). In tRNA^{Ser}(L) and tRNA^{Ser}(H) cell lines the number of tDNA copies was maintained. In tRNA^{Ser}(L) cells, tDNA values were around 0.06 a.u. (6% of tDNA^{Ser} copies) and in tRNA^{Ser}(H) cells, tDNA showed values around 0.09 a.u. (9% of tDNA^{Ser} copies). The tRNA^{Ser}(A) cell line incorporated more copies of the respective tDNA, relative to tRNA^{Ser}(L) and tRNA^{Ser}(H) cell lines (Figure 1-4 B).

Therefore, the expression of the tRNAs and respective tDNA copy number are well correlated indicating that the former may be due to transcriptional regulation by Pol III or tRNA degradation, rather than loss of tDNA copies during evolution. tRNA^{Ser}(A) cell line, is an exception since the decreased mutant tRNA expression is accompanied by a decrease in the copy number.

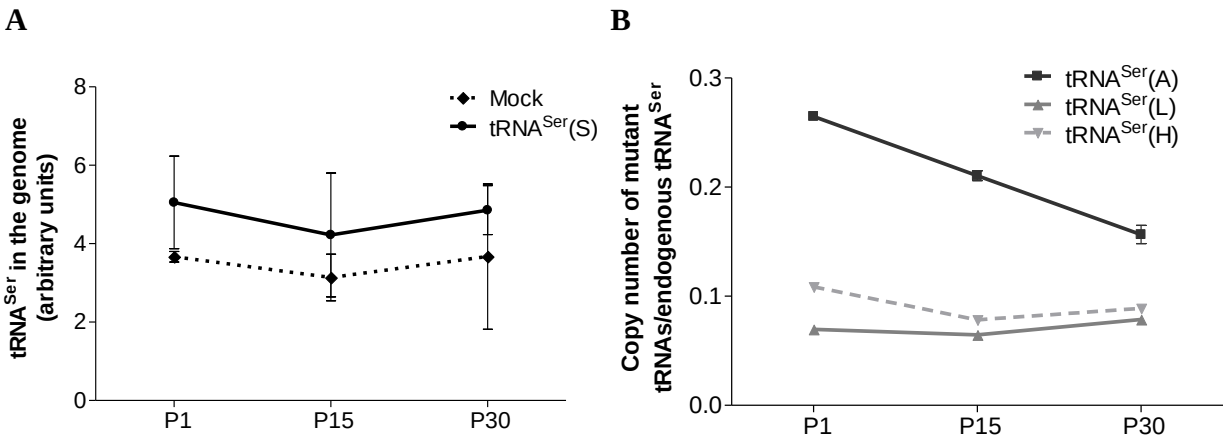

Figure 1-4. Copy number of tRNA^{Ser} and mutant tRNAs. A – tDNA$_{AGA}{}^{Ser}$genomic copy number in Mock and tRNA^{Ser}(S) cell lines, assessed by SNaPshot. **B –** Genomic copy number of the mutant tDNA genes relative to the Wt endogenous tRNA$_{AGA}{}^{Ser}$, assessed by SNaPshot, in tRNA^{Ser}(A), tRNA^{Ser}(L) and tRNA^{Ser}(H) cell lines. tRNA values were normalized to an endogenous control, GAPDH. Data represents Average±SEM of one biological replicate and at least two technical replicates.

1.3.3 Phenotypic effects of PSE

We have accessed cell viability, proliferation, number of anchorage-dependent colonies formed, protein synthesis rate and accumulation of insoluble proteins, as readouts of putative phenotypic effects produced by PSE emerging during evolution of our cell line models.

We used the number of cell passages as landmark of time points during evolution. Since overexpression of Wt tRNA^{Ser} and expression of mutant tRNAs did not affect doubling time of HEK293 cells (approximately 20h), we believed that all cells were approximately in the same generation along the experiment (Figure 1-5).

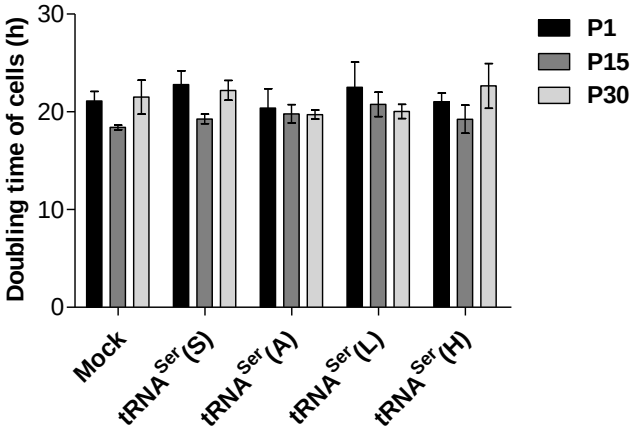

Figure 1-5. Doubling time of cells, assessed by cell counting with Tripan blue. Values represent Average±SEM of three independent experiments in triplicate. One-way ANOVA followed by Dunnett's post-est was used to assess differences between the Mock cell line and cells misexpressing the Wt $tRNA^{Ser}$ ($tRNA^{Ser}$(S)) and expressing mutant tRNAs ($tRNA^{Ser}$(A), $tRNA^{Ser}$(L), $tRNA^{Ser}$(H)) (p>0.05).

In order to test the toxicity of mutant tRNAs and increased copies of the $tRNA^{Ser}$, cell viability was assessed using Tripan blue. Overall, viability was not compromised by the expression of mutant tRNAs or alteration in the tRNA pool (Figure 1-6 A). However, $tRNA^{Ser}$(A) and $tRNA^{Ser}$(L) cell lines showed an increase in viable cells (5.14% and 6.08% respectively), relatively to the Mock in P1 (Figure 1-6 A). This was coincident with the passage in which these mutant tRNAs were most expressed (Figure 1-3 B). During evolution, $tRNA^{Ser}$(A) and $tRNA^{Ser}$(L) cells showed the same pattern of viability, which decreased from P1 and P15 (93% in P1 and a 88% in P15 of viable cells), and recovered from P15 to P30, to a level of viable cells similar to that observed in P1 (~ 93% of viable cells) (Figure 1-6 B).

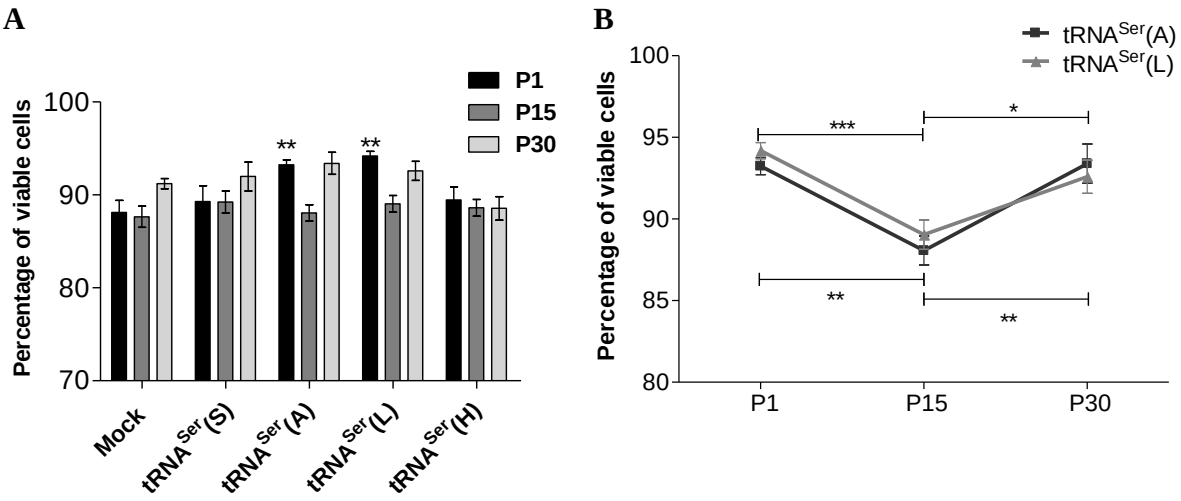

Figure 1-6. Percentage of viable cells in culture determined by cell counting with Tripan blue. A – Percentage of viable cells in comparison with the Mock in each passage (one-way ANOVA, Dunnett's post-test,**p<0.01) **B –** Percentage of viable cells in each time point in $tRNA^{Ser}$(A) and $tRNA^{Ser}$(L) cell lines (one-way ANOVA, Bonferroni's post-test, *p<0.05;**p<0.01;***p<0.001). Values were normalized to the Mock cell line of each passage and represent Average±SEM of three independent experiments in triplicate.

Regarding cell proliferation, assessed with a DNA synthesis–based cell proliferation assay (BrdU), in P1 comparatively to the Mock, there were no alterations (Figure 1-7). In P15, the $tRNA^{Ser}$(A) cell line showed higher proliferation than Mock (1.43 fold), while $tRNA^{Ser}$(H)

cell line showed a decrease of proliferation (0.64 fold) relative to Mock (Figure 1-7 A). In P30, both tRNA^{Ser}(S) and tRNA^{Ser}(A) cell lines proliferated more than the Mock cell line (1.08 fold in both). The tRNA^{Ser}(H) cell line, which showed decrease in proliferation from P1 to P15 (0.33 fold), restored its proliferation values in P30 (1.03 fold) (Figure 1-7 B). The tRNA^{Ser}(A) cell line, which showed an increase in proliferation from P1 to P15 (0.36 fold), in P30 recovered the proliferation values observed in P1 (Figure 1-7 B).

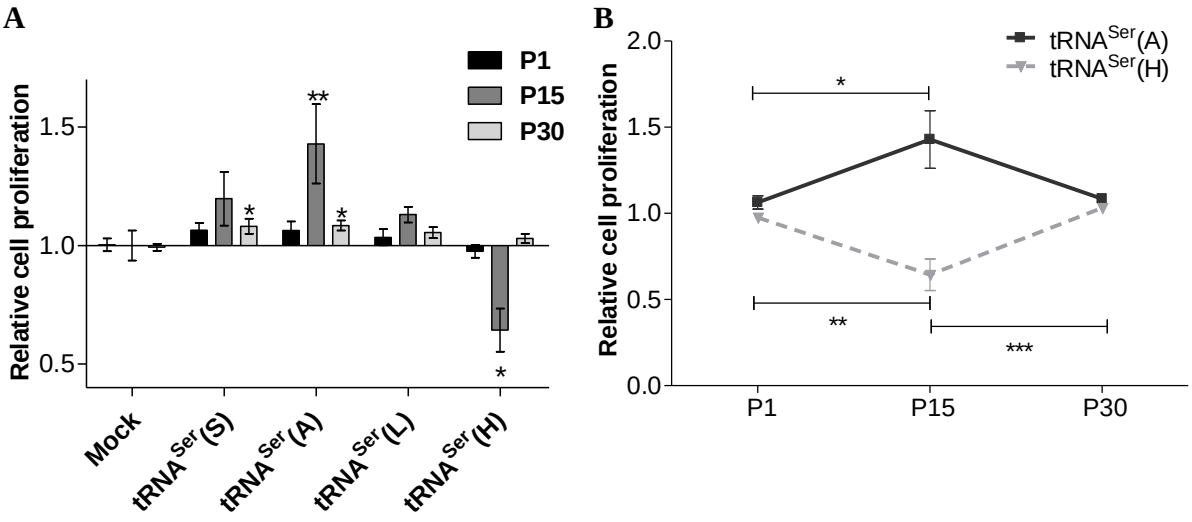

Figure 1-7. Relative cell proliferation determined using a BrdU ELISA Kit. A – Cell proliferation in comparison with Mock in each passage (one-way ANOVA, Dunnett's post-test, (*p<0.05;**p<0.01) **B –** Relative proliferation of tRNA^{Ser}(A) and tRNA^{Ser}(H) cell lines (one-way ANOVA, Bonferroni's post-test, *p<0.05;**p<0.01;***p<0.001).Values were normalized to the Mock cell line of each passage and represent Average±SEM of three independent experiments in triplicate.

Cell proliferation and survival was also assessed using anchorage-dependent colony formation assay, which consists in the ability of a single cell to grow into a colony. Only tRNA^{Ser}(H) cell line had lower colony formation capacity relative to Mock cell line in P15, with an average 12.87 colonies for tRNA^{Ser}(H) vs. 18.44 for Mock (Figure 1-8). This was consistent with proliferation data, as tRNA^{Ser}(H) was the only cell line that displayed decreased proliferation, at this same passage.

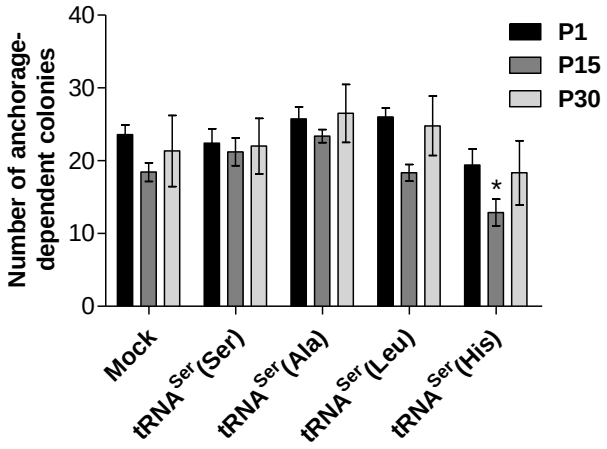

Figure 1-8. Number of colonies formed after 12 days in culture. Values were normalized to the Mock cell line of each passage and represent Average±SEM of three independent experiments in duplicate (one-way ANOVA, Dunnett's post-test, *p<0.05)

Since these engineered cell lines are error prone at the level of protein synthesis, we questioned if protein synthesis rate could be affected during the evolution of these cell lines along 30 passages in culture. To measure protein synthesis rate, we took advantage of the SunSET method, based in the detection of puromycin incorporation into proteins, as described in the methods section [34]. Protein synthesis rate increased in tRNA^{Ser}(A) cells in P1 (1.23 fold) and P15 (1.48 fold) relative to Mock, but decreased in the tRNA^{Ser}(L) cells in P30 (0.61 fold) relative to Mock (Figure 1-9 A). Despite showing increased protein synthesis rate relative to Mock, when we compare the three time points (P1, P15 and P30) of tRNA^{Ser}(A) cell line, there was a decrease from 1.23 fold in P1 to 0.76 fold in P30. The same occurred in tRNA^{Ser}(L) cells, in which protein synthesis rate decreased from 1.20 fold in P1 to 0.61 fold in P30 (Figure 1-9 B).

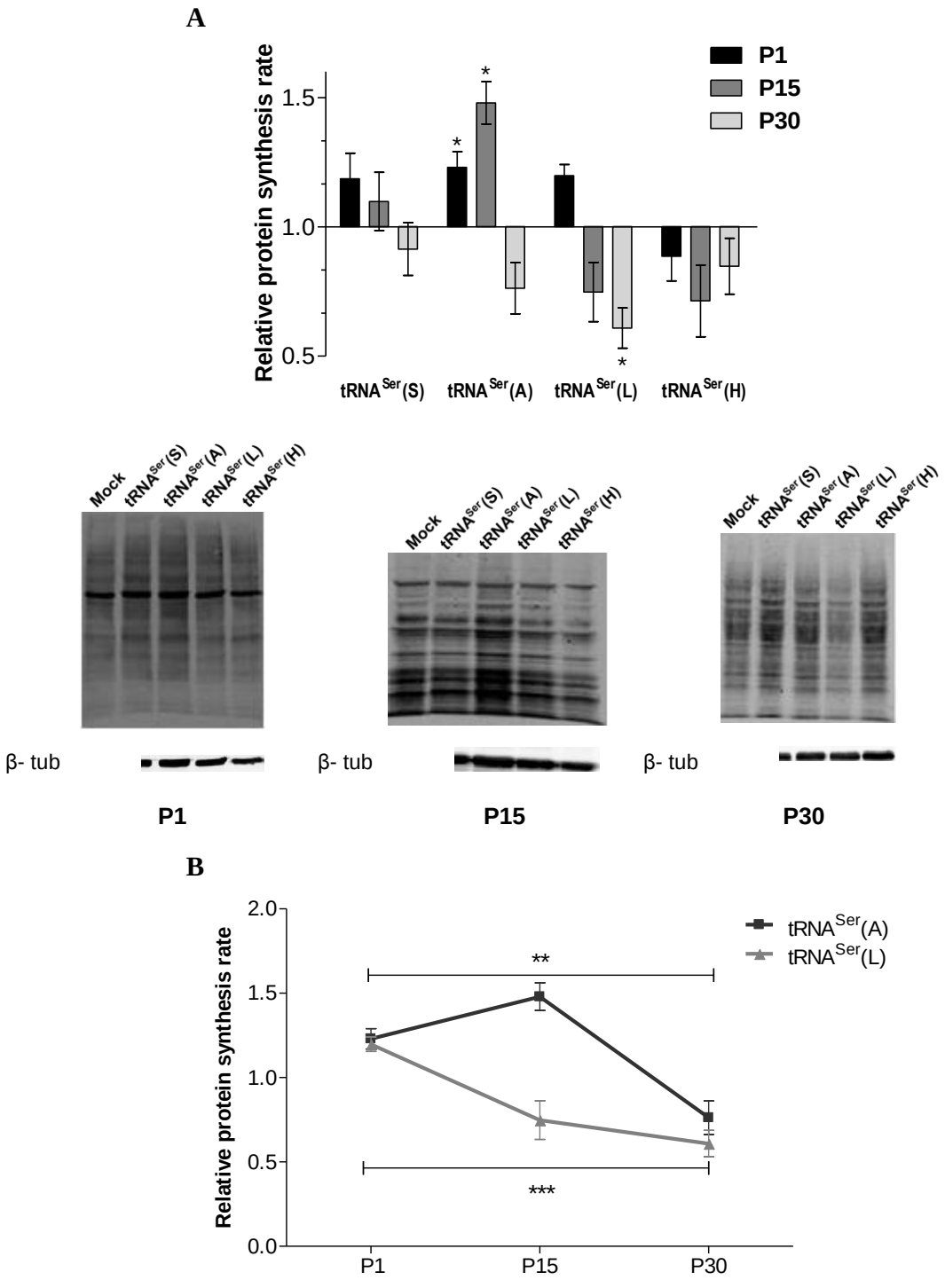

Figure 1-9. Protein synthesis rate determined by SunSET method adapted to immunoblot with anti-puromycin. A – Top panel: Relative protein synthesis rate in comparison with Mock in each passage (one-way ANOVA, Dunnett's post-test, *p<0.05). Mock values for each passage were considered 1 and were not represented in the graph. **Lower panel:** Representative immunoblot images for each time point and cell line and β-tubulin. **B –** Relative protein synthesis rate during evolution of tRNA^{Ser}(A) and tRNA^{Ser}(L) cell lines (one-way ANOVA, Bonferroni's post-test, **p<0.01;***p<0.001). Values were normalized to the Mock cell line of each passage and represent Average±SEM of at least three independent experiments in triplicate.

To test whether mutant and Wt $tRNA^{Ser}$ destabilized the proteome and lead to misfolded protein accumulation and aggregates formation, we have quantified the insoluble protein fraction in P1, P15 and P30. In P15, there was a tendency for increasing levels of insoluble proteins, but it was only statistically significant for the $tRNA^{Ser}$(L) cell line (2.66 fold) (Figure 1-10). This protein aggregation effect was also transient, as the level of insoluble proteins returned to control levels at P30. This result may be explained by the lower expression levels of the mutant tRNAs in P30, but it may also indicate that cells counteracted protein aggregation, through activation of PQC mechanisms. Interestingly, the level of insoluble proteins decreased from P15 (2.1 fold) to P30 (0.71 fold) in the $tRNA^{Ser}$(S) cell line that misexpresses the Wt $tRNA^{Ser}$ (Figure 1-10 B).

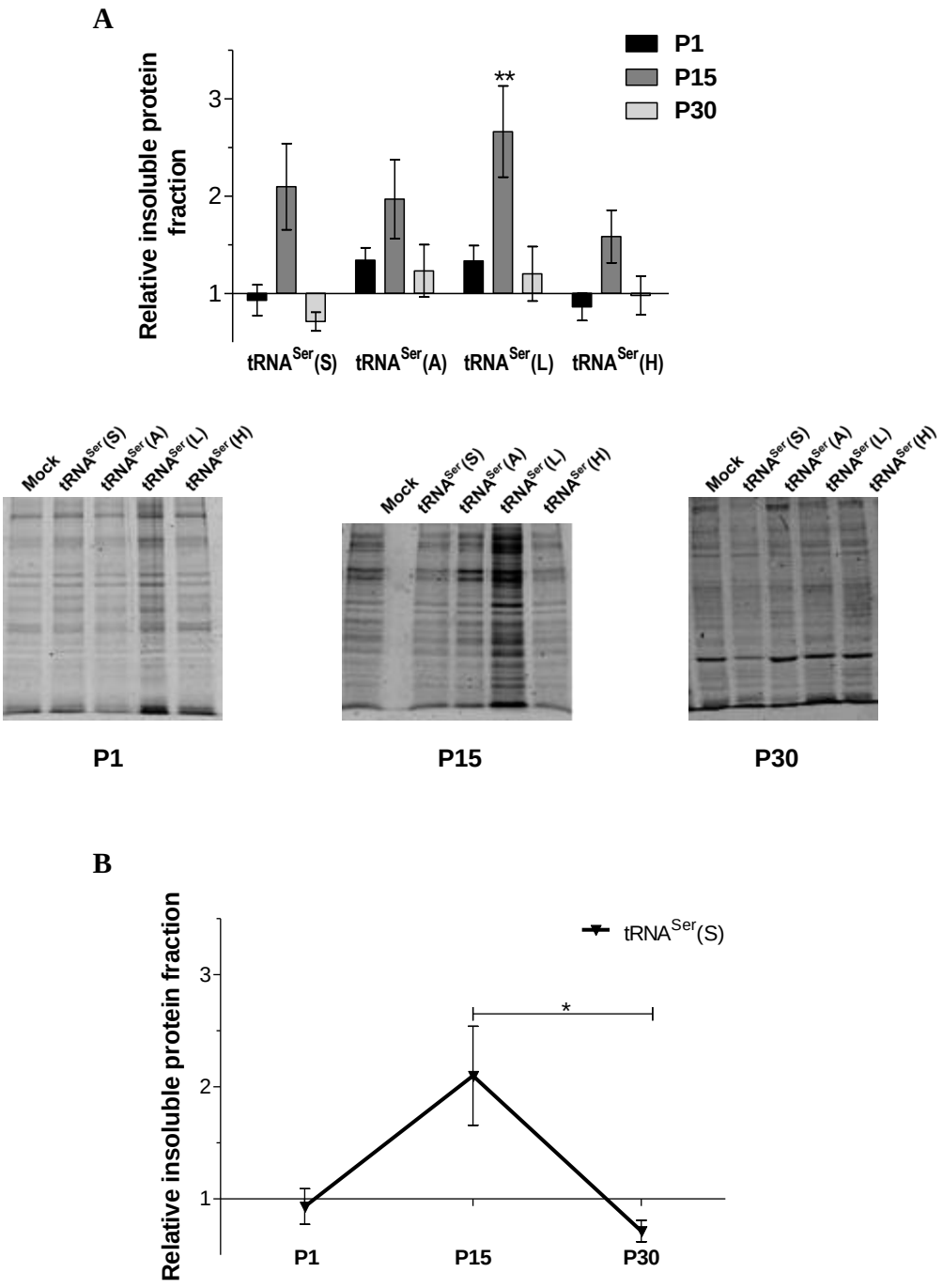

Figure 1-10. Relative insoluble protein fraction. **A – Top panel:** Relative insoluble fraction in comparison with Mock in each passage (one-way ANOVA, Dunnett's post-test, $^{**}p<0.01$). Mock values for each passage were considered 1 and were not represented in the graph. **Lower panel:** Representative acrylamide gel after commassie staining of each time point and cell line. **B –** Protein insoluble fraction during evolution of the tRNA^{Ser}(S) cell line (one-way ANOVA, Bonferroni's post-test, $^{*}p<0.05$). Values were normalized to the Mock cell line of each passage and represent Average±SEM of at least three independent experiments in triplicate.

1.3.4 The impact of PSE in the ubiquitin-proteasome system and molecular chaperones

Eukaryotic cells encompass several mechanisms of PQC to avoid protein aggregation and to eliminate aggregates, if they accumulate. These mechanisms include molecular chaperones, the ubiquitin-proteasome system (UPS), the unfolded protein response (UPR), the endoplasmic reticulum associated protein degradation (ERAD) and autophagy [6, 35, 36]. Since we did not observe significant accumulation of insoluble proteins, particularly in P30, we wondered if erroneous proteins could have been marked by ubiquitin for degradation by the UPS [37, 38]. We observed increased levels of ubiquitinated proteins in the $tRNA^{Ser}$(H) cell line (1.43 fold) in P1 (Figure 1-11 A). In P15, all other cell lines, $tRNA^{Ser}$(S), $tRNA^{Ser}$(A) and $tRNA^{Ser}$(L), also showed higher levels of ubiquitinated proteins (1.36, 1.37 and 1.48 fold respectively) (Figure 1-11 A). In P30, the amount of ubiquitinated proteins in all cell lines was similar to Mock in the same passage. Importantly, from P15 to P30 the amount of ubiquitinated proteins decreased in all cell lines, being statistically significant in $tRNA^{Ser}$(S) (from 1.36 fold in P15 to 0.96 fold in P30) (Figure 1-11 B). The latter data indicates that these cells were able to somehow degrade all proteins targeted by ubiquitination.

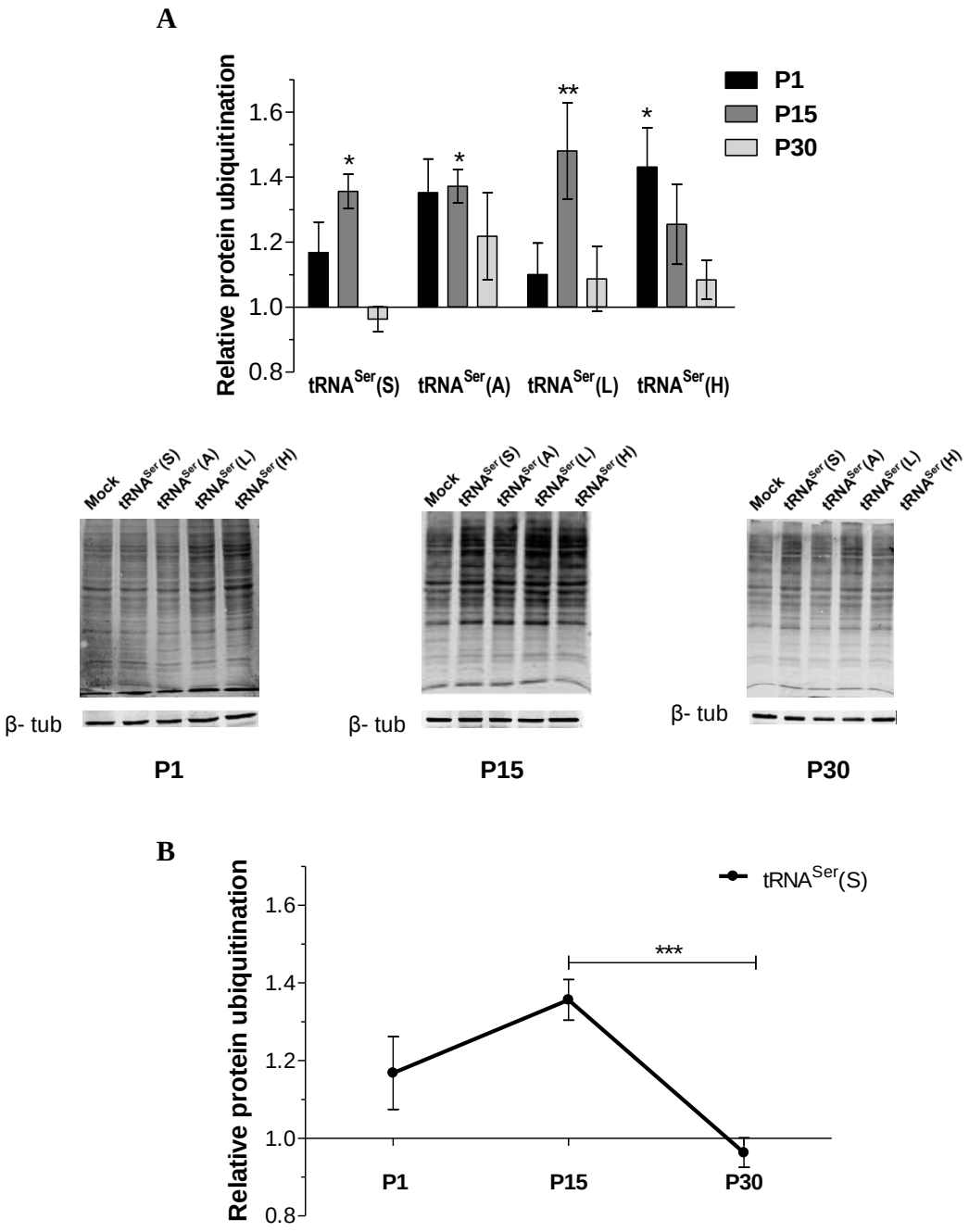

Figure 1-11. Relative protein ubiquitination determined by immunoblot. A – Top panel: Relative protein ubiquitination in comparison with Mock in each passage (one-way ANOVA, Dunnett's post-test, *p<0.05;**p<0.01). Mock values for each passage were considered 1 and were not represented in the graph. **Lower panel:** Representative immunoblot images for each time point and cell line plus β-tubulin are shown. **B –** Relative protein ubiquitination during evolution of the RNA^{Ser}(S) cell line (one-way ANOVA, Bonferroni's post-test, ***p<0.001). Values were normalized to the Mock cell line of each passage and represent Average±SEM of at least three independent experiments in triplicate.

We then checked whether proteasome activity was altered in the same cell lines and time points, using a proteasome activity assay that measures chymotrypsin-like activity. The tRNA^{Ser}(L) cell line showed higher proteasome activity in P1(1.27 fold) (Figure 1-12 A), while tRNA^{Ser}(A) cell line had higher activity relative to Mock in P15 and P30 (2.17 fold and 1.66 fold, respectively) (Figure 1-12 A). However, proteasome activity decreased in the tRNA^{Ser}(L) cell line from 1.85 fold in P15 to 0.97 fold in P30 (Figure 1-12 B). The accumulation of ubiquitinated proteins and insoluble proteins in P15, particularly in this cell line, was likely overwhelming for the proteasome, affecting its degradative capacity. On the other hand, in the tRNA^{Ser}(A) cell line the accumulation of ubiquitinated proteins in P15 was concomitant with increased proteasome activity. tRNA^{Ser}(S) and tRNA^{Ser}(H) cell lines did now show significant alterations in proteasome activity.

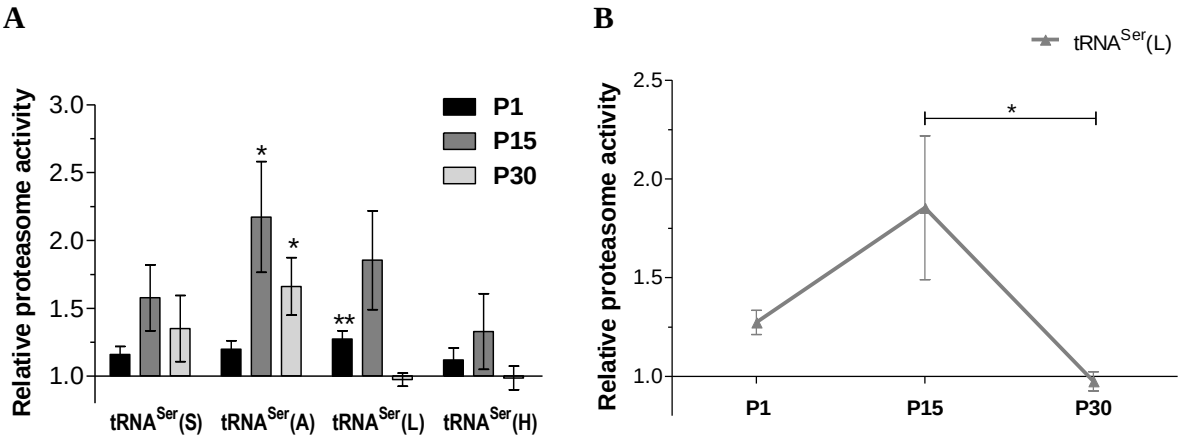

Figure 1-12. Relative proteasome activity. A – Relative proteasome activity assessed by fluorescent measurement of the labeled substrate Suc-LLVY-AMC (one-way ANOVA, Dunnett's post-test, *p<0.05;**p<0.01). Mock values for each passage were considered 1 and were not represented in the graph. **B –** Proteasome activity of the tRNA^{Ser}(L) cell line (one-way ANOVA, Bonferroni's post-test, *p<0.05). Values were normalized to the Mock cell line of each passage and represent Average±SEM of at least three independent experiments in triplicate.

Finally, we checked the molecular chaperones branch of the PQC system. We assessed the expression of those chaperones that are known to play a critical role in protein folding during stress, and whose expression is frequently altered in human diseases, namely Hsp70, Hsp27, Hsp60, Hsp90α and BiP [39, 40]. Hsp70 (heat shock protein 70) binds to a wide range of nascent polypeptides in stress conditions and by shielding hydrophobic regions, prevents aggregation and promotes proper folding. It also recruits ubiquitin ligases, such as CHIP (carboxyl terminus

of Hsp70-interacting proteins) to tag proteins for proteasomal degradation [41]. The expression of Hsp70 did not change in P1 and P15, but decreased in P30 in tRNA^{Ser}(A), tRNA^{Ser}(L) and tRNA^{Ser}(H) cell lines: 0.67, 0.55 and 0.64 fold, respectively (Figure 1-13 A).

In general, the expression of this molecular chaperone decreased during evolution until P30, being this decrease statistically significant in tRNA^{Ser}(A) cells (from 1.02 fold in P1 to 0.67 fold in P30) (Figure 1-13 B).

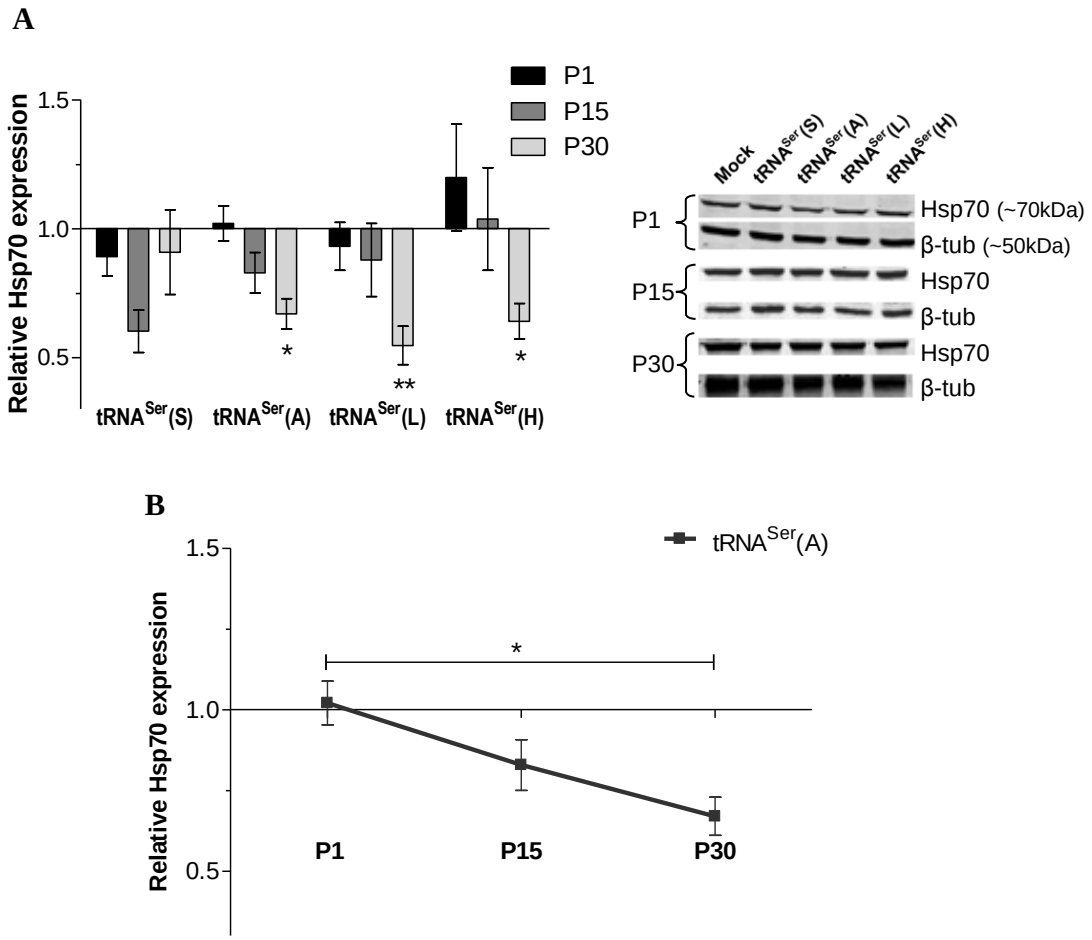

Figure 1-13. Relative HSP70 expression. A – Relative HSP70 expression and respective immunoblots (one-way ANOVA, Dunnett's post-test, *p<0.05;**p<0.01). Mock values for each passage were considered 1 and were not represented in the graph. **B –** Expression in the three different time points of HSP70 in tRNA^{Ser}(A) cell line (one-way ANOVA, Bonferroni's post-test, *p<0.05). Values were normalized to the Mock cell line of each passage and represent Average±SEM of at least three independent experiments in triplicate.

Hsp27 minimizes protein aggregation, by destabilizing aggregates, bind to proteins and aids in the refolding processes, favors degradation of some ubiquitinated proteins by the proteasome and is involved in apoptotic signaling pathways [42]. Its expression increased in

$tRNA^{Ser}$(L) cells in P15 (1.69 fold) and decreased in $tRNA^{Ser}$(L) and $tRNA^{Ser}$(H) cells in P30; 0.53 and 0.56 fold, respectively (Figure 1-14 A). In P15, the increase in Hsp27 levels in the $tRNA^{Ser}$(L) cell line was consistent with the higher levels of insoluble proteins, which may indicate that Hsp27 is being recruited to destabilize aggregated proteins. $tRNA^{Ser}$(S) and $tRNA^{Ser}$(A) cell lines showed increased Hsp27 during early evolution from P1 to P15 (from 0.75 to 1.48 fold and from 0.74 to 1.35 fold, in $tRNA^{Ser}$(S) and $tRNA^{Ser}$(A) cells, respectively). However, from P15 to P30 the level of this chaperone decreased (from 1.49 to 0.96 fold and from 1.35 to 0.69 fold, in $tRNA^{Ser}$(S) and in $tRNA^{Ser}$(A) cells, respectively) (Figure 1-14 B). From P15 to P30, the decrease in the expression of Hsp27 was also statistically significant in $tRNA^{Ser}$(L) (from 1.69 to 0.53 fold) and in $tRNA^{Ser}$(H) cells (from 1.31 to 0.56 fold) (Figure 1-14 C). These alterations in Hsp27 expression are consistent with the dynamics of increased protein ubiquitination in these cell lines in P15.

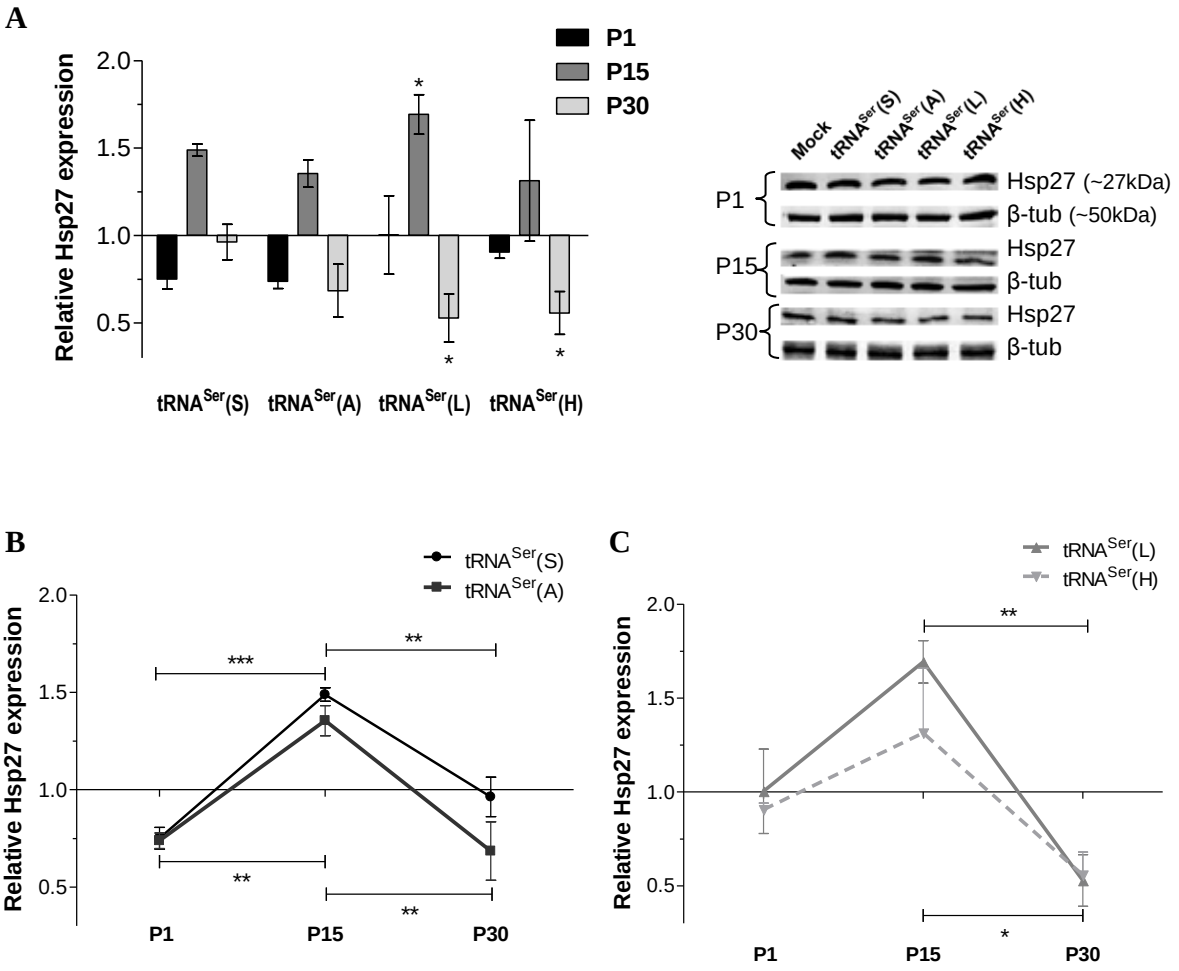

Figure 1-14. Relative Hsp27 expression. **A -** Relative Hsp27 expression the respective immunoblot (one-way ANOVA, Dunnett's post-test, **p*<0.05). Mock values for each passage were considered 1 and were not represented in the graph. **B and C –** Hsp27 expression during evolution line (one-way ANOVA, Bonferroni's post-test, (**p*<0.05;***p*<0.01; ****p*<0.001).Values were normalized to the Mock cell line of each passage and represent Average±SEM of at least three independent experiments in triplicate.

Hsp60 (heat shock protein 60) is a mitochondrial chaperonin involved in protein refolding in the mitochondrial matrix under stress conditions. In our cell lines, the expression of Hsp60 increased in P15 in tRNA^{Ser}(H) cell line (1.48 fold) and decreased in P30 in tRNA^{Ser}(L) (0.69 fold) and tRNA^{Ser}(H) cell lines (0.76 fold) relative to Mock (Figure 1-15 A). The expression of Hsp60 in these two cell lines, increased from P1 to P15 (from 0.83 to 1.4 fold in tRNA^{Ser}(L) cells and from 0.78 to 1.48 fold in tRNA^{Ser}(H) cells), but decreased from P15 to P30 (from 1.4 to 0.69 fold in tRNA^{Ser}(L) cells and from 1.48 to 0.76 fold in tRNA^{Ser}(H) cells) (Figure 1-15 B), indicating that PSE may also affect protein folding in the mitochondria.

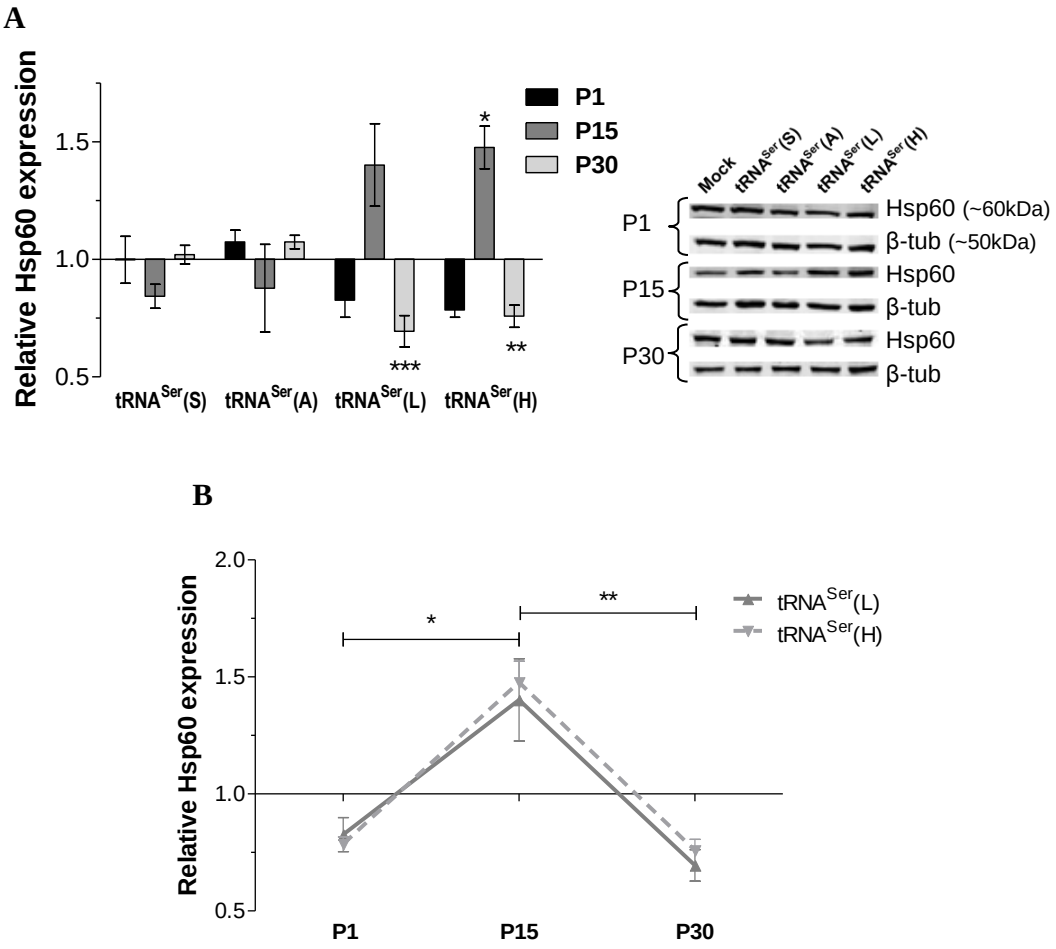

Figure 1-15. Relative Hsp60 expression. A - Relative Hsp60 expression the respective immunoblot (one-way ANOVA, Dunnett's post-test,*p<0.05;**p<0.01; ***p<0.001). Mock values for each passage were considered 1 and were not represented in the graph. **B –** Hsp60 expression during evolution (one-way ANOVA, Bonferroni's post-test, *p<0.05;**p<0.01). Values were normalized to the Mock cell line of each passage and represent Average±SEM of at least three independent experiments in triplicate.

Hsp90α is a molecular chaperone involved in the refolding of specific proteins (normally proteins involved in signal transduction, some of which are ER transmembrane kinases that participate in the UPR) [43]. This protein displayed lower levels in tRNA^{Ser}(L) (0.71 fold) and tRNA^{Ser}(H) (0.69 fold) cell lines in P1, relative to Mock in the same passage (Figure 1-16). In tRNA^{Ser}(S) cell line, Hsp90α increased in P30 (1.31 fold) (Figure 1-16).

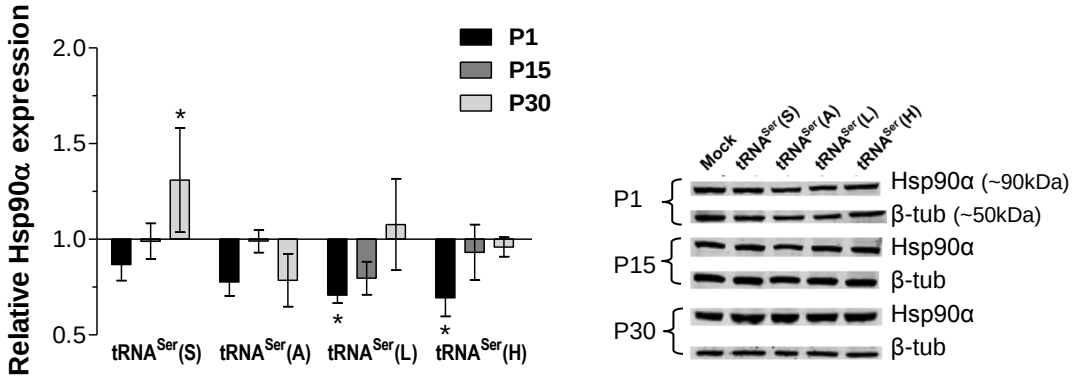

Figure 1-16. Relative Hsp90α expression. Graphic and immunoblot image of Hsp90α expression. Values were normalized to the Mock cell line of each passage and represent Average±SEM of at least three independent experiments in triplicate (one-way ANOVA, Dunnett's post-test, **p*<0.05). Mock values for each passage were considered 1 and were not represented in the graph.

Finally, we accessed the expression of BiP, a molecular chaperone of 70 KDa located in the lumen of the ER that senses ER stress and activates UPR signaling [44]. Its expression was low compared to Mock in tRNA^{Ser}(H) cell line (0.61 fold) in P1 and higher compared to Mock in the tRNA^{Ser}(L) cell line in P30 (1.34 fold) (Figure 1-17 A). In tRNA^{Ser}(L) there was upregulation of this chaperone (from 0.77 to 1.34 fold) from P1 to P30 (Figure 1-17 B), suggesting the presence of misfolded proteins in the ER.

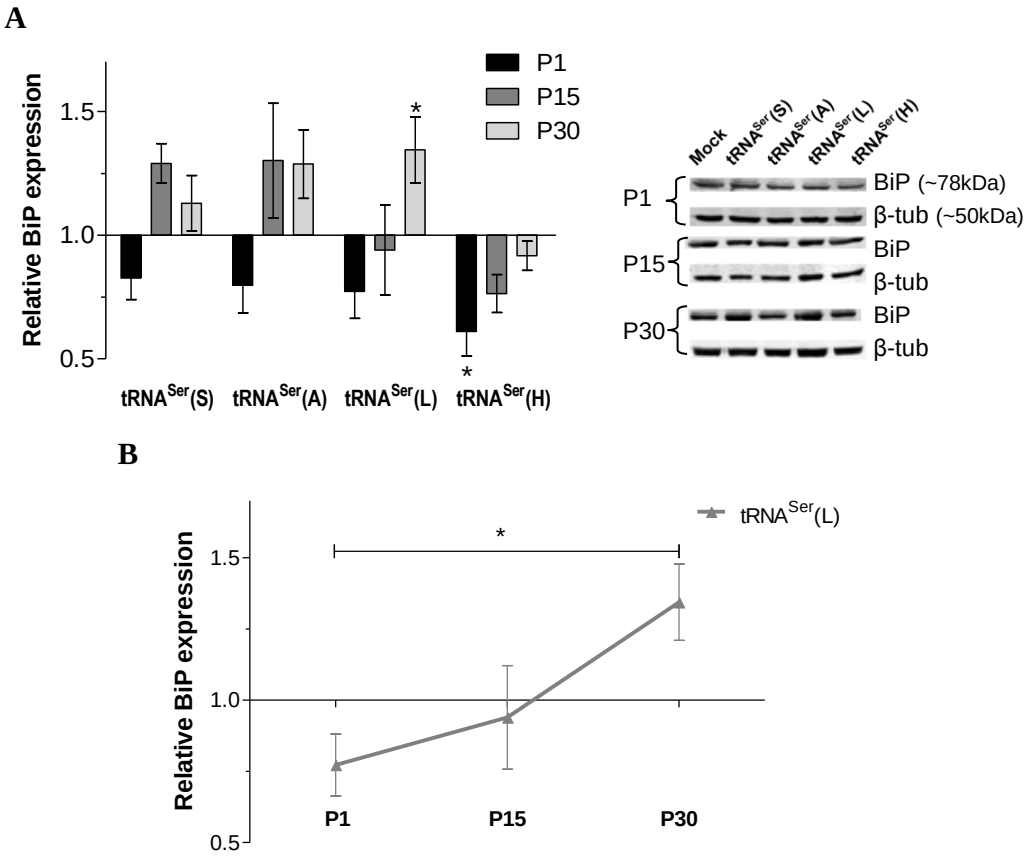

Figure 1-17. Relative BiP expression. A – BiP expression relative to Mock and the corresponding immunoblots (one-way ANOVA, Dunnett's post-test,**p*<0.05). Mock values for each passage were considered 1 and were not represented in the graph. **B –** BiP expression during evolution in tRNA^{Ser}(L) cell line (one-way ANOVA, Bonferroni's post-test, **p*<0.05). Values were normalized to the Mock cell line of each passage and represent Average±SEM of at least three independent experiments in triplicate.

In this part of the study, we have observed accumulation of ubiquitinated proteins in all cell lines, but proteasome activity was only altered in tRNA^{Ser}(A) and tRNA^{Ser}(L) cells. While tRNA^{Ser}(A) cells maintained high proteasome activity, tRNA^{Ser}(L) cells did not. The expression of molecular chaperones changed depending on the cell line and throughout evolution. Hsp70 expression tended to decrease during evolution, while expression of Hsp27 had a peak in P15, which could be correlated with higher levels of ubiquitinated proteins and insoluble proteins in some of the cell lines analyzed. Hsp60 expression was also increased in tRNA^{Ser}(H) cells in P15, but its levels decreased in P30. Hsp90α and BiP presented a different pattern of expression as their expression increased from P1 to P30, in some of our cell lines.

1.3.5 Effects of PSE in the UPR

Accumulation of misfolded proteins in the ER leads to activation of the UPR, which consists in transcriptional activation of genes required for protein folding, ER expansion and ER-associated protein degradation (ERAD). Activation of UPR reduces ER stress, but prolonged activation leads to apoptosis and also the accumulation of reactive oxygen species (ROS) via UPR-regulated oxidative protein folding machinery in the ER, contributing in this way to cell death [45]. To clarify whether constitutive PSE could lead to activation of the UPR, we studied some molecular markers of the UPR branches. Activation transcription factor 6 (ATF6) is a transmembrane protein embedded in the ER. Following ER stress-induced proteolysis, it functions as a nuclear transcription factor [27]. Although in P1 there were no alterations in the ratio of fragmented ATF6/total ATF6 among cell lines, compared to the Mock, $tRNA^{Ser}$(S) cell line displayed an increase in P15 and $tRNA^{Ser}$(A) an increase in P30 (1.69 fold in both cases) (Figure 1-18 A). In $tRNA^{Ser}$(S) cell line the ratio of fragmented ATF6/total ATF6 increased from P1 to P15 (from 0.72 to 1.69 fold) and decreased from P15 to P30 (from 1.69 fold to 0.67 fold) (Figure 1-18 B).

A

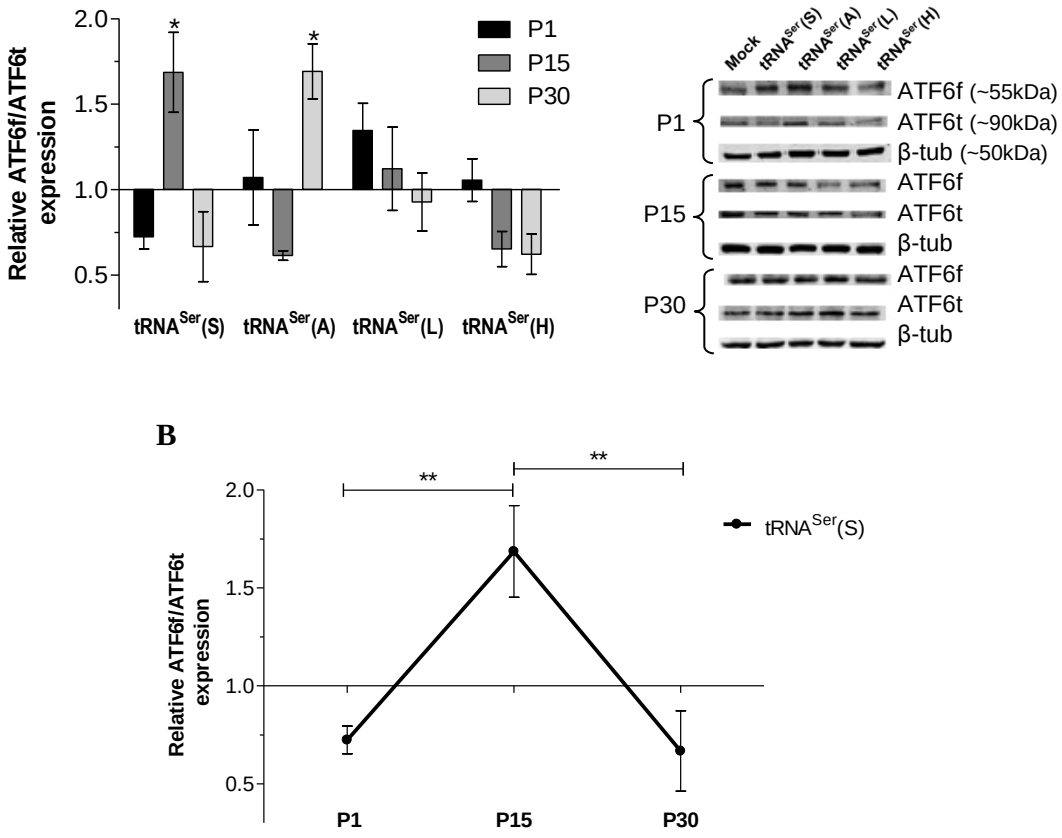

Figure 1-18. Relative ATF6f/ATF6t expression. **A –** ATF6f/ATF6t expression relative to Mock and the corresponding immunoblot (one-way ANOVA, Dunnett's post-test,*p<0.05). Mock values for each passage were considered 1 and were not represented in the graph. **B –** ATF6f/ATF6t expression during evolution in tRNA^{Ser}(S) (one-way ANOVA, Bonferroni's post-test, **p<0.01). Values were normalized to the Mock cell line of each passage and represent Average±SEM of at least three independent experiments in triplicate.

Another marker of UPR activation is the phosphorylation of the eukaryotic initiation factor 2α (eIF2α-P). In cases of ER stress, PERK phosphorylates and inactivates eIF2α, shutting down mRNA translation to reduce protein load in the ER [46]. Only in P30 were observed diffrences in the ratio eIF2α-P/total eIF2α in our cell lines. The ratio eIF2α-P/total eIF2α decreased in tRNA^{Ser}(A) (0.53 fold) and increased in tRNA^{Ser}(L) (1.6 fold), comparing to Mock (Figure 1-19 A). In the latter, this happened gradually throughout evolution, from P1 to P30 (from 0.8 to 1.6 fold) (Figure 1-19 B) and this decrease is consistent with the decreased protein synthesis rate in P30 (Figure 1-9). The decrease of eIF2α-P in the tRNA^{Ser}(A) cell line made us wonder whether it was caused by downregulation of PERK, or upregulation of the eIF2α phosphatase PP1's regulatory domain, GADD34. Our data showed an increase in GADD34 expression only in tRNA^{Ser}(A), in P30 (1.71 fold) (Figure 1-20 A) and from P1 to P30 (from 0.98 to 1.71 fold) (Figure 1-20 B). These results confirm that

GADD34 plays an important role in the maintenance of protein translational rate in this particular cell line.

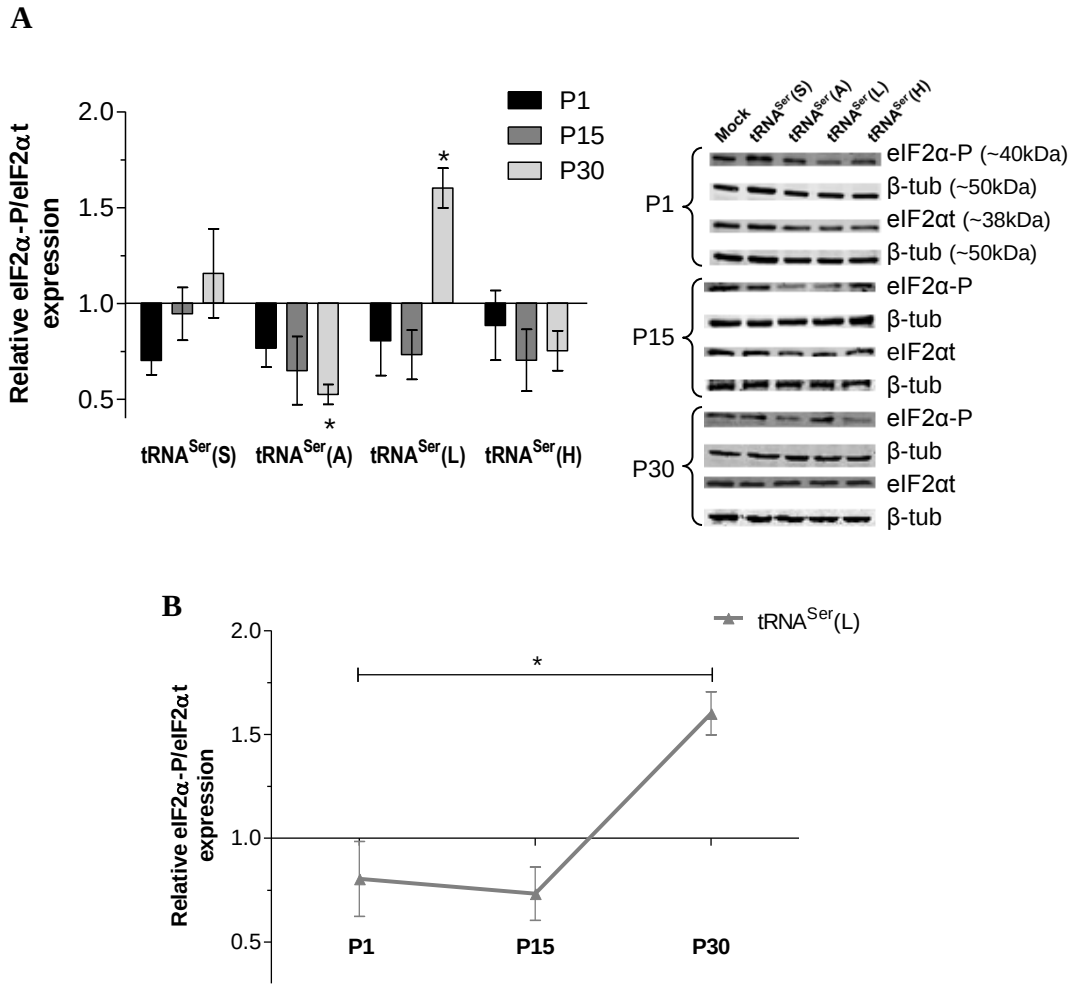

Figure 1-19. Relative eIF2αP/eIF2αt expression. **A –** eIF2αP/ eIF2αt expression relative to Mock and the corresponding immunoblots (one-way ANOVA, Dunnett's post-test,**p*<0.05). Mock values for each passage were considered 1 and were not represented in the graph. **B –** eIF2αP/ eIF2αt expression during evoltution in tRNA^{Ser}(L) cells (one-way ANOVA, Bonferroni's post-test,**p*<0.05). Values were normalized to the Mock cell line of each passage and represent Average±SEM of at least three independent experiments in triplicate.

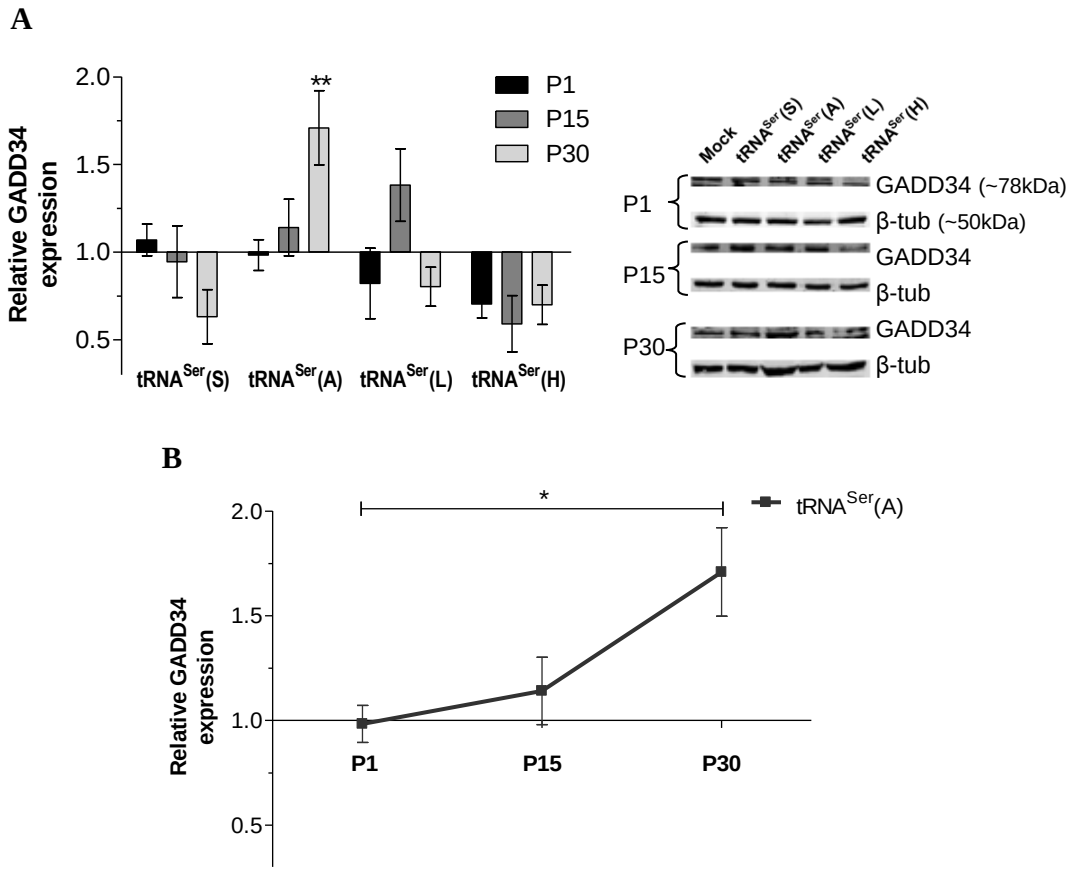

Figure 1-20. Relative GADD34 expression. A – GADD34 expression relative to Mock and the corresponding immunoblots (one-way ANOVA, Dunnett's post-test, **p<0.01). Mock values for each passage were considered 1 and were not represented in the graph. **B –** GADD34 expression during evoltution in tRNA^{Ser}(A) cells (one-way ANOVA, Bonferroni's post-test,*p<0.05). Values were normalized to the Mock cell line of each passage and represent Average±SEM of at least three independent experiments in triplicate.

Therefore, different types of PSE activated different UPR pathways, probably due to differences in ER stress intensity. Indeed, in the tRNA^{Ser}(A) cell line, where protein misfolding levels and ER stress are probably milder (Ser and Ala are chemical similar amino acids), there was an increase in fragmented ATF6, concomitant with increased accumulation of ubiquitinated proteins and proteasome activity. This is physiologically relevant since ATF6 is also responsible for protection against ER stress-induced apoptosis and cell survival [47]. However, in the tRNA^{Ser}(L) cell line, where the level of misfolded proteins and ER stress should be more intense due to bigger chemical differences between Ser and Leu, phosphorylation of eIF2α repressed protein synthesis. This did not happen in the tRNA^{Ser}(A) cell line due to eIF2α dephosphorylation by GADD34, that maintained the levels of protein synthesis rate and allowed a balance between protein degradation and protein synthesis.

1.3.6 Transcriptional deregulation induced by PSE

To obtain a better picture of PQC activation in our model, we have characterized our cell lines using cDNA microarrays. We focused our gene expression data analysis on UPR, UPS, autophagy, translational factors and ribosomal protein genes (Table 2-1). Regarding the UPR genes, *ERN1*(endoplasmic reticulum to nucleus signaling 1, IRE1), *XBP1*(X-box binding protein 1) and *EIF2AK3* (eukaryotic translation factor 2 alpha kinase 3, PERK) were deregulated in our cells. In P1, *ERN1* was downregulated 2.4 fold in tRNA^{Ser}(S), 2.0 fold in tRNA^{Ser}(A) and 1.8 fold in tRNA^{Ser}(L) cells. On the contrary, *XBP1* (wich correspondes to the unspliced transcript) was upregulated 1.5 fold in P1 and 1.8 fold in P15 in tRNA^{Ser}(S) cells. *ERN1* catalyzes the splicing of XBP1 mRNA. Probably, since *ERN1* is downregulated in P1 in tRNA^{Ser}(S) cells, there is an accumulation of *XBP1u*. The upregulation of *XBP1* mRNA in P15, in tRNA^{Ser}(S) cells, is consistent with increased fragmented ATF6. ATF6 can induce not only the expression of ERAD genes, but also *XBP1* gene [48]. During evolution, *EIF2AK3* expression increased from -1.2 fold in P1 to 1.1 fold in P30, relative to Mock in tRNA^{Ser}(L) and decreased in tRNA^{Ser}(H) cells from 1.3 in P1 to -1.2 in P30. *EIF2AK3* encodes the kinase responsible for eIF2α phosphorylation (PERK) and its upregulation is consistent with increased levels of eIF2α-P, in P30, in the tRNA^{Ser}(L) cell line.

The cDNA microarray data also confirmed activation of the UPS, as alterations in the expression of some ubiquitin ligases (*UBE2Z*, *UBE2I* and *SMURF2*) were observed over time. Overall, there was a tendency to increased expression in ubiquitin ligases in P15 in tRNA^{Ser}(S), tRNA^{Ser}(L) and tRNA^{Ser}(H) cells, despite the values were below 1.5 fold. In tRNA^{Ser}(S), *UBE2Z* expression decreased from P15 (1.3 fold) to P30 (-1.3 fold), while *SMURF2* expression increased from P1 (-1.2 fold) to P15 (1.3 fold). For the last one, in tRNA^{Ser}(L), there was also an increase in expression from P1 (0.8 fold) to P15 (1.1 fold). In tRNA^{Ser}(H), the expression of *UBE2I* decreased from P15 (1.1 fold) to P30 (-1.1 fold). Deubiquitinating enzymes (*USP48* and *USP36*) were deregulated in tRNA^{Ser}(S), tRNA^{Ser}(A) and tRNA^{Ser}(L) cell lines. *USP48* was upregulated in tRNA^{Ser}(L) in P30 (1.6 fold). *USP36* was upregulated in tRNA^{Ser}(S) in P15 (1.5 fold) and its expression decreased in tRNA^{Ser}(A) cells from P1 (1.2 fold) to P15 (-1.0 fold). Also, the expression of *PSMC1* gene (proteasome 26S subunit, ATPase 1) suffered alterations during evolution, its expression decreased from P15 to P30 in tRNA^{Ser}(S) (1.3 to -1.0 fold), tRNA^{Ser}(A) (1.1 to -1.1 fold) and tRNA^{Ser}(H) cells (1.2 to -1.1 fold). tRNA^{Ser}(S) cell line presented more alterations in UPS genes comparatively to the other cell lines. We could also observe that UPS related genes tended to

be upregulated in P15, concomitantly with the accumulation of ubiquitinated proteins in most cell lines, with exception for *UPS48* in $tRNA^{Ser}$(S) (upregulated in P30, 1.6 fold).

Regarding autophagy, the microarray data showed upregulation of *ATG16L1* during evolution in $tRNA^{Ser}$(S) (from -1.0 fold in P15 to 1.3 fold in P30), $tRNA^{Ser}$(A) (-1.1 fold in P15 to 2.2 fold in P30) and $tRNA^{Ser}$(H) cells (-2.2 fold in P1 to 1.6 fold in P30). *ATG12* and *ATG5* expression also increased in the $tRNA^{Ser}$(L) cell line, from -1.0 fold in P1 to 1.3 fold in P15 and -1.2 fold in P1 to 1.1 fold in P15, respectively. These two genes encode proteins that form a complex involved in the formation of the autophagosomes and may be involved in the degradation of protein aggregates [49]. These results indicate that autophagy was probably activated in our cell lines. The increase in *ATG12* and *ATG5* is consistent with the higher levels of insoluble proteins in the $tRNA^{Ser}$(L) cell line.

Beyond the above mentioned deregulations, a set of translational factors, namely *EIF4EBP1* (eukaryotic translation initiation factor 4E binding protein 1), *EEF1A1* (eukaryotic translation elongation factor 1 alpha 1) and *EEF2* (eukaryotic translation elongation factor 2), were also deregulated during evolution. *EIF4EBP1* expression decreased in $tRNA^{Ser}$(A) celss from P15 (1.3 fold) to P30 (-1.1 fold). The eIF4EBP1 interacts with eIF4E and inhibits initiation complex assembly with consequent translation repression [50]. The decreased expression of *EIF4EBP1* is in accordance with the translation derepression observed in this cell line. *EEF1A1* expression decreased in $tRNA^{Ser}$(S) and $tRNA^{Ser}$(H) cells from 1.4 fold in P15 to -1.0 fold in P30 and from 1.0 fold in P1 to -1.2 fold in P15, respectively. Also, in $tRNA^{Ser}$(S) cell line, *EEF2* expression was downregulated from 1.0 fold in P15 to -1.5 fold in P30. These data suggest that translation elongation rate may also been affected during evolution, but our data was not able to reveal it. Also, these results may indicate that translation was remodeled for efficient translation of stress genes rather than for global translational repression. Indeed, the *RPS6KL1* (ribosomal protein S6 kinase like 1) that encodes a member of the ribosomal S6 kinase family was upregulated during evolution from -1.3 fold in P15 to 1.0 fold in P30 in $tRNA^{Ser}$(A) cell line. S6 kinases are part of the mammalian target of rapamycin (mTOR) pathway, which is a key regulator of cell growth via the regulation of protein synthesis. S6 kinases are activated by serine/threonine phosphorylation and phosphorylate ribosomal protein 6, increasing translation of a set of proteins, including ribosomal proteins [51].

Altogether, the expression microarrays data are in accordance with our previous results and supported the idea that PQC mechanisms are being activated in a time dependent manner, and in response to mutant tRNAs or tRNA pool deregulation alone. UPR related genes were upregulated ($tRNA^{Ser}$(S) cell line), or showed increased fold change during

evolution (tRNA^{Ser}(L) cell line). UPS related genes were also upregulated in the same cell lines. Variation of expression through time in UPS genes, was observed in tRNA^{Ser}(S), tRNA^{Ser}(A) and tRNA^{Ser}(H) cells. These gene expression alterations are different for each cell line, probably depending on the need for ubiquitinating or deubiquitinating enzymes during each passage. Autophagy seems to play a role in the response against misfolded proteins in our cell lines, since there was an increase in the expression of autophagy related genes through their evolution from P1 to P30. Alterations in translational factors were also seen, as well as a tendency to decreased expression though time in tRNA^{Ser}(S) and tRNA^{Ser}(A) cells, with no implications in the overall protein synthesis rate. Finally, also the expression of a ribosomal protein kinase (*RPS6KL1*) was altered in tRNA^{Ser}(A) and tRNA^{Ser}(H) cell lines.

Table 1-1. Deregulation of PQC genes induced by protein synthesis errors.
Red color represents upregulated genes, fold change above 1.5. Green color represents dowregulated genes, variation below -1.5 fold. Numbers in blue highlight changes in gene expression that occurred during evolution.

		tRNA^{Ser}(S)			tRNA^{Ser}(A)			tRNA^{Ser}(L)			tRNA^{Ser}(H)		
	Time Point / Gene symbol	P1	P15	P30	P1	P15	P30	P1	P15	P30	P1	P15	P30
UPR related genes	*ERN1*	-2.4			-2.0			-1.8					
	XBP1	1.5	1.8										
	EIF2AK3							-1.2	-1.1	1.1	1.3	-1.1	-1.2
UPS related genes	*UBE2Z*		1.3	-1.3									
	UBE2I											1.1	-1.1
	SMURF2	-1.2	1.3					0.8	1.1				
	USP48									1.6			
	USP36		1.5		1.2	-1.0							
	PSMC1		1.3	-1.0		1.1	-1.1					1.2	-1.1
Autophagy related genes	*ATG16L1*		-1.0	1.3		-1.1	2.2				-2.2	1.4	1.6
	ATG12							-1.0	1.3				
	ATG5							-1.2	1.1				
Translational factors	*EIF4EBP1*					1.3	-1.1						
	EEF1A1		1.4	-1.0							1.0	-1.2	
	EEF2		1.0	-1.5		1.0	-1.3						
Ribosomal proteins	*RPS6KL1*					-1.3	1.0					1.1	-1.1

1.4 Discussion

Our study demonstrates that HEK293 cells expressing mutant tRNAs or overexpressing the Wt tRNA^{Ser} are highly tolerant to PSE, despite the accumulation of misfolded proteins over time. PQC mechanisms were activated in a time and stress dependent manner, allowing these cell lines to thrive, after several generations in culture.

PSE destabilize protein structure and cause disease by overloading chaperones and the proteasome and inducing autophagy, increasing protein cleaning up energetic costs, altering cell signaling and metabolism, producing toxic protein aggregates, repressing protein synthesis and inducing major genomic alterations [22, 52–54]. Kalapis and Bezerra have demonstrated recently that a yeast strain misincorporating Ser at Leu sites could adapt to PSE by up-regulating protein synthesis, protein degradation and glucose up-take [55]. Remarkably, clones that evolved for approximately 250 generations were able to reduce protein aggregates and recovered fitness to almost wild type levels, but at a high metabolic cost [55]. Our data are in line with those data. Indeed, protein synthesis and degradation rates increased during evolution in $tRNA^{Ser}$(A) cell line. In contrast, while mistranslation had a major negative initial impact on yeast growth rate and viability, no consequence at all were seen in HEK293 cells doubling time and an increase was even observed in the viability of $tRNA^{Ser}$(A) and $tRNA^{Ser}$(L) cell lines and proliferation of $tRNA^{Ser}$(S) and $tRNA^{Ser}$(A) cell lines (Figure 1-5, Figure 1-6 and Figure 1-7).

Also, tolerance to mutant tRNAs increased in yeast during evolution, while in human cells the mutant tRNAs expression was strongly repressed throughout evolution. These data suggest that yeast adapted to mistranslation using error mitigation mechanisms, while human cells preferred error prevention.

The decrease in protein aggregation levels observed during evolution in yeast and HEK293 cells (namely in $tRNA^{Ser}$(L) cell line) has implications for understanding the biology of protein misfolding diseases. Protein aggregation studies use cell models where expression of aggregation prone proteins is induced and adaptation is not evaluated [56–58]. Even in cases where these proteins are expressed constitutively the norm is to maintain cell passages as low as possible to avoid genomic instability [59]. Considering our data on adaptation during evolution, human cell models of Alzheimer's, Parkinson's and other protein misfolding diseases should be studied to capture the full spectrum of metabolic and physiological changes induced by protein aggregation. Aggregates associated with neurological disorders are known to block proteasome activity and activate mechanisms that lead to the repression of protein synthesis [8, 60], suggesting that these cells are unable to tolerate and adapt to them [61, 62]. However, different types of human cells cope differently with protein aggregation, raising the question of whether adaptation to aggregation may follow different routes in different cell types. Recent studies showing that suppression of eIF2α kinases alleviates Alzheimer's symptoms in mice [63] support this hypothesis.

Different amino acid misincorporations in the proteome activated different cellular responses and led to differential adaption routes during the evolution of our cell lines.

Interestingly, increased expression of the Wt $tRNA_{AGA}^{Ser}$ had phenotypic consequences that were clearly distinct from the Mock (control), suggesting that human cells are highly sensitive to tRNA gene copy number alterations and expression levels. It is known that increased expression of Wt tRNAs (which is common in cancer) alters translation rate, enhances expression of oncogenes and may also increase the level of protein errors, leading to accumulation of misfolded proteins [14, 64]. In P15, we observed accumulation of ubiquitinated proteins, UPS and UPR activation (Figure 1-21) confirming the hypothesis that misexpression of Wt tRNAs may have major physiological consequences due to activation of the stress response and translational deregulation of gene expression [65].

In the $tRNA^{Ser}$(A) cell line there was an initial (P1 to P15) increase in protein synthesis rate, followed by increased proteasome activity (P15 to P30), in other words increased protein synthesis and turnover, as occurred in yeast (Figure 1-21) [55]. Previous studies show that short-living proteins have on average higher aggregation propensity and fewer chaperone interactions than long-living proteins and high protein turnover seems to be sufficient to prevent aggregation [66]. Therefore, the Ser-to-Ala misincorporation model may be relevant to address the biology of PSE for instance in cancer, where PQC mechanisms are highly activated [67], but generalized protein aggregation is not commonly observed. Indeed, PSE have not yet been quantified in a systematic manner in cancer, and it is unclear whether it plays a relevant role, however chaperones are often upregulated in tumors [68], suggesting high demand for protein folding/refolding, which is a hallmark of PSE.

The $tRNA^{Ser}$(L) cell line had higher proteasome activity (P1), but accumulation of aggregated proteins was also visible (P15) (Figure 1-21). Adaptation of this cell line to mutant tRNA expression and protein aggregation was more dependent on UPR activation, namely phosphorylation of eIF2α, and consequent inhibition of protein synthesis rate in order to alleviate ER stress, than other cell lines. At the protein synthesis level, phosphorylation of eIF2α promotes polysome disassembly resulting in the accumulation of untranslated messenger ribonucleoprotein particles (mRPs) that can form stress granules, and are responsible for reprogramming mRNA metabolism and contribute to cell survival [69, 70]. Together with the decrease in protein synthesis rate, also dilution by cell division and autophagy may have contributed to the decrease in protein aggregates observed in P30, in this cell line.

$tRNA^{Ser}$(H) activated mainly PQC mechanisms in P1 and P15, while in P30, a decrease in molecular chaperones occurred (Figure 1-21). With exception of Hsp90α and BiP, there was a general decrease in molecular chaperones expression in our cell lines (Figure 1-21). Decrease in chaperones with aging have been already reported in several studies [71–

74]. Molecular chaperones are, usually, the first line of defense against misfolded proteins, and probably, other mechanisms can be more efficient to remove these proteins after prolonged proteotoxic stress.

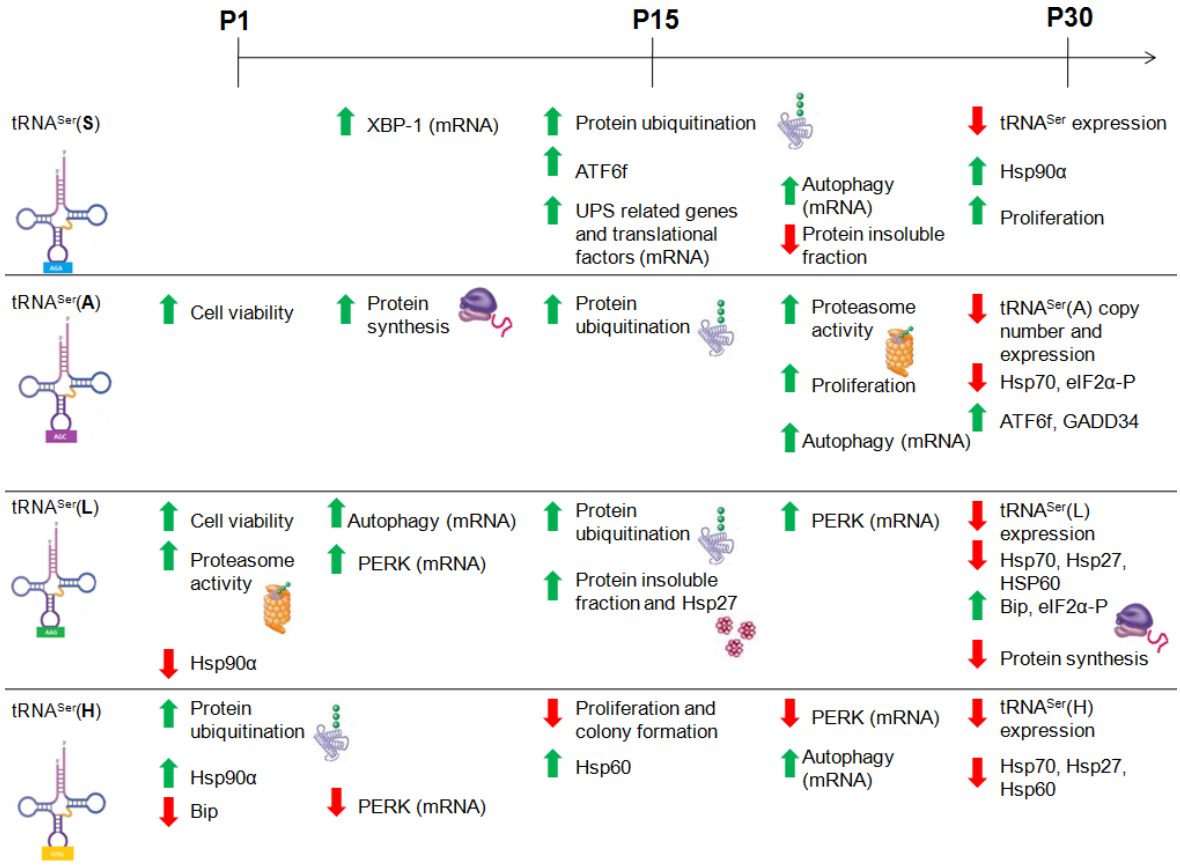

Figure 1-21. Summary of the PQC alterations identified in the different cell lines. Mutant tRNAs and misexpression of $tRNA^{Ser}$ led to accumulation of ubiquitinated proteins, suggesting increased levels of misfolded proteins. PQC mechanisms were recruited in an error type and time dependent manner to counteract proteotoxic stress. Increase in protein turnover and decrease in protein synthesis seem to be two important mechanisms that cells used to thrive in culture after several generations accumulating errors in proteins.

1.5 Conclusion

PSE have been extensively studied in *E. coli* and yeast, but little is known about their biology in human cells. We show here that experimental evolution provides an important tool to study such errors in human cells, although they have only been applied to microorganisms.

HEK293 cells activated PQC mechanisms in order to respond to the accumulation of misfolded proteins caused by the introduction of mutant tRNAs or tRNA pool deregulation. As we expected, this activation depends on the cell passage and the type of proteome

destabilization that we are creating. With evolution of the cell lines, we observed that there was a decrease in protein ubiquitination and in some cases protein aggregates with concomitant increase in UPR activation or protein degradation.

Clearly, and in contrast to models of protein misfolding diseases, we did not observe significant effects on cell viability or proteasome inhibition suggesting that human cells cope better with PSE than with protein aggregation associated with Alzheimer's, Parkinson's and other neuropathies. Adaptation to PSE and protein aggregation may also suggest that protein synthesis and degradation rates are more relevant to mitigate and erase aggregates than chaperones or autophagy. In fact, expression of molecular chaperones was unchanged or decreased during evolution, an effect also observed in yeast, where chaperones expression increases initially but decreases gradually or is even repressed in some cases.

1.6 Materials and Methods

1.6.1 Cell culture

Human embryonic kidney 293 (HEK293) cells were purchased from American Type Culture Collection (ATCC®CRL-1573). Cells were grown in Minimum Essential Medium (Gibco, Cat.41090-028) supplemented with 10% fetal bovine serum (FBS) (Sigma, Cat.F1051), 1% of Pen/Strep (Gibco, Cat.15070-063) and 1% of non-essential amino acids (Gibco, Cat.11140-050) in a humidified atmosphere at 37ºC in the presence of 5% CO_2.

1.6.2 Construction of mutant tRNA plasmids

A DNA fragment of 248kb, corresponding to part of the gene encoding human wild type $tRNA_{AGA}^{Ser}$ (Chr6 tRNA#5) and its flanking region, was amplified by PCR. The primers used were the following: forward 5'-GCCGAATTCAGCTATTATTAAATCCCTAATAAAAGG-3' and reverse 5'-CGCCTCGAGTTGTAAAAGATCGAAAGCCTTTTTA-3'. The region amplified has the following sequence: 5'-AGCTATTATTAAATCCCTAATAAAAGGAGTACAATATGTGATGTATGGAAACAT GTAAGACATTTAATAAGGTTTTTGGTATCTGTAGTCGTGGCCGAGTGGTTAAGG CGATGGACTAGAAATCCATTGGGGTCTCCCCGCGCAGGTTCGAATCCTGCCGAC TACGGCAGTGGGTTTTTGCATCTTCAAGCAGGTTTCATCCGACCGATCGATATTT CACGTGTAAAAAGGCTTTCGATCTTTTACAA-3'. This region was cloned into the

modified vector pIRES2-DsRed with new multiple cloning sites, using the enzymes EcoRI (Thermo Scientific, Cat.ER0271), XhoI (Thermo Scientific, Cat.ER0691) and T4 DNA ligase (Thermo Scientific, Cat.EL0011). To change the anticodon of the $tRNA_{AGA}^{Ser}$, to other anticodons, we performed site-directed mutagenesis. The primers used were the following: forward to $tRNA_{AGC}^{Ser}$ (A) 5'-GTTAAGGCGATGGACTAGCAATCCATTGGGGTCTCCC-3'; reverse to $tRNA_{AGC}^{Ser}$ (A) 5'-GGGAGACCCCAATGGATTGCTAGTCCATCGCCTTAAC-3';forward to $tRNA_{AAG}^{Ser}$ (L) 5'-GGTTAAGGCGATGGACTAAGAATCCATTGGGGTCTCCC-3'; reverse to $tRNA_{AAG}^{Ser}$ (L) 5'-GGGAGACCCCAATGGATTCTTAGTCCATCGCCTTAACC-3';forward to $tRNA_{GTG}^{Ser}$ (H) 5'-GGTTAAGGCGATGGACTGTGATCCATTGGGGTCTCC-3'; reverse to $tRNA_{GTG}^{Ser}$ (H) 5'-GGAGACCCCAATGGATTCACAGTCCATCGCCTTAACC-3'.

Contruction of mutant tRNA plasmids was done by Patrícia Pereira in the RNA Biology Laboratory, Aveiro, Portugal, in 2007.

1.6.3 Generation of mistranslating cell lines

HEK293 cells with approximately 60% of confluency were transfected with 1µg of plasmid DNA using Lipofectamine2000 (Invitrogen, Cat.11668019), following manufacturer's instructions. Cells were transfected with an empty vector (Mock), and with the plasmid carrying $tRNA_{AGA}^{Ser}$(S), $tRNA_{AGC}^{Ser}$(A), $tRNA_{AAG}^{Ser}$(L) or $tRNA_{GTG}^{Ser}$(H) genes. To establish stable cell lines, 72h after transfection, geneticin (Formedium, Cat.G4185) was added to the medium at a concentration of 800µg/ml and selection lasted for 1 month. Cells were kept in low concentration of geneticin (100µg/ml) after selection and during evolution in culture. Geneticin was not added to the medium when cells were plated for the experiments.

1.6.4 Evolution of cells in culture

After transfection with the plasmids and selection, cells were kept in culture dishes (60mm) and subcultured ever 3 days using the same dilution (1/6) until passage 30. Cell culture conditions were the same during evolution. In P1, P15 and P30 cells were plated in 100mm culture dishes, to have enough cells to perform the experiments and extract DNA, RNA and protein.

1.6.5 Total RNA extraction

RNA was extracted using Trizol®Reagent (Thermo Fisher Scientific, Cat.15596026). The content of one well from a 6 well plate, with around $5x10^5$ cells, was collected for each experimental condition. Purification of RNA was done using DNaseI, Amplification Grade kit (Invitrogen, Cat.18068015), following manufacturer's instructions. RNA was then precipitated with a standard Phenol/Chlorophorm/Isoamylalchohol (25:24:1) (Acros Organics, Cat.327111000) extraction protocol and conserved at -80ºC. RNA concentration was determined using NanoDrop1000 (Thermo Scientific). RNA quality was verified using Agilent 2100 Bioanalyser.

1.6.6 Quantification of tRNA expression and tDNA copy number

The expression of the tRNAs was quantified by extracting total RNA from the transfected cell lines. 200ng of total RNA were used for cDNA convertion using NCode™ VILO™ miRNA cDNA Synthesis Kit (Invitrogen, Cat.A11193050), following manufacturer's instructions. To determine the copy number of the Wt $tDNA^{Ser}$ and the mutant tDNA genes, genomic DNA was extracted using Wizard® Genomic DNA Purification Kit (Promega, Cat.TM050), following the manufacturer's instructions. Amplification of the Wt and mutant tRNAs from cDNA (2µL) or DNA (200ng) was done by PCR using the following primers: forward 5'-CGTAGTCGGCAGGATTCGAA-3' and reverse 5'-GTA GTC GTG GCC GAG TGG TT-3'. As an internal control, GAPDH was also amplified in the same PCR reaction, using the following primers: forward 5´-CTC CTG TTC GAC AGT CAG CC -3' and reverse 5'-CCC ACT TGA TTT TGG AGG GA-3'.

PCR conditions for DNA amplification were: 95ºC for 15min, (95ºC for 30 sec, 62ºC for 1 min and 30 sec, 72ºC for 1 min and 30 sec, 3 cycles); (95ºC for 30 sec, 60ºC for 1 min and 30 sec, 72ºC for 1 min and 30 sec, 3 cycles); (95ºC for 30 sec, 58ºC for 1 min and 30 sec, 72ºC for 1 min and 30 sec, 30 cycles) and a final step of extension at 72°C for 10 min. 8µL of the PCR product was run on a 2% agarose gel to confirm the amplification of the two bands (Figure 1-23 A).

PCR conditions for cDNA amplification were: 95ºC for 15min, (95ºC for 30 sec, 62ºC for 1 min and 30 sec, 72ºC for 1 min and 30 sec, 3 cycles); (95ºC for 30 sec, 60ºC for 1 min and 30 sec, 72ºC for 1 min and 30 sec, 3 cycles); (95ºC for 30 sec, 58ºC for 1 min and 30 sec, 72ºC for 1 min and 30 sec, 30 cycles) and a final step of extension at 72°C for 10 min. 5µL

of PCR product were purified with 1µL of ExoI (Thermo Fisher Scientific, Cat.EN0581) and 1µL of FastAp (Thermo Fisher Scientific, Cat.EF0654) for 60min at 37ºC followed by 15min at 85ºC. 2µL of purified PCR product were reamplified. PCR conditions were the same, with the exception of the number of cycles in the last amplification step (cycle 25). 8µL of the PCR product were run on a 2% agarose gel to confirm the amplification of the two DNA fragments (Figure 1-23 B).

5µL of PCR products (from DNA or cDNA) were purified using 1µL of ExoI (Thermo Fisher Scientific, Cat.EN0581) and 1µL of FastAp (Thermo Fisher Scientific, Cat.EF0654) for 60min at 37ºC followed by 15min at 85ºC.

SNaPshot reaction was performed using the following primers: 5'-GGGAGACCCCAATGGATT-3' for tRNAs and 5'-CCC ACT TGA TTT TGG AGG GA-3' for GAPDH and a SNaPshot Multiplex Ready Reaction Mix (Applied Biosystems, Cat.4323163). Reaction cycles for tRNAs were: 96ºC for 10 sec, 54ºC for 5 seconds and 60ºC for 30 sec, 25 cycles. Reaction cycles for GAPDH were: 96ºC for 10 sec, 64ºC for 5 seconds and 60ºC for 30 sec, 10cycles. SNaPshot products were purified with 1µL of FastAp (Thermo Fisher Scientific, Cat.EF0654) for 60min at 37ºC, followed by 15min at 85ºC. Samples were then sequenced and analyzed with Peak Scanner software (Applied Biosystems). The peak area corresponding to each mutant tRNA and Wt $tRNA^{Ser}$ was determined and a ratio calculated. *GAPDH* was quantified and used as a internal control to normalize tRNA expression levels [75, 76].

1.6.7 Cell fitness assessment

To measure cells doubling time, $3x10^4$cells/well were plated in 6-well plates. After 72h, cells were detached and counted in a Neubauer chamber with Tripan blue 0.4% (Lonza, Cat.17-942E). Population doubling time was calculated using the formula: Doubling time=duration*log(2)/(log(final concentration)-log(initial concentration)) [77]. For viability assays, the number of viable cells in culture was determined with Tripan blue exclusion assay. $3x10^4$cells/well were plated in 6-well plates. After 72h, cells were counted in a Neubauer chamber using Tripan Blue 0.4% (Lonza, Cat.17-942E). For the quantification of cell proliferation, we used a colorimetric immunoassay ELISA, based on the measurement of BrdU incorporation during DNA synthesis (Roche, Cat.11647229001), following manufacturer's instructions. $1x10^5$cells/well were plated in a 96-well and analysis was performed after 48h. To access the ability of a single cell to grow into a colony we performed

an anchorage-dependent colony formation assay. 100cells/well were plated in 6-well plates. The medium was renewed every 3 days. After 12 days, cells were fixed in ice-cold methanol and stained with 1% cristal violet (Sigma Aldrich, Cat.C6158) in 20% methanol to count the foci.

1.6.8 Protein synthesis determination

In order to determine protein synthesis rate, we took advantage of a non-reactive fluorescence-activated cell sorting-based assay, called SUnSET [34] with few modifications. $2x10^5$cells/well were plated in 6-well plates and after 48h, puromycin (Sigma Aldrich, Cat. 07635) was added to each well in a final concentration of 10%. Cells were kept in the incubator for 10 min, washed twice with 1%PBS and returned to the incubator for 50 min. After protein extraction with Lysis Buffer (0.5% Triton X-100, 50mM HEPES, 250mM NaCl, 1mM DTT, 1mM NaF, 2mM EDTA, 1mM EGTA, 1mM PMSF, 1mM Na_3VO_4 supplemented with a cocktail of protease inhibitors (Complete, EDTA-free, Roche, Cat. 11873580001); as recommended by the manufacturer) and denaturation, 100 µg of protein were resolved in 10% SDS-PAGE and blotted onto nitrocellulose membranes (0.2µm) (GE Healthcare Life Sciences). Anti-puromycin, clone 12D10 (kindly given by Philippe Pierre) was used (1:5000 dilution) to detect the incorporation of puromycin into proteins. IRDye800 goat anti-mouse secondary antibody (Li-cor Biosciences, Cat.400-33) was used (1:10000 dilution) and detected in an Odyssey Infrared Imaging System (Licor Biosciences). Membranes were also probed with Anti-β-tubulin (Invitrogen, Cat.32-2600) (1:1000 dilution) as a loading control.

1.6.9 Quantification of the insoluble protein fraction

To quantify the insoluble protein fraction, $2x10^5$cells/well were plated in 6-well plates. After 48h cells were detached and 100µL of Lysis Buffer (0.5% Triton X-100, 50mM HEPES, 250mM NaCl, 1mM DTT, 1mM NaF, 2mM EDTA, 1mM EGTA, 1mM PMSF, 1mM Na_3VO_4 supplemented with a cocktail of protease inhibitors (Complete, EDTA-free, Roche, Cat. 11873580001) as recommended by the manufacturer) was added to the cells' pellet. Cells were sonicated with a probe sonicator in 5 pulses of 5 seconds, incubated on ice for 30min and centrifuged at 5000rpm for 15min at 4ºC. 10µL of the supernatant (total protein fraction) were stored to measure protein concentration with bicinchoninic acid (BCA) assay (Thermo Fisher Scientific, Cat. 23225). 80µL of supernatant were centrifuged again at

12000rpm for 20min at 4ºC. The pellet (insoluble fraction) was then washed with 160µL of LB and 40µL of 10%Triton X-100 (Sigma-Aldrich, Cat.X100) and centrifuged at 15000g for 20min at 4ºC. The pellet was solubilized in 50µL of LB. 15µL of samples were denaturated with loading buffer (6x) (0.375M Tris pH 6.8, 12% SDS, 60% glycerol, 0.6M DTT, 0.06% bromophenol blue) at 95ºC for 5 min and resolved in a 10% SDS-PAGE. The gel was stained with 0.1% Comassie Brilliant Blue G solution (Sigma-Aldrich, Cat.B0770) for at least 2h. After destaining with a solution of 10% ethanol and 7.5% acetic acid, gels were scanned using Odyssey Infrared Imaging System (Licor Biosciences). Lane signals corresponding to each sample were quantified and normalized to the total amount of protein determined with BCA assay.

1.6.10 Quantification of proteasome activity

In order to test the activity of the proteasome, $2x10^5$cells/well were plated in 6-well plates. After 48h cells were washed with 1%PBS and resuspended in 100µL of Lysis Buffer (1mM EDTA, 10mM Tris-HCl pH 7.5; 20% glycerol; 4mM DTT; 2mM ATP). Cells were sonicated with a probe sonicator in 5 pulses of 5 seconds, and centrifuged at 13000rpm for 10min at 4ºC. The supernatant was diluted (1:20) and protein content was quantified using Bradford method (Sigma-Aldrich, Cat.B6916). 20µg of protein in Lysis Buffer were incubated with the substrate suc-LLVY-MCA (50µM) (Sigma-Aldrich, Cat.S4939) in the presence or in the absence of the proteasome inhibitor MG132 (10µM) (Sigma-Aldrich, Cat.SML1135) in a medium containing 1mM EDTA, 10mM Tris-HCl pH 7.5; 2mM ATP (final volume 100µL). Substrate degradation was monitored every 5min during 1h at 37ºC in a fluorescence-luminescence detector Synergy™ HT Multi-Mode Microplate Reader (Biotek), set to 380 and 460nm, excitation and emission wavelengths, respectively. Specific proteasome activity was determined by subtracting the values for each sample without MG132 to the values with MG132. Final activity was calculated as fluorescence emission at 0 min subtracted from fluorescence after 1h relative to control (Mock).

1.6.11 Immunoblots

$2x10^5$ cells were plated in 6-well plates. After 48h, cells were washed with 1%PBS and then lysed with protein Lysis Buffer (0.5% Triton X-100, 50mM HEPES, 250mM NaCl, 1mM DTT, 1mM NaF, 2mM EDTA, 1mM EGTA, 1mM PMSF, 1mM Na_3VO_4 supplemented

with a cocktail of protease inhibitors (Complete, EDTA-free, Roche, Cat. 11873580001) as recommended by the manufacturer). Cells were sonicated with a probe sonicator in 5 pulses of 5 seconds. After centrifugation, 16000g for 30min, protein in the supernatants was quantified using the BCA assay (Thermo Fisher Scientific, Cat. 23225). Samples were denaturated with loading buffer (6x) at 95ºC for 5 min.

Protein samples were separated by SDS-PAGE in 10% polyacrylamide gels (or 8% for molecular chaperones and ATF6), transferred to nitrocellulose membranes (0.2µm) and immunobloted. Membranes were incubated with primary antibodies overnight (4ºC), washed and incubated with secondary antibodies (1:10000 dilution, 2h at room temperature), IRDye800 goat anti-mouse (Li-cor Biosciences, Cat.400-33) or IRDye680 goat anti-rabbit (Li-cor Biosciences, Cat.925-68070). Secondary antibodies were detected using an Odyssey Infrared Imaging System (Licor Biosciences). The following primary antibodies were used: anti-ubiquitin (1:1000 dilution) (Sigma-Aldrich, Cat.U0508), anti-Hsp70 (1:1000 dilution) (Stress Marq Biosciences, Cat.SMC-100B), anti-Hsp27 (0.5µg/ml dilution) (Stress Marq Biosciences, Cat.SMC-161A), anti-Hsp60 (1:1000 dilution) (Stress Marq Biosciences, Cat.SPC-105), anti-Hsp90α (1:1000 dilution) (Stress Marq Biosciences, Cat.SMC-147), anti-BiP (1:1000 dilution) (Stress Marq Biosciences, Cat.SPC-180), anti-ATF6 (1:400 dilution) (Stressgen, Cat.70B1413.1), anti-eIF2α (1:1000 dilution) (Cell Signalling, Cat.9722), anti-phosphorylated eIF2α (1:400 dilution) (Abcam, Cat.ab4837), anti-GADD34 (1:500 dilution) (Thermo Fisher Scientific, Cat.PA1-12376), anti-β-tubulin (Invitrogen, Cat.32-2600). β-tubulin was used in all the immunoblots as a loading control.

1.6.12 Gene expression microarrays

Gene expression microarrays profiling was performed using the Agilent protocol for One-Color Microarray Based Gene Expression Analysis Low Input Quick Amp Labeling v6.9 (Agilent Technologies). RNA quality determination was performed using 2100 Bioanalyser (Agilent Technologies) and the kit Agilent RNA 6000 Nano kit (Agilent Technologies, Cat.5067-1512). 100ng of total RNA were used to synthesize labeled cDNA (with Cyanine 3-CTP) using Agilent T7 Promoter Primer and T7 RNA polymerase Blend (Agilent Technologies, Cat.5190-2305). cDNA was purified with RNAeasy mini spin columns (Quiagen, Cat.74104). Dye incorporation was quantified using Nanodrop 1000 Spectophotometer. 600ng of labeled cDNA were hybridized in Sure Print G3 Human Gene Expression 8x60k v2 microarrays (Agilent Technologies, Cat.G4851B). Hybridizations were

carried out using Agilent gasket slides in a rotating oven for 17h at 65ºC. Slides were then washed following manufacturer's instructions and scanned in an Agilent G2565AA microarrays scanner.

Probes signal values were extracted using Agilent Feature Extraction Software. Data were normalized using median centering of signal distribution with Biometric Research Branch BRB-Array tools v3.4.o software [78, 79]. Microarrays statistical analysis was carried out using Mev software (TM4 Microarray Software Suite) [80, 81]. T-test was performed to identify genes that showed differences in expression between control (Mock) and samples. Significant genes that present a fold change above 1.5 or bellow -1.5 were considered for downstream analysis.

The microarray raw data was submitted to the GEO database and has been given the following accession number: GSE93854.

1.6.13 Statistical analysis

For all assays, our data represent at least 3 independent experiments and 3 replicates. Statistical analysis was performed using One-way ANOVA analysis of variance followed by the Dunnett's or Bonferroni's post-tests, as indicated in the figures. In all cases, *p*-values<0.05 were considered statistically significant.

1.7 Supplementary Figures

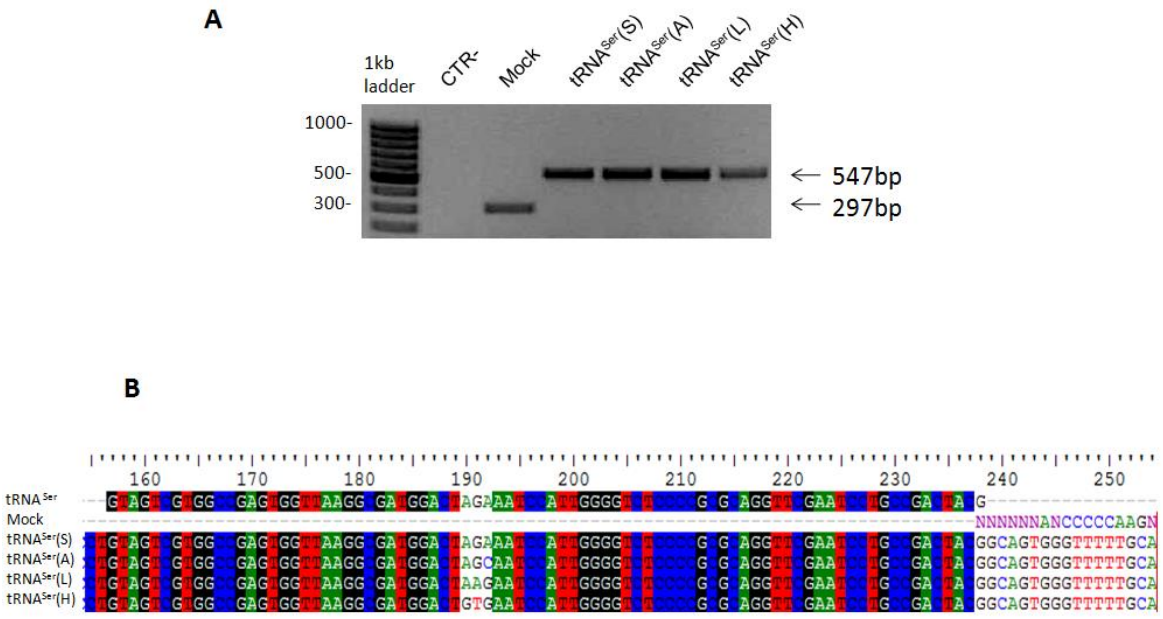

Figure 1-22. tRNA amplification with primers for the plasmid and Sanger sequencing.

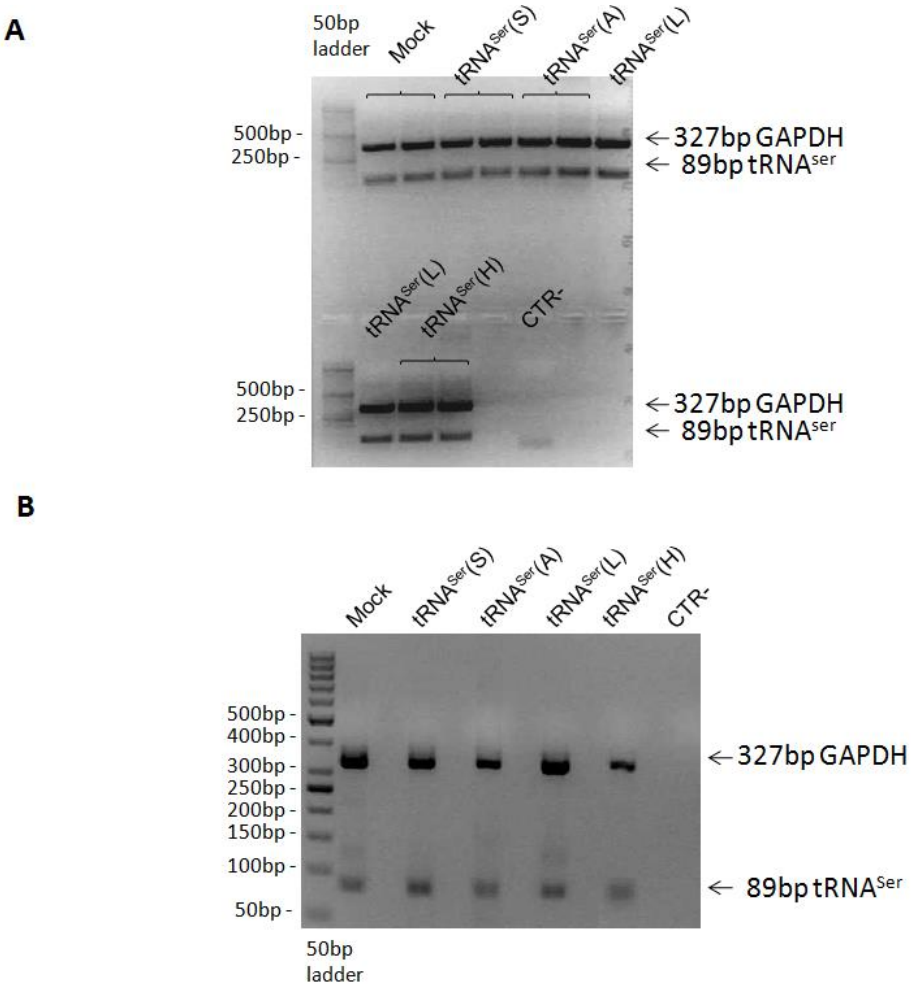

Figure 1-23. SNaPshot analysis – Agarose gels representative of the amplification of tRNA and GAPDH. A – Amplification from DNA of mistranslating cells; **B –** Amplification from cDNA of mistranslating cells.

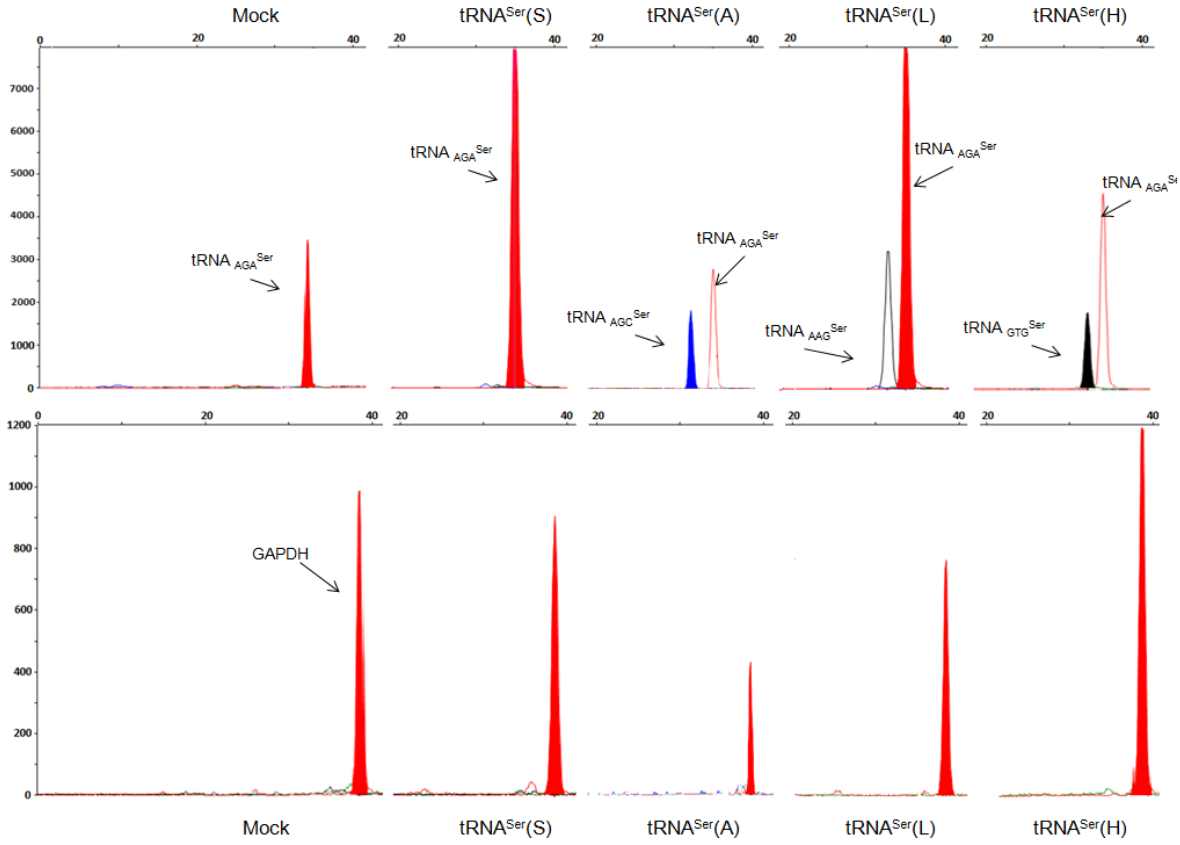

Figure 1-24. SNaPshot peaks of the endogenous tRNA^{Ser}, mutant tRNAs and the respective control, GAPDH. Sequenced samples correspond to cDNA from P1. The primer extension (SNaPshot) reaction utilizes a multiplex kit that contains a reaction mix of four differentially fluorescently labeled ddNTPs, allowing the detection of the incorporated base correspondent to the last base of anticodons. In the case of tRNA^{Ser}(S) cell line, expressing tRNA$_{AGA}^{Ser}$, the peak corresponds to the incorporation of T (red peak). For tRNA^{Ser}(A) cells (expressing tRNA$_{AGC}^{Ser}$), the peak corresponds to the incorporation of G (blue peak). For tRNA^{Ser}(L) (expressing tRNA$_{AAG}^{Ser}$) and tRNA^{Ser}(H) (expressing tRNA$_{GTG}^{Ser}$) cells, the peak corresponds to the incorporation of C (black peak). In tRNA^{Ser}(A), tRNA^{Ser}(L) and tRNA^{Ser}(H) cell lines, the Wt tRNA^{Ser} and mutant tRNAs were detected (upper panel). The peak area corresponding to each mutant tRNA and Wt tRNA^{Ser} was determined for each cell line and a ratio was calculated. Amplification of GAPDH was used as an internal control to normalize the values (lower panel).

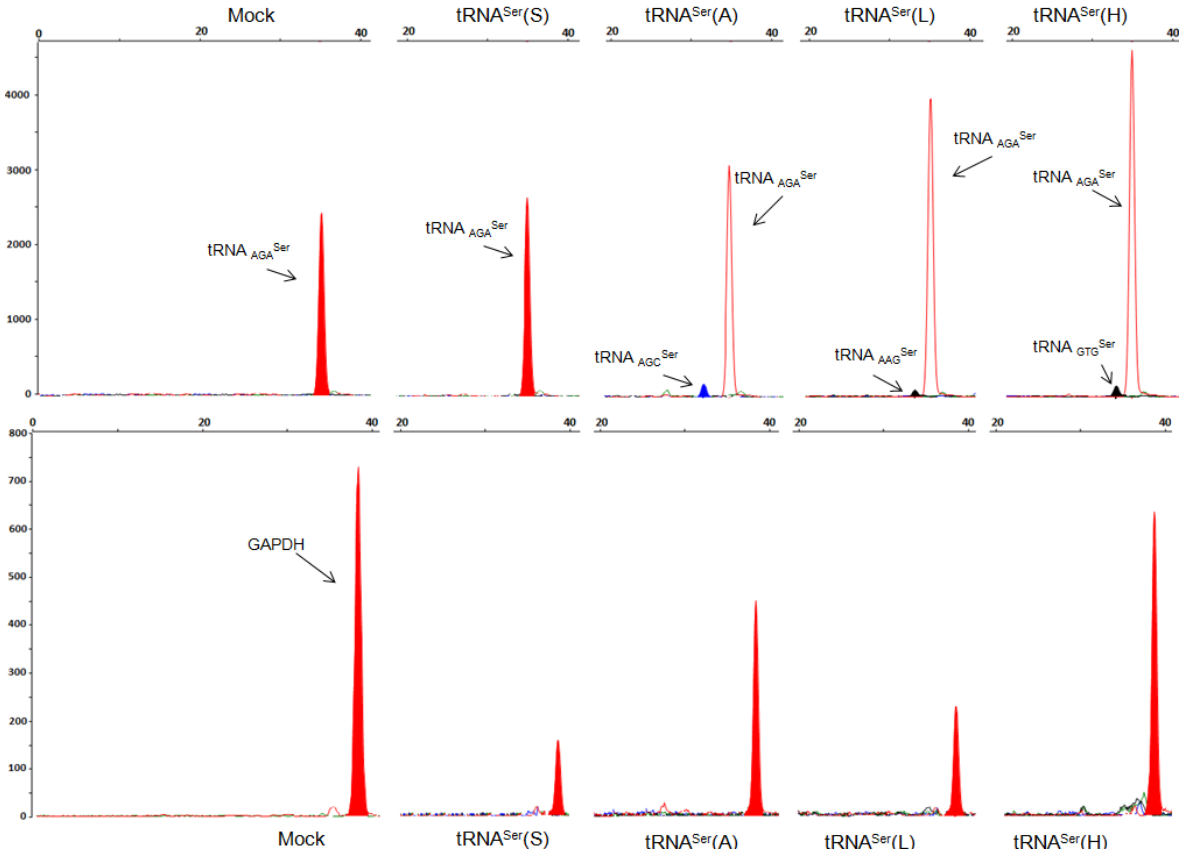

Figure 1-25. SNaPshot peaks of the endogenous tRNA^{Ser}, mutant tRNAs and the respective control, GAPDH. Sequenced samples correspond to cDNA from P15. For tRNA^{Ser}(S) cell line (expressing tRNA$_{AGA}^{Ser}$), the peak corresponds to the incorporation of T (red peak). For tRNA^{Ser}(A) cells (expressing tRNA$_{AGC}^{Ser}$), the peak corresponds to the incorporation of G (blue peak). For tRNA^{Ser}(L) (expressing tRNA$_{AAG}^{Ser}$) and tRNA^{Ser}(H) (expressing tRNA$_{GTG}^{Ser}$) cells, the peak corresponds to the incorporation of C (black peak). In tRNA^{Ser}(A), tRNA^{Ser}(L) and tRNA^{Ser}(H) cell lines, the Wt tRNA^{Ser} and mutant tRNAs were detected (upper panel). The peak area corresponding to each mutant tRNA and Wt tRNA^{Ser} was determined for each cell line and a ratio was calculated. Amplification of GAPDH was used as an internal control to normalize the values (lower panel).

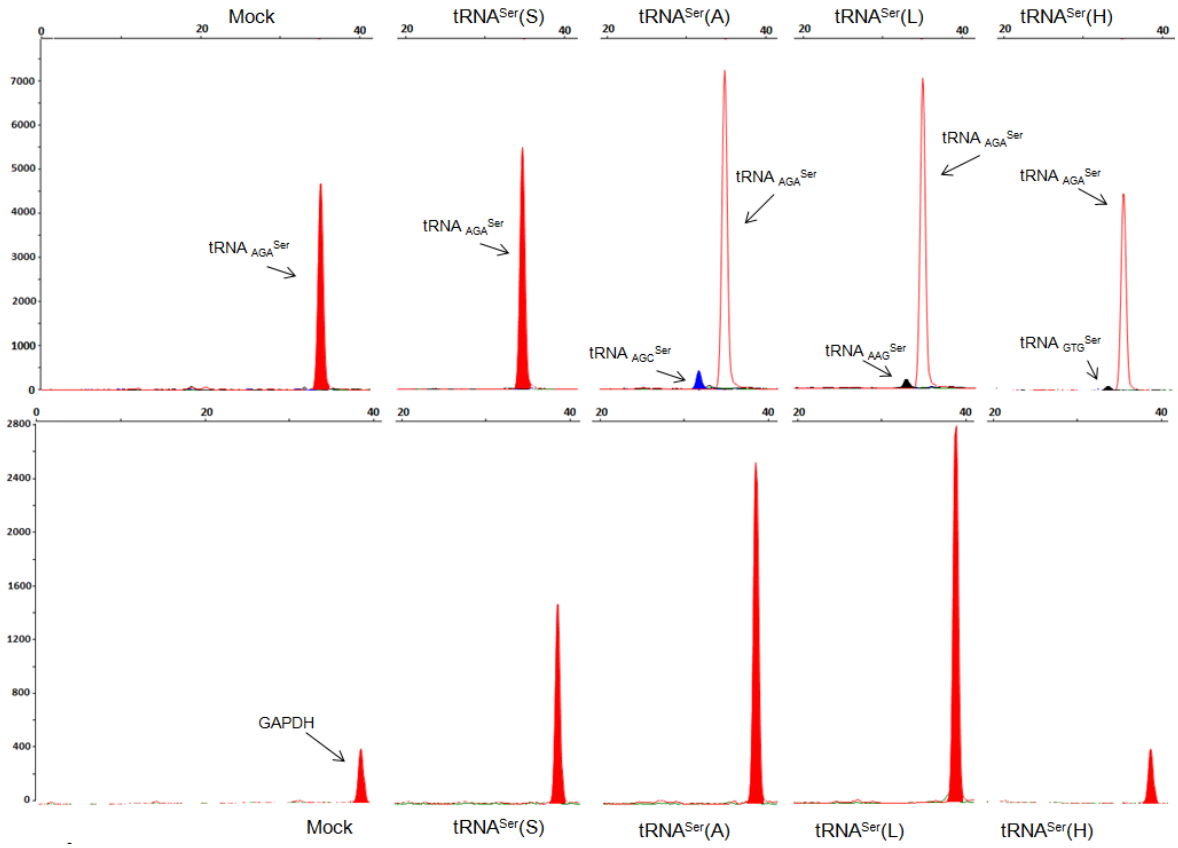

Figure 1-26. SNaPshot peak of the endogenous tRNA^{Ser}, mutant tRNAs and the respective control, GAPDH. Sequenced samples correspond to cDNA from P30. For tRNA^{Ser}(S) cell line (expressing tRNA$_{AGA}^{Ser}$), the peak corresponds to the incorporation of T (red peak). For tRNA^{Ser}(A) cells (expressing tRNA$_{AGC}^{Ser}$), the peak corresponds to the incorporation of G (blue peak). For tRNA^{Ser}(L) (expressing tRNA$_{AAG}^{Ser}$) and tRNA^{Ser}(H) (expressing tRNA$_{GTG}^{Ser}$) cells, the peak corresponds to the incorporation of C (black peak). In tRNA^{Ser}(A), tRNA^{Ser}(L) and tRNA^{Ser}(H) cell lines, the Wt tRNA^{Ser} and mutant tRNAs were detected (upper panel). The peak area corresponding to each mutant tRNA and Wt tRNA^{Ser} was determined for each cell line and a ratio was calculated. Amplification of GAPDH was used as an internal control to normalize the values (lower panel).

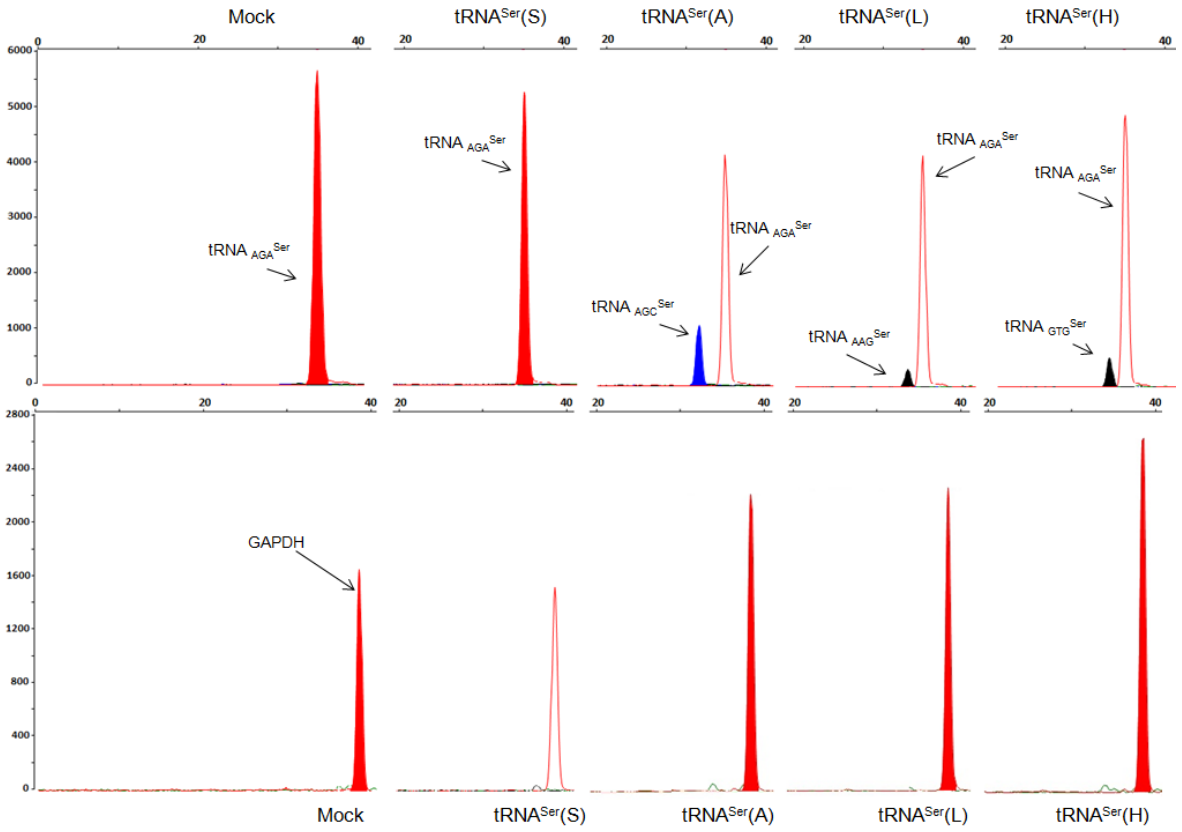

Figure 1-27. SNaPshot peaks of the endogenous tRNA^{Ser}, mutant tRNAs and the respective control, GAPDH. Sequenced samples correspond to DNA from P1. For tRNA^{Ser}(S) cell line (expressing tRNA$_{AGA}^{Ser}$), the peak corresponds to the incorporation of T (red peak). For tRNA^{Ser}(A) cells (expressing tRNA$_{AGC}^{Ser}$), the peak corresponds to the incorporation of G (blue peak). For tRNA^{Ser}(L) (expressing tRNA$_{AAG}^{Ser}$) and tRNA^{Ser}(H) (expressing tRNA$_{GTG}^{Ser}$) cells, the peak corresponds to the incorporation of C (black peak). In tRNA^{Ser}(A), tRNA^{Ser}(L) and tRNA^{Ser}(H) cell lines, the Wt tRNA^{Ser} and mutant tRNAs were detected (upper panel). The peak area corresponding to each mutant tRNA and Wt tRNA^{Ser} was determined for each cell line and a ratio was calculated. Amplification of *GAPDH* was used as an internal control to normalize the values (lower panel).

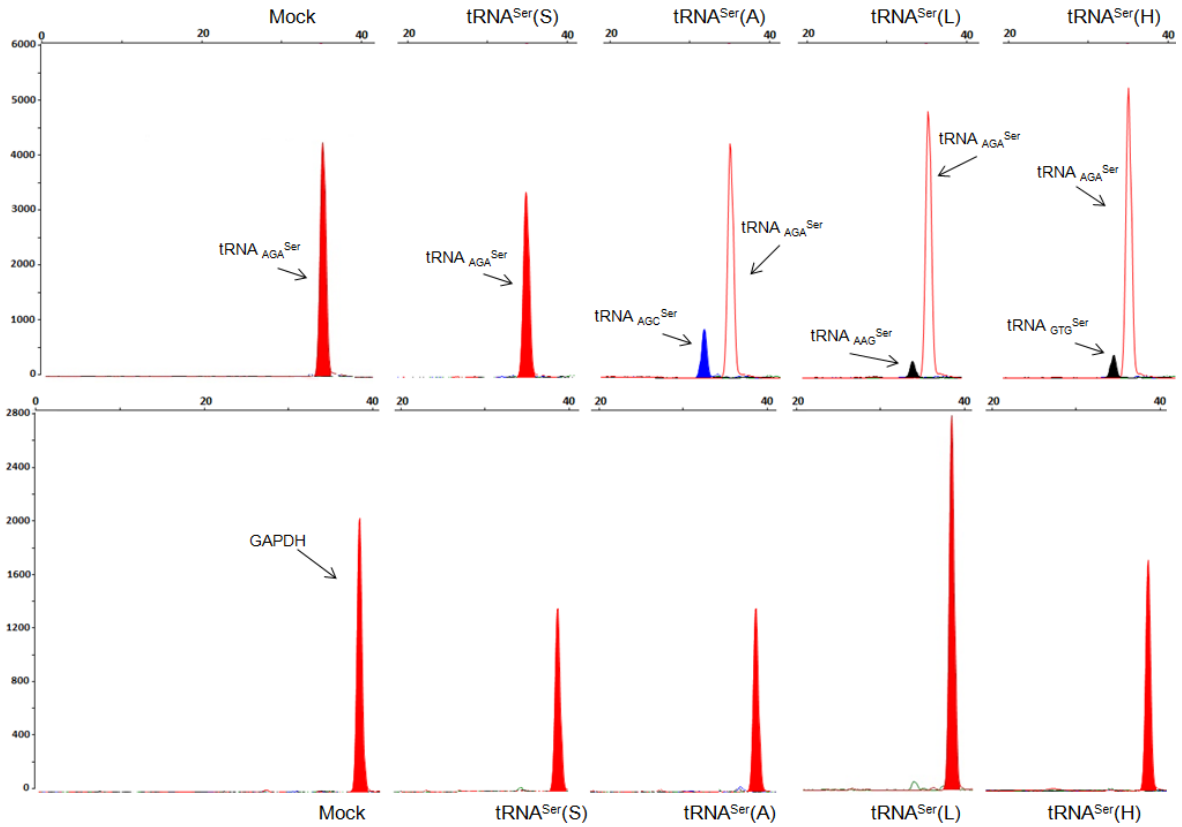

Figure 1-28. SNaPshot peaks of the endogenous tRNA^{Ser}, mutant tRNAs and the respective control, GAPDH. Sequenced samples correspond to DNA from P15. For tRNA^{Ser}(S) cell line (expressing tRNA$_{AGA}^{Ser}$), the peak corresponds to the incorporation of T (red peak). For tRNA^{Ser}(A) cells (expressing tRNA$_{AGC}^{Ser}$), the peak corresponds to the incorporation of G (blue peak). For tRNA^{Ser}(L) (expressing tRNA$_{AAG}^{Ser}$) and tRNA^{Ser}(H) (expressing tRNA$_{GTG}^{Ser}$) cells, the peak corresponds to the incorporation of C (black peak). In tRNA^{Ser}(A), tRNA^{Ser}(L) and tRNA^{Ser}(H) cell lines, the Wt tRNA^{Ser} and mutant tRNAs were detected (upper panel). The peak area corresponding to each mutant tRNA and Wt tRNA^{Ser} was determined for each cell line and a ratio was calculated. Amplification of *GAPDH* was used as an internal control to normalize the values (lower panel).

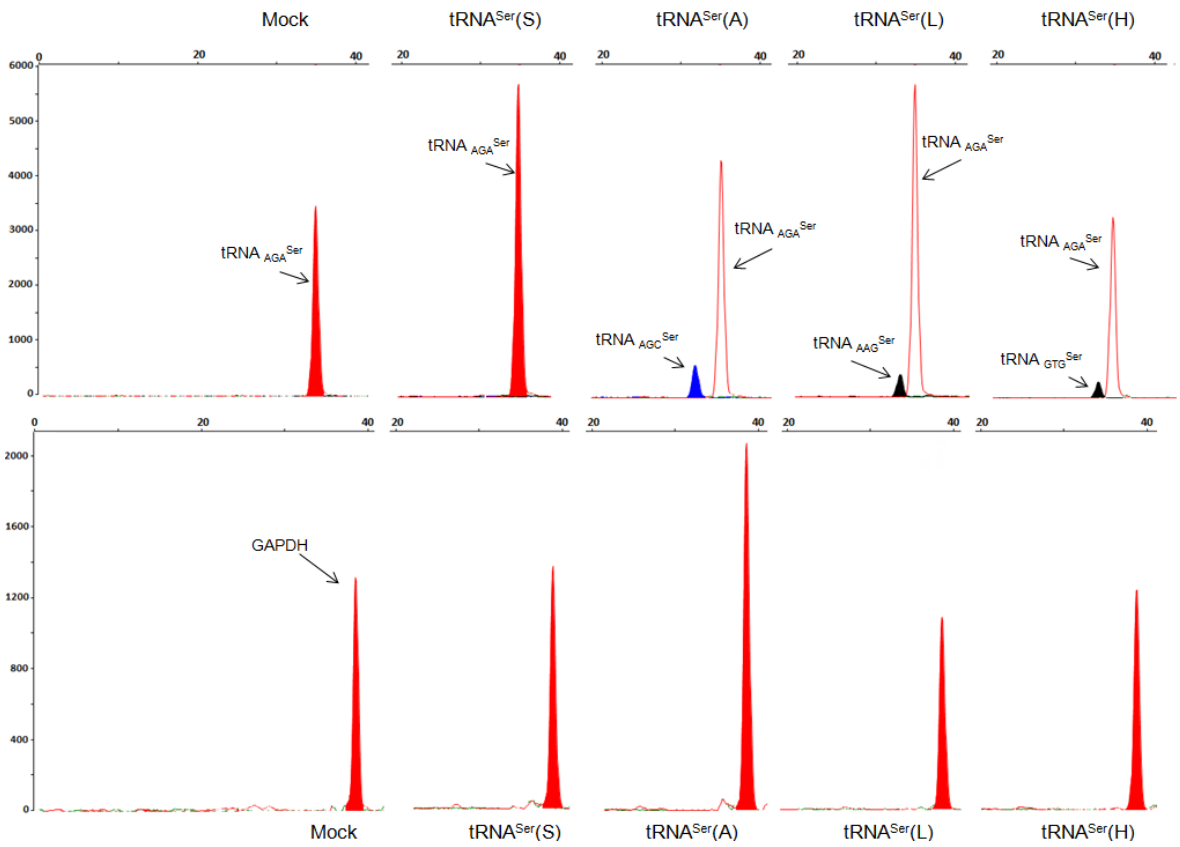

Figure 1-29. SNaPshot peaks of the endogenous tRNA^{Ser}, mutant tRNAs and the respective control, GAPDH. Sequenced samples correspond to DNA from P30. For tRNA^{Ser}(S) cell line (expressing tRNA$_{AGA}^{Ser}$), the peak corresponds to the incorporation of T (red peak). For tRNA^{Ser}(A) cells (expressing tRNA$_{AGC}^{Ser}$), the peak corresponds to the incorporation of G (blue peak). For tRNA^{Ser}(L) (expressing tRNA$_{AAG}^{Ser}$) and tRNA^{Ser}(H) (expressing tRNA$_{GTG}^{Ser}$) cells, the peak corresponds to the incorporation of C (black peak). In tRNA^{Ser}(A), tRNA^{Ser}(L) and tRNA^{Ser}(H) cell lines, the Wt tRNA^{Ser} and mutant tRNAs were detected (upper panel). The peak area corresponding to each mutant tRNA and Wt tRNA^{Ser} was determined for each cell line and a ratio was calculated. Amplification of *GAPDH* was used as an internal control to normalize the values (lower panel).

References

1. Gingold H, Pilpel Y (2011) Determinants of translation efficiency and accuracy. Mol Syst Biol 7:481. doi: 10.1038/msb.2011.14

2. Ruusala T, Andersson D, Ehrenberg M, Kurland CG (1984) Hyper-accurate ribosomes inhibit growth. EMBO J 3:2575–80.

3. Moura GR, Carreto LC, Santos MA (2009) Genetic code ambiguity: an unexpected source of proteome innovation and phenotypic diversity. Curr Opin Microbiol 12:631–637. doi: 10.1016/j.mib.2009.09.004

4. Drummond DA, Wilke CO (2009) The evolutionary consequences of erroneous protein synthesis. Nat Rev Genet 10:715–724. doi: 10.1038/nrg2662

5. Loftfield RB, Vanderjagt D (1972) The frequency of errors in protein biosynthesis. Biochem J 128:1353–1356.

6. Chen B, Retzlaff M, Roos T, Frydman J (2011) Cellular Strategies of Protein Quality Control. Cold Spring Harb Perspect Biol 3:a004374–a004374. doi: 10.1101/cshperspect.a004374

7. Ribas de Pouplana L, Santos M, Zhu JH, et al. (2014) Protein mistranslation: Friend or foe? Trends Biochem Sci 39:355–362. doi: 10.1016/j.tibs.2014.06.002

8. Scheper GC, van der Knaap MS, Proud CG (2007) Translation matters: protein synthesis defects in inherited disease. Nat Rev Genet 8:711–723. doi: 10.1038/nrg2142

9. Kirchner S, Ignatova Z (2015) Emerging roles of tRNA in adaptive translation, signalling dynamics and disease. Nat Rev Genet 16:98–112.

10. Nangle L a, Zhang W, Xie W, et al. (2007) Charcot-Marie-Tooth disease-associated mutant tRNA synthetases linked to altered dimer interface and neurite distribution defect. Proc Natl Acad Sci U S A 104:11239–11244. doi: 10.1073/pnas.0705055104

11. Park SG, Schimmel P, Kim S (2008) Aminoacyl tRNA synthetases and their connections to disease. Proc Natl Acad Sci U S A 105:11043–11049. doi: 10.1073/pnas.0802862105

12. Tsutomu S, Asuteka N, Takeo S (2011) Human mitochondrial diseases caused by lack of taurine modification in mitochondrial tRNAs. Wiley Interdiscip Rev RNA 2:376–386. doi: 10.1002/wrna.65

13. Abbott J a, Francklyn CS, Robey-Bond SM (2014) Transfer RNA and human disease. Front Genet 5:158. doi: 10.3389/fgene.2014.00158

14. Pavon-Eternod M, Gomes S, Geslain R, et al. (2009) tRNA over-expression in breast cancer and functional consequences. Nucleic Acids Res 37:7268–7280. doi: 10.1093/nar/gkp787

15. Zhou Y, Goodenbour JM, Godley LA, et al. (2009) High levels of tRNA abundance and alteration of tRNA charging by bortezomib in multiple myeloma. Biochem Biophys Res Commun 385:160–164. doi: 10.1016/j.bbrc.2009.05.031

16. Frye M, Watt FM (2006) The RNA Methyltransferase Misu (NSun2) Mediates Myc-Induced Proliferation and Is Upregulated in Tumors. Curr Biol 16:971–981. doi: 10.1016/j.cub.2006.04.027

17. Rodriguez V, Chen Y, Elkahloun A, et al. (2007) Chromosome 8 BAC array comparative genomic hybridization and expression analysis identify amplification and overexpression of TRMT12 in breast cancer. Genes Chromosom Cancer 46:694–707. doi: 10.1002/gcc.20454

18. Begley U, Sosa MS, Avivar-Valderas A, et al. (2013) A human tRNA methyltransferase 9-like protein prevents tumour growth by regulating LIN9 and HIF1-α. EMBO Mol Med 5:366–383. doi: 10.1002/emmm.201201161

19. Torres AG, Batlle E, Ribas de Pouplana L (2014) Role of tRNA modifications in human diseases. Trends Mol Med 20:306–314. doi: 10.1016/j.molmed.2014.01.008

20. Liu Y, Satz JS, Vo M-NN, et al. (2014) Deficiencies in tRNA synthetase editing activity cause cardioproteinopathy. TL - 111. Proc Natl Acad Sci U S A 111 VN-:17570–17575. doi: 10.1073/pnas.1420196111

21. Lee JW, Beebe K, Nangle LA, et al. (2006) Editing-defective tRNA synthetase causes protein misfolding and neurodegeneration. Nature 443:50–55. doi: 10.1038/nature05096

22. Reverendo M, Soares AR, Pereira PM, et al. (2014) TRNA mutations that affect decoding fidelity deregulate development and the proteostasis network in zebrafish. RNA Biol 11:1199–1213. doi: 10.4161/rna.32199

23. Bayat V, Thiffault I, Jaiswal M, et al. (2012) Mutations in the mitochondrial methionyl-tRNA synthetase cause a neurodegenerative phenotype in flies and a recessive ataxia (ARSAL) in humans. PLoS Biol. doi: 10.1371/journal.pbio.1001288

24. Geslain R, Cubells L, Bori-Sanz T, et al. (2010) Chimeric tRNAs as tools to induce proteome damage and identify components of stress responses. Nucleic Acids Res 38:e30. doi: 10.1093/nar/gkp1083

25. Bukau B, Weissman J, Horwich A (2006) Molecular chaperones and protein quality control. Cell 125:443–451. doi: 10.1016/j.cell.2006.04.014

26. Hetz C (2012) The unfolded protein response: controlling cell fate decisions under ER stress and beyond. Nat Rev Mol Cell Biol 13:89–102. doi: 10.1038/nrm3270

27. Wang S, Kaufman RJ (2012) The impact of the unfolded protein response on human disease. J Cell Biol 197:857–867. doi: 10.1083/jcb.201110131

28. Tuller T (2012) The Effect of Dysregulation of tRNA Genes and Translation Efficiency Mutations in Cancer and Neurodegeneration. Front Genet 3:201. doi: 10.3389/fgene.2012.00201

29. Wang G, Yang Z-Q, Zhang K (2010) Endoplasmic reticulum stress response in cancer: molecular mechanism and therapeutic potential. Am J Transl Res 2:65–74.

30. Wang M, Kaufman RJ (2014) The impact of the endoplasmic reticulum protein-folding environment on cancer development. Nat Rev Cancer 14:581–597. doi: 10.1038/nrc3800

31. Normanly J, Ollick T, Abelson J (1992) Eight base changes are sufficient to convert a leucine-inserting tRNA into a serine-inserting tRNA. Proc Natl Acad Sci U S A 89:5680–5684. doi: 10.1073/pnas.89.12.5680

32. Lenhard B, Orellana O, Ibba M, Weygand-Durašević I (1999) tRNA recognition and evolution of determinants in seryl-tRNA synthesis. Nucleic Acids Res 27:721–729. doi: 10.1093/nar/27.3.721

33. Gray IC, Barnes MR (2003) Amino Acid Properties and Consequences of Substitutions. Bioinforma Genet 4:289–304. doi: 10.1002/0470867302.ch14

34. Schmidt EK, Clavarino G, Ceppi M, Pierre P (2009) SUnSET, a nonradioactive method to monitor protein synthesis. Nat Meth 6:275–277.

35. Gregersen N, Bross P, Vang S, Christensen JH (2006) Protein misfolding and human disease. Annu Rev Genomics Hum Genet 7:103–24. doi: 10.1146/annurev.genom.7.080505.115737

36. Li X, Zhang K, Li Z (2011) Unfolded protein response in cancer: the physician's perspective. J Hematol {&} Oncol 4:8. doi: 10.1186/1756-8722-4-8

37. Voges D, Zwickl P, Baumeister W (1999) The 26S proteasome: a molecular machine designed for controlled proteolysis. Annu Rev Biochem 68:1015–1068. doi: 10.1146/annurev.biochem.68.1.1015

38. Vilchez D, Saez I, Dillin A (2014) The role of protein clearance mechanisms in organismal ageing and age-related diseases. Nat Commun 5:5659. doi: 10.1038/ncomms6659

39. Macario AJL, Conway de Macario E (2000) Stress and molecular chaperones in disease. Int J Clin Lab Res 30:49–66. doi: 10.1007/s005990070016

40. Broadley SA, Hartl FU (2009) The role of molecular chaperones in human misfolding diseases. FEBS Lett 583:2647–2653. doi: 10.1016/j.febslet.2009.04.029

41. Esser C, Alberti S, Höhfeld J (2004) Cooperation of molecular chaperones with the ubiquitin/proteasome system. Biochim Biophys Acta - Mol Cell Res 1695:171–188. doi: http://dx.doi.org/10.1016/j.bbamcr.2004.09.020

42. Parcellier A, Schmitt E, Gurbuxani S, et al. (2003) HSP27 is a ubiquitin-binding protein involved in I-kappaBalpha proteasomal degradation. Mol Cell Biol 23:5790–5802. doi: 10.1128/MCB.23.16.5790

43. Marcu MG, Doyle M, Bertolotti A, et al. (2002) Heat shock protein 90 modulates the unfolded protein response by stabilizing IRE1alpha. Mol Cell Biol 22:8506–8513. doi: 10.1128/MCB.22.24.8506

44. Wang M, Wey S, Zhang Y, et al. (2009) Role of the unfolded protein response regulator GRP78/BiP in development, cancer, and neurological disorders. Antioxidants {&} redox Signal 11:2307–2316. doi: 10.1089/ars.2009.2485

45. Xu C, Bailly-Maitre B, Reed J (2005) Endoplasmic reticulum stress: cell life and death decisions. J Clin Invest 115:2656–2664. doi: 10.1172/JCI26373.2656

46. DuRose JB, Scheuner D, Kaufman RJ, et al. (2009) Phosphorylation of eukaryotic translation initiation factor 2alpha coordinates rRNA transcription and translation inhibition during endoplasmic reticulum stress. Mol Cell Biol 29:4295–4307. doi: 10.1128/MCB.00260-09

47. Tay KH, Luan Q, Croft A, et al. (2014) Sustained IRE1 and ATF6 signaling is important for

survival of melanoma cells undergoing ER stress. Cell Signal 26:287–294. doi: http://dx.doi.org/10.1016/j.cellsig.2013.11.008

48. Yoshida H, Matsui T, Yamamoto A, et al. (2001) XBP1 mRNA Is Induced by ATF6 and Spliced by IRE1 in Response to ER Stress to Produce a Highly Active Transcription Factor. Cell 107:881–891. doi: 10.1016/S0092-8674(01)00611-0

49. Otomo C, Metlagel Z, Takaesu G, Otomo T (2013) Structure of the human ATG12~ATG5 conjugate required for LC3 lipidation in autophagy. Nat Struct Mol Biol 20:59–66. doi: 10.1038/nsmb.2431

50. Sonenberg N, Hinnebusch AG (2009) Regulation of Translation Initiation in Eukaryotes: Mechanisms and Biological Targets. Cell 136:731–745. doi: 10.1016/j.cell.2009.01.042

51. Dufner a, Thomas G (1999) Ribosomal S6 kinase signaling and the control of translation. Exp Cell Res 253:100–109. doi: 10.1006/excr.1999.4683

52. Ruan B, Palioura S, Sabina J, et al. (2008) Quality control despite mistranslation caused by an ambiguous genetic code. Proc Natl Acad Sci U S A 105:16502–16507. doi: 10.1073/pnas.0809179105

53. Bezerra AR, Simões J, Lee W, et al. (2013) Reversion of a fungal genetic code alteration links proteome instability with genomic and phenotypic diversification. Proc Natl Acad Sci U S A 110:11079–11084. doi: 10.1073/pnas.1302094110

54. Paredes JA, Carreto L, Simões J, et al. (2012) Low level genome mistranslations deregulate the transcriptome and translatome and generate proteotoxic stress in yeast. BMC Biol 10:55. doi: 10.1186/1741-7007-10-55

55. Kalapis D, Bezerra AR, Farkas Z, et al. (2015) Evolution of Robustness to Protein Mistranslation by Accelerated Protein Turnover. PLoS Biol. 13:

56. Khlistunova I, Biernat J, Wang Y, et al. (2006) Inducible Expression of Tau Repeat Domain in Cell Models of Tauopathy: AGGREGATION IS TOXIC TO CELLS BUT CAN BE REVERSED BY INHIBITOR DRUGS . J Biol Chem 281:1205–1214. doi: 10.1074/jbc.M507753200

57. Lim S, Haque MM, Kim D, et al. (2014) Cell-based models to investigate Tau aggregation. Comput Struct Biotechnol J 12:7–13. doi: 10.1016/j.csbj.2014.09.011

58. Falkenburger BH, Saridaki T, Dinter E (2016) Cellular models for Parkinson's disease. J Neurochem. doi: 10.1111/jnc.13618

59. Stansley B, Post J, Hensley K (2012) A comparative review of cell culture systems for the study of microglial biology in Alzheimer's disease. J Neuroinflammation 9:115. doi: 10.1186/1742-2094-9-115

60. Verhoef LGGC, Lindsten K, Masucci MG, Dantuma NP (2002) Aggregate formation inhibits proteasomal degradation of polyglutamine proteins. Hum Mol Genet 11:2689–2700. doi: 10.1093/hmg/11.22.2689

61. Soto C (2003) Unfolding the role of protein misfolding in neurodegenerative diseases. Nat Rev Neurosci 4:49–60. doi: 10.1038/nrn1007

62. Ross C, Poirier M (2004) Protein aggregation and neurodegenerative disease. Nat Med

10 Suppl:S10-7. doi: 10.1038/nm1066

63. Ma T, Trinh M a, Wexler AJ, et al. (2013) Suppression of eIF2α kinases alleviates Alzheimer's disease-related plasticity and memory deficits. Nat Neurosci 16:1299–305. doi: 10.1038/nn.3486

64. Pavon-Eternod M, Gomes S, Rosner MR, Pan T (2013) Overexpression of initiator methionine tRNA leads to global reprogramming of tRNA expression and increased proliferation in human epithelial cells. RNA 19:461–466. doi: 10.1261/rna.037507.112

65. Goodarzi H, Nguyen HCB, Zhang S, et al. (2016) Modulated Expression of Specific tRNAs Drives Gene Expression and Cancer Progression. Cell 165:1416–1427. doi: 10.1016/j.cell.2016.05.046

66. de Baets G, Reumers J, Blanco JD, et al. (2011) An evolutionary trade-off between protein turnover rate and protein aggregation favors a higher aggregation propensity in fast degrading proteins. PLoS Comput Biol. doi: 10.1371/journal.pcbi.1002090

67. Trcka F, Vojtesek B, Muller P (2012) Protein quality control and cancerogenesis. Klin Onkol Cas Ces a Slov Onkol Spol 25 Suppl 2:2S38-44.

68. Calderwood SK, Khaleque MA, Sawyer DB, Ciocca DR (2006) Heat shock proteins in cancer: Chaperones of tumorigenesis. Trends Biochem Sci 31:164–172. doi: 10.1016/j.tibs.2006.01.006

69. Kedersha N, Stoecklin G, Ayodele M, et al. (2005) Stress granules and processing bodies are dynamically linked sites of mRNP remodeling. J Cell Biol 169:871–884. doi: 10.1083/jcb.200502088

70. McEwen E, Kedersha N, Song B, et al. (2005) Heme-regulated inhibitor kinase-mediated phosphorylation of eukaryotic translation initiation factor 2 inhibits translation, induces stress granule formation, and mediates survival upon arsenite exposure. J Biol Chem 280:16925–16933. doi: 10.1074/jbc.M412882200

71. Hay DG, Sathasivam K, Tobaben S, et al. (2004) Progressive decrease in chaperone protein levels in a mouse model of Huntingt ... Hum Mol Genet 13:1389–1405. doi: 10.1093/hmg/ddh144

72. Arumugam T V, Phillips TM, Cheng A, et al. (2010) Age and energy intake interact to modify cell stress pathways and stroke outcome. Ann Neurol 67:41–52. doi: 10.1002/ana.21798

73. Njemini R, Lambert M, Demanet C, Mets T (2006) The effect of aging and inflammation on heat shock protein 27 in human monocytes and lymphocytes. Exp Gerontol 41:312–319. doi: 10.1016/j.exger.2006.01.006

74. Ben-Zvi A, Miller E a, Morimoto RI (2009) Collapse of proteostasis represents an early molecular event in Caenorhabditis elegans aging. Proc Natl Acad Sci 106:14914–14919. doi: 10.1073/pnas.0902882106

75. Carvalho J, Van Grieken NC, Pereira PM, et al. (2012) Lack of microRNA-101 causes E-cadherin functional deregulation through EZH2 up-regulation in intestinal gastric cancer. J Pathol 228:31–44. doi: 10.1002/path.4032

76. Hurst CD, Zuiverloon TCM, Hafner C, et al. (2009) A SNaPshot assay for the rapid and

simple detection of four common hotspot codon mutations in the PIK3CA gene. BMC Res Notes 2:66. doi: 10.1186/1756-0500-2-66

77. Roth V (2006) Doubling Time Computing.

78. Simon R, BRB-ArrayTools Development Team BRB-ArrayTools.

79. Simon R, Lam A, Li M-C, et al. (2007) Analysis of Gene Expression Data Using BRB-Array Tools. Cancer Inform 3:11–17.

80. Saeed AI, Sharov V, White J, et al. (2003) TM4: A free, open-source system for microarray data management and analysis. Biotechniques 34:374–378. doi: 12613259

81. Saeed A, Bhagabati N, Braisted J, et al. (2006) TM4 microarray software suit. Methods Enzymol 411:134–193. doi: 10.1016/S0076-6879(06)11009-5

Annex C – Ana Fidaldo Master's Dissertation

Disclosure of interests: The autor of this thesis, Mafalda Santos, has mentored this Master's Dissertation; supervised all experiments except for the proteasome activity assay; developed the cellular models together with Ana Fidalgo; helped with results analysis; and reviewed this manuscript.

Universidade de Aveiro Departamento de Biologia
2015

Ana Patrícia Figueiredo Fidalgo

The contribuition of tRNA pool deregulation in the acquisition of a malignant phenotype

A contribuição da desregulação da pool de tRNA na acquisição do fenótipo maligno

DECLARAÇÃO

Declaro que este relatório é integralmente da minha autoria, estando devidamente referenciadas as fontes e obras consultadas, bem como identificadas de modo claro as citações dessas obras. Não contém, por isso, qualquer tipo de plágio quer de textos publicados, qualquer que seja o meio dessa publicação, incluindo meios eletrónicos, quer de trabalhos académicos.

Annex C

Universidade de Aveiro **Departamento de Biologia**
2015

Ana Patrícia Figueiredo Fidalgo

The contribuition of tRNA pool deregulation in the acquisition of a malignant phenotype

A contribuição da desregulação da pool de tRNA na acquisição do fenótipo maligno

Dissertação apresentada à Universidade de Aveiro para cumprimento dos requisitos necessários à obtenção do grau de Mestre em Biologia Molecular e Celular, realizada sob a orientação científica da Doutora Ana Raquel Santos Calhôa Mano Soares, bolseira de Pós-Doutoramento do Instituto de Biomedicina de Aveiro.

À Tua memória.

O júri

Presidente	**Doutora Maria de Lourdes Gomes Pereira** **Professor associada do departamento de Biologia da Universidade de Aveiro**
Arguente	**Doutora Patrícia Joana Morais Ferreira Oliveira** **Bolseira de pós-doutoramento do i3S/IPATIMUP**
Oritentador Científico	**Doutora Ana Raquel Santos Calhôa Mano Soares** **Bolseira de pós-doutoramento do Instituto de Biomedicina de Aveiro**

Agradecimentos

Ao Professor Manuel Santos pelo voto de confiança, dando me a oportunidade de integrar a sua equipa para concretizar esta dissertação.

À Doutora Ana Raquel Soares a orientação ao longo deste percurso, a disponibilidade, apoio e o voto de confiança.

À Mafalda Santos pelo trabalho em conjunto na construção do modelo em estudo, pelo apoio essencial em todas as fases deste projeto e por ter partilhado comigo o melhor que sabia. Juntamente com a Sofia Varanda, a vossa disponibilidade, a confiança que sempre depositaram em mim e o bom humor enriqueceram este desafio.

A toda à equipa do Laboratório de Biologia do RNA pelo auxílio, pela integração, pela ajuda e pelos momentos de descompressão.

À Carla, à Sara, à Ana, e à Débora pelo companheirismo, pela partilha e pelos momentos de diversão.

À Joana, à Rita e à Filipa por acreditarem em mim, celebrarem comigo cada conquista e partilharem o peso de cada derrota.

À Tertúlia das Pitecas pelo constante incentivo, pela amizade e pela presença constante apesar da distância.

Ao Hugo por ser a minha rede de queda, por todos os dias me lembrar do que sou capaz, por me ajudar a ir mais longe e pela infinita paciência.

Aos meus Avós pelo carinho, pelo conforto e pela alegria em os ter.

À Sara pela alegria e simplicidade com que preenche as nossas vidas.

À minha Irmã por despertar o melhor de mim e me fazer acreditar que temos o mundo nas mãos. Pelo orgulho, cumplicidade, partilha e ternura.

Aos meus Pais, acima de tudo. Por me apoiarem nas conquistas e nas derrotas, por permitiram que todos os dias me realize um pouco mais, pelo amor e pela confiança. Por possibilitarem que esta esta etapa se concretizasse. É a minha e a vossa dedicação.

Palavras-chave **Síntese proteica,** pool **de tRNAs,** codon usage**, stress proteotóxico, vias de controlo de qualidade proteica, tumorigénese.**

Resumo

Os tecidos humanos exibem diferentes padrões de expressão de tRNAs que se correlacionam com o codon usage **de genes altamente expressos, o que pode representar um controlo ao nível da tradução tendo em conta que os tRNAs são intervenientes importantes durante a síntese proteica. Nas células cancerígenas é observada a desregulação de componentes do processo de tradução, nomeadamente elevados níveis de tRNAs específicos estão correlacionados com a expressão preferencial de genes relacionados com o cancro. Assim, a desregulação da** pool **de tRNAs pode aumentar a eficiência de tradução desses genes, promovendo a transformação maligna.**

O processo tumorigénico é acompanhado por aumento do conteúdo proteico celular. A evasão à apoptose, a instabilidade do genoma e as mutações frequentes são também observadas em células cancerígenas. Isto pode promover a acumulação de proteínas mutantes que desencadeia o stress **proteotóxico e a produção elevada de HSPs, de forma a contrariar a instabilidade proteica. Para além disso, elevados níveis de proteínas incorretamente enoveladas, derivadas da elevada taxa de síntese proteica, induzem outras vias de controlo de qualidade proteica que auxiliam a ação dos chaperons: a resposta das proteínas não enoveladas e o sistema de degradação associado ao retículo endoplasmático.**

Este estudo teve como objetivo avaliar a influência da desregulação da pool **de tRNAs na aquisição do fenótipo maligno e a contribuição das vias de controlo de qualidade proteica na transformação celular. Globalmente, os resultados mostraram que a desregulação da** pool **de tRNAs induzida pela sobre expressão do $tRNA^{Ser}$ leva à aquisição de um fenótipo intermédio entre as células normais e as células cancerígenas. Assim, concluímos que esta desregulação pode representar um promotor da aquisição da malignidade celular.**

Keywords **Protein synthesis, tRNA pool, codon usage, proteotoxic stress, protein quality control pathways, tumorigenesis**

Abstract

Human tissues display different tRNA expression patterns correlated with the codon usage of highly-expressed genes, which may represents a translational control since tRNAs are critical players during protein synthesis. In cancer cells it is observed misregulation of components of translational machinery, namely elevated levels of tRNAs in a specific fashion, correlated with a preferential expression of cancer-related genes. Therefore, misregulation of tRNA pool may enhance the translational efficiency of these genes, promoting the malignant transformation.

The tumorigenic process is accompanied by increasing cellular protein load. Evasion of apoptosis, genome instability and frequent mutations are also observed in cancer cells. This may promote accumulation of mutated proteins that leads to proteotoxic stress and high production of HSPs, in order to counteract protein instability. Furthermore, high levels of misfolded proteins derived from the high rate of protein synthesis induce other protein quality control pathways to support the action of chaperones: the unfolded protein response and the endoplasmic reticulum-associated degradation system.

This study aimed to evaluate the influence of tRNA pool deregulation in the acquisition of a malignant phenotype and the contribution of protein quality control pathways in cell transformation. In general, the results showed that the deregulation of tRNA pool prompted by $tRNA^{Ser}$ overexpression leads to the acquisition of an intermediary phenotype between normal cells and cancer cells. Therefore, we concluded that this deregulation may be a driven force for cellular malignancy.

I. Contents

II. List of Figures

III. List f Tabels

IV. List of abreviations

5’ UTR - 5’ Untranslated Region

A
A – Adenosine
aaRS – aminoacyl tRNA synthetase
aa-tRNA – aminoacylated tRNA
ALK - Anaplastic Lymphoma Kinase
AMP – Adenosine Monophosphate
ATF4 – Activating Transcription Factor 4
ATF6 – Activating Transcription Factor 6
ATP – Adenosine Triphosphate

B
BiP – Binding immunoglobulin Protein
bp –base pair

C
C – Cytosine
CMA – Chaperones-Mediated Autophagy
cMET - mesenchymal-epithelial transition factor
CSC – Cancer Stem Cell

E
EGFR - epidermal growth factor receptor
eIF – eukaryotic Initiation Factor
eRF - eukaryotic Release Factor
EML - Echinoderm Microtubule-associated protein-Like 4
EMT - Epithelial-Mesenchymal Transition
ER – Endoplasmic Reticulum
ERAD – Endoplasmic Reticulum Associated Degradation

G
G – Guanosine
GAP – GTPase Activating Protein
GDP – Guanosine-5’-Diphosphate
GTP – Guanosine-5’-Triphosphate
GPR78 - G Protein-Coupled Receptor 78

H
HSF1 – Heat Shock Factor 1
HSP – Heat Shock Protein
HSR –Heat Shock Response

I
IRE1α – Inositol Requiring kinase 1
IRES- Internal Robosome Entry Sites
ITAF – IRES Trans-Acting Factor

K
K-ras - Ki-ras2 Kirsten rat sarcoma viral oncogene homolog

L
Leu – Leucine

M
MAPK – Mitogen-Activated Protein Kinase
Met - Metionine
mRNA – messenger RNA
mTOR – mammalian Target Of Rapamycin

N
NSCLC – Non-Small Cell Lung Cancer

O
ORF – Open Reading Frame

P
PABP – Poly(A) Binding Protein
PERK – PKR-like Endoplasmic Reticulum Kinase
PI3K - phosphoinositide 3-kinase
PIC – Preinitiation Complex
PKR – Protein Kinase RNA-activated
PPi – Pyrophosphate
PTC – Peptidyl Transferase Center

R
RB – Retinoblastoma protein
ROS – Reactive Oxygen Species
rRNA – ribosomal RNA

S
SCLC - Small Cell Lung Cancer
Ser – Serine

T
TFIIIB - RNA polymerase III-specific transcription factor
tRF – tRNA derived Fragment
tRNA – transfer RNA
Tyr – Tyrosine

U
U – Uridine
UPR – Unfolded Protein Response
UPS – Ubiquitin-Proteasome System

V
VCP – Valosin Containing Protein
VEGF - Vascular Endothelial Growth Factor

X
XBP1 - X-box binding protein 1

CHAPTER 1

V. Introduction

1.1.The Genetic Code

The central dogma of molecular biology states that the genetic information is coded in DNA molecules confined to the nucleus, which are transcribed in messenger RNA (mRNA) molecules that, in turn, will originate proteins in a process called translation. Translation is the last step of gene expression and it occurs according with the rules established by the genetic code, proposed by F. Crick in 1968.[1,2]

The mRNA is composed by codons that are non-overlapping nucleotide triplets, among adenosine (A), guanosine (G), cytosine (C) and uridine (U). Despite the 64 possible combinations between the ribonucleotides only 20 amino acids are coded, demonstrating the degenerative character of the genetic code (Figure 1).[3] The number of possible codons for each amino acid is variable, known as synonymous codons, but only one exists to start the translation of all proteins, the start codon methionine (AUG) and 3 stop codons (UAA, UAG, UGA) in eukaryotes to ensure the translation termination.[3–5] However, the universal genetic code is flexible since deviations to the canonical genetic code are described both in eukaryotes and bacteria, suggesting that it is still evolving.[6]

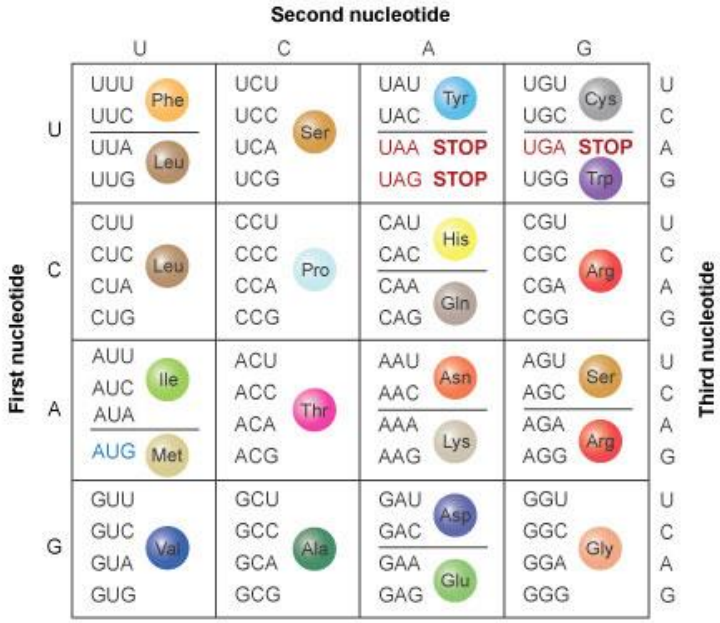

Figure 1. **The genetic code**. Clancy, S. and Brown, W. 2008

Amino acids are transported by transfer RNAs (tRNAs) that recognize the corresponding codon through interactions with its anticodon. The interaction between the first and second position of mRNA with tRNA is based on the canonical Watson-Crick pairing rules, by which an A or a G (purines) pairs an U or a C (pyrimidines), respectively. Furthermore, in 1996, F. Crick proposed that the third position, also known as the wobble position, could pair with the perfectly matched tRNA anticodon or adopt a non-canonical interaction to allow the same tRNA to recognize more than one codon, giving rise to the "Wobble Hypothesis".[7,8]

1.2.Codon Usage

The genetic code degeneracy allows a choice between different codons for the same amino acid in the transcriptome, which will affect the efficiency and accuracy of translation. This is known as codon usage. The codon usage has a close relation with the cellular availability in tRNAs (tRNA pool), that is regulated at several levels such as transcription, posttranscriptional processing, amino acid loading and degradation. The balance between these two factors affects protein production levels and the cellular fitness in a global view.[9–11] Non-optimal codon usage derived from poor correlation between codon usage and the tRNA pool may result in incorrect allocation of resources, namely the increase of ribosomes sequestration due to translation speed decrease, reducing the global cellular fitness.[12–14]

Highly expressed genes are often codon optimized to match the tRNA pool so they can be translated more efficiently. These genes are under a higher pressure for translational efficiency and accuracy, in particular the speed by which they are recognized by the ribosome and the corresponding tRNA selection. Thus, codon usage has a crucial role in modelling gene expression and can increase the expression of a gene more than 1000-fold. Moreover, alternative nucleotide sequences arising from synonymous codons may have a direct influence in protein folding and stability of secondary structures.[9–12,15]

The transcriptome's codon usage and the cellular tRNA pool are dynamic and adapted to biological conditions and tissue requirements, allowing different translation patterns accordingly with the cellular microenvironment.[12,15] Recently, Gingold *et al.* verified that cells' content in tRNAs and the respective codons in the transcriptome have approximately

the same gene copy numbers, suggesting that changes in tRNA's basal levels are required to restore the balance between codon usage and tRNA pool when the first is altered.[15]

1.3.Eukaryotic Translation

Translation is the process whereby information encoded in mRNAs is converted in polypeptide chains. This process is carried out in the core of ribosomes, where the interaction between mRNA codons and acylated-tRNA anticodons is allowed.[16] Ribosomes are ribonucleoproteins, complexes with several proteins and ribosomal RNAs (rRNAs), comprising a large and a small subunit, known as the 60S and 40S in respect with its sedimentation rate. In their inactive state, ribosomal subunits are apart and they only form complexes in the presence of mRNA transcripts that need to be translated, acquiring distinct functions. The small subunit offers the suitable environment for interaction between tRNAs and mRNA codons, while in the large subunit occurs the formation of peptide bonds between the recently added amino acids.[16]

The ribosome moves along the mRNA transcript by reading the nucleotide triplets from its 5' end to 3' end, giving rise to the polypeptide chain from the N-terminal to the C-terminal. The ribosome has one binding site for mRNA chains and three binding sites for tRNAs, which are the A-site, the P-site and the E-site, allowing amino acid adding in three major steps: tRNA binding, peptide bond formation and large and small subunits translocation, in a processes fully described below.[16,17]

a. Initiation

The initiation of translation requires several eukaryotic initiation factors (eIFs) and their isoforms. Generally in eukaryotes and for most cellular mRNAs, initiation occurs in a CAP-dependent manner, with the start codon AUG being recognized through scanning of the mRNA transcript.[18,19] The ternary complex is the major player in the scanning process and is fundamental in CAP-dependent translation, comprising the eIF2-GTP (guanosine-5'-triphosphate) and the initiator $tRNA_i^{Met}$.[20–23] The α-subunit of eIF2 (eIF2α) is crucial for translation regulation during initiation. Its phosphorylation at Ser51 prevents GDP (guanosine-5'-diphosphate) recycling triggered by eIF2B, hindering the interaction of eIF2 with the additional ternary complex components and consequent inhibition of protein

synthesis. This inhibition usually occurs during stress conditions to reduce protein synthesis rate and to enhance the translation of mRNAs that allow the adaptation to stress and the recovery of translation.[23]

Anyhow, translation initiation only occurs in the presence of the 43S preinitiation complex (PIC) that comprises the ternary complex, the 40S ribosomal subunit and the factors eIF3, eIF1, eIF1A and probably eIF5. The mRNA 5' CAP is recognized by the multimeric eIF4F complex, composed by eIF4E, the CAP-binding protein stabilized by the ATP-dependent RNA helicase eIF4A, and the eIF4G, a scaffold protein that links the mRNA and the ribosome using the eIF3. This complex unwinds the structures in the 5' untranslated region (5' UTR) and, together with eIF3 and poly(A) binding protein (PABP), attaches the 3'-poly(A) tail allowing the PIC to scan mRNAs for the initiation codon.[20–23] When the initiation codon, localized in a favorable context as Kozak sequence, is recognized in the P-site by the anticodon of the Met-$tRNA_i^{Met}$ in the ternary complex, the scanning is arrested and GTP is irreversible hydrolyzed by the GTPase-activating protein (GAP) eIF5, consequentially releasing the eIF2-GDP and other eIFs. At this point, the eIF5B-GTP promotes the association between the 60S ribosomal subunit and the complex formed by the 40S small subunit, the initiation aminoacyl-tRNA and the mRNA chain. When GTP is hydrolyzed, the eIF5B is released from the ribosome, dictating the final of the initiation.[21–23]

However, CAP-independent translation represents an alternative to CAP-dependent translation both under normal and stress conditions, such as endoplasmic reticulum (ER) stress, hypoxia, nutrient deprivation, mitosis and cell differentiation and it is used not only by eukaryotic cells but also by virus that infect them as a strategy to express their mRNAs. At stress conditions, CAP-dependent translation is compromised leading to a significant increase in cellular Internal Ribosome Entry Sites (IRES)-mediated translation that recruits both canonical and non-canonical initiation factors, IRES trans-acting factors (ITAFs) and 40S ribosomal subunits.[24,25]

b.Elongation

Translation elongation is conserved among Eukarya, Bacteria and Archaea and it follows the initiation process.[21] In the beginning of elongation the P-site is occupied by the Met-$tRNA_i^{Met}$ and the A-site is empty. Then, the aminoacyl-tRNA whose anticodon complements

the second codon, or the cognate aminoacyl-tRNA, is added to the A-site due to the formation of another tertiary complex comprising the cognate aa-tRNA and the eEF1A-GTP. The interaction between this tRNA and the mRNA codon involves conformational changes in the decoding center of the 40S ribosomal subunit and the GTP hydrolysis ensures the presence of the cognate tRNA. If the complementarity is assured, the eEF1A-GTPase becomes activated. Then, eEF1A-GDP is released and the aminoacyl tRNA is accommodated in the A-site.[17,21,26,27]

The next step is the peptide bond formation between Met and the recently added amino acid, in the peptidyl transferase center (PTC) located in the large ribosomal subunit. The Met accommodated in the P-site moves to the A-site of this center and a peptide bond can be made with the second amino acid still attached to its cognate tRNA, in a peptidyl transferase induced reaction. Then, the P-site is occupied with a deacylated tRNA connecting the mRNA in the small subunit and the 3' CCA in the E-site of the large subunit. Also, the peptidyl tRNA is in a hybrid state as its acceptor arm is in the P-site and the anticodon arm forming a mRNA-tRNA duplex in the A-site of the small subunit.[21,26,27] The eEF2-GTP is required to restore the canonical positions in the A and P-sites, in a process named translocation. GTP hydrolysis turns the ribosome free to move temporarily three codons towards the mRNA 3' end. Posttraslocation state accounts for a deacylated tRNA in the E-site, a peptidyl-tRNA in the P-site and a new codon in the A-site to be decoded. At this point, a new codon can be read and this cyclic mechanism is repeated until a stop codon is detected.[21,27]

c. Termination

When the ribosome detects a stop codon in the A-site a signal to finish the translation and to release the polypeptide chain is recognized. Stop codon recognition can be made by the ribosome, by external factors that interact with the ribosome and by the combined action of both.[17,28] This signal activates the eukaryotic release factor 1 (eRF1), a class I release factor that binds the ribosome at the A-site. It is responsible for high-fidelity stop codon recognition and peptidyl-tRNA hydrolysis, promoting the addition of a water molecule to the peptide chain.[27] eRF1 may also open a channel that triggers the incoming of water molecules into the ribosome; engender conformational changes in the ribosome so the water molecule can reach the active center; activate the water molecule and the ester bond so peptidyl-tRNA hydrolysis can occur.[21] This step destroys the attachment of the carboxyl end

to the ribosome, and the recently synthetized polypeptide is finally released. eRF1 activity and connection with the ribosome is supported by a class II release factor, the eRF3-GTPase whose hydrolysis removes eRF1 from the ribosome.[17,21,28]

d.Recycling

The ribosomal subunits have to be recycled after the synthesis of a newly polypeptide chain, so another translational cycle could be performed. Therefore, the mRNA chain and the deacylated-tRNA have to be released as well as the ribosomal subunits have to be separated in a process called recycling, a mechanism that lacks fully explanation in the eukaryotic model.[27]

Nevertheless, partial dissociation of ribosomes is also observed in a mechanism termed reinitiation. In these cases, the ribosome translates further Open-Reading Frames (ORFs) in the same mRNA without complete recycling of the ribosomal machinery. In this way, translation of the same ORF can be done, through incomplete recycling potentially taking place in the stop codon, allowing scanning along the 3' UTR and triggering the 40S transference to the 5' UTR. Although interactions involved in this process are not completely known, there is a potential hypothesis based on the role of PABP, eRF3, eIF4E and eIF4G in a mechanism that potentiate a close proximity between the mRNA 5' and 3' ends.[21,27]

The eIF3 has an active role in the recycling process in higher eukaryotic translation, since it directly binds to and induces conformational changes in the 40S small subunit surface avoiding its reconnection with the 60S large subunit until a new mRNA emerge to be translated.[20,21,27]

1.4.Transfer RNAs

Transfer RNAs (tRNAs) are universally conserved small and ubiquitous RNA molecules that are the interface between the genetic information encoded in mRNA transcripts and the proteins. [29,30] The secondary structure of tRNA (Figure 2) has a cloverleaf shape derived from a single nucleotide chain with 73 to 90 nucleotides in length and 4 domains organized in unpaired and paired regions: acceptor arm, D arm, anticodon arm and TΨC arm. The acceptor arm has a 3' CCA tail that links covalently the cognate amino acid, and the anticodon arm has a three nucleotide sequence in the unpaired region, the anticodon loop,

that interacts with the mRNA codon. Unpaired regions also mold loops in the D and the TΨC arms and an unpaired region between the anticodon and the TΨC arms represents the variable arm, also known as extra arm. [16,29–31] The size of the variable arm can range from 3 to 21 bases and dictates tRNA grouping in class I or II. The first includes the majority of tRNA molecules and is characterized by small extra arms, while class II tRNAs, comprising Leucine (Leu), Serine (Ser) and Tyrosine (Tyr), have larger variable arms and a R_{13}-R_{22} base pair (bp) in the D-loop.[16,32]

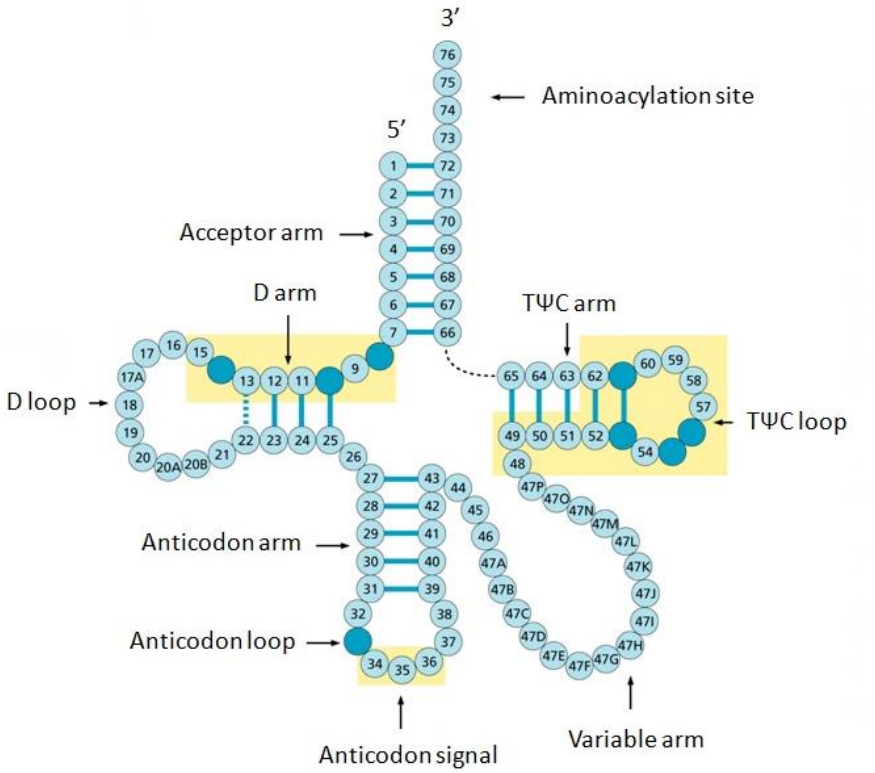

Figure 2. **tRNA secondary structure**. Adapted from Zvelebil, M. and Baum, J. O. 2007

Functional and mature tRNAs acquire a L-shape tertiary structure through the stacking between acceptor stem and TΨC arm and between D-arm and anticodon arm, both stacks forming a continuous A-helix. Thus, functional tRNAs are characterized by an amino acid accepting branch where cognate amino acid covalently links an adenosine in 3' CCA tail and an anticodon branch that connects with the codons in mRNAs. This highly stable structure is obtained from the interaction between conserved and semi conserved nucleotides in the tRNA chain and it is substantially altered according to its functional state.[29–31,33]

tRNAs are codified by 506 genes [Genomic tRNA Database] that are transcribed by the RNA polymerase III, whose activation is regulated by cellular nutrient availability and other environmental features. To become functional, tRNA transcripts should be processed to get the standard length and be posttranscriptionally modified (Figure 3). Still in the nucleus, the ribonucleoprotein RNase P performs endonucleolytic cleavage of the 5' ladder sequence in precursor tRNA. Then, endonucleases (such as RNase E and RNase III) cleave the 3' trailer extensional sequence and exonucleases (such as RNase T and RNase PH) cleave the residual trailer sequence. In some cases where CCA tail is absent, it is added by the CCA-adding enzyme following the discriminator base N_{73}. Next, the splicing of remaining introns occurs, as well as modification of several nucleotide residues.

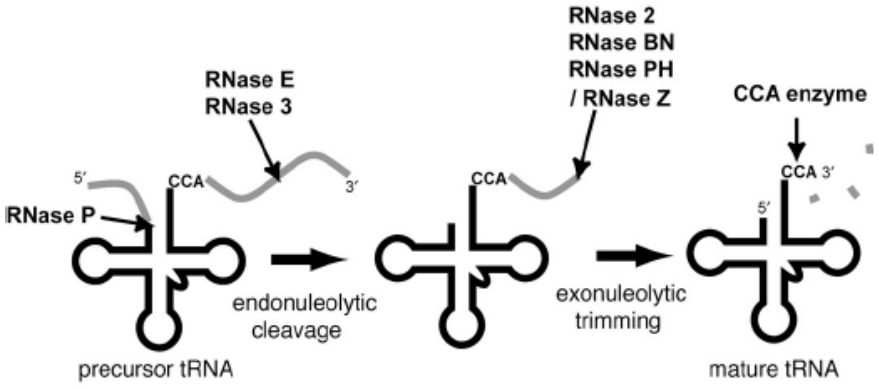

Figure 3. **tRNA processing**. Nakanishi, K and Nureki, O. 2005

These posttranscriptional modifications are divided in two types, according to its target: modifications in the loops of D and TΨC arms have the purpose to stabilize the tertiary L-shape structure, while modifications in the anticodon loop promote precise codon pairing and accurate recognition by the cognate aminoacyl tRNA synthetase (aaRS).[33,34]

In spite of tRNAs being mainly associated with its role during translation, these molecules also participate actively in other cellular functions, both in prokaryotic and eukaryotic cells. Uncharged tRNAs act as signaling molecules that activate cellular stress responses in the presence of nutritional stress, to stimulate the expression of genes related to amino acid synthesis and their uptake and to aminoacyl-tRNA synthetases, thus contributing to cell survival.[29,31] Additionally, tRNAs are mediators in non-ribosomal processes, as the peptide bond formation between peptidoglycans in bacterial cell wall biosynthesis and in the modification of phospholipids that form the cell membrane.[35] These molecules can also label

proteins for degradation, participate in the regulation of apoptosis and in antibiotic biosynthesis.[31,36]

Recently, tRNA-derived fragments (tRFs), resulting from tRNA degradation, were also found to be functional forms that can actively participate in regulation of gene expression at translational level under stress conditions and in gene silencing.[31,37,38]

Since tRNAs can have a variety of functions, it is not surprising that their biosynthesis occurs under several control pathways, which recognize and degrade misfolded or hypomodified forms. Also, tRNAs account for more than 15% of total RNA amount and comprise one of the most abundant transcripts in the cells.[29]

1.5.Aminoacyl-tRNA Synthetases

Aminoacyl-tRNA synthetases (aaRSs) are a highly conserved enzyme family that catalyzes tRNA aminoacylation with the cognate amino acid. The aminoacylation reaction occurs in two steps, illustrated in Figure 4. From the first step results a stable complex between the active site of aaRS and the cognate amino acid, in an ATP dependent reaction. In this way, a firmly bounded aminoacyl-adenylate is formed, releasing a pyrophosphate (PPi). In the second step, the tRNA binds the amino acid by the 3' end adenosine in the acceptor stem, releasing AMP and esterifying the tRNA at 3' end.[39]

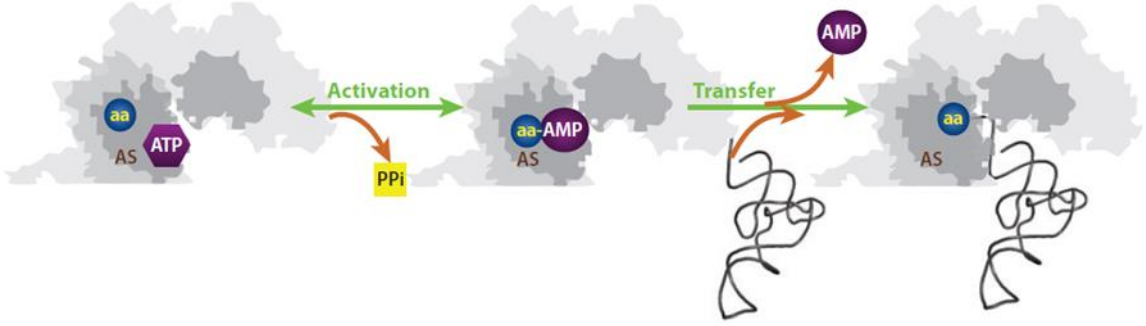

The recognition of tRNAs by its cognate aaRSs is based on the interaction with specific elements, as the discriminator base N_{73}, the acceptor stem and the anticodon region. Less often, interactions with elements in the extra arm, the D stem, the core of the tRNA tertiary

Figure 4. Schematic representation of **aminoacylation reaction**. AS, active site; aa, amino acid; PPi, pyrophosphate. Jiqiang Ling, J. *et al*. 2009

structure and the phosphate backbone or with modified nucleotides and the wobble base can occur.[39]

To avoid inaccuracy derived from tRNA charging with the incorrect amino acid, aaRSs have an editing capacity encoded by a different active site. The double-sieve model suggests that the editing capacity allows aaRSs to discriminate amino acids with similar properties, and it can occur before or after amino acid transference to the tRNA, the pretransfer editing and posttransfer editing, respectively. Pretransfer editing is based on the hydrolysis of amino acids incorrectly activated before transference to the tRNA, while posttransfer editing requires the interaction between the tRNA 3' CCA tail with the aaRS editing site. Trans editing was recently proposed and relies on the capacity of other proteins to recognize and hydrolyze incorrectly charged tRNAs.[40–42] Moreover, the editing capacity is wider and it can act through discrimination between tRNAs by direct interaction, recognition of the acceptor stem nucleotide sequence and by contact with key nucleotides in the tRNA.[17,41] This editing capacity is essential to avoid protein synthesis errors and its disturbance can be associated with various pathologies, which severity varies inversely with the editing capacity.[40]

1.6.Protein Folding and Misfolding

Proteins are the most structurally and functionally complex molecules, thus its activation requires more than its translation. After leaving the ribosome, the polypeptide chain has to be modified to get its unique three-dimensional conformation. Protein-modifying enzymes bind small-molecule cofactors essential for protein activity or assemble proteins with other protein subunits.[17,43]

The information necessary for these modifications is encoded by the amino acid sequence itself and its biochemical properties. The interaction between amino acids from different regions of the polypeptide occurs by weak non-covalent bonds that taken together determine the protein folding stability. Also, folding is influenced by the hydrophobic character of the side chains, as the non-polar tend to cluster in the interior of the molecules forming a hydrophobic core, while polar amino acids are exposed and form hydrogen bonds with other molecules. These interactions result in a three dimensional structure that lacks the conformation of lowest free energy, without losing the flexibility to interact with other molecules that may influence protein function.[16,17,43]

Incorrect folding results in misfolded and nonfunctional proteins characterized by exposed hydrophobic amino acids. Alterations in cell homeostasis caused by stochastic fluctuations, destabilizing mutations, stress conditions or metabolic alterations resulting from processes such as cancer and aging, trigger wrong interactions, unfolding or denaturing of proteins and inhibit interactions between subunits of larger protein complexes. These alterations can be dangerous for the cell because misfolded/unfolded proteins can aggregate in toxic forms and give rise to several human diseases. Thereby, cells account with several mechanisms to maintain the stability of the proteome, ensuring misfolded proteins refolding, degradation or sequestration.[17,44–46]

1.7.Proteotoxic Stress and Protein Quality Control Pathways

The endoplasmic reticulum (ER) is the cellular compartment responsible for structural maturation of one-third of all eukaryotic proteins. Proteins remaining in the cytoplasm and mitochondria are under constant vigilance of chaperones responsible for its maturation. Proteins matured in the ER, when leaving this compartment, no longer need the assistance of chaperones, meaning that only correctly folded proteins leave the ER. In this way, highly sophisticated and robust quality control systems are required to avoid release of aberrant proteins to perform their functions.[43,47] However, as a result of errors during transcription and translation, aberrant proteins are produced and their accumulation leads to homeostatic perturbations and proteotoxic stress.[2,48,49]

To counteract the proteotoxic stress, several quality control responses are activated to promote the refolding of misfolded proteins or, if not possible, its degradation. The activation of these pathways aims to restore homeostasis and to avoid apoptosis induction. Homeostasis is achieved by upregulation of the ER folding capacity, increasing chaperones availability and foldases as well as ER size; through downregulation of biosynthetic load, inhibiting protein synthesis at transcriptional and translational levels; and increasing elimination of unfolded proteins through upregulation of Endoplasmic Reticulum Associated Degradation (ERAD) protein clearance mechanism.[2,45–47,49] It is estimated that 30% to 70% of proteins do not pass the quality control mechanisms and end up being degraded.[50]

If cells are unable to activate these control pathways or if these pathways become overloaded, waste of nutrients occurs and misfolded and nonfunctional proteins that can aggregate in toxic forms are produced, dictating cell death as the final fate.[2]

a. Chaperones and Heat Shock Response

Molecular chaperones are proteins that assist noncovalent folding of newly synthesized polypeptides, assembly of protein subunits, preventing or reversing incorrect folding. This large protein family, first discovered in 1978 by Laskey *et al.*, recognizes and binds reactive surfaces exposed in the client protein, avoiding incorrect interactions. Still, chaperones assist oligomeric structures synthesis in the transport of proteins through membranes, by preventing the three-dimensional folding that can be a hitch in the membrane crossing, maintaining the protein in an unfolded and more flexible status. Chaperones can also signal the protein for degradation.[16,46,51]

A significant number of chaperones are designated heat shock proteins (HSPs), term that derives from its overexpression in cells exposed to higher temperatures. While chaperones have the folding as their major role during normal metabolism, stress conditions induce higher levels of HSPs that assist the refolding and repair of damaged proteins, to prevent protein denaturation and aggregation. HSPs derive from the transcription of distinct gene families and they are classified according to their approximate relative molecular mass in five main HSP families: Hsp70, Hsp90, Hsp60, small HSP and large HSP families. The genes encoding chaperones have three differently regulated classes: constitutively expressed chaperones, during growth and development; constitutively and induced chaperones and strictly induced chaperones.[51–54]

Regarding their action, HSPs can be classified, not exclusively, in holding and folding proteins. The first group comprises HSP70 and HSP90 families and they recognize and bind exposed hydrophobic domains in unfolded polypeptides. They can act during mRNA translation to prevent premature self-association of nascent polypeptide chains; during heat shock response through interaction with totally or partially unfolded proteins and constitutively to bind unstable tertiary structures. In this process a large complex is formed, comprising five core proteins that accounts for Hsp90, the scaffold protein Hop, the p23 protein as mediator of substrate selection and the complex HSP70/HSP40 to mediate the interaction between HSP90 and the client protein. These complexes interact with many

accessory proteins, also known as co-chaperones, to facilitate substrate selection and cycles of association and dissociation from the client protein. Once the correct folding is achieved, HSPs are released from proteins in an ATP-dependent mechanism.

Folding activity can be performed individually by Hsp70, Hsp40 or co-chaperone GrpE or in a chaperonin system comprising a large oligomeric assembly that lodges unfolded proteins and promotes a suitable environment for their folding. Also, Hsp90 together with Hsp70 acts directly with specific classes of proteins involved in signal transduction, thereby maintaining the target in an appropriate function until it is stabilized through the interaction with other components of the pathway.[16,44,54]

The transcription of HSPs is dependent on heat shock factor 1 (HSF1) transcription factor that binds the promoters of *HSP* genes, inducing HSP mRNA transcription. Activation of HSF1 is still under investigation but some explanations were proposed. HSF1 is inhibited by its products, which in stress conditions may be sequestrated in protein aggregates, thus de-repressing HSF1. Another mechanism for HSF1 activation relies on the heat-induced binding to large non-coding RNAs, which are known to be involved in the regulation of a wide range of genes, complexed with eEF1A. Besides, during stress conditions, a rapid phosphorylation of serine 326 in the HSF1 occurs, correlated with the onset of *HSF* gene transcription, suggesting that this serine has a role in stress response regulation prompted by HSF1: the heat shock response (HSR).[52,53]

The HSR is a cellular mechanism activated in the presence of a wide range of stress conditions that triggers protein inactivation. This response is based on a combination of events called thermotolerance, a condition directly related with the coordinated synthesis of HSPs. [44,52,53]

b. Unfolded Protein Response

The UPR relies on the activation of different but complementary signal pathways triggered by three ER transmembrane proteins: the inositol requiring kinase 1 (IRE1α), the double-stranded RNA-activated protein kinase (PKR)-like endoplasmic reticulum kinase (PERK) and the activating transcription factor 6 (ATF6), schematically represented in Figure 5. During homeostatic conditions these proteins are inactivated by formation of stable complexes with the ER stress sensor GPR78, also known as binding immunoglobulin protein

(BiP). However, presence of unfolded proteins leads to a competition for BiP, derepressing the signal pathways.[45,55,56]

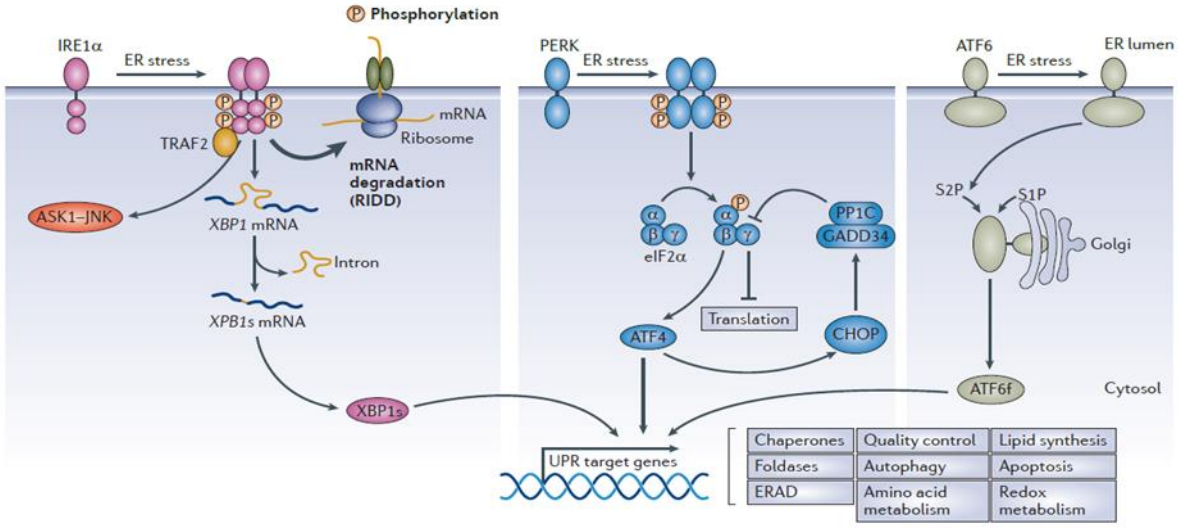

Figure 5. Schematic representation of the **unfolded protein response**. Adapted from Claudio Hetz *et al.* 2013

When IRE1α is dissociated from BiP, it undergoes dimerization and autophosphorylation, activating its endonuclease activity for mRNA processing. IRE1α activates the X-box binding protein 1 (XBP1), through splicing of its mRNA transcript. When active, XBP1 upregulates the expression of genes encoding proteins that have roles in protein folding, insurance of its quality and ERAD activation.[45,55–57]

After being released from BiP, PERK becomes activated through dimerization and autophosphorylation, activating its kinase activity. PERK activation prompts global protein synthesis inhibition through inhibitory phosphorylation of eIF2α, to reduce the influx of newly synthetized proteins into the ER. The downregulation of translation upregulates the activating transcription factor 4 (ATF4) that promotes cell survival since it regulates genes involved in oxidative stress, amino acid synthesis, protein folding and cell differentiation. [45,55–57]

Finally, ATF6 is released from BiP and translocated to the Golgi compartment. There, ATF6 is cleaved by the site-1 and site-2 proteases releasing its N-terminal fragment, the cytoplasmic domain, which acts as a transcription factor. In the nucleus, ATF6 fragment promotes upregulation of UPR target genes, such as XBP1, and ERAD associated proteins.[45,55–57]

c. Endoplasmic Reticulum Associated Degradation Response

ERAD is fundamental to eliminate misfolded proteins, maintaining the equilibrium between protein synthesis and degradation, in a demand to prevent proteotoxicity, ER stress and subsequent apoptosis.[57]

The ERAD response promotes degradation of aberrant proteins by the Ubiquitin-Proteasome System (UPS), the major eukaryotic proteolytic pathway. This process is initiated with the recognition of substrate and its translocation across the ER lipid bilayer to the cytoplasm. In the cytoplasm, proteins are polyubiquitinated, signaling for degradation by the 26S proteasome subunit.[46,58]

d. Autophagy

Autophagy is an evolutionarily conserved protein and organelle degradation mechanism with a complex molecular background, missing full explanation. Autophagy can be characterized into three different types: macroautophagy, microautophagy and chaperones-mediated autophagy (CMA). All end up with the delivery of the target, the cargo, into the lysosome where it occurs protein unfolding and degradation by the action of proteases.[59]

Regarding the protein quality control, the autophagic process represents an important mechanism to eliminate aggregation prone proteins. It functions as a backup of ERAD since its impairment leads to an upregulation of autophagy, as a strategy to recognize and degrade protein aggregates.[46,60] Also, autophagy has a role during stress caused by nutrient and oxygen deprivation, and biosynthetic and homeostatic functions. Examples are the degradation of mitochondria, known as mitophagy, as an approach to control their reliability and to avoid the production of reactive oxygen species (ROS), or the degradation of peroxisomes that are no longer needed, the pexophagy. [59,61]

1.8. Tumorigenesis

The tumorigenic process starts with a normal cell that becomes transformed by acquisition of autonomous proliferation features driven by accumulation of genetic alterations, leading to immortalization. Acquisition of malignancy is the result of tumour progression rather than transformation. During tumour progression, cancer cells lose their original shape and polarity. Finally, they acquire the capacity to invade nearby tissues and metastasize to distant locations through the blood or lymphatic system.[62,63]

Variability is an intrinsic characteristic of tumors that promotes functional and phenotypic heterogeneity in tumors established in the same organ, known as intertumoral heterogeneity, and even within individual tumors, the intratumoral heterogeneity.[62] The intertumoral heterogeneity is associated with different genetic and epigenetic mutations, distinct cells in the origin of tumor, different molecular profiling characterization, different specific markers expression and different morphological features.[62]

Intratumoral heterogeneity can be explained by the cancer stem cell (CSC) and the clonal-evolution models.[62] The first proposes that the tumor has its origin in normal self-renewing stem cell or downstream progenitor with limited or no self-renewal. Considering that the expansion of the progenitor cell may originate downstream cells which accumulate different mutations, CSCs can originate different clones within the same tumor, thus contributing to its heterogeneity.[64,65] In turn, the clonal evolution model suggests that a single cell accumulates mutations that are hereditarily transmitted through successive generations and the most advantageous for the tumor are selected through natural selection.[64] The genetic and epigenetic changes which provide the cell with the more aggressive, invasive and drug-resistant phenotype are those prevailing. However, these models cannot be applied in a mutually exclusive characterization since all the events interact to define the tumor histopathology and behavior.[62,64,65]

In a global view, cancer cells can be characterized based on traits that enable them with distinct but complementary capabilities. These features allow tumor growth and metastatic dissemination and they are known as the hallmarks of cancer (Figure 6). The acquisition and development of these hallmarks are possible due to genome instability, product of several random and particular genetic mutations and chromosomal rearrangements, and the inflammatory state of established or premalignant lesions that is supported by immunologic cells.[66]

Figure 6. The **hallmarks of cancer** and enabling characteristics. Adapted from Hanahan, D. and Weinberg, R, 2011

Cancer cells present deregulation of growth-promoting signals, leading to sustained proliferative signaling. Moreover, cancer cells are also able to evade growth suppressors that could inhibit its proliferation.[66,67]

The programmed cell death is essential to prevent cancer development. The most relevant player in responses to stress, damage and regulation of apoptosis is the p53. In cancer cells, mutations in *TP53* gene or in its upstream or downstream effectors are frequent, allowing apoptosis evasion, invasion, metastasis, proliferation and cell survival.[66,68,69]

Proliferation of normal cells is limited by a number of successive division cycles in a process controlled by the size of telomeres, which triggers cell death when they become too short to protect the chromosomes. In cancer cells, the DNA telomerase is highly expressed, opposing to what happens in normal cells, which is correlated with resistance to senescence and acquisition of replicative immortality.[66]

Cancer cells are also associated with the capacity to induce angiogenesis, in a process triggered by deregulated proangiogenic signals that give rise to aberrant neovascularization. Considering that tumor microenvironment is characterized by hypoxia, nutrient deprivation and low pH, angiogenesis may be induced as an alternative to obtain nutrients and oxygen and to discard metabolic wastes and carbon dioxide.[66]

Lastly, malignant cells have the capacity to invade, to avoid apoptosis and to disseminate, in a process called metastization, closely related to the regulatory program "epithelial-mesenchymal transition" (EMT). The reprogramming of energy metabolism and the capacity

of tumor cells to avoid immune surveillance are now emerging as new hallmarks of cancer, as major evidences are emerging to prove its crucial role in cancer development.[66,70]

1.9.Lung Cancer and Non-Small Cell Lung Cancer

Cancer is the leading cause of death in the world with a continuous increase in the number of cases, particularly in developing countries, estimated at over 20 million per year at 2025.[71] Lung cancer represents the main cancer related death and it is associated to cigarettes active smoking, followed by passive smoking and occupational exposure to chemical and physical carcinogenic agents as nickel, asbestos, arsenic, radiation and air pollution. Susceptibility to lung cancer is also allied with individual inherent susceptibility to these agents and familiar history of lung cancer, without overlooking lifestyle factors as diet and physical inactivity, established diagnosis of acquire lung diseases and HIV related infections.[72] The stage and degree of tobacco epidemic have a close relationship with countries socioeconomic development. Countries that had its smoking peak in the middle of 20th century are currently detecting a decrease in lung cancer rates; instead, countries where tobacco consumption epidemic was established recently are handling increasing rates. Yet, as the rate of smokers decreases it is observed a greater frequency of lung cancer among passive smokers. Another bequest of socioeconomic development is the increase in smoking habit among women, resulting in 50% of cancer related death in this gender and 80% in men.[72–74]

Lung cancer is classified in two major subtypes based on histological features and response to conventional therapies: small cell lung cancer (SCLC) and non-small cell lung cancer (NSCLC), the last accounting for 85% of all lung cancers. SCLC type can be also divided in classical small cell carcinoma, large cell neuroendocrine and combined, while NSCLC comprises adenocarcinoma, squamous cell carcinoma and large cell carcinoma.[74–76]

Lung cancer has a 5-years survival rate of 15%, as result of late diagnosis of advanced tumors.[74,75] Diagnosis of lung cancer is achieved by analysis of complete medical history and physical examination that can reveal suggestive signs and symptoms of lung disease, such as alterations in expectoration quantity, amount and presence of blood, shortness of breathing, wheezing, chest pain and frequent respiratory infections. Then the physician

should proceed with more conclusive and chest located tests as radiography and also computed tomography and magnetic resonance imaging, which can identify metastatic episodes and support a differential diagnosis. Adenocarcinoma and large cell carcinoma have preferential localization in the periphery of lung, lining the small airways while squamous cell carcinoma and SCLC have their origin in epithelial cells that line the larger airways in the central area of chest. At the cellular level, cytological analysis can be made after expectoration collection, being enough to diagnose 80% of lung tumors. To improve diagnostic capacity and precision, a bronchoscopy and fine-needle biopsy of lung and metastatic lesion or lymph node may be done.[75,77]

NSCLC has a complex molecular character underlying his pathogenesis that is not fully understood. However, it is crucial to understand and characterize diagnostic and prognostic biomarkers and therapeutic targets so worry rates associated to lung cancer can be weakened.[78] The epidermal growth factor receptor (EGFR) is responsible for the activation of phosphoinositide 3-kinase (PI3K)/AKT and RAS/RAF/MAPK pathways that ultimately lead to the active transcription of genes involved in cell survival, proliferation, angiogenesis, invasion and metastasis. Mutations in *EGFR* are presented in 10% of NSCLC cases and are closely related with tobacco consumption, being inversely proportional to the degree of smoking.[76,79] Mutations on the V-Ki-ras2 Kirsten rat sarcoma viral oncogene homolog (K-*ras*) gene are present in 20-30% of NSCLCs, with influence on cell proliferation and apoptosis via MAPK and on cell survival responses via PI3K. These represents 90% of all *ras* mutations in adenocarcinomas and they are common in smokers and patients that were exposed to asbestos, being more prevalent in women.[76,79,80]

Despite those factors are markedly involved in the carcinogenic process of NSCLC, others have been identified. The vascular endothelial growth factor (VEGF) is highly expressed in NCSLC and it is critical in physiologic and pathologic angiogenesis, through promotion of survival and tumor growth. Its overexpression relates to poor prognosis.[76] Similarly, overexpression, amplification or gain-of-function of the mesenchymal-epithelial transition factor (c-MET) are evident in lung adenocarcinoma, participating in tumor growth, differentiation and metastasis and thus contributing to a poor prognosis.[77,81,82]

The rearrangement of the anaplastic lymphoma kinase (*ALK*) gene derived from the fusion with the echinoderm microtubule-associated protein-like 4 (*EML4*) gene was classified as a gain of fusion mutation. *EML4-ALK* fusion was identified in 2% to 7% of

NCSLC, in the absence of *KRAS* and *EGFR* mutations, with a positive influence in neoplastic transformation and cell survival.[76,83]

1.10. tRNA Pool Deregulation in Cancer

The deregulation of protein synthesis machinery and tRNA pool, in particular, are observed in a wide range of tumors, suggesting that misregulation of translation components are involved in malignant transformation.[84]

Pavon-Eternod *et al*. observed a significant overexpression of tRNAs in breast cancer cell lines and tumor tissues when compared with non-cancer-derived breast epithelial cell lines and normal breast tissues.[85] In particular, $tRNA^{Ser}$, $tRNA^{Tyr}$ and $tRNA^{Thr}$ were the most expressed and its overexpression seems to favor the codon usage of cancer-related genes, important in tumor initiation and progression, but not the house-keeping genes and cell-line specific genes. Also, the overexpressed tRNAs carry polar amino acids that are targets of protein kinases and phosphatases, demonstrating a possible mechanism for potentiating posttranslational regulation of proteins involved in signal transduction.[85] Notably, the overexpression of tRNAs in cancer cells is accompanied by altered metabolic activity and unregulated growth.[86]

Differential expression of tRNAs regulates the efficiency of translation through the codon usage of specific genes and it is possible that during active cell growth there is a correlation between the tRNA pool and the codon usage of highly translated genes.[85] So, deregulation of the tRNA pool in cancer may be responsible for the quantitative and qualitative alterations in protein expression, since this deregulation leads to preferential expression of key proteins in tumor progression and development, such as growth factors, cell-cycle promoters and oncoproteins, particularly c-Myc and VEGF, the last known to be upregulated in NSCLC tumors.[76,85,86]

The deregulation of RNA polymerase III is also observed in several tumors, explained by the releasing of pol III-specific transcription factor TFIIIB from the inhibitory effect provided by RB (retinoblastoma protein) and p53, which are often mutated in cancer cells.[84,85] Also, TFIIIB is activated by the upregulation of c-Myc and mutations in *KRAS*, alterations observed in NSCLC cells.[80,87] Must be noted that tRNA transcription via pol III is globally regulated by environmental signals, as nutrient availability, and the transcription

of tRNA genes is coordinately regulated by common transcription factors that act in highly related promoter sequences.[86]

Cellular stress leads to an alteration in the codon usage of demanded genes and so the request for tRNAs by certain codons increases and the availability in tRNAs for other codons decreases. It is also known that codons that became preferentially expressed under these conditions corresponded to tRNAs that are represented by the lowest gene copy number.[15]

In another study, Pavon-Eternod *et al*. verified that induction of the elongator $tRNA_e^{Met}$ does not alter significantly its levels but punctual changes in levels of several other tRNAs not induced experimentally are observed. This can be explained by a regulatory feedback mechanism related with overexpression of $tRNA_i^{Met}$.[86]

Nonetheless, the knowledge available about effects derived from overexpression of tRNAs and the mechanisms of response from cells to these perturbations is very limited yet.[86]

1.11. Proteotoxic Stress in Cancer

The process of malignant transformation is accompanied by increased protein load. Likewise, evasion of apoptosis, genome instability and frequent mutations are observed in cancer cells, which may promote accumulation of mutated proteins and sustained activation of proliferation signals.[88] Qualitative and quantitative alterations of the proteome induce cellular proteotoxic stress that is faced by the induction of HSPs as an attempt to repair and refold aberrant products. In cancer cells, an increase in HSF1 levels is observed through a process not yet understood but that may be related with increased transcription and translation as well as epigenetic regulation.[53,88]

The relation between increased chaperoning capacity and tumorigenesis can be explained by the "addiction to chaperones" hypothesis. This assumption is based on the increased necessity for chaperoning the larger protein load due to rising in mRNA translation derived from highly metabolic and proliferative rates and the polyploidy observed in several cancer cells. The instability created in the proteome is supported by chaperones in an addictive process since high protein expression and gene mutations are driven forces of tumor growth and progression. Interestingly, in studies where the Hsp90 chaperone is inhibited downregulation of several oncogenes is observed, probably because the instability

of mutant and aberrant proteins is not counteracted and they are eliminated by quality control pathways.[53]

Moreover, HSPs activity in cancer cells supported by HSF1 seems to affect a wide range of pathways that are essential to sustain the malignant phenotype. Evidences exist to prove their role in the acquisition of cancer hallmarks, excluding the evasion of growth suppressors where the role of chaperones is still inconclusive.[53] Hsp90 seems to be the main chaperone in tumorigenesis, acting to maintain the active conformation of mutant and signal proteins as an approach for faster information flux in response to extracellular signals, essential to development and cell renewal.[53,54] Hsp90 and Hsp70 overexpression in cancer allows to stabilize precancerous proteins, such as growth factor receptors, survival-signaling kinases, oncogenes and mutated proteins, supported by Hsp27 that is known to be upregulated in many cancers.[53,89] In the NSCLC context, low levels of HSP90 are correlated with better prognosis and pharmaceutical inhibitors of Hsp90 also impair EGFR activity, useful when no *KRAS* mutations are present.[90]

Cancer cells grow in an environmental context that differs from normal cells as it is hypoxic and with lower pH and nutrient availability, as a result of low vascularization. The higher tumor growth rate outdoes new blood supply, although in an inefficiently manner because the synthesis of new vessels is aberrant and the blood flow dynamics are altered.[57,91] The low nutritional availability directly influences protein glycosylation and ATP production, which triggers synthesis of misfolded proteins, an event also supported by the lack of oxygen that is crucial for disulfide bond formations in proper protein folding. These perturbations lead to ER stress with consequent activation of quality control pathways, at which cancer cells can adapt and so escape to apoptosis.[57,92]

Cancer cells have high activation of the UPR and take advantage from activation of characteristic signal pathways, in a chronic manner. BiP is known to be increased in aggressive malignant forms, including lung cancer and it seems to promote cell survival, tumor progression, metastasis and resistance to therapeutics.[57,93] This is possible since overexpression of BiP has a crucial role in pro-survival and cytoprotective responses in malignant cells, by diverse mechanisms such as inactivation of caspase-7.[57]

Despite its role in tumorigenesis is not entirely explained, IRE1α inhibition appears to prompt reduction in tumor growth, in angiogenesis and in blood perfusion of tumor. It is known that IRE1α induces cellular proliferation through XBP1 splicing and the axis IRE1α-

XBP1 seems to be regulated by the pro-apoptotic proteins BAX and BAK, suggesting a close relation between the UPR and the apoptotic pathway. Deletion of *Xbp1* increases sensitivity to hypoxia-induced cell death and consequent decrease in tumor formation capacity, since it is a major transcription factor in the adaptive response to ER stress, solid tumor growth and survival under hypoxic conditions. The activation of such related factors promotes induction of proangiogenic factors like VEGF, highlighting its role in angiogenesis and proposing as possible therapeutic targets.[57,92]

PERK can have an active role in tumor growth and proliferation through limitation of oxidative stress derived from ATF4 activation, which also stimulates transcription of pro-survival genes and upregulation of adhesion proteins, VEGF and type 1 collagen inducible protein, important factors for angiogenesis.[92,94] Furthermore, ATF4 expression triggers cell survival by negative regulation of genes related with cellular senescence.[57] Moreover, the upregulation of the autophagosomal membrane LC3B by ATF4 allows lysosomal degradation of unnecessary cellular components and thereby cell survival. In a global view, inhibition of PERK remarkably reduces cells adaptation and survival under hypoxic conditions.[57] Recently, Fan *et al.* detected an active form of ATF4 phosphorylated at Ser 245 highly expressed in NSCLC tumors that may contribute to its progression, particularly in metastasis, since it promotes adaptive response to ER stress and triggers stress-induced angiogenesis. However, the mechanism involved in its upregulation is still unclear.[57,94]

Although few studies have been conducted, it is know that ATF6 is required to malignant transformation. Its functionally active form improves tumor survival by activating the mammalian target of rapamycin (mTOR) signaling pathway, which has been associated with malignant transformation, taking into account its influence in cell growth and proliferation.[59,97] Particularly in NSCLC, the mTOR activation, AKT-dependent or independent, has been correlated with the proliferative character of cancer cells.[82,100]

Regarding the ERAD system, its regulation is also visible in cancer cells as a way to evade apoptosis and to reduce the accumulation of misfolded proteins that may be toxic for the cell. The valosin containing protein (VCP), an AAA ATPase molecular chaperone, is upregulated in several tumors. VCP controls ubiquitin mediated degradation of misfolded proteins and it is involved in protein folding, cell cycle control and apoptosis.[57] Valle *et al.* demonstrated that the inhibition of VCP in cells from a NSCLC suppresses tumor growth and induces apoptosis *in vitro* and in xenograft murine models.[96]

Autophagy can act both as tumor suppressive and as oncogenic player. As tumor suppressive, autophagy intervenes in cell cycle arrestment, strives for maintenance of genome and organelle integrity and promotes inhibition of necrosis and inflammation. On the other hand, autophagy promotes cell survival under the conditions of metabolic stress created by the tumor microenvironment, through elimination of damaged mitochondria, ROS and protein aggregates, which cause DNA damage and activation of tumorigenesis.[59,97]

VI. Aim of Study

The deregulation of tRNA pool has been reported in different tumors and correlated with the expression of cancer-related genes.[85,86] However, a major question remains: is tRNA pool deregulation a cause or a consequence in the acquisition of a malignant phenotype?

In order to contribute to the clarification of this issue, this study proposed to evaluate the influence of tRNA deregulation in the acquisition of a malignant phenotype and the contribution of protein quality control pathways in cell transformation. Therefore, the following cellular mechanisms were evaluated:

- Phenotypic profiling;
- Transformation ability *in vitro*;
- Induction of proteotoxic stress;
- Activation of protein quality control mechanisms;
- Insoluble protein expression profile.

CHAPTER 2

VII. Experimental Design

To assess the effects of tRNA overexpression for the acquisition of a malignant phenotype, a comparative study was performed between a normal human cell line derived from the bronchial epithelium (BEAS-2B cell line) and a NSCLC cell line (NCI-H460 cell line) derived from a large cell lung carcinoma. Since Pavon-Eternod *et al*. observed a particular overexpression of $tRNA^{Ser}$ in breast cancer cell lines and breast tumor tissues.[85]

Therefore, BEAS-2B cells were stably transfected with a pIRES2-DsRED plasmid containing $tRNA^{Ser}$ to induce $tRNA^{Ser}$ overexpression and so promote deregulation of the cellular tRNA pool. This transfection created BEAS-2B $tRNA^{Ser}$ cell line. Also, BEAS-2B cells and NCI-H460 cells were stably transfected with the empty pIRES2-DsRED plasmid, given rise to the BEAS-2B Mock cell line and NCI-H460 Mock cell line, respectively. BEAS-2B Mock cell line is the control in the assays performed.

VIII. Material and Methods

2.1.pIRES2-DsRED plasmid

To induce overexpression of $tRNA^{Ser}$ in a stable cell line we used the pIRES2 DsRed-Express2 vector, a bicistronic expression vector (Figure 7) that allows simultaneously the expression of the $tRNA^{Ser}$ coding sequence and the Ds-Red Express2 fluorescent protein, useful to identify cells expressing the $tRNA^{Ser}$ gene through fluorescence microscopy. Also, this vector contains a kanamycin/neomycin resistance gene, suitable for selection of *Escherichia Coli* (*E. Coli*) competent cells with the plasmid using kanamycin, and for the selection of stably transfected mammalian cells using geneticin (G418) (Formedium^{Tm}). Previously co-workers inserted the coding sequence for the $tRNA^{Ser}$ using EcoRI and XhoI restriction enzymes into the vector. A pIRES2 DsRed-Express2 vector without the $tRNA^{Ser}$ coding sequence was used to normalize the effect of plasmid insertion.

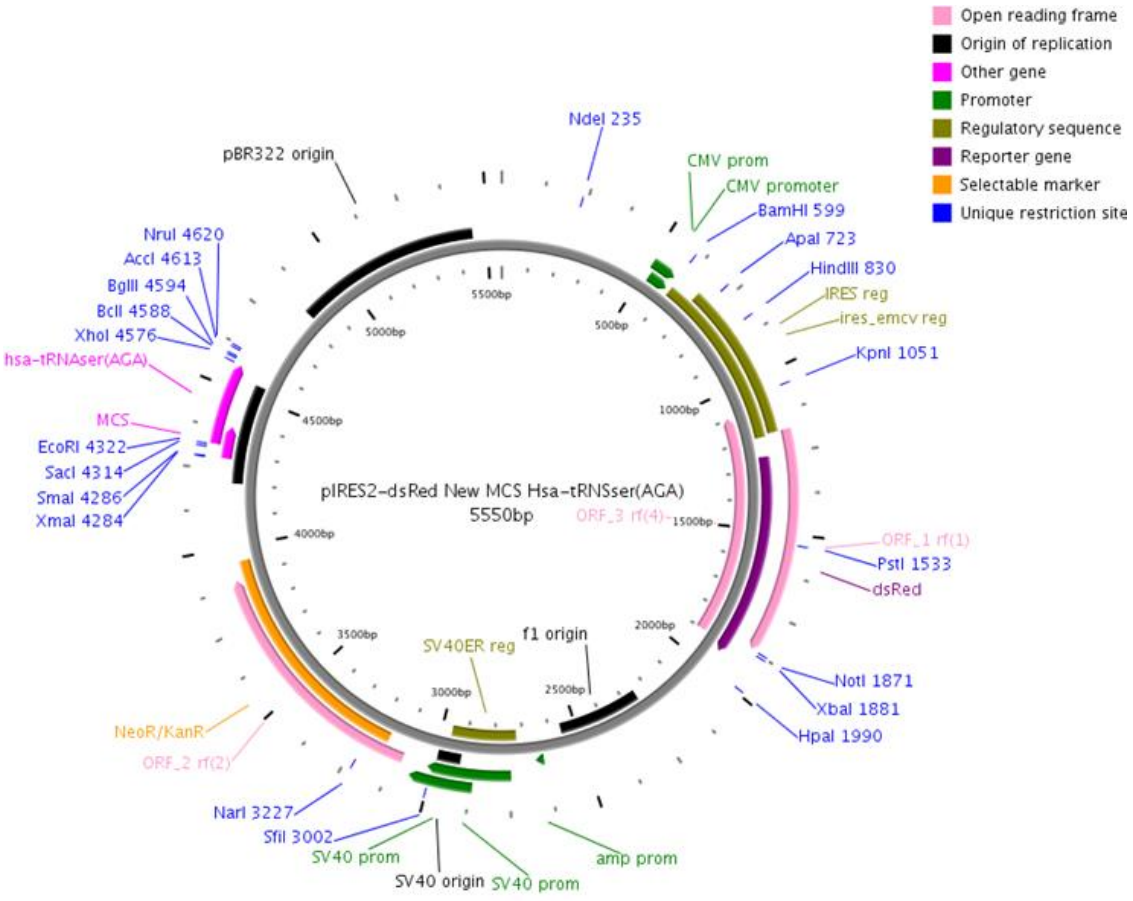

Figure 7. **pIRES-DsRed containg the $tRNA^{Ser(AGA)}$** coding sequence.

2.2.*Escherichia Coli* Competent Cells

E. Coli cells were grown to obtain enough amount of plasmids to create our cell lines. Previously, co-workers transformed these cells with the pIRES2-DsRED containing the $tRNA^{Ser}$ and the empty pIRES2-DsRED plasmid and stored at -20ºC. To cultivate the *E. Coli* cells, Lysogeny Broth (LB) medium was supplemented with kanamycin. After homogenization, 20µl of transformed *E. Coli* cells were added to the medium and maintained overnight in a shaking incubator at 37ºC.

2.3.Extraction and Quantification of pDNA

Plasmid DNA (pDNA) from transformed *E. Coli* was extracted with MiniPrep Nzytech Kit, according with the manufacturer's instructions. After extraction, the pDNA concentration was quantified with the NanoDrop spectrophotometry (ThermoScientific). The system was calibrated using 1.5µl of miliQ H_2O and purity values were calculated through the ratios 260nm/280nm and 260nm/230nm.

2.4.Polymerase Chain Reaction

To verify if the *E. Coli* selected carried our plasmid without alterations, we amplified the tRNA region of our plasmid by PCR using 50ng of pDNA. The reagents were acquire to Invitrogen (Thermo Scientific) and primers' sequences are represented in Table I. Note that primers are the same for the amplification of pIRES2-DsRED containing the $tRNA^{Ser}$ and the empty pIRES2-DsRED plasmid since the flaking regions are equivalent. The PCR reaction comprised 35 cycles and occurred in the MyCycler™ Thermal Cycler (Bio-Rad).

Table I. Primers used and respective sequences

Primer	Sequence
Primer Forward	CAATACGCCCGCGTTTCTT
Primer Reverse	TTATCCAAAAAGGATCTTCACCTAGA

2.5.Agarose Gel Electrophoresis

PCR amplification products were analyzed by performing an agarose gel electrophoresis, a technique that allows the separation of DNA fragments, according with their molecular size, under an electric field.[98] Five µl of PCR products were run in 1% agarose with 0.01% ethidium bromide (EtBr) at 80V and in an electrophoretic thank containing 1X Tris-Acetate-EDTA (TAE) (GRiSP). After electrophoresis, gels were scanned in the UV-Transilluminator (Bio-Rad) and results were visualized with Quantity One 4.2.1 software.

2.6.Purification of PCR products

PCR purification was performed using the QIAquick PCR Purification Kit (Qiagen), following the manufacturer's instructions. After the purification, DNA concentration was evaluated in the NanoDrop, as described in 2.3.

2.7.DNA Sequencing

To confirm the nucleotide sequences of the pIRES2-DsRED containing the $tRNA^{Ser}$ and the empty plasmid, purified PCR products were prepared to be sequenced by GATC Biotech. For that, microtubes with 5µl of 80ng/µl of amplified DNA were prepared for each sample as well as microtubes with the forward and reverse primers with 5µl of 5µM, according to the recommendations of the LIGHTRUN sequencing kit. Results were analyzed using the FinchTV v.04 software (Geospiza Inc).

2.8.Cell Culture

BEAS-2B cell line was kindly provided by Professor Maria Carmen Alpoim, from IBILI, University of Coimbra and NCI-H460 were obtained from IPATIMUP's Cell Bank. BEAS-2B cells were cultured in LHC-9 medium (Gibco, Life Technologies) supplemented with 1% of Penicillin-Streptomycin (Pen/Strep) (Gibco, Life Technologies). NCI-H460 cells were cultured in RPMI 1640 medium (Gibco, Life Technologies), supplemented with 10% Fetal Bovine Serum (FBS) (Sigma) and 1% Pen/Strep. Cells were maintained in an incubator at 37ºC with 5% CO_2 and 95% relative humidity.

To execute the following procedures, cells were detached using trypsin (Sigma). Then, BEAS-2B cells were resuspended in trypsin neutralizer solution [0.5% FBS in 1X Phosphate Buffered Saline (PBS)] while NCI-H460 cells were resuspended in complete RPMI 1640 medium. Cells were then centrifuged at room temperature (RT) and ressuspended in complete medium or 1X PBS, depending on the following procedure.

2.9.Lipotransfection

Lipotransfection is a procedure that uses cationic lipids formulations to deliver the foreign genetic material into eukaryotic cells. [99]

Transfection protocols using Lipofectamine® 3000 Transfection Kit (Invitrogen), for BEAS-2B and NCI-H460, were carefully optimized to reach close to 100% transfection efficiency. 1.0 x 10^5 BEAS-2B cells and 5.0 x 10^4 NCI-H460 cells were plated in MW24 plates and after 48h cells were transfected with small alterations to manufacturer's protocol. BEAS-2B were transfected using 1µg of plasmid DNA and 1µL of Lipofectamine® 3000, whereas NCI-H460 were transfected using 1.5µg of plasmid DNA and 0.75µL of Lipofectamine® 3000. In this transfection, while a set of BEAS-2B cells were transfected with the pIRES2-DsRED containing the $tRNA^{Ser}$ another set of BEAS-2B cells were transfected with the empty pIRES2-DsRED plasmid. NCI-H460 cells were transfected with the empty pIRES2-DsRED plasmid.

Since the goal was the integration of the plasmid in the genome and the expansion of these cells, cell lines were on culture for three weeks and under the selection of G418 in a concentration of 200µg/ml in BEAS-2B cells culture and 800µg/ml in NCI-H460 cells culture (concentrations previously optimized through a death curve).

Despite this methodology allowed the creation of a stable NCI-H460 Mock cell line, BEAS-2B Mock cell line or BEAS-2B $tRNA^{Ser}$ cell line were not successfully created since these cells lost the plasmid during selection and died.

2.10. Electroporation

As an alternative to create stable BEAS-2B derived cell lines, we used electroporation, which is a technique that relies in the use of electric pulses to transiently alter the cell membrane permeability, allowing the DNA to enter the cell.[99] To perform the electroporation, BEAS-2B cells were seeded in 100mm dishes and cultured until 70-90% of

confluence was reached. Cells were detached as described in 4.8 and the pellet was resuspended in Hepes Buffered Saline (HBS) solution (Appendix) to improve the transfection efficiency. Then, 4mm electroporation cuvettes were prepared with 10µg of plasmid and 0.5ml of cell suspension was added, mixing carefully. For each sample, two conditions were tested differing in the voltage applied, 230V and 260V, both with capacitance of 1500µF and resistance of 125Ω. This step was performed using ECM Electro Cell Manipulator (BTX, Harvard Apparatus). Immediately after the electroporation, 1ml of LHC-9 culture medium was added, homogenizing carefully, and the mixture was transferred to 60mm dishes, already prepared with 3ml of LHC-9 culture medium.

The stable cell lines BEAS-2B Mock and BEAS-2B $tRNA^{Ser}$ were obtained by selection with G418 in a concentration of 200µg/ml for three weeks, as in the lipotransfection.

2.11. Fluorescence Microscopy

pIRES2-DsRED plasmid codifies for the red fluorescent protein DsRed-Express2, which allows to validate its integration in the cell genome through fluorescence microscopy. For that, a coated coverslip (Corning™) was placed in the well or culture dish of each culture cell line in the moment of transfection, so the cells could adhere and grown into it. 48h later, the culture medium was removed and the well/culture dish was washed ten times with 1X PBS. Then, enough volume of Hoechst dye (1µg/ml) was added to the coverslip and incubated during 15min at RT, protected from the light. The coverslip was washed five times with 1X PBS, the excess was removed and it was transferred to a microscope slide containing the Fluoroshield mounting medium (Sigma), leaving to dry for 15min. Fluorescence was detected in the Zeiss MC80 Axioplan 2 Light microscope with the filter set HE38. Photographs were taken using an AxionCam HRc camera.

2.12. Extraction and Quantification of gDNA

To ensure the plasmid did not acquire mutations when integrated in the genome, gDNA was extracted to be sequenced as described in 2.7. For that, it was used the NZY Tissue gDNA Isolation Kit, following the recommended instructions, and gDNA concentration was quantified in the NanoDrop, as described in 2.3.

2.13. Cellular Viability Assay

To perform this assay 1.5 x 10^5 cells/well of BEAS-2B Mock cells, BEAS-2B $tRNA^{Ser}$ cells and NCI-H460 Mock cells were seeded in a 24-well plate. After two days in culture, cells were detached and equal volumes of cell suspension and trypan blue were mixed. Finally, cell viability (%) was obtained by counting the live and death cells using a $TC10^{Tm}$ Automated Cell Counter (Bio-Rad). This assay was performed with triplicates and repeated three times.

2.14. Cellular Proliferation Assay

To evaluate cellular proliferation, 5.0 x 10^4 cells/well of BEAS-2B Mock cells, BEAS-2B $tRNA^{Ser}$ cells and NCI-H460 Mock cells were seeded into four 24-well treated culture plates, so cell counting could be performed before the first cellular division (0h) and over the next three days (24h, 48h, 72h). Cells were detached and equal volumes of cell suspensions and trypan blue were mixed and viable cells were counted in a Neubauer chamber at each time point. The procedure accounted with triplicates and it was repeated three times.

2.15. Anchorage-Dependent Colony Formation Assay

To access the tumorigenic ability of our cell lines *in vitro* we performed an anchorage-dependent colony formation assay. This assay requires well individualized cells, so suspensions of 300 cells of BEAS-2B Mock cells, BEAS-2B $tRNA^{Ser}$ cells and NCI-H460 Mock cells were seeded in 60mm dishes and maintained on culture during two weeks. After, the colonies were fixed using ice cooled methanol and maintained at -30ºC during 30min. Methanol was removed and a solution of 0.1% crystal violet in methanol was added and the plates were laid on stirring at least for 30min. When colonies were stained, each well was washed with H_2O milliQ to remove excess dye and the colonies were counted. This assay was performed with triplicates and repeated four times.

2.16. Total Protein Extraction

To obtain total protein from the three cell lines, BEAS-2B Mock cells, BEAS-2B $tRNA^{Ser}$ cells and NCI-H460 Mock cells were seeded on 60mm dishes and maintained on culture until they reached about 90% confluence. At that time, the culture medium was removed and the plates were washed with 1X PBS. Cells were detached and pelleted as described in 2.8.

The next step was to lyse cellular membranes to release their content, by resuspending the pellet in lysis buffer (Appendix) (volume was adjusted regarding the size of the cell pellet) and incubating during 30min. From this point, sample manipulation should be performed on ice to avoid proteases activity. During the incubation with lysis buffer, each sample was sonicated in a Branson Sonifier S-250A (Fisher Scientific) and centrifuged at 4ºC and 16000*g* for 30min in a Centrifuge 5415R (Eppendorf®). Finally, the supernatants were collected and the samples were concentrated in a DNA 120 SpeedVac System (Thermo Scientific) until a volume of 50µl was reached.

Protein quantification was accessed through the Pierce BCA Protein Kit (Thermo Scientific), according to the recommendations of the manufacturer. Absorbance at the 575nm wavelength was obtained using a microplate reader (iMark™ Microplate Reader, Bio-Rad), and results were analyzed in the Microplate Manager Software v6.3 (Bio-Rad Laboratories, Inc.).

2.17. Western Blot

Western blot is a technique that separates proteins based on its molecular weight under an electric field, which are then transferred to a solid supported and identified using specific and labeled antibodies.[100] Proteins were separated by sodium dodecylsulfate-polyacrylamide gel electrophoresis (SDS-PAGE), which allows proteins to migrate according to their molecular weight. Accordingly with the molecular weight of proteins in study, 8% and 10% polyacrylamide gels (Appendix) were prepared.

Protein quantity was optimized for each protein studied (ranging from 30µg to 60µg of protein) and protein samples preparation required addition of 6X SDS Protein Loading Buffer (Appendix). Proteins were denatured at 95ºC for 5min in the Thermomixer Comfort (Eppendorf®). The denatured proteins were then loaded into gels in an electrophoretic thank filled with 1X running buffer (Appendix), under a voltage of 80V when running in the stacking

gel and 100V during migration in the running gel. After their separation, proteins were transferred from gels to 0.2µm nitrocellulose membranes (GE Healthcare Life Sciences) in a transference system filled with cold transfer buffer (Appendix) under the constant voltage of 100V, for 1h30min at 4ºC. As a transference quality control, the membranes were stained with 0.1% (m/v) Ponceau S (Sigma-Aldrich) in 5% (m/v) acetic acid during 1min at RT and excess dye was removed with distilled H2O (dH2O). Staining was removed by washing the membranes with Tris-Buffered Saline – Tween (TBS-T) (Appendix).

To avoid antibody unspecific hybridization, membranes were incubated with blocking solution [5% BSA in TBS-T] for 1h at RT and then washed three times with TBS-T for 5 min each. At this point, the membranes were ready for hybridization with the primary antibodies: anti-Hsp27, anti-Hsp70, anti-Hsp90α, anti-BiP and anti-ubiquitin (StressMarq, Biosciences Inc.) prepared in blocking solution with 1:1000 dilution factor. Their hybridization occurred overnight at 4ºC. After the incubation, membranes were washed three times with TBS-T for 5 min each.

The secondary antibodies goat anti-mouse IgG and goat anti-rabbit IgG (Odyssey, LI-COR) diluted 1:10000 in blocking solution were incubated by 2h at RT, protected from the light. Anti-β tubulin (StressMarq, Biosciences Inc.) was used as internal control and its hybridization occurred for 2h at RT and also 2h with the secondary antibody goat anti-mouse IgG. Primary antibodies and the correspondent secondary antibodies are represented in Table II.

After secondary antibody hybridization, membranes were washed two times with TBS-T for 5min each and 15min with TBS and scanned in the Odyssey Infrared Imaging System (LI-COR, Biosciences Inc.). Data was obtained with the software Odyssey v3.0.16 (LI-COR, Biosciences Inc.).

TABELA II**. Primary antibodies** and respective **secondary antibodies**

Primary antibody	Secondary antibody
Anti-Hsp27	Goat anti-mouse IgG
Anti-Hsp70	
Anti-Hsp90α	
Anti-ubiquitin	
Anti-β tubulin	

Anti-BiP	Goat anti-rabbit IgG

For multiple probing, membranes were incubated with stripping solution (Appendix) at RT, long enough to dissociate the antibodies from the membrane.

2.18. Proteasome activity assay

Proteasome activity can be determined by measuring the intensity of fluorescence derived from the cleavage of a labeled peptide (Suc-LLVY-AMC), a substrate for enzymes with chemotrypsin-like activity.[101]

The three different cell lines were seeded in 60mm dishes and maintained in culture until 90% of confluence was reached. At this point, culture medium was removed and cells were washed with PBS. Then, proteasome lysis assay buffer (Appendix) was added to the culture plates placed on ice and, after an incubation of 5min at RT, cells were scrapped and collected to 2ml microcentifuge tubes. Total protein extraction was performed as described in 2.16.

Protein quantification was obtained through the Bradford method, Bradford reagent was obtained from Bio-Rad and absorbance was read in the absorbance microplate reader (iMark™ Microplate Reader, Bio-Rad).

To assess proteasome activity, 20µg of protein were incubated with proteasome activity buffer (Appendix) in a black 96 multiwell plate (Costar™) to avoid light interferences, platting 6 wells for each sample. To eliminate unspecific proteasome activity, the proteasome inhibitor MG132 (Sigma) was added to 3 wells per sample. The fluorescence emitted from the cleavage of Suc-LLVY-AMC (Sigma) was accessed in the fluorometer system of Synergy 2 (BioTek®), for one hour with reads every 5min, using 360nm wavelength for excitation and 460nm for emission. Results were analyzed in the Gen5™ v.1.11.5 software (BioTek). Each experiment was performed with triplicates and repeated seven times.

2.19. SUnSET Method

As a strategy to obtain a similar number of cells to perform the assay, 5.0×10^5 cells of BEAS-2B Mock cells and BEAS-2B $tRNA^{Ser}$ cells and 1.0×10^5 cells of NCI-H460 Mock cells were seeded in 100mm dishes and maintained in culture for three days. 10µg/ml puromycin in 1X PBS was added to the culture medium of each culture dish, in a volume

corresponding to 10% of culture medium. After 10 min incubation at 37ºC with 5% CO_2, the culture medium was removed and replaced by fresh culture medium. Cells were once again placed in the incubator for 50 min, after which the culture medium was removed and 1X PBS was added to wash the culture plate. Cells were detached and pelleted as described in 2.8.

Total protein extraction was performed using proteasome lysis assay buffer and as described in 2.16 and protein quantification was achieved by the Bradford method, described in 2.18.

Incorporation of puromycin was detected by immunoblotting, so samples were prepared to SDS-PAGE. 100µg of total protein was loaded into 10% polyacrylamide gels, separated and transferred to nitrocellulose membranes. For the detection of puromycin, membranes incubated with anti-puromycin clone 12D10 primary antibody (1:5000 in blocking solution) overnight at 4ºC and with goat anti-mouse IgG secondary antibody by 2h at RT, protected from the light. Anti-β tubulin was used as internal control and secondary antibody fluorescence detection occurred as described in 2.17.

2.20. Insoluble Protein Fraction

BEAS-2B Mock cells, BEAS-2B $tRNA^{Ser}$ cells and NCI-H460 Mock cells were seeded on 60mm dishes and maintained on culture until about 90% confluence was reached. Cells were detached and pelleted, as described before, and suspensions with 5.0 x 10^6 cells were aliquoted after total cell counting in a Neubauer chamber.

To perform protein extraction, cellular pellets were resuspended in lysis buffer and maintained on ice for 30min. Meanwhile, samples were sonicated in a Branson Sonifier S-250A (Fisher Scientific). Then, samples were centrifuged for 15min at 2300*g* and at 4ºC in a Centrifuge 5415R (Eppendorf®). Supernatants were collected and 5µl was kept apart to quantify total protein with the BCA method. The supernatant was centrifuged for 20min at 16000*g*, 4ºC. At this point, the supernatant (the soluble protein fraction) was separated from the pellet (the insoluble fraction). The pellet was ressuspended in protein lysis buffer and 10% Triton X-100. Another centrifugation was performed for 20min at 16000*g* and at 4ºC. To finish, the supernatant was discarded and the pellet was resuspended in 50 µl of lysis buffer.

Relative expression of insoluble protein fraction was obtained though SDS-PAGE, as described in 4.6. Samples were solubilized with 2% urea SDS loading buffer (Appendix), denatured at 95ºC in the Thermomixer Comfort (Eppendorf®) and loaded into 10% polyacrylamide gels. Then, gels were stained with Coomassie Brilliant Blue (Appendix) during 2h and the excess was removed with distaining solution (Appendix). Gels were scanned in the Odyssey Infrared Imaging System (LI-COR, Biosciences Inc.) and data was obtained with the software Odyssey v3.0.16 (LI-COR, Biosciences Inc.). This assay was performed with triplicates and repeated three times.

2.21. Statistical analysis

Statistical analysis was performed in the GraphPad Prim® v6.01 software, applying the one-way ANOVA test with Tukey post-test for all the experiments except for proliferation assay, which was analyzed with two-way ANOVA test with Tukey post-test.

CHAPTER 3

IX. Results

3.1.Stable cell lines construction

To obtain the three stable cell lines two different approaches were applied. BEAS-2B Mock cell line and BEAS-2B $tRNA^{Ser}$ cell line were obtained through electroporation while NCI-H460 Mock stable cell line was obtained by lipotransfection.

The pIRES-DsRED plasmid contains the coding sequence for the DsRed Express2 fluorescent protein, therefore 48h after transfection it was possible to detect the integration of plasmid in cells through fluorescent microscopy and images of transfected BEAS-2B are shown in Figure 8 as well images of transfected NCI-H460 cells are shown in Figure 9.

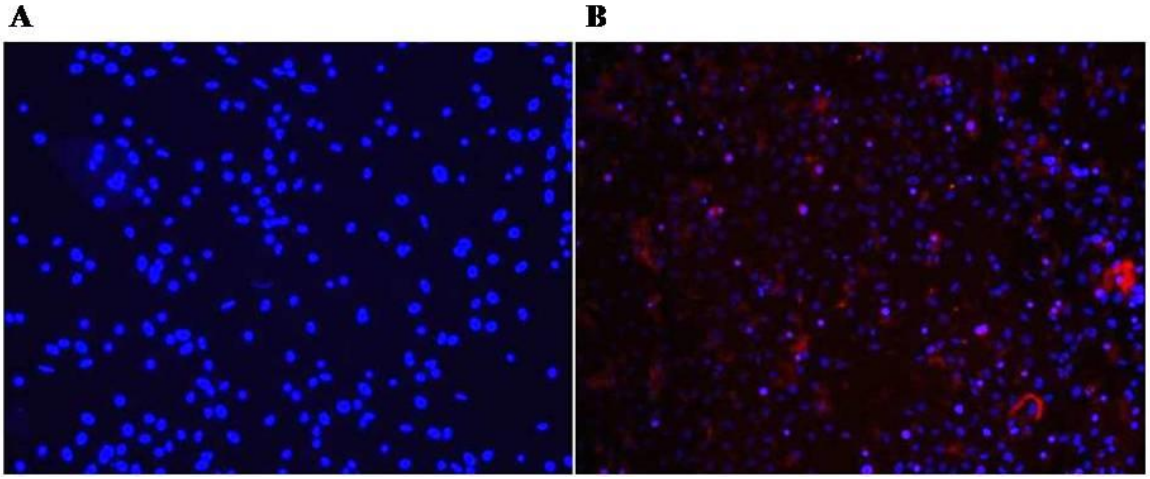

Figure 8. **A**. BEAS-2B non-transfected and stained with Hoechst dye (20x). **B**. BEAS-2B transfected with 1µg of plasmid pIRES-DsRED and stained with Hoechst dye (20x).

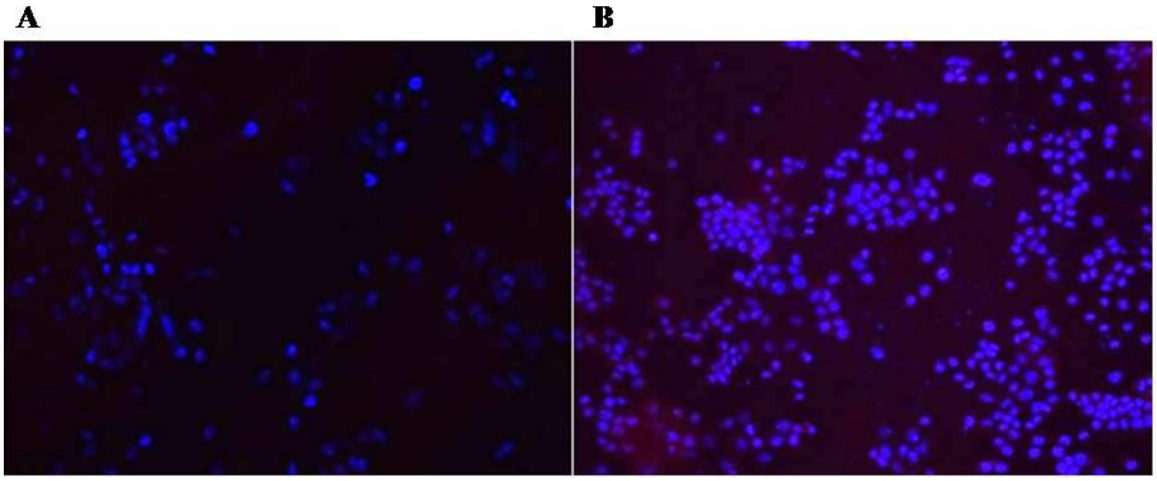

Figure 9. **A**. NCI-H460 non-transfected and stained with Hoechst dye (20x). **B**. NCI-H460 transfected with the empty pIRES-DsRED plasmid and stained with Hoechst dye (20x).

To ensure that stable cell lines retained the plasmid in their genomes it was performed a PCR and the PCR product was sequenced to check if no mutations occurred.

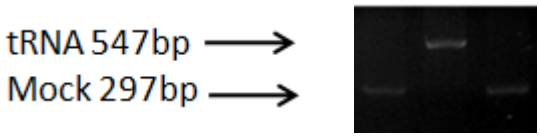

Figure 10. Results from pIRES-DsREd plasmid PCR amplification of BEAS-2B Mock, BEAS-tRNA^{Ser} and NCI-H460 Mock cells.

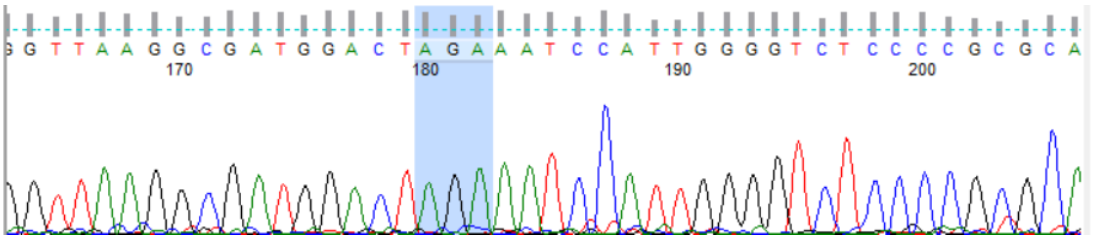

Figure 11. **Sequencing results from BEAS-2B tRNA^{Ser} cells** PCR products. In the highlighted zone is the tRNA^{Ser} anticodon.

Results from PCR (Figure 10) confirm the genome's integration of pIRES-DsRED plasmid containing the tRNA^{Ser} in BEAS-2B tRNA^{Ser} cell line and the empty pIRES-DsRED plasmid in BEAS-2B Mock cell line and NCI-H460 Mock cell line. Also, the results from sequencing (Figure 11) ensure the absence of mutations. Therefore, the cell line models were validated and the study proceeded.

3.2. Phenotypic Profilling

a. Cellular Viability

Cellular viability was assessed by determining the number of viable cells applying the Trypan Blue dye exclusion test. This test is based on the assumption that live cells have intact membranes that exclude particular dyes, such as trypan blue. So, nonviable cells present blue stained cytoplasm while viable cells have no staining.[102] The percentage (%) of viability resulted from the ratio between the number of live cells and the total number of cells and it is represented in Figure 12.

Cellular viability assay excluded the possibility of plasmid toxicity in the three cell lines since no differences were visible in their cellular viability.

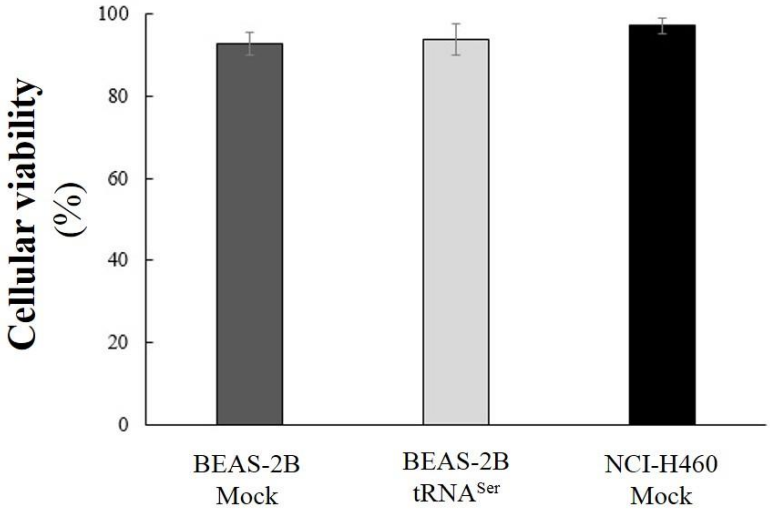

Figure 12. Effect of pIRES2-DsRED plasmid on **cell viability**. No differences are observed. Graphic represents mean ± SD of three independent experiments. Statistical analysis was performed using the One-Way ANOVA with Tukey's post-test ($p > 0.05$).

b. Cellular Proliferation

Cellular proliferation was accessed to verify if deregulation of tRNA pool promotes alterations in the proliferative capacity of BEAS-2B tRNA^{Ser} cells. To do so, cells from the three cell lines were counted in a Neubauer chamber excluding nonviable cells, according to the trypan blue exclusion principle. The first counting was done before their doubling, at 0h, and over the next three days: after 24h, 48h and 72h. Results are represented in Figure 13.

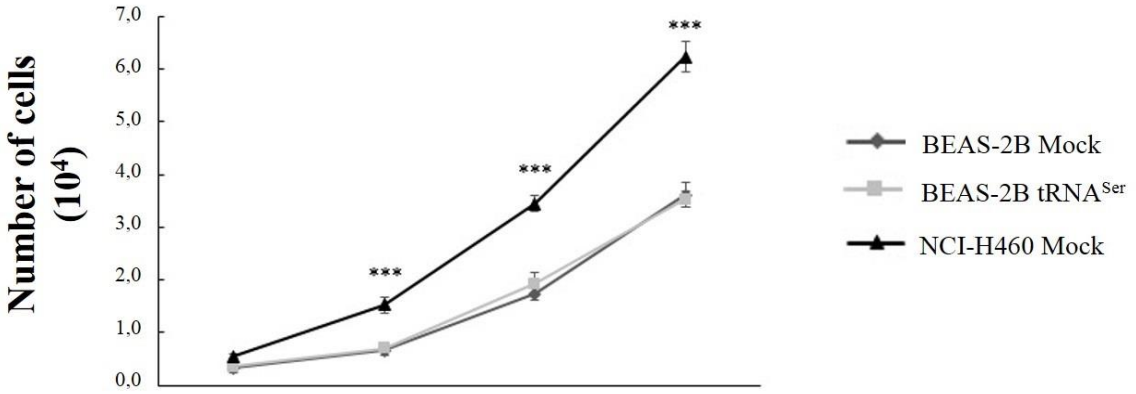

Figure 13. **Proliferation capacity** of the three cell lines. NCI-H460 Mock cell line has higher proliferation capacity than BEAS-2B tRNA^{Ser} cell line and the control. No differences are observed between BEAS-2B Mock and BEAS-2B tRNA^{Ser} cell lines. Graphic represents mean ± SEM of three independent experiments. Statistical analysis was performed using the Two-Way ANOVA with Tukey's post-test (***$p < 0.001$).

In normal cells the production and release of growth-promoting signals is tightly controlled so cells can enter and progress through the cell cycle in conditions that favor homeostasis. However, deregulation of growth and proliferation promoting signals is obvious in cancer cells, which leads to unregulated cell cycle divisions and aberrant cell proliferation.[66] In this context, results obtained through the proliferation assay show differences in NCI-H460 proliferative capacity when compared with BEAS-2B derived cell lines, as early as 24h. Proliferation promoting signals are related with other biological properties such as cell growth, firmly expressed by the bigger cell size, and the energy metabolism, which is typically altered.[66]

When comparing BEAS-2B tRNA^{Ser} cells to the control no differences are observed in their proliferative capacity. However, Pavon-Eternod *et al.* verified that induced overexpression of tRNA$_i^{Met}$ in normal breast cells was enough to prompt increase in proliferation capacity but overexpression of other tRNAs failed to do so.[86] Withal, the same research group verified that the different range of doubling times between normal and cancer breast cells has no correlation with mitochondrial and nuclear global tRNA content.[85]

3.3.Tranformation Ability

The anchorage-dependent colony formation assay was done to access the transformation ability of each cell line through their capacity to form colonies consisting in 50 cells, at least[103] (Figure 14).

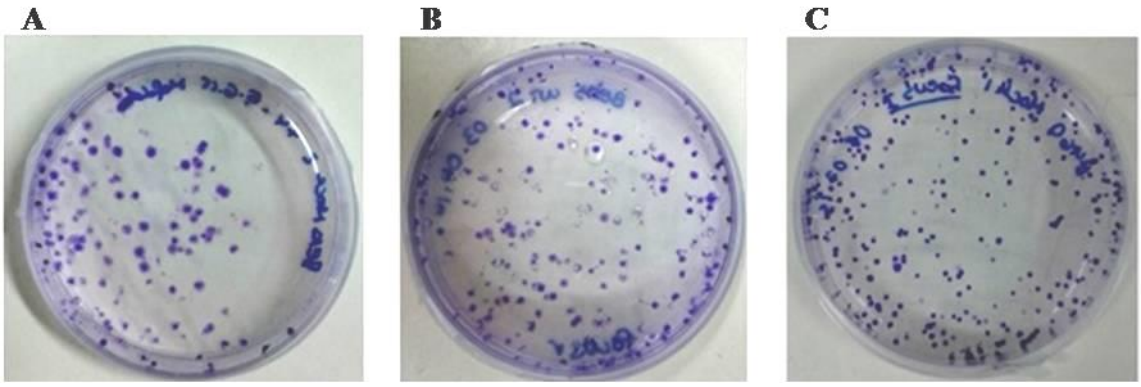

Figure 14. **Anchorage-dependent colony formation assay**. Cells were seeded at low density to assure their individualization and were maintained in culture for two weeks. Then colonies were fixed, stained and counted. **A**. BEAS-2B Mock cells; **B**. BEAS-2B tRNA^{Ser} cells; **C**. NCI-H460 Mock cells. Image represents results from one independent experiment.

This assay was performed to characterize the unlimited reproductive capacity of BEAS-2B tRNA^{Ser} cells and compare it to cancer cells colony formation capacity. Results are shown in Figure 15. A significant increase of transformation ability *in vitro* was visible in BEAS-2B tRNA^{Ser} cells with no statistical differences comparing with NCI-H460 Mock cells. This suggests that overexpressing tRNA^{Ser} is enough to prompt the acquisition of transformation ability *in vitro* in a level comparable with cancer cells. This represents further evidence for the hypothesis that deregulation of translational machinery can be a driving force for cellular transformation.[104]

Similarly, De Marco *et al.* observed that BEAS-2B cells carrying a mutation on AKT1 does not show alterations in proliferation capacity in complete medium but increased tumorigenic capacity demonstrated by higher transformation ability *in vitro* and induction of tumor formation *in vivo*.[105]

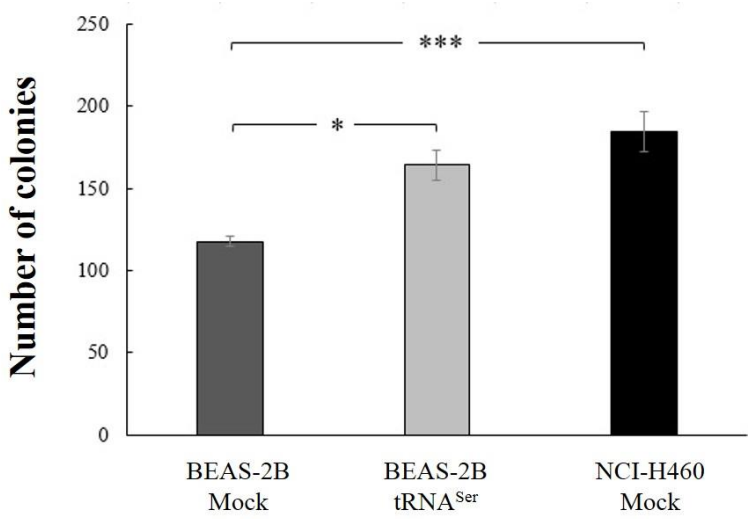

Figure 15. Evaluation of **transformation ability *in vitro***, based on the number of colonies. Both BEAS-2B $tRNA^{Ser}$ and NCI-H460 Mock cells showed higher tumorigenic capacity when compared with the control. No statistical significant differences were observed between BEAS-2B $tRNA^{Ser}$ cell line and NCI-H460 Mock cell line. Graphic represents mean ± SEM of four independent experiments. Statistical analysis was performed using the One-Way ANOVA with Tukey's post-test (*$p < 0.05$; ***$p < 0.001$).

The assay was carried out *in vitro* conditions that do not mimic *in situ* microenvironment, like cell-to-cell interactions, oxygen and nutrient availability and pH levels. Thus, it is not possible to ensure the *in vivo* behavior of these cells and so *in vivo* assays should be performed to evaluate the influence of tRNA pool deregulation to the acquisition of tumorigenic capacity.

3.4.Study of Proteotoxic Stress Induction and Activation of Protein Quality Control Pathways

Despite the protein quality control systems, errors still occur during protein synthesis, which can prompt proteotoxic stress resulting from the toxic character of aberrant proteins that became nonfunctional and aggregate.[49] Proteotoxic stress and quality control pathways activation were evaluated in this study by assessing chaperones availability, protein synthesis, activation of UPS system and insoluble protein fraction evaluation. These mechanisms were chosen based on previously results by co-workers indicating their alteration when facing proteotoxic stress conditions.

a. Expression of chaperones

The Western Blot assay was performed to assess the expression of Hsp90, Hsp70 and the small Hsp27 (Figure 16).

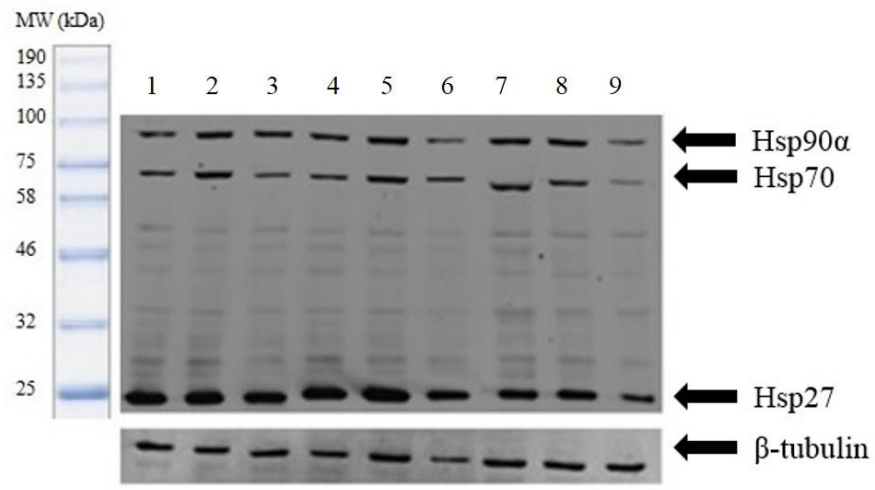

Figure 16. **Expression of Hsp90, Hsp70 and Hsp27**. β-tubulin represents the internal control. Total protein was extracted from BEAS-2B Mock cells (lanes 1, 2 and 3), BEAS-2B $tRNA^{Ser}$ (lanes 4, 5 and 6) and NCI-H460 Mock cells (lanes 7, 8 and 9). 10% polyacrylamide gels were loaded with 50µg of total protein. Image represents results from one independent experiment.

Surprisingly, the results of HSPs expression obtained from western blot analysis (Figure 17) do not agree with the "addiction to chaperones" hypothesis, which dictates that high levels of chaperones are required to stabilize the increased protein load containing aberrant

proteins, characteristic of cancer cells.[53] In our study, a downregulation of Hsp90α is clear in NCI-H460 Mock cells and a tendency is observed in BEAS-2B tRNA^{Ser} cells.

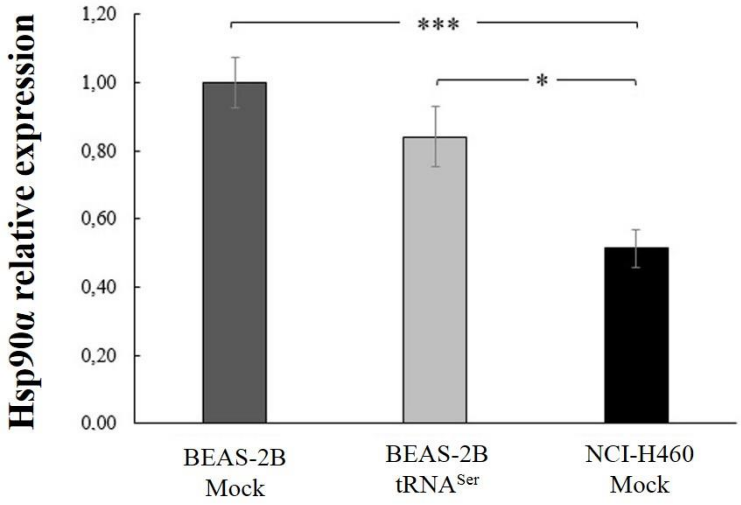

Figure 17. **Relative expression of Hsp90α**. β-tubulin was used as internal control and data was normalized to the control. Statistical analysis indicates decreased expression of Hsp90α in NCI-H460 Mock cells comparing with BEAS-2B Mock cells and with BEAS-2B tRNA^{Ser} cells. No differences in the expression of Hsp90α are observed between control and BEAS-2B tRNA^{Ser}. Graphic represents mean ± SEM of eight independent experiments. Statistical analysis was performed using the One-Way ANOVA with Tukey's post-test (*$p < 0.05$; ***$p < 0.001$).

Recently, Gallegos Ruiz *et al.* performed an integrated genome wide screening to analyze resected tumor samples from NSCLC patients and they described a deletion on chromosome 14. This deletion was presented in 44% of samples and correlated with overall survival, comparing with NSCLC patients with normal gene dosage at the same locus.[90] The study revealed that this deletion only affects the expression of *HSPAA1* and the consequent lower levels of Hsp90α seems to have a crucial role to promote sensitivity to therapeutics, probably derived from the more unstable status of oncoproteins when Hsp90α is expressed at lower levels.[90]

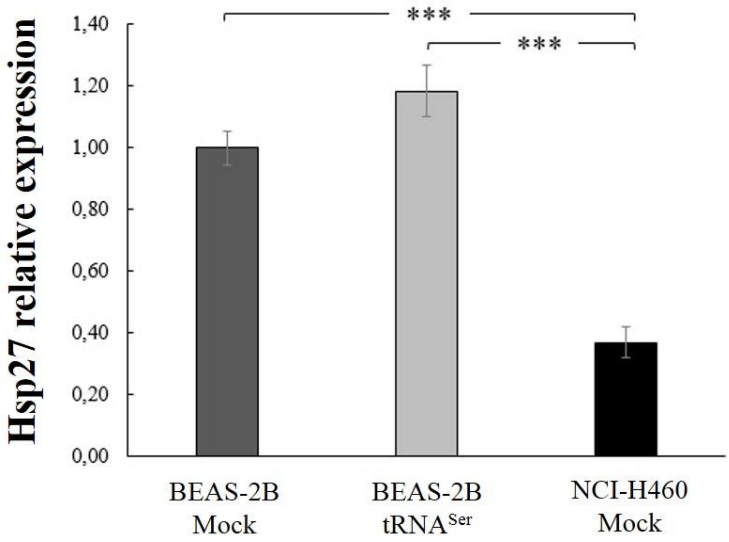

Figure 18. **Relative expression of Hsp70**. β-tubulin was used as internal control and data was normalized to the control. Statistical analysis indicates decreased expression of Hsp70 in NCI-H460 Mock cells comparing with control and BEAS-2B $tRNA^{Ser}$ cells. No differences are observed between control and BEAS-2B $tRNA^{Ser}$. Graphic represents mean ± SEM of three independent experiments. Statistical analysis was performed using the One-Way ANOVA with Tukey's post-test (*$p < 0.05$).

Results of Hsp70 expression also did not match the 'addiction to chaperones' hypothesis since it is observed a decreased relative expression of Hsp70 in NCI-H460 Mock cells in relation with control and BEAS-2B $tRNA^{Ser}$ cells (Figure 18).

Despite the contribution of Hsp70 to achieve the malignant phenotype, a protective role in lung cancer development is also supported by high levels of this chaperone. Overexpression of Hsp70/Hsc70 can sequester mutant p53 and reduce the inhibition of wild-type p53 due to association with mutant p53. In this way, p53 is free to perform its antiproliferative activity, suggesting that high levels of Hsp70 can be detrimental to maintenance of tumorigenesis and they can be related with survival advantage.[106,107] Note that mutations in *TP53* are present in 50% of NSCLC cancers.[108]

The results of Hsp27 relative expression are represented in Figure 19, demonstrating a clear decrease in the expression of this chaperone in NCI-H460 Mock cells.

Despite being normally overexpressed amongst different tumors[89], Huang Qi *et al.* did not observe differences in Hsp27 expression in tissue samples from patients with NSCLC, suggesting that the high levels of Hsp27 detected in other tumors are related with the different functions of Hsp27 in different cell types.[109] Alain Michils *et al.* did not observed differences in Hsp27 expression NSCLC samples as well, instead, they detected low levels

of Hsp27 in a small set of samples.[89] In another study, it was concluded that Hsp27 overexpression is correlated with a longer survival rate in tissues from NSCLC.[107]

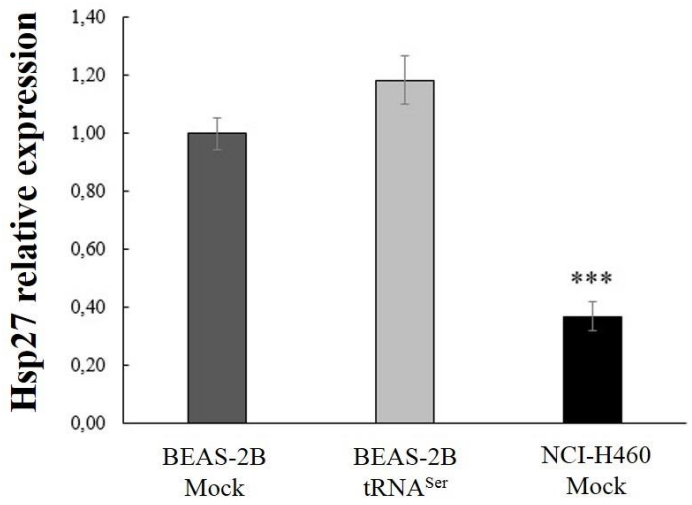

Figure 19. **Relative expression of Hsp27**. β-tubulin was used as internal control and data was normalized to the control. Statistical analysis indicates decreased expression of Hsp27 in NCI-H460 Mock cells comparing with control and BEAS-2B $tRNA^{Ser}$. No differences are observed between control and BEAS-2B $tRNA^{Ser}$. Graphic represents mean ± SEM of four independent experiments. Statistical analysis was performed using the One-Way ANOVA with Tukey's post-test (***$p < 0.001$).

However, even in cells from normal lung different HSP expression patterns are detected.[107] In a study performed by Marcel Bonay *et al.* it was observed that only a set of normal human lung cells were positive for Hsp90 and Hsp70, meaning that only a subset of cells in lung expresses high levels of HSPs. Also, they suggest that high levels of inducible Hsp70 and Hsp90 reflect the differentiated states of bronchial epithelial cells, since they are required to specific functions accordingly with the physiological state.[110]

Considering the dynamic expression of HSPs in the different types of normal and cancer cells and even in different physiological and differentiation states, other cell lines from normal lung and cancer lung tissues should be tested to better understand the behavior of HSPs in normal and lung cancer cells and in the presence of an inducible tRNA overexpression.

Regarding the cells in study, NCI-H460 cell line was obtained from pleural effusions of patients with large cell carcinoma, which is commonly located in the periphery of lung in the line of airways, while BEAS-2B cell line has its origin in bronchus. The different origins

of cells can also have influence in the unexpected results and derail the normalization with the control.

Still, it should be noted that in this study the total protein was obtained from cell cultures *in vitro.* The model *in vitro* abolishes the great influence of microenvironment of cancer cells, particularly the hypoxia, the low pH and nutrient availability, which are important sources of proteotoxic stress.[57]

b. Protein Synthesis Rate

Almost all types of stress prompt reduced translation at global levels as a strategy to decrease energy costs and production of proteins that could be prejudicial in the demand against the cellular stress. At the same time, synthesis of proteins that support cell survival under stress is favored.[23]

The Surface Sensing of Translation (SUnSET) method represents a strategy to evaluate the protein synthesis rate. It is based on the incorporation of puromycin, an analog of aminoacyl tRNAs, into nascent polypeptide chains, inhibiting its elongation. Thus, puromycin incorporation directly infers about *in vitro* translation rate.[111] Detection of puromycin was done by western blot and results are represented in Figure 20.

Results show that deregulation of tRNA pool does not promote alterations in the protein synthesis rate *in vitro*, but there is a clear increase in protein synthesis rate in NCI-H460 Mock cells.

The protein synthesis rate is closely related with the protein content, the DNA content and the cell size.[112] The tumorigenic process is accompanied by increased protein load related with overexpression of oncogenes and polyploidy.[53] Particularly, higher levels of anti-apoptotic and pro-mitotic proteins are common in cancer cells that are accompanied by overexpression of eIF2α.[113] Increased levels of this factor allows the cell to maintain the increased metabolism and to progress in the cell cycle. At the same time, higher rates of protein synthesis allows to outdo metabolic consequences of stress conditions intrinsic to cancer cells, as they are the environment stressors and free radicals production.[113] Thus, it should be interesting to quantify the eIF2α expression and its phosphorylation status to explore the mechanisms underlying the protein synthesis deregulation in NCI-H460 Mock cells.

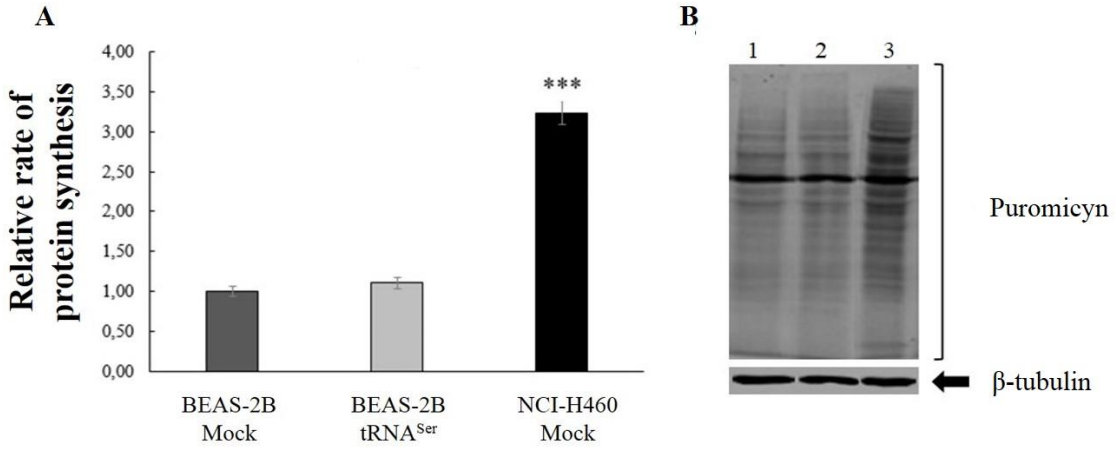

Figure 20. **A**. **Relative rate of protein synthesis.** β-tubulin was used as internal control and data was normalized to the control. Statistical analysis indicates increased relative rate of protein synthesis in NCI-H460 Mock cells compared with BEAS-2B Mock cells and BEAS-2B $tRNA^{Ser}$. No differences are observed between control and BEAS-$tRNA^{Ser}$ cells. Graphic represents mean ± SEM of four independent experiments. Statistical analysis was performed using the One-Way ANOVA with Tukey's post-test (***$p < 0.001$). **B**. **Expression of puromycin**. β-tubulin represents the internal control. Total protein was extracted from BEAS-2B Mock cells (lane 1), BEAS-2B $tRNA^{Ser}$ (lane 2) and NCI-H460 Mock cells (lane 3). 10% polyacrylamide gels were loaded with 100µg of total protein. Image represents results from one independent experiment.

c. Unfolded Protein Response Activation

The stress sensor BiP is the main player of the UPR since it recognizes and bind unfolded proteins during ER stress, aiming to restore its conformational structure. This leads to BiP dissociation from IRE1α, PERK and ATF6 which become activated and up-regulate genes that encode proteins involved in protein folding, insurance of its quality and ERAD activation.[57]

To assess the relative expression of BiP in the three cell lines it was performed a western blot assay (Figure 21).

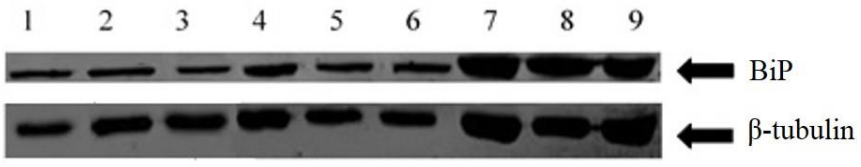

Figure 21. **Expression of BiP.** β-tubulin represents the internal control. Total protein was extracted from BEAS-2B Mock cells (lanes 1, 2 and 3), BEAS-2B $tRNA^{Ser}$ (lanes 4, 5 and 6) and NCI-H460 Mock cells (lanes 7, 8 and 9). 8% polyacrylamide gels were loaded with 60µg of total protein. Image represents results from one independent experiment.

Results show (Figure 22) that the induced overexpression of $tRNA^{Ser}$ prompt overexpression of BiP without differences compared to NCI-H460 Mock cells.

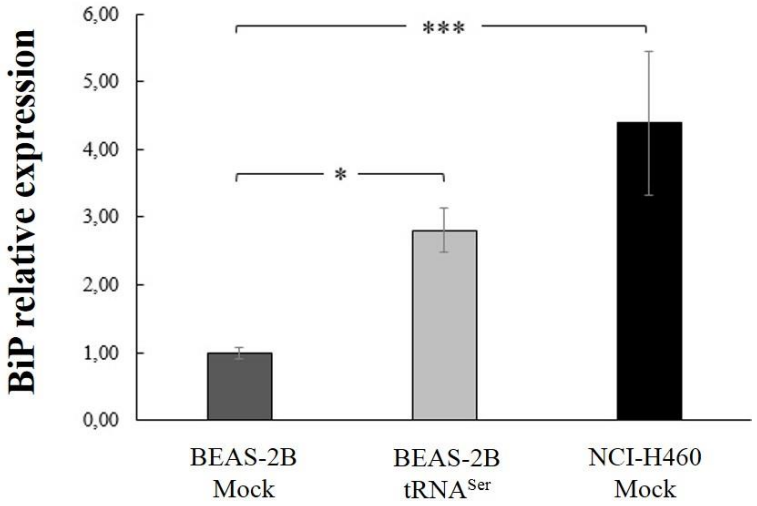

Figure 22. **Relative expression of BiP**. β-tubulin was used as internal control and data was normalized to the control. Statistical analysis indicates increased relative expression of BiP in BEAS-2B $tRNA^{Ser}$ and NCI-H460 Mock cells compared to the control. No differences are observed between BEAS-tRNASer and NCI-H460 Mock cells. Graphic represents mean ± SEM of five independent experiments. Statistical analysis was performed using the One-Way ANOVA with Tukey's post-test (*$p < 0.05$); ***$p < 0.001$).

Cancer cells are known to be under ER stress triggered by the particular features of the microenvironment. So, elevated BiP levels in cancer cells are required to activate pro-survival and cytoprotective responses to counteract this chronic stress. BiP may interact directly with apoptotic pathway intermediates and block caspase activation, leading to apoptosis inhibition and cell survival, being overexpressed in malignant forms of cancer such as lung cancer.[57,114] Likewise, *Qi Wang et al.* detected an overexpression of BiP in cancer lung tissues comparing with normal lung tissues, without differences between types of lung cancer despite their intrinsic morphological and molecular heterogeneity. Also, it was observed an increase in BiP expression correlated with the tumor stage, suggesting that elevated expression of BiP can be a feature of lung cancer which is correlated with its origin and progression.[115]

It seems that tRNA pool deregulation is enough to activate the UPR response. However, the activation of the different branches of UPR should be analysed to understand if the activation of UPR in BEAS-2B $tRNA^{Ser}$ occurs similarly to UPR activation and modulation in cancer cells.

d. Ubiquitin-Proteaseome System Activation

The UPS is an important system to retain the equilibrium between protein synthesis and protein destruction, controlling the turning over of proteins and maintaining the homeostasis.[57] The 26S proteasome is an ATP-dependent proteolytic complex consisting in two subunits, the 20S proteolytic core and the 19S ATP-dependent regulatory cap, which degrades polyubiquitinated polypeptide chains to ensure the elimination of damaged or no longer essential proteins.[101]

Ubiquitin is involved in the regulation of proteolysis as well as other biological functions, namely DNA repair, autophagy and signal transduction. The polyubiquitination of proteins, allows protein unfolding and degradation in the 26S proteasome.[116,117] The relative protein ubiquitination was assessed by western blot and results are shown in Figure 23.

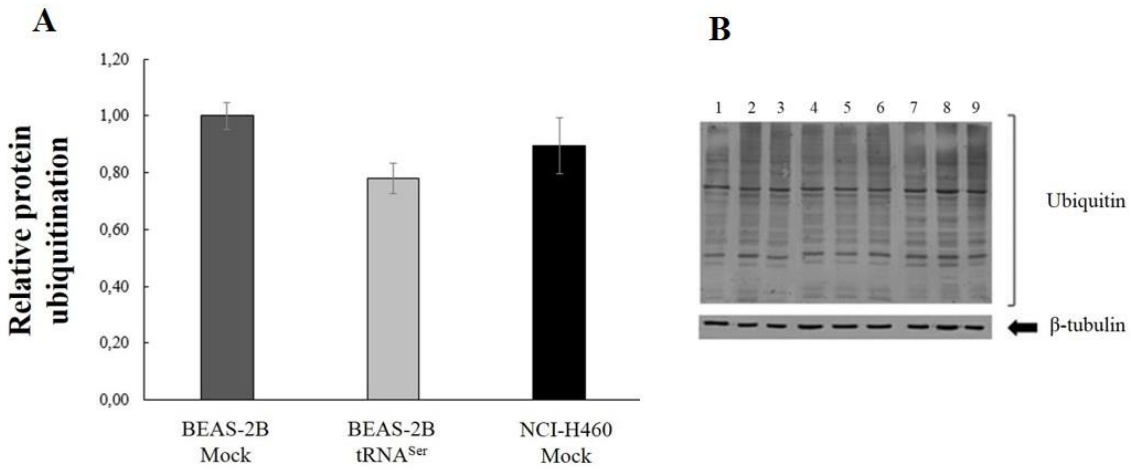

Figure 23. **A**. **Relative protein ubiquitination.** β-tubulin was used as internal control and data was normalized to the control. No differences are observed between control, BEAS-2B $tRNA^{Ser}$ cells and NCI-H460 Mock cells. Graphic represents mean ± SEM of five independent experiments. Statistical analysis was performed using the One-Way ANOVA with Tukey's post-test. **B**. **Expression of ubiquitin.** β-tubulin represents the internal control. Total protein was extracted from BEAS-2B Mock cells (lanes 1, 2 and 3), BEAS-2B $tRNA^{Ser}$ (lanes 4, 5 and 6) and NCI-H460 Mock cells (lanes 7, 8 and 9). 10% polyacrylamide gels were loaded with 50µg of total protein. Image represents results from one independent experiment.

Results showed no differences in the levels of polyubiquitinated proteins among the three cell lines, but apparently proteins with higher molecular size are more ubiquitinated, as we can see in Figure 23 B.

Alain Michils *et al.*, in a comparative study between cell lysates from lung carcinomas and cell lysates from non-cancerous tissues, also verify that no differences exist in the

expression of ubiquitin between the samples.[89] Considering its involvement in basic cellular processes whose perturbation leads to malignant transformation, these results were not expected.[89]

Proteasome activity was determined by measuring the intensity of fluorescence derived from the cleavage of a labeled peptide (Suc-LLVY-AMC), a substrate for enzymes with chymotrypsin-like activity[101] and results are represented in Figure 24.

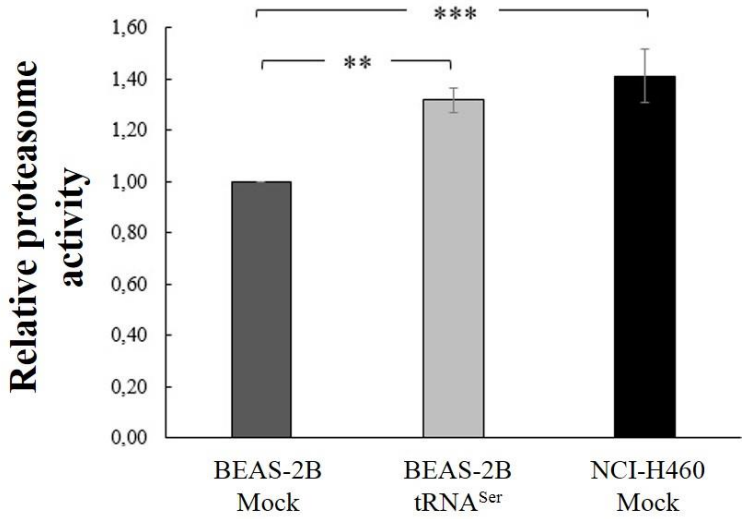

Figure 24. **Relative proteasome activity.** β-tubulin was used as internal control and data was normalized to the control. Statistical analysis indicate increase in the relative proteasome activity in BEAS-2B $tRNA^{Ser}$ cells compared with the control as well as in NCI-H460 Mock cells. No differences are observed between BEAS-2B $tRNA^{Ser}$ cells and NCI-H460 Mock cells. Graphic represents mean ± SEM of seven independent experiments. Statistical analysis was performed using the One-Way ANOVA with Tukey's post-test (**$p < 0.01$; ***$p < 0.001$).

Results show that deregulation of tRNA pool through the expression of a single tRNA boost the activity of proteasome at levels similar to that observed in NCI-H460 Mock cells.

UPS is the major eukaryotic proteolytic pathway and it is responsible for eliminate most of the soluble misfolded proteins.[46] Upregulation of UPS system is evident in cancer cells as a strategy to reduce the accumulation of proteins and so to evade apoptosis. Also, proteasome is responsible for degradation of cell cycle regulatory proteins, allowing the cells to bypass cell cycle checkpoints. Inhibition of 26S proteasome activity has been study as a therapeutic in lung cancer.[118,119]

e. Insoluble protein fraction

To verify if alterations exist in protein insoluble profiles, we analyzed insoluble protein fractions by SDS-PAGE (Figure 25).

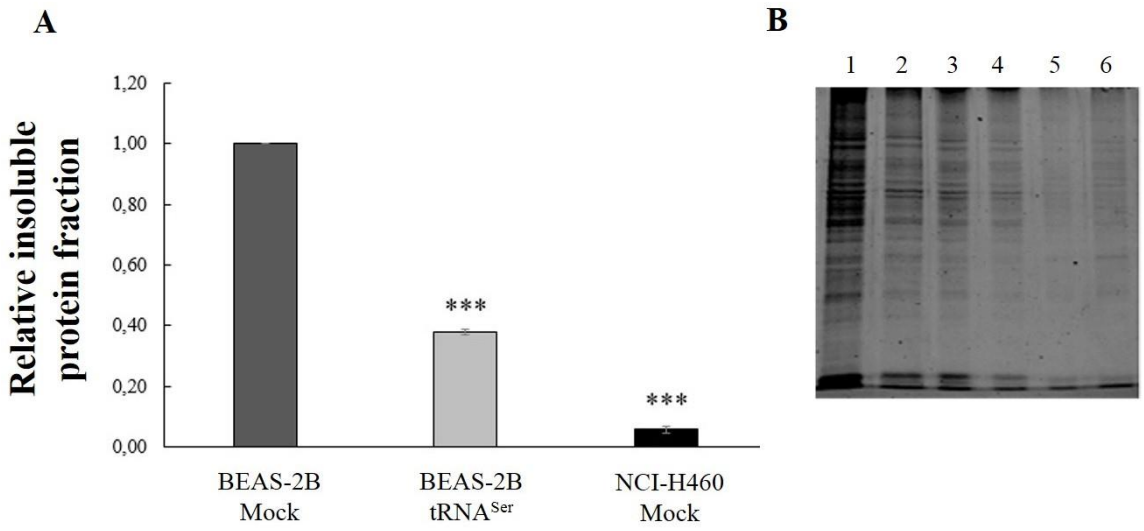

Figure 25. **A**. **Relative insoluble protein expression**. β-tubulin was used as internal control and data was normalized to the control. Statistical analysis indicates decrease of relative insoluble protein fraction in BEAS-2B $tRNA^{Ser}$ cells and in NCI-H460 Mock cells. Graphic represents mean ± SEM of three independent experiments. Statistical analysis was performed using the One-Way ANOVA with Tukey's post-test (***$p < 0.001$). **B**. **Expression of insoluble protein fraction** obtained through SDS-PAGE. Insoluble protein fraction was extracted from BEAS-2B Mock cells (lanes 1 and 2), BEAS-2B $tRNA^{Ser}$ cells (lanes 3 and 4) and NCI-H460 Mock cells (lanes 5 and 6). 10% polyacrylamide gels were loaded with 20µl of insoluble protein fraction. Image represents results from one independent experiment.

Results show a clear decline of the insoluble protein fraction both in BEAS-2B $tRNA^{Ser}$ cells and NCI-H460 Mock cells, suggesting that induced $tRNA^{Ser}$ overexpression leads to alterations in protein expression profiles. Probably, these alterations are advantageous to the acquisition of the malignant phenotype, since it is visible that BEAS-2B $tRNA^{Ser}$ cells adopted an intermediate phenotype.

Cancer cells have quantitative and qualitative alterations in protein expression, with a preferential expression of key proteins in tumor progression and development, such as growth factors, cell-cycle promoters and oncoproteins, particularly c-Myc and VEGF, the last known to be upregulated in NSCLC tumors.[76,104] This alterations in insoluble protein expression in BEAS-2B $tRNA^{Ser}$ and in NCI-H460 Mock cells can be associated with those alterations in insoluble protein expression due to deregulation of tRNA pool.

X. Discussion

Differential expression of tRNAs may represent a mechanism of translational control through the codon usage of specific genes.[85,120] Between human tissues there are differences in individual tRNA expression correlated with the codon usage of highly-expressed tissue specific genes.[85] The deregulation of tRNA pool and mutations in tRNA genes are associated with human diseases.[121] Also, deregulation of transcriptional machinery is common in cancer cells and it has been proposed as a trigger for the acquisition of the malignant phenotype.[84] Elevated levels of tRNAs have already been documented in breast cancer in a specific fashion since there is a preferential overexpression of tRNAs accordingly with the chemical properties of their cognate amino acids.[85]

To date, data about the effects of tRNA overexpression and how cells respond to it are very limited. In this work, a model to study the effects of $tRNA^{Ser}$ overexpression in BEAS-2B cells was successfully generated, allowing a comparative analysis between effects derived from $tRNA^{Ser}$ overexpression and the acquisition of a malignant phenotype *in vitro*. BEAS-2B cell line and NCI-H460 cell line were already used to infer about the acquisition of malignant features by other researchers.[122]

However, it should be noted that the profile of tRNA pool in cells with induced tRNA overexpression is dependent on different factors, such as tRNA identity, cells' genetic background and the site of integration in the genome.[86] Also, it is still unknown the role of individual tRNAs in different cell types and their effect in the transcriptome and the cellular physiology and how they are affected by these two factors.[11]

In general, cells with overexpression of $tRNA^{Ser}$ seem to acquire an intermediate behavior between control and cancer cells. The transformation ability of cells with induced tRNA overexpression is equivalent to that observed in NCI-H460 Mock cells which suggests the acquisition of tumorigenic features.

A study performed by Stoletzki and Eyre-Walke, provided evidences that codon usage in *E. Coli* is adapted to highly expressed genes to reduce the energy costs derived from missense errors that can lead to non- or misfunctional proteins production.[123] In multicellular eukaryotes the quantification of gene expression and tRNA abundance are difficult due to their variation between tissues and developmental stages.[124] However, it was observed a

positive correlation for the adaptation of codon usage to higher expressed genes, supporting the hypothesis that the equilibrium between tRNA pool and codon usage may increase translation accuracy and efficiency in a demand to reduce mistranslation.[124–126] Thus, we cannot exclude the possibility of misfolded protein synthesis derived from tRNA pool perturbation by overexpression of $tRNA^{Ser}$.

Results from relative expression of BiP and proteasome activity suggest that UPR and UPS quality control pathways were activated in response to proteome instability in BEAS-2B $tRNA^{Ser}$. Since no alteration in size, proliferation capacity and in protein synthesis rate are observed, contrarily to NCI-H460 Mock cells, it seems that overexpression of $tRNA^{Ser}$ does not trigger increase in protein load, but it rather affects proteins that are being produced as well as translation speed and accuracy of those proteins. The increase in proteasome activity to similar levels to those observed in NCI-H460 Mock cells, suggest an increasing demand to eliminate aberrant proteins. Therefore, we can conclude that tRNA pool deregulation prompts activation of UPR and UPS similarly to NCI-H460 Mock cells. In cancer cells the activation of these pathways is chronic and cancer cells can adapt to it and use to their advantage the cytoprotective benefits of its activation to survive and progress.[57]

The analysis of insoluble protein fractions indicates a progressive reduction of insoluble proteins from control cells to NCI-H460 Mock cells, with BEAS-2B $tRNA^{Ser}$ expressing an intermediate phenotype. This reduction in the insoluble protein content can be explained by alterations in gene expression profiles but also by a reduction in protein aggregates, whose toxic character is incompatible to the higher metabolism of cancer cells, which eliminates them by upregulating the autophagy.[127]

XI. Conclusion and Future Work Suggestions

Is tRNA pool deregulation a driven force or a by-product of malignant transformation? The question remains unanswered. However, we can conclude that tRNA pool deregulation by a unique tRNA overexpression is enough to prompt the acquisition of an intermediated behavior suggestive of progressive acquisition of the malignant phenotype. The activation of protein quality control pathways show that $tRNA^{Ser}$ overexpression suggests interferences in the stability of the proteome but more studies should be performed to confirm and unveil its origin, namely through mass spectrometry.

To better understand the mechanism of UPR activation it should be quantified the activation of IRE1α, PERK and ATF6 branches by western blot. Since autophagy is essential for cancer cells to eliminate the protein aggregates derived from highly metabolism, this could represent another phenotypic trait to evaluate BEAS-2B $tRNA^{Ser}$ cells in the acquisition of malignancy, and it could be assessed by western blotting or flow cytometry analysis.

Considering the evidences that cancer cells express higher levels of tRNAs and that induction of an unique tRNA isoacceptor leads to other tRNAs overexpression[86], through the tRNA microarray technology we could confirm the $tRNA^{Ser}$ overexpression in BEAS-2B $tRNA^{Ser}$ cell line and assess other perturbations in the tRNA pool. Likewise, patters of tRNA pool in NCI-H460 Mock cell line would be obtained, allowing to perform a correlation with the tRNA patterns in BEAS-2B $tRNA^{Ser}$ cells. Besides, the application of cDNA microarray technology would be useful to confirm alterations in gene expression patterns in BEAS-2B $tRNA^{Ser}$ cells and to establish a correlation with gene expression profiles of NCI-H460 Mock cells. Thereby, a correlation between tRNA patterns and the codon usage of specific genes in BEAS-2B $tRNA^{Ser}$ would be possible and we could understand if tRNA pool deregulation is a trigger to preferential expression of cancer-related genes.

XII. References

1. Crick, F. H. The Origin of the Genetic Code. *J. Mol. Biol* **38,** 367–379 (1968).

2. Reynolds, N. M., Lazazzera, B. a & Ibba, M. Cellular mechanisms that control mistranslation. *Nat. Rev. Microbiol.* **8,** 849–56 (2010).

3. Agris, P. F. Decoding the genome: a modified view. *Nucleic Acids Res.* **32,** 223–38 (2004).

4. Chavatte, L., Kervestin, S., Favre, A. & Jean-Jean, O. Stop codon selection in eukaryotic translation termination: Comparison of the discriminating potential between human and ciliate eRF1s. *EMBO J.* **22,** 1644–1653 (2003).

5. Mitarai, N. & Pedersen, S. Control of ribosome traffic by position-dependent choice of synonymous codons. *Phys. Biol.* **10,** 056011 (2013).

6. Knight, R. D., Freeland, S. J. & Landweber, L. F. Rewiring the keyboard: evolvability of the genetic code. *Nat. Rev. Genet.* **2,** 49–58 (2001).

7. Grosjean, H., de Crécy-Lagard, V. & Marck, C. Deciphering synonymous codons in the three domains of life: Co-evolution with specific tRNA modification enzymes. *FEBS Lett.* **584,** 252–264 (2010).

8. Agris, P. F., Vendeix, F. a P. & Graham, W. D. tRNA's Wobble Decoding of the Genome: 40 Years of Modification. *J. Mol. Biol.* **366,** 1–13 (2007).

9. Novoa, E. M. & Ribas de Pouplana, L. Speeding with control: Codon usage, tRNAs, and ribosomes. *Trends Genet.* **28,** 574–581 (2012).

10. Plotkin, J. B. & Kudla, G. Synonymous but not the same: the causes and consequences of codon bias. *Nat. Rev. Genet.* **12,** 32–42 (2011).

11. Gingold, H. *et al.* A Dual Program for Translation Regulation in Cellular Proliferation and Differentiation. *Cell* **158,** 1281–1292 (2014).

12. Gingold, H. & Pilpel, Y. Determinants of translation efficiency and accuracy. *Mol. Syst. Biol.* **7,** 481 (2011).

13. Sørensen, M. a, Kurland, C. G. & Pedersen, S. Codon usage determines translation rate in Escherichia coli. *J. Mol. Biol.* **207,** 365–377 (1989).

14. Kudla, G., Murray, a. W., Tollervey, D. & Plotkin, J. B. Coding-Sequence Determinants of Gene Expression in Escherichia coli. *Science (80-.).* **324,** 255–258 (2009).

15. Gingold, H., Dahan, O. & Pilpel, Y. Dynamic changes in translational efficiency are deduced from codon usage of the transcriptome. *Nucleic Acids Res.* **40,** 10053–10063 (2012).

16. Lewin, B. *Genes VIII*. (Pearson Prentice Hall, 2004).

17. Alberts, B. *et al. Molecular Biology of The Cell*. (Garland Science, 2008).

18. Holcik, M., Sonenberg, N. & Korneluk, R. G. Internal ribosome initiation of translation and the control of cell death. *Trends Genet.* **16,** 469–473 (2000).

19. Malys, N. & McCarthy, J. E. G. Translation initiation: Variations in the mechanism can be anticipated. *Cell. Mol. Life Sci.* **68,** 991–1003 (2011).

20. Jackson, R. J., Hellen, C. U. T. & Pestova, T. V. The mechanism of eukaryotic translation initiation and principles of its regulation. *Nat. Rev. Mol. Cell Biol.* **11,** 113–127 (2010).

21. Kapp, L. D. & Lorsch, J. R. The molecular mechanics of eukaryotic translation. *Annu. Rev. Biochem.* **73,** 657–704 (2004).

22. Sonenberg, N. & Hinnebusch, A. G. Regulation of Translation Initiation in Eukaryotes: Mechanisms and Biological Targets. *Cell* **136,** 731–745 (2009).

23. Holcik, M. & Sonenberg, N. Translational control in stress and apoptosis. *Nat. Rev. Mol. Cell Biol.* **6,** 318–27 (2005).

24. Komar, A. a. & Hatzoglou, M. Cellular IRES-mediated translation: The war of ITAFs in pathophysiological states. *Cell Cycle* **10,** 229–240 (2011).

25. Martínez-Salas, E., Piñeiro, D. & Fernández, N. Alternative Mechanisms to Initiate Translation in Eukaryotic mRNAs. *Comp. Funct. Genomics* **2012,** 1–12 (2012).

26. Rodnina, M. V & Wintermeyer, W. Fidelity of Aminoacyl-tRNA Selection on the Ribosome: Kinetic and Structual Mechanisms. *Annu. Rev. Biochem.* **70,** 415–435 (2001).

27. Dever, T. E. & Green, R. The elongation, Termination, and Recycling Phases of Translation in Eukaryotes. *Cold Spring Harb Perspect Biol* **4,** (2012).

28. Kisselev, L., Ehrenberg, M. & Frolova, L. Termination of translation: interplay of mRNA, rRNA and release factors? *EMBO J.* **22,** 175–182 (2003).

29. Gebetsberger, J. & Polacek, N. Slicing tRNAs to boost functional ncRNA diversity. *RNA Biol.* **10,** 1798–806 (2013).

30. Giegé, R. Toward a more complete view of tRNA biology. *Nat. Struct. Mol. Biol.* **15,** 1007–1014 (2008).

31. Raina, M. & Ibba, M. tRNAs as regulators of biological processes. *Front. Genet.* **5,** 171 (2014).

32. Giegé, R. *et al.* Structure of transfer RNAs: Similarity and variability. *Wiley Interdiscip. Rev. RNA* **3,** 37–61 (2012).

33. Nakanishi, K. & Nureki, O. Recent progress of structural biology of tRNA processing and modification. *Mol. Cells* **19,** 157–166 (2005).

34. Phizicky, E. M. & Hopper, A. K. tRNA biology charges to the front. *Genes Dev.* **24,** 1832–1860 (2010).

35. Shepherd, J. & Ibba, M. Lipid II-independent trans editing of mischarged tRNAs by the penicillin resistance factor MurM. *J. Biol. Chem.* **288,** 25915–25923 (2013).

36. Shepherd, J. & Ibba, M. Direction of aminoacylated transfer RNAs into antibiotic synthesis and peptidoglycan-mediated antibiotic resistance. *FBES Lett.* **587,** 2895–2904 (2013).

37. Sobala, A. & Hutvagner, G. Small RNAs derived from the 5 ' end of tRNAs can inhibit protein translation in human cells. *RNA Biol.* **10,** 553–563 (2013).

38. Haussecker, D. *et al.* Human tRNA-derived small RNAs in the global regulation of RNA silencing. *Spring* **16,** 673–695 (2010).

39. Ibba, M. & Söll, D. Aminoacyl-tRNA synthesis. *Annu. Rev. Biochem.* **69,** 617–650 (2000).

40. Schimmel, P. Development of tRNA synthetases and connection to genetic code and disease. *Protein Sci.* **17,** 1643–1652 (2008).

41. Ling, J., Reynolds, N. & Ibba, M. Aminoacyl-tRNA synthesis and translational quality control. *Annu. Rev. Microbiol.* **63,** 61–78 (2009).

42. Ahel, I., Korencic, D., Ibba, M. & Söll, D. Trans-editing of mischarged tRNAs. *Proc. Natl. Acad. Sci. U. S. A.* **100,** 15422–15427 (2003).

43. Van Anken, E. & Braakman, I. Versatility of the endoplasmic reticulum protein folding factory. *Crit. Rev. Biochem. Mol. Biol.* **40,** 191–228 (2005).

44. Morimoto, R. Proteotoxic stress and inducible chaperone networks in neurodegenerative disease and aging. *Genes Dev.* 1427–1438 (2008). doi:10.1101/gad.1657108.GENES

45. Schröder, M. & Kaufman, R. J. ER stress and the unfolded protein response. *Mutat. Res.* **569,** 29–63 (2005).

46. Chen, B., Retzlaff, M., Roos, T. & Frydman, J. Cellular strategies of protein quality control. *Cold Spring Harb. Perspect. Biol.* **3,** 1–14 (2011).

47. Bukau, B., Weissman, J. & Horwich, A. Molecular chaperones and protein quality control. *Cell* **125,** 443–51 (2006).

48. Paredes, J., Carreto, L. & Simões, J. Low level genome mistranslations deregulate the transcriptome and translatome and generate proteotoxic stress in yeast. *BMC Biol* **10,** 55 (2012).

49. Gregersen, N., Bross, P., Vang, S. & Christensen, J. H. Protein misfolding and human disease. *Annu. Rev. Genomics Hum. Genet.* **7,** 103–24 (2006).

50. Lipatova, Z. & Segev, N. A Role for Macro-ER-Phagy in ER Quality Control. *PLOS Genet.* **11,** (2015).

51. Ellis, R. J. Molecular chaperones: assisting assembly in addition to folding. *Trends Biochem. Sci.* **31,** 395–401 (2006).

52. Calderwood, S. K. *et al.* Signal Transduction Pathways Leading to Heat Shock Transcription. *Sign. Transduct. Insights* **2,** 13–24 (2010).

53. Ciocca, D. R., Arrigo, A. P. & Calderwood, S. K. Heat shock proteins and heat shock factor 1 in carcinogenesis and tumor development: an update. *Arch. Toxicol.* **87,** 19–48 (2013).

54. Calderwood, S. K., Khaleque, M. A., Sawyer, D. B. & Ciocca, D. R. Heat shock proteins in cancer: Chaperones of tumorigenesis. *Trends Biochem. Sci.* **31,** 164–172 (2006).

55. Schröder, M. & Kaufman, R. J. The mammalian unfolded protein response. *Annu. Rev. Biochem.* **74,** 739–789 (2005).

56. Korennykh, A. & Walter, P. Structural Basis of the Unfolded Protein Response. *Annu. Rev. Cell Dev. Biol.* **28,** 251–277 (2012).

57. Wang, W.-A., Groenendyk, J. & Michalak, M. Endoplasmic reticulum stress associated responses in cancer. *Biochim. Biophys. Acta* **1843,** 2143–9 (2014).

58. Olzmann, J. A., Kopito, R. R. & Christianson, J. C. The Mammalian Endoplasmic Reticulum-Associated Degradation System. *Cold Spring Harb Perspect Biol* **5,** (2013).

59. Glick, D., Barth, S. & Macleod, K. F. Autophagy : cellular and molecular mechanisms. *J Pathol.* **221,** 3–12 (2010).

60. Vembar, S. S. & Brodsky, J. L. One step at a time: endoplasmic reticulum-associated degradation. *Nat. Rev. Mol. Cell Biol.* **9,** 944–957 (2008).

61. Klionsky, D. J. The molecular machinery of autophagy: unanswered questions. *J. Cell Sci.* **118,** 7–18 (2005).

62. Visvader, J. E. Cells of origin in cancer. *Nature* **469,** 314–322 (2011).

63. Scholzová, E., Malík, R., Sevcík, J. & Kleibl, Z. RNA regulation and cancer development. *Cancer Lett.* **246,** 12–23 (2007).

64. Michor, F. & Polyak, K. The origins and implications of intratumor heterogeneity. *Cancer Prev. Res.* **3,** 1361–1364 (2010).

65. Marusyk, A. & Polyak, K. Tumor heterogeneity: Causes and consequences. *Biochim. Biophys. Acta - Rev. Cancer* **1805,** 105–117 (2010).

66. Hanahan, D. & Weinberg, R. a. Hallmarks of cancer: the next generation. *Cell* **144,** 646–74 (2011).

67. Burkhart, D. L. & Sage, J. Cellular mechanisms of tumour suppression by the retinoblastoma gene. *Nat. Rev. Cancer* **8,** 671–682 (2008).

68. Junttila, M. R. & Evan, G. I. p53--a Jack of all trades but master of none. *Nat. Rev. Cancer* **9,** 821–829 (2009).

69. Muller, P. A. J. & Vousden, K. H. P53 muations in cancer. *Nat. Cell Biol.* **15,** 2–8 (2013).

70. Chew, V., Toh, H. C. & Abastado, J. P. Immune microenvironment in tumor progression: Characteristics and challenges for therapy. *J. Oncol.* **2012,** (2012).

71. Ferlay, J. *et al.* Cancer incidence and mortality worldwide : Sources , methods and major patterns in GLOBOCAN 2012. **386,** (2015).

72. Alberg, A. J., Brock, M. V, Ford, J. G., Samet, J. M. & Spivack, S. D. Epidemiology of lung cancer: Diagnosis and management of lung cancer, 3rd ed: American College of Chest Physicians evidence-based clinical practice guidelines. *Chest* **143,** e1S–29S (2013).

73. Jemal, A., Center, M. M., DeSantis, C. & Ward, E. M. Global patterns of cancer incidence and mortality rates and trends. *Cancer Epidemiol. Biomarkers Prev.* **19,** 1893–907 (2010).

74. Molina, J. R., Yang, P., Cassivi, S. D., Schild, S. E. & Adjei, A. a. Non-small cell lung cancer: epidemiology, risk factors, treatment, and survivorship. *Mayo Clin. Proc.* **83,** 584–594 (2008).

75. Cersosimo, R. J. Lung cancer: A review. *Am. J. Heal. Pharm.* **59,** 611–642 (2002).

76. Raparia, K., Villa, C., DeCamp, M. M., Patel, J. D. & Mehta, M. P. Molecular profiling in non-small cell lung cancer: a step toward personalized medicine. *Arch. Pathol. Lab. Med.* **137,** 481–91 (2013).

77. Garber, M. E. *et al.* Diversity of gene expression in adenocarcinoma of the lung. *Proc. Natl. Acad. Sci. U. S. A.* **98,** 13784–13789 (2001).

78. Trigka, E. A. *et al.* A detailed immunohistochemical analysis of the PI3K/AKT/mTOR pathway in lung cancer: correlation with PIK3CA, AKT1, K-RAS or PTEN mutational status and clinicopathological features. *Oncol. Rep.* **30,** 623–36 (2013).

79. Mello, R. A. De. Epidermal growth factor receptor and K-Ras in non-small cell lung cancer-molecular pathways involved and targeted therapies. *World J. Clin. Oncol.* **2,** 367 (2011).

80. Aviel-Ronen, S., Blackhall, F. H., Shepherd, F. a & Tsao, M.-S. K-ras mutations in non-small-cell lung carcinoma: a review. *Clin. Lung Cancer* **8,** 30–38 (2006).

81. Nakamura, Y. *et al.* c-Met activation in lung adenocarcinoma tissues: An immunohistochemical analysis. *Cancer Sci.* **98,** 1006–1013 (2007).

82. Agarwal, S. *et al.* Association of constitutively activated hepatocyte growth factor receptor (Met) with resistance to a dual EGFR/Her2 inhibitor in non-small-cell lung cancer cells. *Br. J. Cancer* **100,** 941–949 (2009).

83. Harris, A. *et al.* Anaplastic Lymphoma Kinase Inhibition in Non–Small-Cell Lung Cancer. *N Engl J Med* **363,** 609–619 (2010).

84. Ruggero, D. & Pandolfi, P. P. Does the ribosome translate cancer? *Nat. Rev. Cancer* **3,** 179–192 (2003).

85. Pavon-Eternod, M. *et al.* tRNA over-expression in breast cancer and functional consequences. *Nucleic Acids Res.* **37,** 7268–80 (2009).

86. Pavon-Eternod, M., Gomes, S., Rosner, M. R. & Pan, T. Overexpression of initiator methionine tRNA leads to global reprogramming of tRNA expression and increased proliferation in human epithelial cells. *RNA* **19,** 461–6 (2013).

87. Mitani, S. *et al.* Analysis of c-myc DNA amplification in non-small cell lung carcinoma in comparison with small cell lung carcinoma using polymerase chain reaction. *Clin. Exp. Med.* **1,** 105–111 (2001).

88. Wang, H., Tan, M.-S., Lu, R.-C., Yu, J.-T. & Tan, L. Heat shock proteins at the crossroads between cancer and Alzheimer's disease. *Biomed Res. Int.* **2014,** 239164 (2014).

89. Michils, a *et al.* Increased expression of high but not low molecular weight heat shock proteins in resectable lung carcinoma. *Lung Cancer* **33,** 59–67 (2001).

90. Gallegos Ruiz, M. I. *et al.* Integration of gene dosage and gene expression in non-small cell lung cancer, identification of HSP90 as potential target. *PLoS One* **3,** e0001722 (2008).

91. Koumenis, C. ER stress, hypoxia tolerance and tumor progression. *Curr. Mol. Med.* **6,** 55–69 (2006).

92. Wang, S. & Kaufman, R. J. The impact of the unfolded protein response on human disease. *J. Cell Biol.* **197,** 857–867 (2012).

93. Hetz, C., Chevet, E. & Harding, H. P. Targeting the unfolded protein response in disease. *Nat. Rev. Drug Discov.* **12,** 703–19 (2013).

94. Fan, C. F., Miao, Y., Lin, X. Y., Zhang, D. & Wang, E. H. Expression of a phosphorylated form of ATF4 in lung and non-small cell lung cancer tissues. *Tumor Biol.* **35,** 765–771 (2014).

95. Yoshizawa, A. *et al.* Overexpression of phospho-eIF4E is associated with survival through AKT pathway in non-small cell lung cancer. *Clin Cancer Res;* **16,** 240–248 (2010).

96. Valle, C. W. *et al.* Critical role of VCP/p97 in the pathogenesis and progression of non-small cell lung carcinoma. *PLoS One* **6,** 1–12 (2011).

97. Yang, Z. & Klionsky, D. J. Eaten alive: a history of macroautophagy. *Nat. Cell Biol.* **12,** 814–822 (2010).

98. Rapley, R. *Principles and Techniques of Biochemistry and Molecular Biology*. *Saudi Med J* **33,** (Cambridge University Press 2010, 2012).

99. Al-Dosari, M. S. & Gao, X. Nonviral Gene Delivery: Principle, Limitations, and Recent Progress. *AAPS J.* **11,** 671–681 (2009).

100. Walker, J. M. *The Protein Protocols Handbook*. (Humana Press, 2009). doi:10.1007/978-1-59745-198-7

101. Kisselev, A. F. & Goldberg, A. L. Monitoring activity and inhibition of 26S proteasomes with fluorogenic peptide substrates. *Methods Enzymol.* **398,** 364–378 (2005).

102. Strober, W. Trypan blue exclusion test of cell viability. *Curr. Protoc. Immunol.* **Appendix,** A.3B.1–A.3B.2 (2001).

103. Brown, J. M. & Attardi, L. D. The role of apoptosis in cancer development and treatment response. *Nat. Rev. Cancer* **5,** 231–237 (2005).

104. Pandolfi, P. P. Aberrant mRNA translation in cancer pathogenesis: an old concept revisited comes finally of age. *Oncogene* **23,** 3134–7 (2004).

105. Marco, C. De *et al.* Mutant AKT1-E17K is oncogenic in lung epithelial cells. *Oncotarget* 1–17 (2015).

106. Jolly, C. & Morimoto, R. I. Role of the heat shock response and molecular chaperones in oncogenesis and cell death. *J. Natl. Cancer Inst.* **92,** 1564–1572 (2000).

107. Malusecka, E. W. a *et al.* Stress Proteins HSP27 and HSP70i Predict Survival in Non-small Cell Lung Carcinoma. *Anticancer Res* **28,** 501–506 (2008).

108. Mogi, A. & Kuwano, H. TP53 Mutations in Nonsmall Cell Lung Cancer. *J. Biomed. Biotechnol.* **2011,** 1–9 (2011).

109. Qi, H., Yukun, Z. U., Xiangning, F. U. & Tangchun, W. U. Expression of Heat Shock Protein 70 and 27 in Non-small Cell Lung Cancer and Its Clinical Significance. *J Huazhong Univ Sci Technol. Med Sci* **25,** 693–695 (2005).

110. Bonay, M. *et al.* Expression of heat shock proteins in human lung and lung cancers. *Am. J. Respir. Cell Mol. Biol.* **10,** 453–461 (1994).

111. Schmidt, E. K., Clavarino, G., Ceppi, M. & Pierre, P. SUnSET, a nonradioactive method to monitor protein synthesis. *Nat. Methods* **6,** 275–277 (2009).

112. Dolfi, S. C. *et al.* The metabolic demands of cancer cells are coupled to their size and protein synthesis rates. *Cancer Metab.* **1,** 1–13 (2013).

113. White-Gilbertson, S., Kurtz, D. T. & Voelkel-Johnson, C. The role of protein synthesis in cell cycling and cancer. *Mol Oncol* **3,** 402–08 (2009).

114. Wang, M., Wey, S., Zhang, Y., Ye, R. & Lee, A. S. Role of the unfolded protein response regulator GRP78/BiP in development, cancer, and neurological disorders. *Antioxid. Redox Signal.* **11,** 2307–2316 (2009).

115. Wang, Q. *et al.* Overexpression of endoplasmic reticulum molecular chaperone GRP94 and GRP78 in human lung cancer tissues and its significance. *Cancer Detect. Prev.* **29,** 544–551 (2005).

116. Schwartz, D. C. & Hochstrasser, M. A superfamily of protein tags: Ubiquitin, SUMO and related modifiers. *Trends Biochem. Sci.* **28,** 321–328 (2003).

117. Mani, a. The Ubiquitin-Proteasome Pathway and Its Role in Cancer. *J. Clin. Oncol.* **23,** 4776–4789 (2005).

118. Scagliotti, G. Proteasome inhibitors in lung cancer. *Crit. Rev. Oncol. Hematol.* **58,** 177–89 (2006).

119. Escobar, M., Velez, M., Belalcazar, A., Santos, E. S. & Raez, L. E. The role of proteasome inhibition in nonsmall cell lung cancer. *J. Biomed. Biotechnol.* **2011,** 806506 (2011).

120. Dittmar, K. a., Goodenbour, J. M. & Pan, T. Tissue-specific differences in human transfer RNA expression. *PLoS Genet.* **2,** 2107–2115 (2006).

121. Shah, P. & Gilchrist, M. a. Effect of correlated tRNA abundances on translation errors and evolution of codon usage bias. *PLoS Genet.* **6,** e1001128 (2010).

122. Malanga, D. *et al.* The Akt1/IL-6/STAT3 pathway regulates growth of lung tumor initiating cells. *Oncotarget* 1–20 (2015). doi:10.18632/oncotarget.5626

123. Stoletzki, N. & Eyre-Walker, A. Synonymous codon usage in Escherichia coli: Selection for translational accuracy. *Mol. Biol. Evol.* **24,** 374–381 (2007).

124. Duret, L. & Mouchiroud, D. Expression pattern and, surprisingly, gene length shape codon usage in Caenorhabditis, Drosophila, and Arabidopsis. *Proc. Natl. Acad. Sci. U. S. A.* **96,** 4482–4487 (1999).

125. Drummond, D. A. & Wilke, C. O. Mistranslation-Induced Protein Misfolding as a Dominant Constraint on Coding-Sequence Evolution. *Cell* **134,** 341–352 (2008).

126. Carlini, D. B. & Stephan, W. In vivo introduction of unpreferred synonymous codons into the Drosophila Adh gene results in reduced levels of ADH protein. *Genetics* **163,** 239–43 (2003).

127. Lozy, F. & Karantza, V. Autophagy and cancer cell metabolism. *Semin. Cell Dev. Biol.* **23,** 395–401 (2012).

XIII. Appendix

1X PBS (1L)	
Reagent	Mass (g)
NaCl	0.10
KCl	0.20
Na_2HPO_4	1.44
KH_2PO_4	0.24
In 1L dH_2O	
Adjust pH to 7.4	

HBS (1L)	
Reagent	Mass (g)
Hepes	0.25
NaCl	0.40g
KCl	0.0185
Na2HPO4	0.005
D(+) glucose	0.054
In 1L dH_2O	
Adjust pH to 7.14	

Protein lysis buffer	
Reagent	Volume (µl)
ELB	4645
DTT (1M)	5
NaF (1M)	5
EDTA (0.5M)	20
EGTA (0.1M)	50
Na_3VO_4 (0.1M)	50
For 5 aliquots of 955µl	
Adjust pH to 7.14	
1M PMSF	25
Complete Mini EDTA-free protease inhibitor cocktail tablets	20
Add to aliquots immediately before use	

2 Polyacrylamide gels			
Reagents	Running gel		Stacking gel
	10%	8%	4%
H_2O miliQ	3.6ml	3.8ml	3.465ml
Tris-HCl 1.5M pH 8.8	3.75ml	3.960ml	-------
Tris-HCl 0.625M pH 6.8	-------	-------	1.0ml
40% Acrylamide/bis-acrylamide solution, (29:1)	2.5ml	2.1ml	500µl
10% SDS	100µl	100µl	50µl
10% APS	100µl	50µl	50µl
TEMED	10µl	10µl	10µl

6X SDS Protein Loading Buffer	
Reagent	
Tris-HCl	375 mM
SDS	9%
Glycerol	50%
Bromophenol Blue	0.03%

10X Running buffer	
Reagent	Mass (g)
Glycine	144
Tris	30.2
SDS	10
In 1L dH_2O	

Dilute 10X to use

Transfer Buffer	
Reagent	
Tris Base	3.03g
Glycine	14.4g
Methanol	200ml
dH_2O	800ml

TBS 10X	
Reagent	Mass (g)
NaCl	80
KCl	2
Tris base	30
In 1L dH_2O	

Dilute 10X to use

Stripping solution	
Reagent	
Glycine	1.5g
SDS	0.1g
Tween-20	1ml
In 100ml dH_2O	

Adjust pH to 2.2

Proteasome lysis assay buffer	Proteasome activity buffer
0.5M EDTA	500mM EDTA
200mM Tris-HCl pH8	100mM Tris-HCl pH8
40% Glycerol	1mM Suc
H_2O miliQ	------
1M DTT	------
1M ATP	1M ATP

In 10ml solution

Add immediately before use

2% Urea SDS loading buffer	Coomassie Brilliant Blue	Distaining solution
Reagent	Reagent	Reagent
8M urea	0.25% (w/v) Comassie Blrilliant Blue R in ethanol	Ethanol
2% SDS	dH_2O	dH_2O
50mM DTT	Acetic acid	Acetic acid
50mM Tris pH7.4	[5:5:1]	[5:5:1]
A trace of bromophenol		